DESTABILISATION OF THE MEDIAL MENISCUS: IMAGING AND MECHANICS OF A MURINE SURGICAL OSTEOARTHRITIS MODEL

Jonathan Moodie

Thesis submitted for the degree of
Doctor of Philosophy

Department of Bioengineering
Imperial College London

August 2011

Declaration

This Thesis describes work carried out by the author in the Department of Bioengineering at Imperial College, London

This Thesis describes original work, which has not been submitted for a higher degree at any other University and is the work solely of the author, except where acknowledged in the text.

Jonathan Moodie

Abstract

Destabilisation of the medial meniscus (DMM) is a murine surgical instability model of osteoarthritis (OA). In this thesis the bone and cartilage changes were examined at different time points and in different strains of mice in the DMM model.

In the first study C57Bl/6 mice underwent DMM surgery and were culled four and eight weeks post-operatively. Tibiae were examined using confocal scanning laser microscopy (CSLM) for cartilage changes and micro-computed tomography (micro-CT) for bone changes. Additional mice underwent laxity testing. The tibia exhibited significant loss of cartilage and bone on the posterior plateau. A significant increase of anterior-posterior laxity suggested that damage of the anterior cruciate ligament had occurred during surgery, which permitted the femur to relocate to posterior tibia causing bone and cartilage damage.

A second study investigated early stage bone changes in the DMM model. CSLM and micro-CT were used in conjunction with non-decalcified histology. Mice received calcein injections three and six days prior to sacrifice, and were culled two weeks after surgery. There was an increase of epiphyseal bone volume. No change in cartilage was observed with CSLM. A significant increase of mineralising surface/bone surface and osteoid surface/bone surface occurred at two weeks.

A final study compared the bone response of two mice strains (BALB/c and C57Bl/6). Laxity was compared between strains eight weeks post operatively. Epiphyseal bone increased in both strains, more so in the BALB/c which had initially less epiphyseal bone volume. There was no change in histological mineralisation parameters or laxity measures.

In this work multi-modal imaging techniques were developed to determine the change in bone and cartilage in the DMM model.

Acknowledgments

I would like to acknowledge the support, wisdom and patience of my supervisor Sandra Shefelbine, who provided the original inspiration for undertaking a PhD. The project was funded by a CASE award provided the EPSRC and Smith & Nephew for whom I am grateful. I must also acknowledge the help and facilities offered by Nikki Horwood and her group at the Kennedy Institute of Rheumatology, the IDEA league and Ralph Muller's group at ETH.

I would also like to thank Warren MacDonald for his broad and ready dispensable knowledge, as well as his cheer and entertainment, Max Vanleene and Mike Doube for technical advice and Alessandra Carriero for being a friendly (and tolerant) desk neighbour.

I would like to thank the members of Bioengineering for making the department and enjoyable place to work, Dominic Southgate, Joe Prinold and Robin Jones deserve a special mention for providing continual vertical distraction.

I would also like to thank Simon Moodie and Samantha Blackham, both of whom provided significant and contrasting reasoning to help get me across the finish line.

Contents

Table of Figures

1. Introduction

1.1 Rationale

Osteoarthritis (OA) is a complex disease compounded by its heterogeneous nature. Predisposing risk factors, causes of initiation and rate of disease progression all vary across patients. Osteoarthritis is a disease not just of cartilage, but of all the tissues in a synovial joint. The complexity and transiency of OA necessitates the use of animal models for investigating disease pathology and the efficacy of treatments. Effective animal models must be reproducible and mimic the human form of the disease under investigation (Bendele 2001). It is therefore, necessary to obtain a detailed understanding of OA initiation and progression in a model in order to ascertain its relevance. The destabilised medial meniscus (DMM) model is a widely used murine OA model; it is an instability model which requires the surgical transection of the medial menisco-tibial ligament. At present few papers have characterised the changes seen in the DMM model. Cartilage changes at four and eight weeks post operatively have been characterised (Glasson 2007) as have bone changes at eight weeks (Botter 2009). This thesis provides further understanding of tissue changes in the DMM model.

1.2 Relevance

Tissue response to OA is variable across animal OA models and knowledge of the sequence of tissue changes is necessary in any model prior to usage for investigating therapy efficacy. The work in this thesis illustrates the nature and timings of tissue changes, uses novel methods to analyse these changes and highlights the biomechanical impact of meniscal destabilisation. This thesis also illustrates possible errors that could be encountered during surgical induction of the DMM model. The thesis also develops murine knee joint laxity testing, non-decalcified histology and multi-modal imaging techniques, namely confocal scanning laser microscopy for cartilage analysis, and micro-computed tomography for bone analysis.

1.3 Outline

The original focus of my PhD project was to design and validate a device to distract the articulating surfaces of the murine knee joint. The joint distraction device was to be used to investigate the effect of unloading on cartilage repair. The intention was to apply joint distraction to mice which had received surgical destabilisation of the medial meniscus (DMM). Nine months in to the project I travelled to ETH Zurich on an IDEA League fellowship to learn confocal scanning laser microscopy (CSLM) and micro-CT techniques, with the intention of using them to investigate the efficacy of joint distraction. On returning to London the surgical collaborators withdrew support for the joint distraction project, to focus instead on fracture healing. This was because of the perceived difficulty in developing the required intricate small-scale orthopaedic device. Consequently the focus of the project shifted to developing a deeper understanding of tissue structural changes in the DMM model, using the aforementioned techniques. Joint distraction progressed as far as the development of a prototype distractor, capable of unloading the articular surfaces. Details of the joint distraction project and the scientific reasons for its termination are contained in Appendix A.

The legs of 23 mice with DMM surgery were taken to ETH for CSLM and micro-CT analysis. Though I received valuable training in the techniques, the automatic methods for micro-CT analysis used in Switzerland were deemed unsuitable for the bone changes that were produced in the DMM model. Because bone morphology of the DMM affected tibiae deviated significantly from normal morphology, the automated methods used at ETH were unable to accurately measure bone parameters. On returning to London all micro-CT scan data was reanalysed manually. Limitations with the CSLM method also became apparent, as the ETH CSLM method produced reconstructed cartilage volumes with approximately three times the thickness of murine tibial cartilage. I repeated all the CSLM scans with an improved method that I developed. Measurements of joint laxity were initially to be incorporated into the joint distraction project to determine if distractor application

reduced laxity. However, laxity testing was used in subsequent studies to characterise the mechanical effects of DMM surgery as well as the effects of tissue changes on joint laxity.

In Chapter 3 the mice received DMM surgery and were culled 0, four and eight weeks post operatively. Joint laxity was assessed in the 0 week group to determine how DMM surgery affects joint mechanics. Changes in bone and cartilage were assessed in the four and eight week groups with micro-CT and CSLM, respectively. This study revealed substantial tissue changes on the posterior-medial plateau that had not been described with the DMM model, but were evident through the 3D imaging techniques. On the basis of these results, the studies described in Chapters 4 and 5 were designed and initiated, in order to (1) determine how early tissue changes occurred and (2) if mouse strain, particularly initial bone density, affects OA bone changes. Upon completion of the experimental programme of work for the thesis and initial analysis of these results, the surgical technique described in Chapter 3 was re-examined. It was established that the mice in that study probably received medial menisco-tibial ligament transection accompanied with variable damage to the anterior cruciate ligament. The study in Chapter 3 was published in Osteoarthritis and Cartilage in February 2011.

The experimental programmes of work described in Chapters 4 and 5 were conducted simultaneously. Chapter 5 compares bone changes in two different mouse strains with DMM. The two mouse strains had a different apparent bone density and produced a different bone response to OA.

Early stage bone changes in the DMM model were investigated as described in Chapter 4. The experimental design used was based on the severe bone changes originally reported in Chapter 3, before establishing that the DMM surgery had anterior cruciate ligament damage. Although this surgical procedure was different it was not detrimental to the reported outcomes as the procedures were independent of one another. The conclusions presented in Chapter 4 showed that the tibial epiphyseal bone formation occurred in the early stages of OA in the DMM model.

The main contributions to the thesis are highlighted in Chapter 6 and further topics for potential future work are also suggested.

2. Literature Review

2.1 Components of a Joint

2.1.1 Cartilage

Articular cartilage is a load bearing structure, resistant to compressive, tensile and shear forces, with little mechanical distortion (Gray 2008). It allows almost frictionless motion between the two joint surfaces. It has limited vascularisation and therefore slow metabolism. On its surfaces it is lubricated and nourished by synovial fluid, composed of hyaluronic acid, lubricin and phagocytic cells. Cartilage is composed of chondrocytes embedded in a fibrous extracellular matrix (ECM). The immature cells found in cartilage tissue are called chondroblasts; the mature cartilage cells are called chondrocytes and are larger, spherical and are embedded in lacunae in the ECM. The role of the chondrocytes is to produce and maintain the cartilage ECM.

Articular cartilage thickness ranges from 1-7 mm in humans and 30-70 µm in mice (Stok 2009a). The structure of cartilage varies at different depths (Figure 2-1). The tangential layer is formed from collagen fibres arranged tangentially to the cartilage surface, which provides resistance to shear occurring at the articular surface. The chondrocytes in this zone are elongated in appearance and preferentially express lubricin and similar protective proteins rather than proteoglycans expressed in the transitional and deep layers (Wong 1996). In the transitional layer the collagen fibres are thicker and in a less ordered oblique arrangement. Chondrocytes in this layer are round in shape. Extending deeper, the cells form in rows, perpendicular to the tidemark (Nordin 2012).

This occurs to a lesser extent in the mouse, as the non calcified cartilage is approximately five cells thick. The deepest layer of cartilage is calcified, here the collagen fibres merge together and are anchored to the bone (Aspden 1981; Pearle 2005).

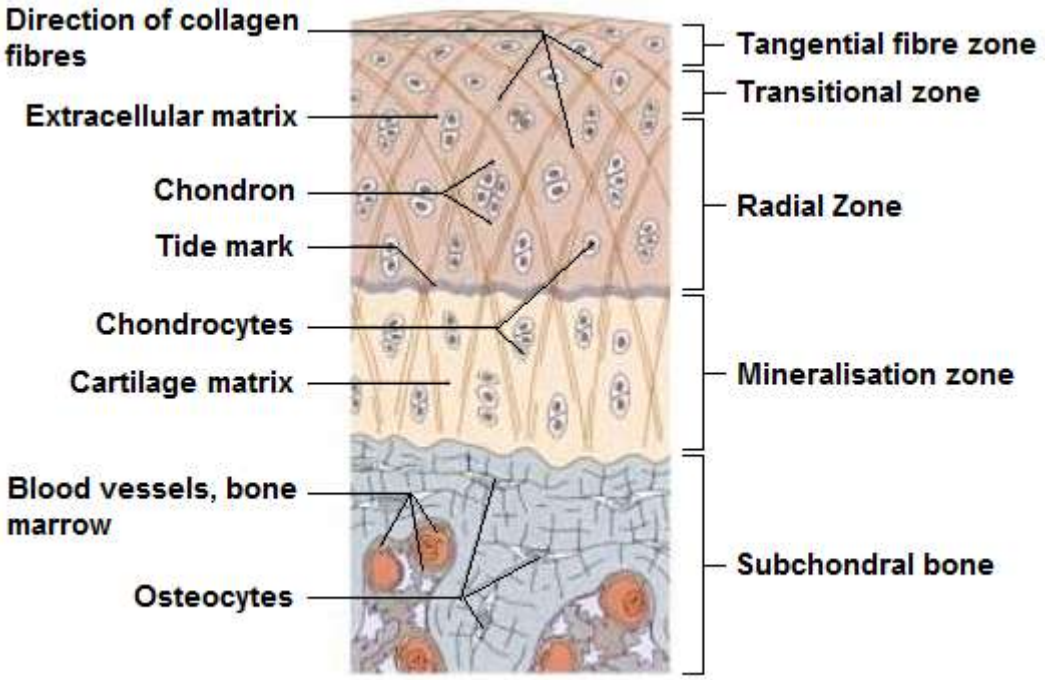

Figure 2-1. Zonal structure of articular cartilage (Schünke 2006).

The tidemark lies between the hypertrophic region of the deep cartilage and the calcified cartilage, it delineates the calcified cartilage from the overlying cartilage, marking the mineralising front of the cartilage. The calcified cartilage reduces the mechanical gradient between the compliant cartilage and the stiffer subchondral bone (Radin 1986). The tidemark advances with the progression of the mineralised front during aging (Hunziker 2002; Hughes 2005; Ge 2006; Gray 2008).

Articular cartilage is avascular and the chondrocytes are maintained by diffusion of nutrients. When chondrocytes undergo proliferation and matrix production the demand for nutrients increases. This drives the formation of canals within the cartilage which contain capillaries, forming an environment which favours bone formation.

The extracellular matrix (ECM) of cartilage gives it its mechanical characteristics. Cartilage ECM is approximately 70% water, 20% type II collagen, 6% proteoglycan (PG) and the remainder are other non-collagenous proteins. This varies with age, pathology and location within a joint, for example OA

cartilage has increased water content, especially in the middle zone, and decreased PG content (Venn 1977). The ECM is biphasic: the proteoglycan and collagen form the solid phase, which has a low permeability to the aqueous fluid phase.

The proteoglycans give cartilage their resistance to compression (Pearle 2005). They take the form of aggrecans, which are huge aggregates of proteoglycans and are formed primarily from two glycosaminoglycans (GAGs), chondroitin sulphate and keratan sulphate, which are non covalently bonded to a molecule of hyaluronate (Figure 2-2). The GAGs are negatively charged and retain large quantities of water, accounting for the hydrophilic properties of cartilage. The high water content of cartilage gives it its ability to withstand large hydrostatic compressive stresses. The osmotic pressures caused by water uptake are resisted by tension from the collagenous network. The collagen network is also responsible for resisting tensile and shear forces.

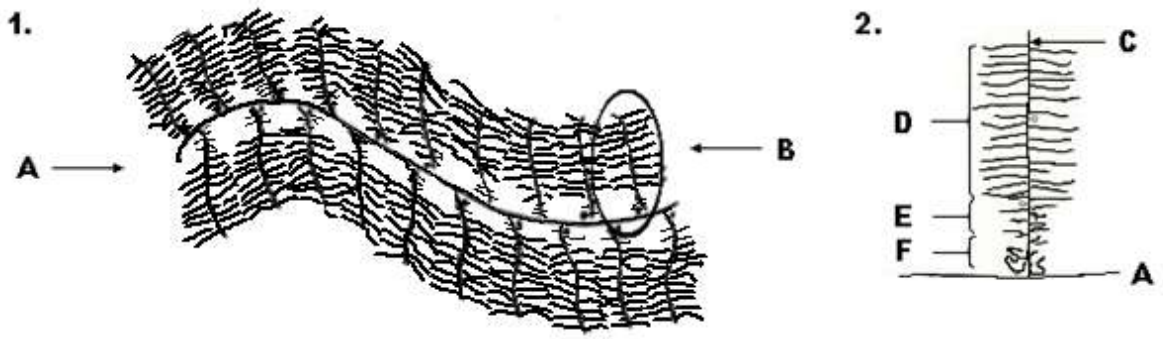

Figure 2-2. (1) Proteoglycan and (2) Glycosaminoglycan structure. A. Hyaluronic acid backbone. B. Proteoglycan. C. Core Protein. D. Chondroitin sulphate region. E Keratan sulphate region. F. Binding region.

2.1.2 Bone

Bone structure

Bones possess a hard outer layer, known as cortical bone which is dense with a low porosity, and accounts for 80% of skeletal bone mass. The remainder of skeletal mass is trabecular bone which is found in the interior of bones. Trabecular bone is formed from an interconnected network of rod and plate like bone elements (trabeculae) forming an open cell porous structure. The trabeculae in

porous bone are remodelled so as to preferentially align parallel with the principal component of an external load (Biewener 1996; Bilezikian 2008).

The long bones are the bones of the skeleton which have a length substantially greater than their width, and are characterised by a long shaft. The long bones tend to be the larger bones in the appendicular skeleton, such as the femur, tibia, ulna and humerus, and are associated with larger loads and motion.

Articular cartilage covers portions of the ends of long bones. Underneath this articular cartilage lies a region of cortical bone referred to as the subchondral plate. The tubular shaft of a long bone is referred to as the diaphysis and contains the marrow cavity. The wide end region of a long bone is referred to as the epiphysis, and the metaphysis is a region between the diaphysis and the epiphysis adjacent to the growth plate (Figure 2-3). The growth plate is responsible for longitudinal growth of the bone and ossifies at skeletal maturity, when this occurs longitudinal bone growth stops. In humans, skeletal maturity occurs between the ages of 15 and 20 depending on the bone, whereas in mice the growth plate can remain unfused throughout the mouse's lifetime. However, in some mouse strains, growth plate ossification is described as occurring after four months (Silbermann 1977; Somerville 2004), in the C57Bl/6 used in this thesis, the growth plates had not fused at the latest time point of 20 weeks.

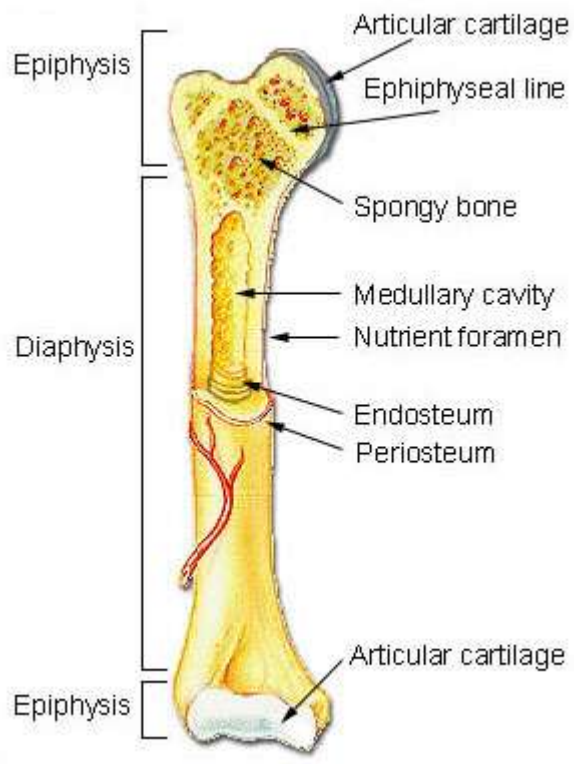

Figure 2-3. Illustration of bone compartments (Seer 2001).

Trabecular bone is found in the epiphyseal and metaphyseal regions of long bones, this region is highly vascularised and typically contains red bone marrow which produces blood cells and platelets. The marrow cavity of the diaphysis contains primarily yellow marrow which is mostly adipose tissue. The outer surfaces of bones are covered by a membranous layer called the periosteum. This is comprised of two layers, the inner cambium layer and the outer fibrous layer. The cambium contains osteoprogenitor cells, which differentiate into bone forming cells. The fibrous layer is formed from dense irregular connective tissue, and is supplied with nerves and blood vessels which enter the bone via perforating canals. The inner surface of bone is covered with a thin layer of connective tissue known as the endosteum. (Bilezikian 2008).

Bone tissue is comprised of both a cellular component and an extracellular matrix. Bone is predominantly extracellular matrix, which can be subdivided into an organic phase and a mineral phase. The mineral phase of bone is hydroxyapatite ($Ca_{10}(PO_4)_6(OH)_2$), which is formed on collagen

fibrils and gives bone its stiffness and resistance to compressive stresses (Junqueira 2005). Carbonate substitution (for phosphate) can occur in the mineral and is often used as an indication of age of the crystal. The mineral phase also contains small quantities of calcium precipitates, ions and impurities. The organic phase of extracellular matrix consists of collagen (90% collagen type I, with a small amount of type V and XII), glycosaminoglycans, non-collagenous proteins such as osteocalcin, osteonectin and bone sialoprotein and various growth factors. (Junqueira 2005).

Bone Cells

There are five types of cell associated with bone tissue: osteoblasts, osteocytes, osteoclasts, bone-lining cells and osteoprogenitor cells. With the exception of osteoclasts, the four other cell types derive from the same cell line, starting with the mesenchymal stem cells. Osteoprogenitor cells are immature bone cells, the first in the cell line to be formed. Osteoprogenitor cells are flat in shape, and are found in the innermost layers of the periosteum and endosteum, they respond to molecular stimuli by transforming into osteoblast cells (Ross 2006).

The osteoblast is a secretory cell responsible for forming new bone (Figure 2-4). Osteoblasts are found in clusters on the surface of the bone usually adjacent to a layer of new matrix of which they are producing. Osteoblasts produce new bone by first forming the organic phase of the ECM called osteoid. Osteoid is composed of over 90% collagen type I, and also contains a GAG gel with calcium binding proteins (osteonectin and osteocalcin). The osteoblast then mineralises the osteoid. Mineralisation is restricted to osteoid tissue because co-expression of collagen type I and tissue non-specific alkaline phosphatase (TNAP) is required for mineral deposition. TNAP is an enzyme which cleaves pyrophosphate (PP_i), an inhibitor of bone mineralisation (Murshed 2005). Humans and mice deficient in PP_i production exhibit mineralisation of soft tissues (Rutsch 2003). Osteoblasts secrete alkaline phosphatase which provides phosphate groups necessary to form hydroxyapatite in bone mineralisation (Chenu 1990). The osteoblast responds to mechanical stimuli to attenuate or initiate

bone remodelling. When osteoblasts are active they are located on bone surfaces and are cuboidal or polygonal in shape; quiescent osteoblasts are flatter in appearance. Osteoblasts aggregate into a thin layer on bone surface when forming bone. During mineralisation the osteoblast is embedded to become an osteocyte (Ross 2006).

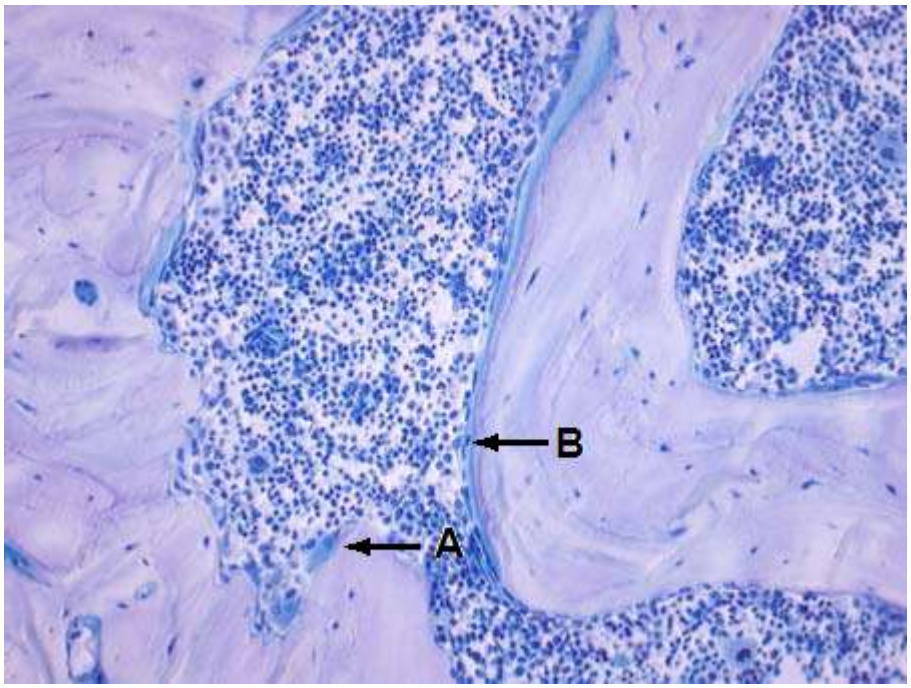

Figure 2-4. A 5 µm ×100 non decalcified toluidine blue stained histology image of primate vertebra (SkeleTech 2001). A. Osteoclast resorption. B. Osteoblast formation.

The osteocyte is a mature cell that exists in a lacuna enclosed by bone matrix and maintains the surrounding bone matrix (Figure 2-5). Mechanical forces on bone alter osteocyte gene expression, a process known as mechanotransduction. Osteocytes possess cytoplasmic processes which extend through canaliculi in the matrix between lacunae; they connect to neighbouring osteocytes by gap junctions[1]. The necrosis or apoptosis of osteocytes initiates resorption of the surrounding matrix by osteoclasts, which is followed by osteoblast remodelling (Ross 2006).

[1] A gap junction is an intercellular connection that allows molecules and ions to be exchanged between two cells.

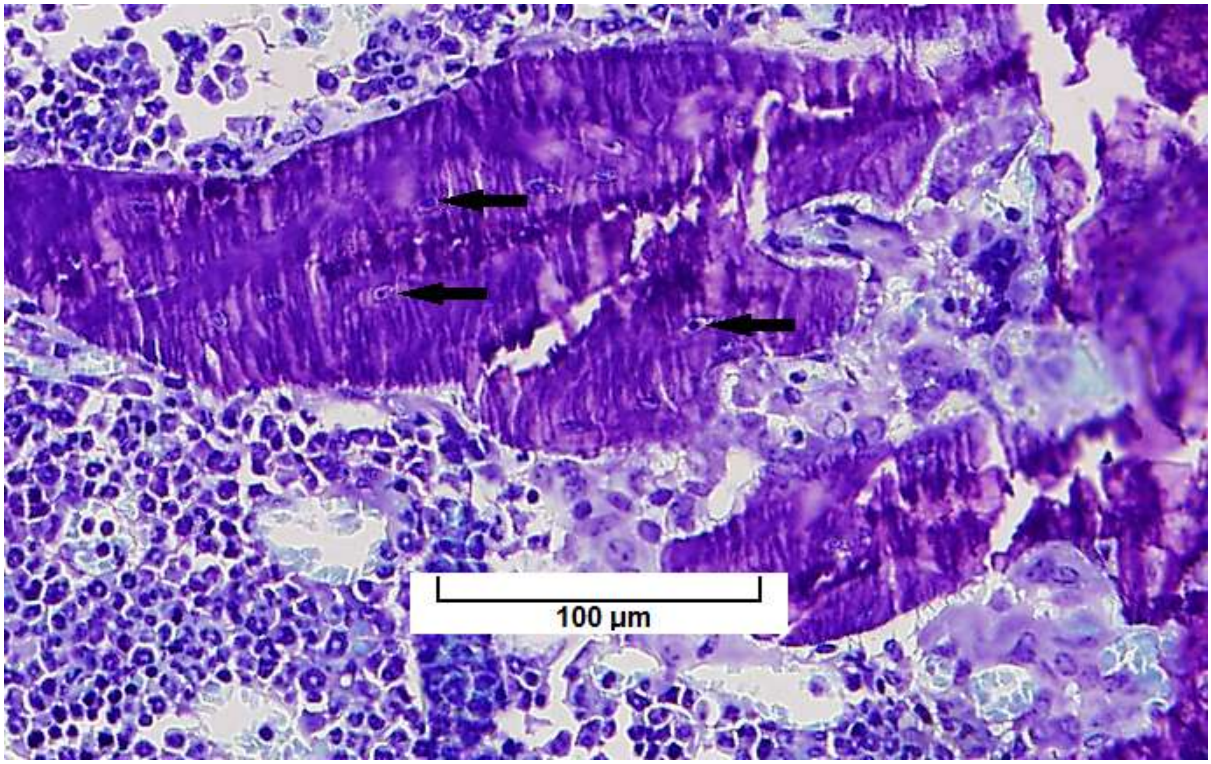

Figure 2-5. A non decalcified toluidine blue stained histology image of murine trabeculae. Arrows denote osteocytes. (Image taken from a histology section used in Chapter 4 of this thesis).

Osteoclasts resorb bone and are found in resorption pits (Figure 2-4). The osteoclast is multinucleate and larger in size than other bone cells, it derives from haematopoietic cells of the mononuclear lineage. When resorbing bone, the osteoclast exhibits a ruffled border formed from folds in the membrane adjacent to the bone. In this region the osteoclast secretes protons and lysosomal hydrolases by exocytosis into the extracellular space of the folds. The hydrolytic enzymes include cathepsin K and MMPs (matrix metalloproteinases), which degrade collagen and other organic bone matrix components (Ross 2006). Prior to resorption the matrix is decalcified by secretion of protons. The protons are formed from dissolution of carbonic acid in the cytoplasm, protons are secreted by proton pumps in the ruffled border. The acidic environment produced by excess protons in the extracellular space initiates dissolution of the mineral component.

The bone surface is covered by bone-lining cells in sites where no remodelling is occurring. They are found on both endosteal and periosteal surfaces. The bone-lining cell is derived from the

mesenchymal stem cell lineage. Bone-lining cells are interconnected through gap junctions, and through canaliculi connecting them to osteocytes on the inner surface of bone. Their function is to maintain and support embedded osteocytes, and to transport calcium and phosphate out of the bone (Ross 2006).

Bone Microstructure

Bone can take the form of woven or lamellar bone, which is determined by its collagen pattern. The fundamental difference between lamellar bone and woven bone is that lamellar bone has a highly organised secondary and tertiary structure which results in a stronger tissue (Weiner 1999).

Lamellar bone is composed of cylindrical structural units called osteons (Figure 2-6), which feature a central canal containing a blood vessel, and surrounding concentric cylindrical layers of bone called lamellae. The osteon can be categorised as either a primary or a secondary osteon. Secondary osteons are formed during the replacement of pre-existing bone. Formation of secondary osteons are initiated by osteoclasts, which tunnel a resorption cavity approximately 2000 μm long with a diameter of 150 – 300 μm parallel to the principal loading direction (Petrtyl 1996). Osteoblasts then synthesise matrix on the tunnel walls, in successive concentric lamellae, until the tunnel diameter is reduced to approximately 50 - 90 μm (Bronner 2005) (the process of bone remodelling is discussed in greater detail in the next section). This central space in the osteon is called the Haversian canal, which contains a blood vessel. Diffusion through mineralised tissue is highly limited; therefore, vasculature in the bone is required to deliver nutrients close to the osteocytes in the interior of the bone tissue. Volkmann's canals run perpendicular between two adjacent osteons, and carry vessels that link the Haversian vessels (Bronner 2005)(Figure 2-6). At the outer diameter of an osteon is the cement line, a border of under mineralised bone tissue with a higher degree of compliance than the osteon. The cement line is thought to reduce fracture propagation through energy absorption and crack deflection (Qiu 2009).

The concentric lamellae in an osteon possess a tertiary structure, in which the collagen fibres of each individual lamella are highly organised. The collagen fibres in one lamella are arranged in a predominantly parallel direction with a preferred orientation within the whole lamella. The preferential fibre direction in adjacent lamellae are then arranged up to 90° to each other, akin to grain direction in plywood (Pazzaglia 2011).

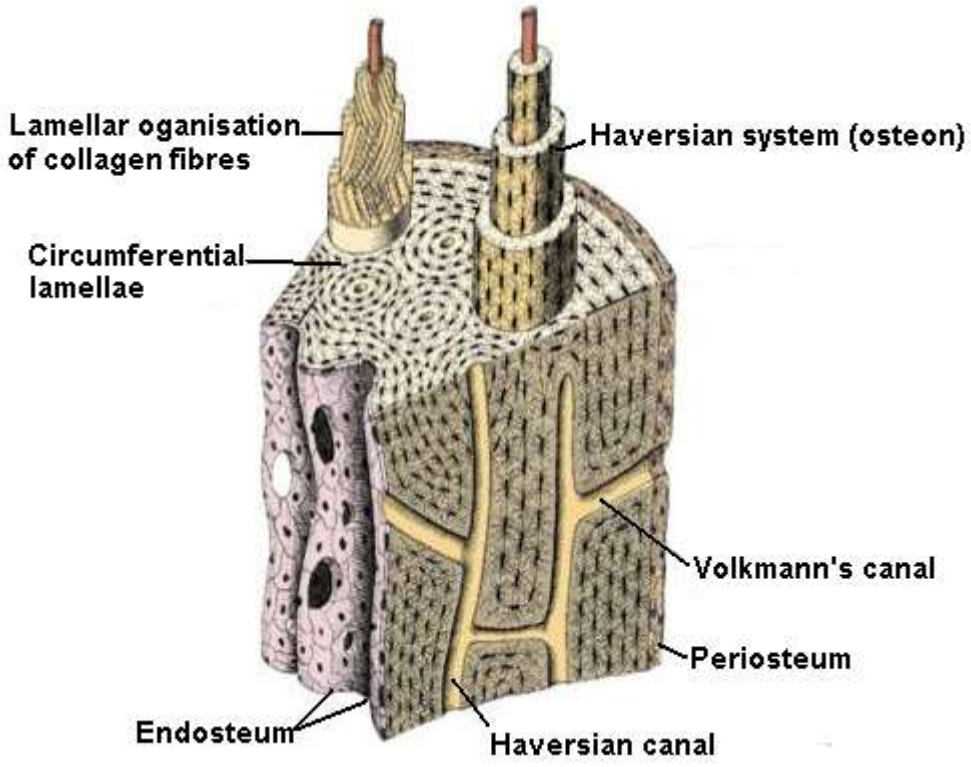

Figure 2-6. Illustration of Haversian system in cortical bone (Junqueira 2005).

Woven bone is formed when osteoid is produced rapidly by the osteoblasts. It does not possess an organised lamellar structure; instead collagen fibres are interlaced with a lower extent of mineralisation. It is the only type of bone that can be formed without requiring pre-existing bone or cartilage. Due to its rapid formation, collagen fibres are randomly orientated and it is therefore weaker (Ross 2006).

Bone Microstructure in Mice

In young mice, the cortex of long bones comprises mostly woven bone from endochondral ossification. As the mouse ages, circumferential lamellae are added to the periosteal surface and the woven bone is slowly resorbed. By 3-4 months the cortical bone of the mouse is predominantly lamellar bone. Mouse cortical bones lack the Haversian systems seen in humans. The Haversian systems seen in human bone are a result of continual remodelling, mouse cortical bone is rarely remodelled and as a result, exhibits the circumferential lamellar structure that is ordered concentric to the medullary canal (figure 2-7) (Treuting 2011).

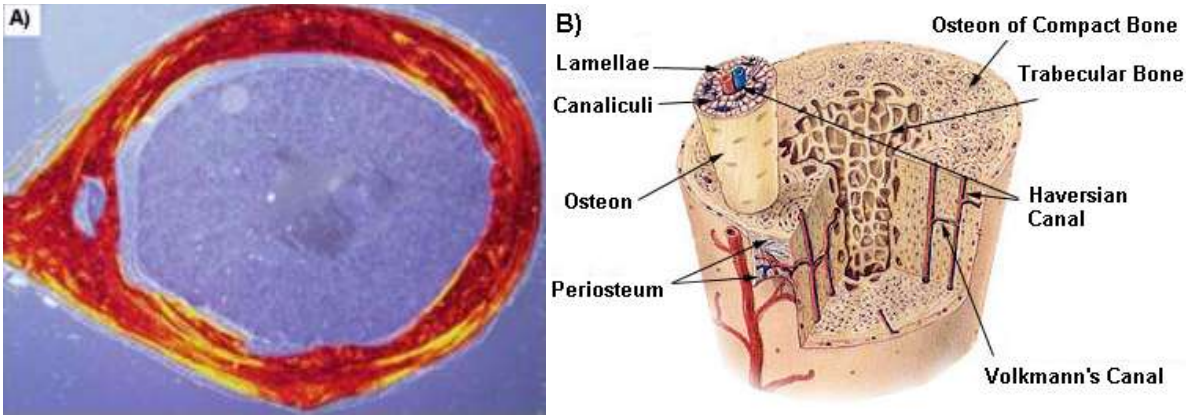

Figure 2-7 A) Cross section of mouse tibia displaying circumferential lamellae (Treuting 2011). B) Diagram of human bone structure which comprises of trabecular bone, and compact bone which, unlike mice bone, is organised into osteons (Seer 2001).

Bone remodelling

Bone remodelling is a coupled process in which old bone undergoes resorption and is replaced by newly formed bone. As well as replacing old bone, remodelling also enables bone to adapt to mechanical stresses that occur during loading. In healthy adults the extent of bone resorption and formation is balanced. Bone remodelling occurs in discrete regions on the surface of bone, which are formed from packets of cells called basic multicellular units (BMUs). The main cells involved in remodelling are the osteoclasts and osteoblasts. The remodelling process in human cortical bone differs to that of trabecular bone, with the differences being primarily morphological. In cortical

bone, remodelling establishes an osteon where osteoclasts in the BMU resorb a cylindrical tunnel through the bone parallel to the primary loading direction (Petrtyl 1996). Osteoblasts then form concentric layers of bone on the walls of the tunnel establishing a secondary osteon. Trabecular bone is more actively remodelled than cortical bone. In trabecular remodelling the osteoclast forms a trench (or resorption pit), which moves across the surface of a trabecula and is filled in by osteoblasts.

There are four separate stages in the remodelling cycle. The first stage is the resportion phase which begins with the migration of the osteoclasts onto the bone surface. Initiation of the osteoclast is triggered by RANKL (receptor activator NF-kappa ligand, a member of the TNF family). Interaction of RANKL with RANK receptors on the surface of the osteoclast precursor cell initiates differentiation and activation of resorption by the osteoclast (Hsu 1999). Integrins expressed on the surface membrane of the osteoclast facilitate its binding to proteins within the bone matrix (Davies 1989). Osteoclasts then resorb the bone matrix by acidic and proteolytic dissolution of the bonds between hydroxyapatite crystals and the collagen network. Once the mineral phase is dissolved, the collagen fibres are then digested with collagenases and cathepsins, to form resorption cavities on the surface of bone. RANKL also extends the lifetime of the osteoclast by delaying apoptosis (Hsu 1999). Osteoclast resorption is regulated by various systemic hormones and locally acting cytokines (implicated species include interleukin-1 (IL-1) (Xu 1996), insulin-like growth factor-1 (IGF-1) (Hou 1997), various androgens (Mizuno 1994), thyroid-hormone (Abu 1997) and calcitonin (Warshawsky 1980).

The next phase of the remodelling cycle is the reversal phase, in which the osteoclasts undergo apoptosis, and the osteoblast precursor cells differentiate into osteoblasts for synthesis of new bone. This process is facilitated by osteoprotegerin (OPG), which is produced by cells in the osteoblast lineage to block the activities of RANKL, this prevents osteoclast differentiation and induces osteoclast apoptosis (Hofbauer 2004).

Once the reversal phase has completed, the formation phase takes place, starting with the differentiation of mesenchymal stem cells into osteoblasts. Osteoblasts line the bottom of a resorption pit, and are responsible for forming osteoid, which is mineralised to form new bone that fills the resorption pit. The resting phase begins when mineralisation ends. The osteoblasts apoptose or revert back to bone lining phenotype and the resting bone surface is maintained until the next wave of remodelling occurs (Raggatt 2010)(Figure 2-8).

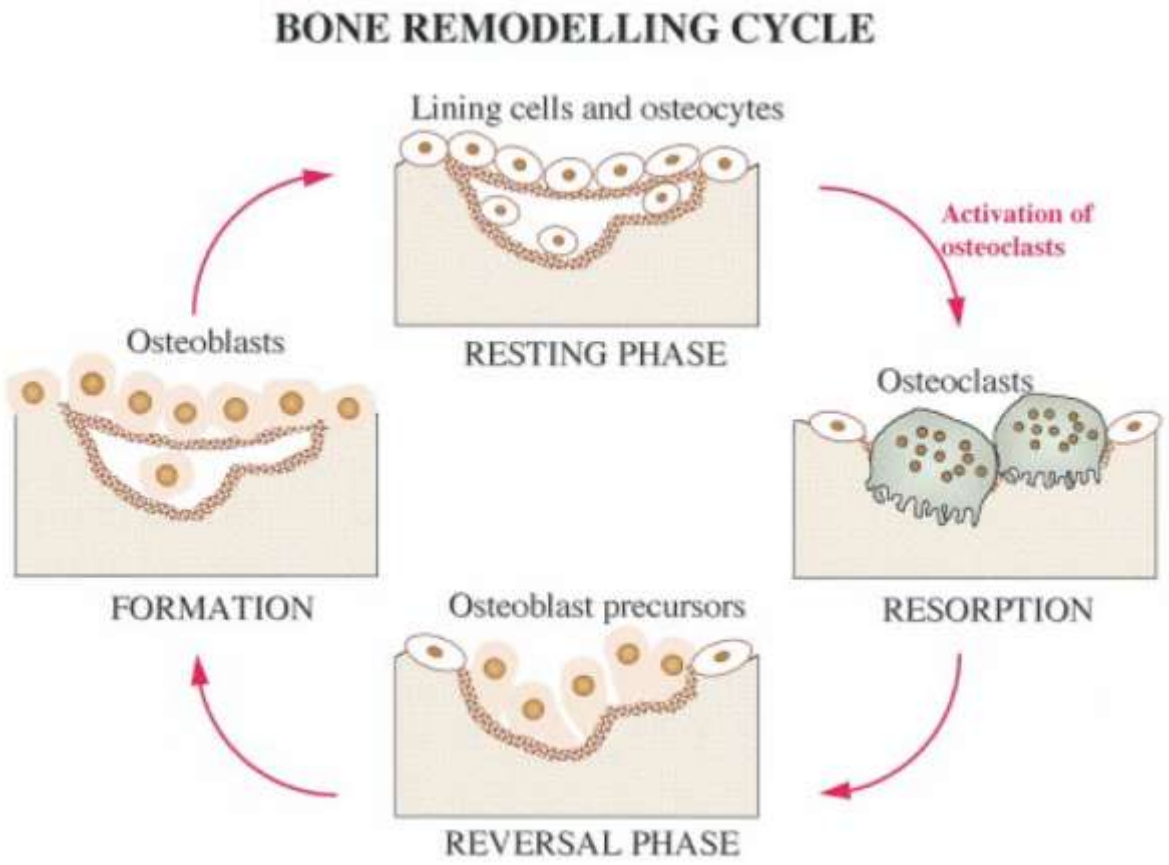

Figure 2-8 .The stages of the bone remodelling cycle (Hill 1998).

Local versus systemic control of the bone remodelling process

The involvement of RANKL and OPG suggests that local control of bone remodelling is important. The ratio of OPG to RANKL has a strong effect on the extent of osteoclast differentiation, activation resorption and apoptosis (Hofbauer 2000). This system is further modulated by various cytokines

including IL-10, TNF-α and β which affect RANKL or OPG production (Hadjidakis 2006). As well as local control, there is also evidence for systemic control of bone remodelling. In this regard, parathyroid hormone plays a key role in calcium homeostasis, calcitriol controls mineral absorption and therefore mineralisation, and glucocorticoids, androgens and estrogens have all been shown to regulate the cells involved in bone remodelling (Weinstein 1998; Srivastava 2001; Wang 2004).

Endochondral ossification

Endochondral ossification is the process by which long bones are formed in the developing foetal skeleton (Figure 2-9), and occurs alongside the process of intramembranous ossification, which is responsible for formation of flat bones during foetal skeleton development.

The primary distinguishing feature of endochondral ossification, compared to the process of intramembranous ossification, is the presence of a progressively mineralised cartilage template upon which long bone formation takes place (Gilbert 2000).

The cartilage template is formed from aggregated mesenchymal stem cells, this process is initiated by paracrine factors which induce the expression of transcription factors PAX1 and scleraxis from mesodermal cells (a type of embryonic germ cell) which activate cartilage specific genes (Cserjesi 1995; Sosic 1997). The mesenchymal stem cells differentiate into chondrocytes, which proliferate rapidly and secrete cartilage specific extracellular matrix to form the cartilage template (Figure 2-9A-B). Eventually the chondrocytes cease dividing and become hypertrophic, whereby their volume increases substantially (Figure 2-9C). At this point the composition of the secreted ECM changes, collagen X is now produced and fibronectin production is increased, and there is also an upregulation of matrix metalloproteinases including MMP 13. These changes in matrix structure allow the matrix to be mineralised (Ortega 2004; Mahmoodian 2011). These changes in ECM composition and synthesis also accompany the release of vascular endothelial growth factor (VEGF) by the chondrocyte (Ortega 2004). The cartilage model then undergoes vascular invasion as the

chondrocytes apoptose (Figure 2-9D). Osteoprogenitor cells invade the cartilage model and differentiate into osteoblasts which begin forming bone on the cartilage template (Figure 2-9E) (Hatori 1995).

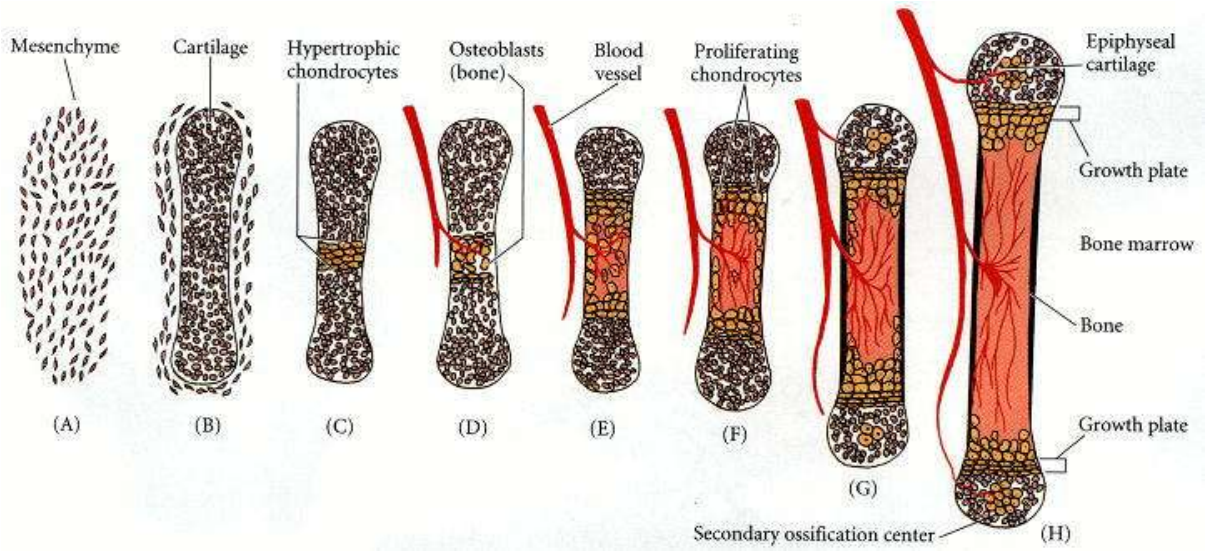

Figure 2-9. Diagram of the stages of endochondral ossification. A) and B) Mesenchymal cells condense and differentiate into chondrocytes which form the cartilage model. C) Chondrocytes in the centre of the model undergo hypertrophy and alter the composition of the matrix for mineralisation to begin. D) The release of VEGF by the chondrocytes and their apoptosis permits vascular invasion. E) The vessels bring in osteoblasts which mineralise the degrading matrix. F) A mineralising front is established which originates outward from the primary centre of ossification. The mineralising front is ordered into zones of proliferating, hypertrophic and apoptosing chondrocytes. G) Secondary centres of ossification are established near the ends of the bone (Gilbert 2000).

In mammalian long bones endochondral ossification progresses outward, ossification originates from the centre of the bone and progresses towards the ends of the long bones (Figure 2-9F and G); this is known as the primary front of ossification. A secondary site of ossification also appears in the ends of long bones at around birth (Figure 2-9H). In the primary front of ossification, chondrocytes ahead of the ossification front are in a state of proliferation. The proliferating chondrocytes increase the volume of the cartilage model by pushing out the cartilage model ends (Gilbert 2000). This cartilaginous area adjacent to the site of mineralisation is known as the epiphyseal growth plate (Figure 2-10). The growth plate consists of chondrocytes organised into distinct layers. Chondrocytes

in the layer closest to the mineralising front are in a state of apoptosis, leaving cavities into which bone forming cells invade. The layer beyond this consists of hypertrophic chondrocytes, and adjacent to this again is the aforementioned layer of proliferating chondrocytes. Finally, in the layer furthest away from the mineralising front there is a region of resting chondrocytes (Figure 2-10)(Chen 1995).

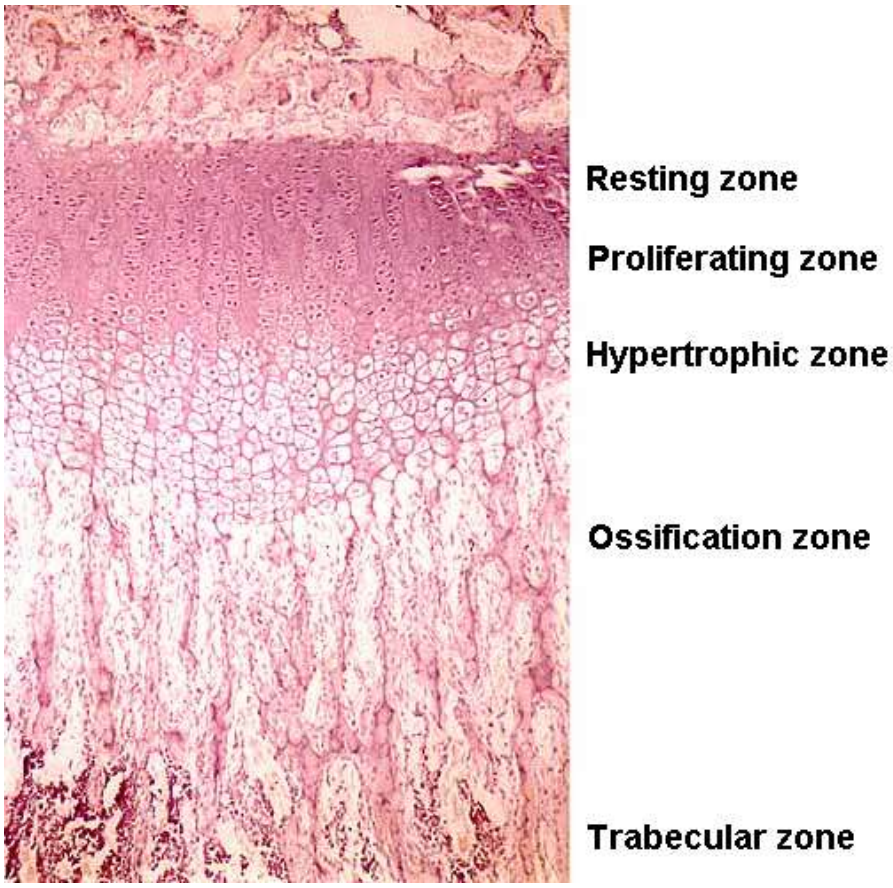

Figure 2-10. A hematoxylin and eosin stained section of a murine epiphyseal growth plate of a two week old mouse, with the separate regions of the growth plate labelled (Naski 1998).

The interstitial growth of bones continues as long as the epiphyseal plate remains unfused and is responsible for the long bones increasing in length. The bones grow in width by a process called periosteal apposition, whereby osteoblasts add bone material on the periosteal bone surface. The periosteum is comprised two layers, a fibrous outer layer and an inner layer termed the cambium. The cambium contains osteoprogenitor cells which differentiate into osteoblasts, these then secrete

new bone material forming ridges that envelope periosteal blood vessels, the osteoblast continues to form concentric layers of bone around them (Rauch 2005).

Intramembranous ossification

Intramembranous ossification is the process by which flat bones (e.g. the skull and scapula) are formed in the developing foetal skeleton (Figure 2-11).

The process of intramembranous ossification is initiated when mesenchymal stem cells proliferate and condense to form a dense aggregate of cells, known as a nodule. Once in the nodule, the mesenchymal stem cells differentiate into osteoprogenitor cells, which further differentiate into osteoblasts. This process is controlled by the transcription factor CBF1A, the transcription of which is activated by the presence of various bone morphogenic proteins (BMPs) (Ducy 1997).

Once osteoblast cells have been generated they secrete a collagen-proteoglycan extracellular matrix called osteoid, in which the principle collagen component is type I. The osteoid matrix is secreted into the centre of the nodule and is surrounded by osteoblasts that line the nodule periphery. The osteoid is then calcified by the osteoblasts, which secrete hydroxyapatite containing membrane bound vesicles into the osteoid. Hydroxyapatite crystals precipitate from within these vesicles and mineralise the collagen fibres in the osteoid matrix (Ozawa 2008). As the process of matrix secretion and mineralisation progresses, some of the osteoblasts lining the periphery of the nodule become trapped in the matrix and differentiate into osteocytes. The calcified matrix also forms into spicules (needles of calcified osteoid) that radiate out from the centre of the nodule. These calcified spicules become surrounded by compact mesenchymal stem cells leading to the formation of the periosteum. The mesenchymal stem cells on the inner surface of the periosteum differentiate into osteoblasts and continue to deposit matrix on the existing spicule. As the process continues, spicules fuse and aggregate into woven bone (Bilezikian 2008).

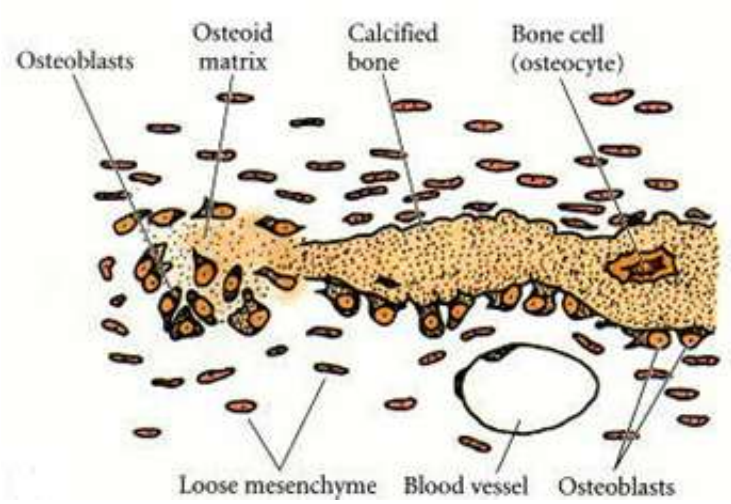

Figure 2-11. The process of intramembranous ossification. Mesenchymal stem cells condense and differentiate into osteoblasts, which deposit osteoid matrix. The osteoblasts become arrayed along the calcified region of the matrix. Some of the osteoblasts become trapped within the bone matrix and become osteocytes (Gilbert 2000).

2.1.3 Tendons and Articular Ligaments

Tendons and ligaments are soft collagenous connective tissues, the former connects muscle to bone and the latter connects bone to bone. The composition of tendon is 55% water and 38% collagen (primarily type I). Ligaments have a similar composition, but with a slightly increased proteoglycan content. The collagen allows tendons and ligaments to resist tensile stresses and the proteoglycans maintain spacing between fibres to help withstand deformation during loading (Scott 1981; Puxkandl 2002). Both structures have a similar composition and a similar hierarchical structure which determines their mechanical behaviour. Ligaments and tendons are formed from smaller subunits called fascicles. The fascicles contain collagen fibrils, aligned along the long axis of the tissue and are maintained by fibroblasts. At this level the fibril features a crimp structure, which appears as a wave like pattern under a microscope. This structural characteristic contributes significantly to the nonlinear stress-strain relationship seen in ligaments and tendons. During small deformations, tendons and ligaments exhibit low stiffness as the crimps become uncrimped, this is referred to as the toe region on a stress-strain (or load–extension) curve (Figure 2-12). As the fibrils

become uncrimped, the collagen fibril itself becomes stretched increasing stiffness; this region is referred to as the linear region (Ker 2002; Silver 2003).

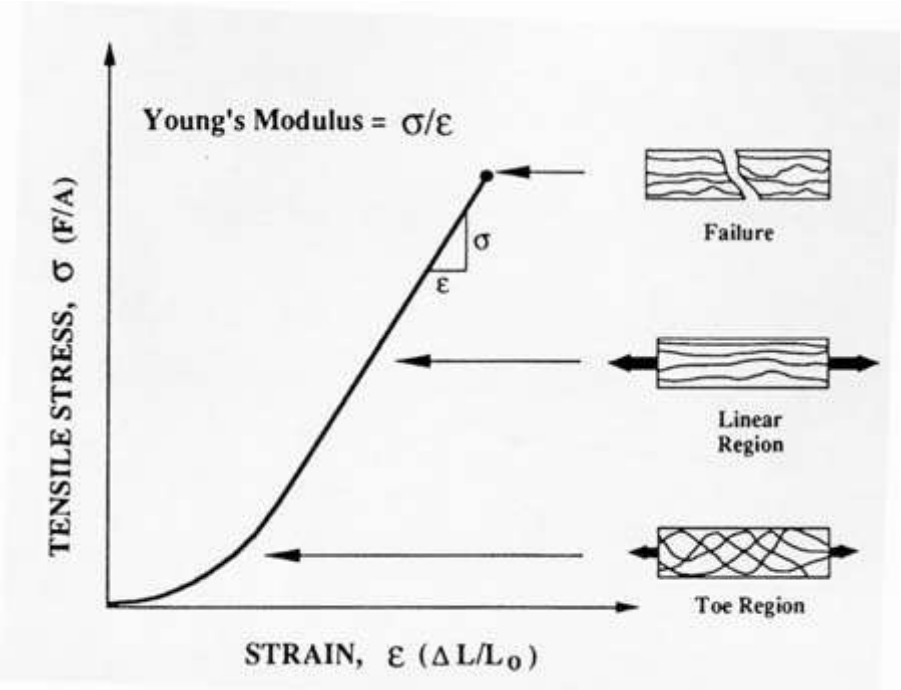

Figure 2-12. Stress-strain curve illustrating the toe and linear region for a ligament (Maffulli 2005).

2.1.4 Synovial fluid and the Capsule

The articular capsule is a bilayer structure which encapsulates a synovial joint. The outermost layer is white fibrous tissue; the inner layer is the synovial membrane which produces the synovial fluid. The role of the synovial fluid is to reduce friction during articulation of the joint, and to provide nourishment through diffusion to the chondrocytes within the cartilage (Brujan 2011). Synovial fluid composition is similar to interstitial fluid but with increased levels of hyaluronic acid and lubricin amongst others. Hyaluronic acid increases the viscosity of synovial fluid and provides lubrication at low loads, whereas under high loads it is the lubricin that is the primary component for lubrication. Synovial fluid also contains phagocytes which remove wear debris (Tortora J R 2002). Synovial fluid forms as a fluid film layer on the surface of the cartilage; this layer provides the two articulating surfaces with hydrodynamic lubrication. Some of the synovial fluid in a joint is contained within the

cartilage, which is extruded out under load, to maintain lubrication during loading (Tortora J R 2002). Synovial fluid is non-Newtonian, that is, its coefficient of viscosity increases proportional to applied shear forces. It is this non-Newtonian nature of synovial fluid which helps it to maintain lubrication during loading. The electrostatic attraction between the long chains of the hyaluronic acid gives synovial fluid its complex non-Newtonian properties (Marguerite 2008; Mathieu 2009).

2.1.5 Knee anatomy

The knee is formed of four bones: the femur, tibia, patella and fibula. In mice the tibia and fibula are fused distally (Bab 2007). Mice also possess two additional sesamoid bones: the lateral and medial fabella which are located caudally to the distal femur (Figure 2-13B). There are two types of ligaments found in both murine and human knees, the collateral and cruciate ligaments (Saunders 1933). The two collateral ligaments connect the femur to the tibia on the medial and lateral aspects of the knee. In mice the collateral ligaments exist as a thickened band on the capsule. Primary restraint to valgus and varus rotation is provided by the medial collateral ligament and the lateral collateral ligament respectively (Nielsen 1984). They also restrict axial displacement of the tibia in the distal direction.

There are two cruciate ligaments, the anterior cruciate ligament (ACL) and the posterior cruciate ligament (PCL) (Figure 2-13A). The ACL and PCL originate from within the femur intercondylar notch and attach to the tibial head. The ACL restrains the tibia from moving anteriorly in relation to the femur, and the PCL restrains in the posterior direction. Transection of the ACL results in increases instability in anterior drawer and internal/external rotation. The ACL also limits hyper extension (Furman 1976). Transection of the PCL results in increased posterior drawer and external rotation (Gill 2003).

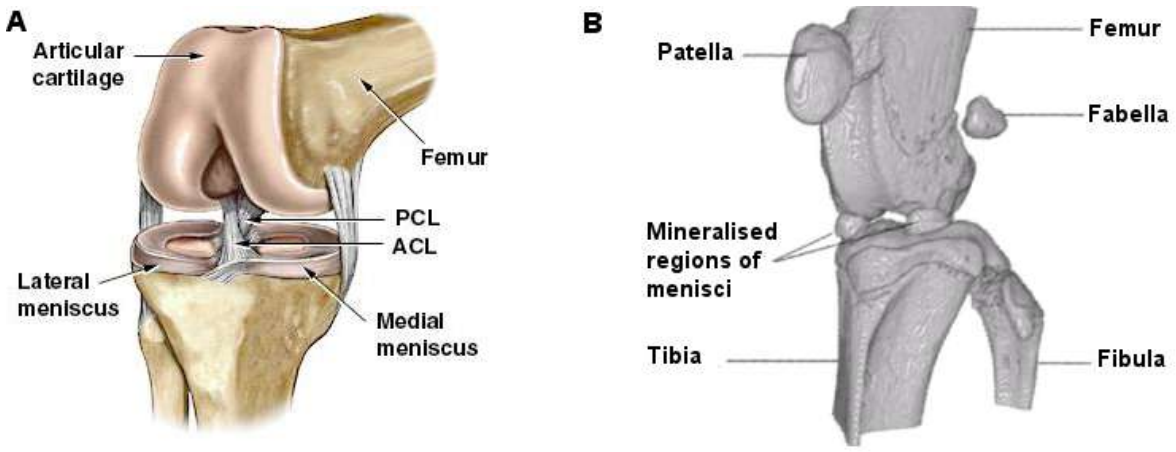

Figure 2-13. A) Ligamentous structures in the human knee (Media 1999-2011). B) Mineralised structures of the murine knee (3D reconstruction from micro-CT data obtained as part of experimental work in Chapter 3).

The menisci are fibrocartilage structures that partially separate the articular surfaces. The lateral and medial menisci are crescent shaped and are anchored to the tibial head at the anterior and posterior intercondylar fossa, which prevents the meniscus from being extruded under load. The function of the meniscus is to disperse peak contact force on the articular surfaces, helping to reduce cartilage tissue stresses. The menisci also play a role in proprioception and joint stability (Aagaard 1999). The menisci are wedge shaped in cross section. When loaded axially, stresses are transformed into circumferential hoop stresses. The circumferential arrangement of collagen fibres in the meniscus supports this hoop stress. The meniscus is composed of 72% water and 22% collagen (predominantly collagen type I), and the remainder is GAG (Messner 1998). In rodents and some other quadrupeds, the meniscus is partially mineralised, and is most likely related to the different biomechanics of quadrupeds (Ganey 1994; Kilts 2009). Meniscectomy in humans and canines increases varus-valgus rotation, but has no effect on anterior translation unless the ACL is also sectioned (Hsieh 1976; Oretorp 1978; Oretorp 1978; Levy 1982; Shoemaker 1986).

2.2 Osteoarthritis in the Clinic

The term arthritis refers to a group of conditions that damage the joints of the body. Osteoarthritis (OA) is the most prevalent form of arthritis. OA typically affects the larger weight-bearing joints such as the hip, knee and spine, but it can also affect the smaller joints such as those in the hands and feet (Buckwalter 1997). OA can occur rapidly but most forms will progress slowly over a number of years and it is possible for symptoms to stabilise or decrease. In the UK it is estimated that over 8.5 million people suffer from OA (Ge 2006), which costs an estimated £5.5 billion per year (Brown 2006).

2.2.1 Symptoms

The primary symptom of OA is persistent joint pain, resulting in loss of mobility and joint stiffness. The pain associated with OA is usually exacerbated by activity and therefore increases throughout the day, but decreases with inactivity. The joint can often exhibit crepitus (grating or crackling sensation within the joint) when moved. The patient may experience muscle spasms and tendon contractions. As the OA progresses the joint becomes enlarged, with effusion and abnormal bone growth taking place. In larger joints nodules of bone, called osteophytes may appear on the periarticular bone surface (Altman 1986). In smaller joints, such as the hand, cone growths called Heberden's and Bouchard's nodes appear in the distal and proximal interphalangeal joints; in the foot bunion formation can precede or accompany OA symptoms.

2.2.2 Primary and Secondary OA

Osteoarthritis can be divided into two categories, primary (idiopathic) and secondary (post-traumatic). Primary OA is the most common form and occurs in the absence of a known cause, typically in the middle aged and elderly (Buckwalter 1997; Nuki 1999). Secondary OA usually results

from an injury or insult to the joint. For example, 70% of patients who receive a meniscectomy or suffer a cruciate ligament injury develop secondary OA symptoms within 20 years (Nuki 1999). Secondary OA may also result from genetic, developmental, hereditary or metabolic factors. In the lower extremity it is estimated that the percentages of secondary OA of all OA cases are: 1.6% of the hip, 9.8% of the knee and 79.5% of the ankle(Brown 2006). Both types have very similar progression and end stage results.

2.2.3 Diagnosis

Osteoarthritis is usually diagnosed by a clinical examination then confirmed using radiographic techniques (Hunter 2006). A clinical assessment examines the range of motion, location of pain, muscle strength and ligament stability. Patients with advanced OA are often examined radiographically for joint space narrowing, osteophyte formation and altered subchondral bone. The subchondral bone changes are usually in the form of increased density (termed subchondral sclerosis[2]) and abnormal trabeculae structure. MRI can also be used in OA diagnosis and is helpful for distinguishing OA from other sources of knee pain.

2.2.4 Risk Factors of OA

Risk factors can be divided into systemic and local. Theories exist that suggest systemic factors increase a patient's vulnerability to cartilage damage, injury or limit repair. Whereas it is the local biomechanical factors that cause the degeneration of the joint. Examples of systemic and local factors are given below (Felson 1998a):

[2] Sclerosis is the hardening of tissue, in bone it specifically refers to an increase of bone density (osteosclerosis) and appears as a bright band on radiographs.

Systemic Risk Factors:

Ageing: Studies in the US suggest that 6% of over 30s and 33% of the population over 60 years have symptomatic OA (Felson 1998a). Osteoarthritis is prevalent in the elderly but OA is not caused by ageing alone. Rather, ageing causes failure of the protective mechanisms within a joint, such as decreased chondrocytic response to growth factors, which reduces the reparative capacity of an aged joint. An increase of ligament laxity can occur with age, reducing joint stability and increasing likelihood of injury (Sharma 2004). Gradual decrease in strength and slowing of neurological responses also occurs with age, and both play a role in the protection of a joint (Sharma 1997). In addition, the chondrocyte increases apoptosis and decreases its mitotic and synthetic activity with age, resulting in a decreased ability to maintain cartilage matrix (Martin 2002; Robertson 2006).

Gender: There is a higher incidence of OA in men under 50 years old than in women, but in those over 50 years old, women have a higher incidence (Felson 1998a). The reason for this remains undetermined. There is no clear relationship between female hormone loss and OA, neither is there a relationship between estrogen replacement therapy and OA (Felson 1998b). Early onset of OA in males is frequently attributed to secondary factors, such as knee injury in sports. Whereas the prevalence of OA increases in women after menopause (Nadkar 1999), with evidence suggesting that hormone replacement therapy has a chondroprotective effect (Hannan 1990).

Genetics: There is evidence to suggest that a genetic predisposition to OA exists. Early familial aggregation studies have suggested that inherited factors can increase the incidence of OA in first degree relatives (Kellgren 1963). Twin pair studies have also indicated a heritable component to OA, studies using mono- and dizygotic twin pairs have found that prevalence and progression of OA was higher in the monozygotic pairs, suggesting a genetic effect on OA (MacGregor 2000; Zhai 2007). It is difficult to assess the precise contribution of genetics to OA pathogenesis, as there is a range of possible genes involved in OA, and these may have a combined effect (Valdes 2008b), but various studies have been performed to identify candidate genes that may explain the inheritability of OA.

Genetic association studies (GWAS) aim to quantify the effect that different gene variants have on the incidence of OA. These studies have raised a number of candidate genes, in general many of the genes implicated can be categorised as belonging to the following family of molecules or pathways, that is: Inflammation, ECM molecules, bone morphogenic proteins, proteases and those involved modulating osteocyte and chondrocyte behaviour. Two heavily implicated genes are *FRZP* and *GDF5*, the former encodes for a transmembrane receptor involved in Wnt signalling, a pathway that has been demonstrated to be involved in OA (Enomoto-Iwamoto 2002; Lories 2007). The latter, *GDF5*, encodes for a bone morphogenic protein (BMP), BMPs mediate a number of cellular responses in the cells of bone and cartilage. Further investigations of these two genes have confirmed their involvement in OA, for example, GDF5 murine knockout models induced OA in mice (Masuya 2007)and FRZP knockouts exhibited an increased cartilage loss in an instability model (Lories 2007).

Genome wide association studies investigate the whole genome for gene-variants associated with a disease, they are capable of identifying haplotypes associated with large groups of individuals afflicted with a particular disease. For OA, GWAS has been used in a number of studies to highlight associated genes. As a result of these studies a number of candidate gene variants have been identified, including genes encoding for COX-2 (Valdes 2008a), GDF5, DIO-2 (Loughlin 2010), genes on the 7q22 loci (Kerkhof 2010) and CALM 1 (Mototani 2005). The latter is an example of a gene variant identified with GWAS which, with further investigation, has been shown to be less involved in OA (Loughlin 2006). So far GWAS has not yet identified a single large genetic effect in OA, but instead suggested that carrying a predisposing genetic variant increases the risk of OA (Valdes 2009).

Local Biomechanical Factors:

Joint Injury or Surgery: Osteoarthritis can develop in a joint affected by trauma. Animal models of OA utilise damage to structures of a joint to initiate OA and will be discussed in section 2.2.3. In humans, ACL and meniscal ligament injury are strongly associated with OA (Nuki 1999).

Muscular weakness: Deterioration of muscle function may also be a risk factor for osteoarthritis (Slemenda 1997).The quadriceps provide anterior-posterior stability to the knee. OA patients often exhibit quadriceps weakness, normally attributed to disuse atrophy. The quadriceps reduce impulsive loading of the knee by providing a braking function prior to heel strike.

Neuromuscular control and proprioception: Patients with unilateral knee arthritis exhibit a bilateral impairment of proprioception, raising the possibility that the impairment is not a result of the OA, but a cause (Sharma 1997). Coordination of the musculature is necessary for reducing instability in the joint and for reducing peak force during gait. For example, normal patients have a five-fold increase of load magnitude after a femoral nerve block (Jefferson 1990; Radin 1991). This indicates that lack of neuromuscular control may increase tissue loading and initiate degeneration.

Developmental abnormalities: Misshapen joints increase local contact stresses between articulating surfaces. Developmental disorders include slipped capital femoral epiphysis (a separation of the femoral head at the growth plate), developmental hip dysplasia (malformed acetabulum results in hip dislocation at birth) and Legg-Perthes disease (idiopathic adolescent avascular osteonecrosis of femoral head) (Harris 1986; Wedge 1991). Malalignment of knee joints predisposes to OA (Sharma 2001) presumably through increased contact stresses. Excessive varus and valgus alignment results in OA progression of the medial and lateral compartments respectively.

Obesity increases the risk of developing OA and the risk of OA progressing. Obesity has been identified as one of the most important factors in the progression of OA, especially in the knee (Dougados 1992; Manninen 1996; Sharma 2000). Increased physical strain on the joints due to injury may not fully explain the association between OA and obesity. Due to the increased incidence of hand OA with obesity, it is likely that metabolic factors are also present. For example, adipocytes may be involved in the regulation of bone and cartilage cells, leptin a hormone produced in such cells is implicated in the initiation and progression of OA (Dumond 2003).

2.2.5 Disease Progression in OA

The first histological change to be observed in OA is the fraying and fibrillation of the superficial layer of articular cartilage. As OA progresses fibrillation turns into clefts which extend deeper into the cartilage and roughening of the articular surface increases. As clefts grow, the tops of the superficial cartilage fibrillations begin to break, releasing fragments into the joint. Eventually degradation erodes the articular cartilage leaving only thickened and possibly necrotic bone. Loss of articular cartilage causes the symptoms of OA, which include joint pain and loss of motion. Cartilage loss in primary OA is more prevalent in those of increasing age, possibly because of the reduced chondrocyte anabolic capacity associated with age, which diminishes the tissue's ability to maintain itself (Buckwalter 1997). Cartilage-like tissue is formed at the periosteum-synovium junction, which gradually ossifies through endochondral ossification to form an osteophyte (Blom 2004). Osteophytes are considered to contribute to pain and loss of motion. It is thought that osteophytes may be a repair mechanism to stabilise the joint (Pottenger 1990), a product of increased metabolism in the surrounding tissues (van Beuningen 1998), or a result of altered loading in the region. Inflammation can occur in osteoarthritis but its severity is often mild in comparison to rheumatoid arthritis. Historically, OA is termed a non-inflammatory disease because of the comparatively low leukocyte count found in the synovial fluid of OA affected joints. One feature of osteoarthritis is the increased production of pro-inflammatory mediators; such mediators have been found to increase the progression of osteoarthritis. Of the many pathways that are activated in the tissues of an osteoarthritic joint, a number are associated with inflammation, for example IL-1 and TNF-(α) signalling. Major functions of these cytokines are to induce catabolic processes, inhibit matrix production and induce cell apoptosis (Pelletier 2001). Other inflammatory mediators of interest to the pathogenesis of OA include NO, prostaglandin E_2 and COX-2 (Amin 1995; Amin 1997).

2.2.6 Current Treatments

Surgical

Osteotomy is the surgical procedure whereby the bone is cut or shortened to alter its alignment or length. Usually in arthritic joints the aim is to alter the alignment of the joint in such a way that the patient redistributes body weight off the damaged cartilage. Biopsies from the femoral condyle of an osteotomised knee have shown the formation of new fibrocartilage over exposed bone. Clinical outcomes are mixed and the result declines over time (Buckwalter 1994; Ge 2006).

Muscle Release is the surgical severing of specific muscles that act on an arthritic joint in order reduce the loading experienced by the joint, and transfer load from an area of damaged cartilage and onto a healthy region. Muscle release has been shown in studies to increase joint space width and reduce pain. However, it weakens the joint and limits the options for total joint replacement.

Lavage (rinsing of the joint) and debridement (the removal of loose fragments of cartilage and menisci by shaving the degenerated articular structures) was originally shown to be a promising treatment for osteoarthritis (Harwin 1999), but subsequent studies have convincingly demonstrated that arthroscopic treatments are not effective at treating osteoarthritis (Moseley 2002; Kirkley 2008; Laupattarakasem 2008).

Microfracture of subchondral bone stimulates formation of fibrocartilage on regions where bone is exposed due to cartilage loss. This process can be induced by drilling, abrasion or piercing of the subchondral bone. Penetrating the subchondral bone disrupts the underlying blood vessels causing the formation of a fibrin clot. If this clot is not severely loaded then it can be replaced with repair tissue, which may range from hyaline cartilage to dense fibrous tissue (Frisbie 1999; Hunt 2002). Formation of a fibrocartilage repair surface does not automatically decrease symptoms. Examination shows that compared to normal cartilage it is lacking in structure, mechanical properties and durability. Its failure to absorb loads may result in persistence of symptoms and continued degeneration (Bae 2006). Additionally this procedure requires extensive healing of the soft tissues

(Steadman 2003; Kreuz 2006). This technique is better suited to isolated full thickness lesions and is rarely used as a treatment for osteoarthritis.

Resection arthroplasty is the removal of articular surfaces and some underlying bone. The space between the bones fills with a fibrin clot followed by granulation tissue. If resection arthroplasty can be combined with passive joint motion the granulation tissue can be replaced with fibrocartilage. Resection arthroplasty removes tissue from the articulating surfaces reducing the stability of the joint (Buckwalter 1994).

The treatment options for end-stage OA are arthrodesis or endoprosthesis. Endoprosthesis is the replacement of the articular joint with an internal artificial prosthesis. Arthrodesis is artificial fusing of a joint, performed to relieve pain that cannot be managed, often performed after a failed arthroplasty.

Pharmacological

Non-steroidal anti-inflammatory drugs (NSAIDs) and paracetamol are the main pharmacological treatment for OA. NSAIDS are able to relieve pain and increase mobility in approximately 60% of OA cases (Watson 2006). Paracetamol is frequently administered as an analgesic and is often preferred over NSAIDs as they are less likely to produce adverse gastrointestinal affects (Towheed 2006). Chondroitin and glucosamine have also been used to treat OA and appear to increase proteoglycan production, but their effect is modest. For patients with local inflammation, intra articular steroids can be administered for short term restoration of function (Ge 2006; Hunter 2006). For some time pharmacological treatments have been moving away from therapies that target the symptoms of OA towards strategies for halting or reducing the progression of the disease, for example, by developing an inhibitor for IL-1β (e.g. Diacerein). Other examples pharmacological strategies include targeting the suppression of bone turnover, catabolic enzyme production or synovial inflammation (Martel-Pelletier 2011).

Physical Therapy

Physical therapy is often the first treatment for mild and moderate OA. Weight loss, exercise to increase muscle strength, stretching and joint mobilisation can also be implemented. Braces and orthotics can be used to treat instability or joint misalignment (Hunter 2006).

Transplantation and grafting

Tissue grafting between debrided or resected articular surfaces introduces a new population of cells and matrix to the damaged tissue. Often the grafted tissue can be fascia, muscle, tendon, periosteum or perichondrium. Cartilage and meniscal grafts have the benefit that their composition closely resembles the material which they are replacing, the inter condylar notch is often a source of cartilage for autografts. Osteochondral allografts have greater availability and their incorporation into the host tissue has been demonstrated (Buckwalter 1994; Ge 2006). Typically these treatments are applied to osteochondral defects, and are not usually applied to those over the age of 50, or those with advanced OA (Gomoll 2011). A number tissue engineered scaffolds to replace matrix in cartilage defects are also under development (Gomoll 2011).

2.3 Animal models of OA

The development of osteoarthritis in humans is difficult to study. The pathological changes can take several decades to develop in humans. It is very rare to see early stage OA, as patients usually present themselves for diagnosis when pain occurs with moderate to severe OA. Diagnostic methods can only visualise tissue changes when joint space narrowing occurs, more sensitive methods such as histology are too invasive. The progression of human OA is also highly variable, due to a broad range of genetic and environmental differences, including lifestyle, nutrition, occupation and hormones (Felson 2004b).

OA animal models have been developed to study OA pathology and investigate therapeutic treatments. Animal models allow the study of tissues over time; which is important in a disease such as OA. They allow more invasive techniques to be employed, which facilitate the investigation of microstructural and biochemical changes. Animal models are also used to investigate and demonstrate how interventions may prevent or reduce OA (Bendele 2001; Ameye 2006).

It is essential that an OA animal model mimics the characteristics of the human disease. OA by definition involves a heterogeneous set of changes affecting the tissues of a synovial joint. Therefore it is difficult for an OA animal model to directly mimic human OA when the disease itself is varied. For example, humans with traumatic injury unweight the affected limb until it has restabilised. Most animals, including rodents and canines do not. As with primary and secondary OA in humans, animal OA models can be categorised into either spontaneously occurring or experimentally induced ones.

2.3.1 Spontaneously occurring OA models

Dunkin Hartley guinea pigs

DH guinea pigs are frequently used as spontaneous OA models. OA develops more quickly in male guinea pigs possibly due to a greater body weight. Lesions appear bilaterally on the medial tibial plateau at approximately three months of age in 50% of animals (Bendele 2001). At this time PG loss and chondrocyte death are present but subchondral bone and meniscal changes are not. At six months 90% of animals exhibit bilateral medial tibial lesions, small osteophytes and altered proteoglycan synthesis. At nine months, mild to moderate cartilage damage on the tibia and femur and sclerosis of the subchondral bone is apparent. At one year fibrillation extends into the deep zone of cartilage, subchondral sclerosis is extensive, and bone cysts and meniscal degeneration are present (Bendele 2001).

Prevalence of OA in the DH guinea pig is attributed to knee laxity (Quasnichka 2006). An increased toe region of the cruciate ligament on a force-extension curve was found in the DH guinea pig, when compared to a control strain. The toe region represents the normal physiological range of ligament strain (Figure 2-12), it is a function of the tertiary structure of the collagen in the tissue, and is less sensitive to ligament cross section area. An increase in the toe region is more likely to be caused by a change in the ligament matrix rather than shape. There is increased collagen turnover in the DH guinea pig compared to the control strain, which probably accounts for the increased cruciate laxity (Quasnichka 2005; Quasnichka 2006).

Mice

BALB/c, C57Bl/6 and STR/Ort mice have been studied as spontaneous OA models (Silberberg 1964; Walton 1977). C57Bl/6 develop ultra-structural abnormalities in the superficial cartilage of the femur and patella from the age of two months (Stanescu 1993). Collagen degradation is evident on the lateral plateau of the tibia after one year in the C57Bl/6. Similarly the BALB/c mouse also develops cartilage lesions on the medial plateau after one year (Stoop 1999). The STR/Ort mouse develops mild histopathological lesions in one or both knees at ten weeks of age. At twenty weeks lesions are present in most animals. Cartilage damage typically appears on the medial tibial plateau. Timing of OA onset is variable between STR/Ort mice (Mason 2001). One study of the cruciate ligament of STR/Ort mice found high levels of MMP-2 indicating an upregulation of collagen metabolism and a decrease of mechanical strength in the ligament when compared to a control strain (Anderson-MacKenzie 1999). These changes took place before any radiographic signs of OA, suggesting that like the DH guinea pig, cruciate laxity could be the cause of spontaneous OA (Anderson-MacKenzie 1999). The STR/Ort mouse also grows at a faster rate and to a greater body mass than other strains. Furthermore, STR/Ort mice first develop histological changes on the patella femoral joint, attributed to internal tibial torsion and medial patellar dislocation inherent in the strain (Naruse 2009).

Macaques

Spontaneous OA has been observed in the knee joints of macaques (Carlson 1996). Management, cost, emotional attachment and ethical controversy mean that this model is rarely used, despite its genetic similarity to humans (Little 2008).

2.3.2 Experimentally Induced OA Models

Destabilisation

Surgical destabilisation models are widely used in OA research. They involve simple procedures, are reproducible, and have a known initiation time. Two such models are the ACL transection (Pond 1973) and meniscectomy models (Moskowitz 1973). These were used originally in dogs and rabbits, but they have been used in a variety of animals since. Instability models work by redistributing loads on the articular surfaces. When a joint is immobilised immediately after destabilisation the joint is protected from degeneration (Palmoski 1980; Palmoski 1982). Models of this form typically produce an inflammatory response and attempted joint repair through increased chondrocyte metabolism (Colombo 1983). The cartilage in these models continues eroding and subchondral bone changes occur (Brandt 1991). Instability models on small animals (mice and rats) allow large numbers to be used and are useful for investigating pharmacological treatments for OA (Shimizu 2007), genetic studies can also be implemented in mice. Larger animals allow long term changes to be studied with non invasive methods (Dedrick 1993) and have a larger volume of cartilage so biochemical analysis of synovial fluid and cartilage can be performed (Ehrlich 1975). Most animals resume weight bearing immediately after trauma, whereas humans reduce weight bearing until some degree of restabilisation has occurred. This means animal destabilisation models accelerate the progression of OA in comparison. The permanent trigger (surgical trauma) reduces the efficacy of therapeutic intervention.

The work performed and described in this thesis used a mouse model of joint destabilisation. The model utilised surgical destabilisation of the medial meniscus (DMM) to induce degenerative changes. The DMM model is discussed in detail in Chapter 4 of the thesis.

Trauma

Direct defects can be introduced directly onto the articulating surfaces of a joint. These defects then initiate joint degeneration. One such model is the groove model of OA, performed in canine knee (stifle) joints and ovine metacarpophalangeal joints, in which a groove less than 0.5 mm deep is cut into the cartilage of a joint using a Kirschner wire. The model can be applied uni- or bi- laterally and is usually followed by loading from enforced exercise. Trauma models produce slow progression of cartilage degeneration and osteophyte formation with subchondral bone changes (Marijnissen 2002a; Intema 2008; Mastbergen 2008).

Biomechanical

Mechanical loading is able to alter articular cartilage structure, which is evident as strenuous physical activity and occupations that apply high joint loads are risk factors for OA. Displaced load models induce degenerative joint changes by redistributing load across the joint without affecting joint stability. Examples of these include osteotomy, overload and immobilisation. Tibial osteotomy typically produces milder lesions than destabilisation models (Panula 1997).

Cartilage damage and bone remodelling occur with excessive or repetitive compressive loading across the joint (Poulet; Dekel 1978; Radin 1978). These models have the advantage that the frequency and magnitude of load can be controlled or removed completely. Exercise and overuse models also share this same benefit, where animals are subject to treadmill exercises, exercise on

hard surfaces or forced jumping. The overuse induces osteoarthritic changes (Brown 1984; Lapvetelainen 1995).

Joint immobilisation can induce cartilage degradation and osteopenia. Immobilisation can be performed either by cast, external fixator or by unweighting (tail suspension) (Videman 1982; Säämänen 1990; O'Connor 1997; Leroux 2001). The effects can be limited or reversed by remobilisation (Säämänen 1990).

Chemical

OA can be induced by intra-articular injection of biological agents, such as collagenase, papain and growth factors. Collagenase works by degrading ligaments and introducing instability into the joints (van der Kraan 1990). Papain is an enzyme which degrades cartilage, growth factors induce degeneration by altering metabolic processes (van Beuningen 2000). Many of the models induce local inflammation. These models are easy to induce; however, they may not be entirely relevant for modelling human OA. For example, agents that degrade aspects of the joint such as papain (Havdrup 1977; Karadam 2005) or collagenase (Botter 2008) induce degradation on certain tissue matrix components by proteolysis, which is not seen in human OA. The processes seen in inflammatory models do not replicate the sequence of degradation seen in human OA (Little 2008).

2.4 Pathophysiology of OA

During the progression of OA, cartilage undergoes a series of changes that alter its molecular composition and structure. As OA progresses these changes result in a loss of mechanical properties which then result in damage to the surface of cartilage. The changes seen in the cartilage matrix are reflected by changes in the chondrocyte. The chondrocyte exhibits increased proliferation and an upregulation of matrix components. This is followed by an increase in catabolic enzymes, whereby

production of proteinases results in degradation of proteoglycans and collagen in the cartilage extracellular matrix. (Goldring 2010).

The initial loss of the proteoglycan aggrecan precedes the degradation of the collagen network. Degradation of aggrecan reduces its aggregation and chain length, adversely affecting the compressive stiffness of the cartilage. Damage to the collagen tissue network then results in a loss of tensile properties of cartilage. These changes increase the matrix permeability, causing a decrease of matrix stiffness and an increase of water content. This reduces the ability of the matrix to withstand mechanical load (Goldring 2010). An increase of water content is also attributed to damage on the collagen network which reduces restraint on osmotic forces (Venn 1997)

Aggrecanases are the principal proteases attributed to the cleavage of aggrecan, in particular ADAMTS-4 and ADAMTS-5, which are members of the ADAMTS (A Disintegrin And Metalloproteinase with ThromboSpondin motifs) family. Genetic knockout studies of ADAMTS-5 demonstrated decreased severity of OA and demonstrated protection against aggrecan degradation, suggesting that ADAMTS-5 is an important enzyme for aggrecan degradation (Glasson 2005; Ilic 2007; Majumdar 2007). A knock-in model was generated, whereby aggrecan expression was altered such that ADAMTS-5 was blocked from cleaving it by a specific site. This resulted in a reduction of cartilage loss and a potential increase of cartilage repair (Little 2007). However, a knockout model of ADAMTS-4 had no effect on the progression of surgically induced OA (Glasson 2004).

Collagen has been shown to be degraded by MMP-1, MMP-8, MMP-13 and MMP-14 (Billinghurst 1997; Imai 1997), the expression of which, significantly increases in the superficial zone of OA cartilage (Tetlow 2001). Elevated levels of MMPs are found in synovial fluid and in OA damaged cartilage. MMP-13 is potentially the most significant due to its specificity toward collagen type II (Knäuper 1996). A number of inhibitor studies have demonstrated that collagenase MMP-13 plays a significant role in OA (Piecha 2010).

The early stages of OA are believed to involve inflammation in the synovium, suggesting inflammatory factors are mediators that affect metabolism of the bone and cartilage right from the early stages of OA (Ayral 2005). IL-1β and TNF are key proinflammatory cytokines in the pathophysiology of OA. IL-1β is heavily associated with degradation of cartilage, elevated levels are seen in osteoarthritic bone and cartilage, as well as the synovial membrane and synovial fluid. It is believed IL-1β reduces production of aggrecan and collagen type II (Chadjichristos 2003), whilst stimulating the release of MMPs (-1, -3 and -13), and inducing the expression of IL-6 and various chemokines. The role of IL-1β in OA is complex, despite its catabolic effects on the chondrocyte and upregulation of MMPs, knockout studies actually demonstrate an increase of OA progression (Clements 2003). TNF is heavily involved in stimulating systemic inflammation, its over expression is seen in the same osteoarthritic tissues as IL-1β, and its effect on osteoarthritic tissues is heavily linked to IL-1β (Saklatvala 1986). For example, studies in animal models have demonstrated that both cytokines have a greater osteoarthritic inducing effect when combined, than when either are administered separately (Henderson 1989).

IL-1β and TNF are thought to increase OA progression by stimulating the production or release of other species which are also involved in OA degradation. Examples of these species are IL-6, IL-8, inducible nitric oxide synthase (iNOS), CC-chemokine ligand 5, cyclooxygenase 2 (COX-2), prosta-glandin E_2 (PGE_2) and nitric oxide (NO) (Lotz 1992; Alaaeddine 2001; Kapoor 2011). The last two, (NO and PGE_2) are known to promote production of MMPS, reduce proteoglycan and collagen synthesis and promote chondrocyte apoptosis.

IL-1β and TNF are known to stimulate the increased production of IL-6. The role of IL-6 is unclear, IL-6 knockout mice have a decreased PG synthesis and an increased incidence and severity of spontaneous OA, suggesting IL-6 has a protective role (de Hooge 2005). Whereas IL-6 injected into osteoarthritic mice knee joints reduced cartilage damage (Van de Loo 1997).

IL-17 is another proinflammatory cytokine potentially involved in OA pathophysiology, it is potentially secreted by $CD4^+$ cells (mature T helper cells of the innate immune system), but it is unclear if this occurs in OA (Kapoor 2011). IL-17 stimulates chondrocytes to produce IL-1β, TNF, IL-6, NO, and MMPs (Benderdour 2002; Pacquelet 2002).

Inhibitory cytokines include IL-4, IL-10 and IL-13, as they decrease the activities of proinflammatory cytokines. Their effects have only been demonstrated in-vivo, where IL-4 and IL-10 demonstrated a chondroprotective effect (Joosten 1997). Insulin-like growth factor 1 (IGF-1) and transforming growth factor β (TGF-β) are potentially involved in the cartilage repair process. They may act to regulate chondrocyte gene expression (van den Berg 1999). Various fibroblast growth factors may interact with these cytokines to promote certain chondrocyte functions

2.4.1 Chondrocyte Response to Mechanical Loading

Homeostasis is necessary for healthy articular cartilage; synthesis and degradation however, need to be balanced to prevent degradation. Mechanical loading and physiological processes combine to mediate cartilage homeostasis (O'Hara 1990). Two types of cartilage loading identified in mathematical models result from everyday usage of an articular joint. These are shear stress and hydrostatic stress (Carter 1988; Eckstein 2005). Different physical activities or injury will affect the ratio of hydrostatic to shear stress experienced by cartilage ECM. In vitro studies suggest that two different types of stress have different effects on chondrocyte metabolism. Shear stress increases expression of pro-inflammatory mediators and decreases gene expression of matrix macromolecules (Mohtai 1996; Lee 2002; Lee 2003a; Lee 2003b). Hydrostatic stress enhances expression of matrix macromolecules and inhibits pro inflammatory mediators (Smith 1996; Smith 2000; Trindade 2004). Risk factors for OA such as increased loading or joint laxity may affect the distribution, magnitude and proportion of shear and hydrostatic stress in favour of shear. Exposure to elevated levels of

shear stress is likely to result in increased inflammation, increased enzymatic matrix degradation and decreased matrix production.

2.4.2 Bone Changes in Osteoarthritis

Bone Changes in Studies on Human OA

It is well known that in addition to cartilage degradation, bone changes occur in human OA. In OA of both the hand and larger joints, advancement and thickening the tidemark is usually observed (Goldring 2009) . The subchondral bone undergoes thickening and the trabeculae coalesce to form thick trabeculae (Havdrup 1976; Ding 2003; Goldring 2009). Sclerosis of the bone varies with the extent of damage to the overlying cartilage, severe sclerosis is seen where cartilage is very thin. Where the bone has become denuded bone tissue contains necrotic osteocytes. Osteophytes also appear on the periphery of articular cartilage. Osteophyte formation is driven by progenitor cells in the synovium or periosteal tissue (Aigner 1995; Blom 2004). Osteophyte formation occurs in non-weight bearing areas of a joint, their role in providing mechanical stability or increasing surface contact area is frequently proposed, but also questioned by some. It is possible they are a by-product of increased metabolism that occurs in OA. Transforming growth factor-beta (TNF-β), a protein known to stimulate PG production in chondrocytes, when injected into murine knee joints resulted in osteophyte formation (van Beuningen 1994). Murine injection of BMP2 achieved a similar effect on osteophyte formation (van Beuningen 1998).

Most studies investigating human OA use samples from the end stage of the disease, where the bone is removed prior to joint arthroplasty. Some studies, however, have used bone from donors with early stage OA, which can provide clues as to timing of changes in the tissue. Studies of early stage OA suggest that there is an initial thickening of the subchondral epiphyseal trabeculae and subchondral bone plate (Radin 1972; Ding 2003) and an increase of bone turn over and bone mineral density (Dieppe 1993; Dequeker 1997; Bailey 2004). Despite thickening and increased bone mineral

density, osteoarthritic subchondral bone has reduced mechanical properties (Ding 2003; McErlain 2008), due to hypomineralisation (Bailey 2004). A number of studies have reported that the presence of bone marrow lesions in epiphyseal bone on MRI scans can predict regions of cartilage loss (Felson 2003; Hunter 2006; Roemer 2009). This localised resorption of epiphyseal bone in early human OA may be analogous to early stage bone resorption seen in various animal models of OA (Layton 1988; Dedrick 1993; Hayami 2006; Intema 2010).

Increased bone formation continues with the progression of OA into the late stage. Bone formation occurs in both the epiphyseal bone and subchondral plate (Grynpas 1991; Bobinac 2003; Chappard 2006). In end stage OA the reduced material properties are still present (Li 1997a; Li 1997b; Yamada 2002).

Not all studies of human OA show a uniform increase of subchondral epiphyseal bone. One study using MRI to investigate epiphyseal trabecular bone of the femur and tibia found a loss of trabecular bone occurs between mild and severe OA groups (Beuf 2002). Other MRI studies have been performed on early and severe OA patients, which were categorised by radiographic and clinical assessment. Medial cartilage loss was associated with increased epiphyseal bone volume fraction in the medial compartment. At the same time the epiphyseal bone in the lateral compartment decreased, possibly caused by mal-alignment due to cartilage damage in the medial plateau, which may cause lateral unweighting (Lindsey 2004).

Bone Changes in Animal Models of OA

Animals offer a greater scope for assessing longitudinal bone changes, as invasive methods are available. Animal models also benefit from an identifiable cause (the induction method) and known time point of disease initiation. Despite the large number of review articles discussing subchondral changes there are few experimental papers that feature longitudinal experimental studies observing bone changes. In general the existing temporal studies use either spontaneous models with the DH

guinea pig, or various ACLT models on the dog or rat. There appears to be a disparity of outcomes of subchondral bone changes on animal OA models.

One key criterion of OA models is that their pathologic changes mimic the human form of OA under investigation. If different animal models produce different subchondral bone responses then these responses should be investigated to determine their suitability as models. Furthermore, much could be learned about OA initiation and progression by investigating the factors that produce these different responses.

2.4.3 The Role of Bone in Osteoarthritis

The role of bone in the initiation and progression of OA has been the focus of much debate. Bone undoubtedly plays a role in OA, evident from the gross morphological changes that occur in the disease, but its role as an initiator is not widely accepted.

There is certainly evidence that bone changes occur early in OA, and that thickening of the subchondral plate occurs before radiographic joint space narrowing in humans (Buckland Wright 2004). In guinea pigs, MRI has been used to demonstrate that thickening of subchondral bone precedes cartilage degeneration assessed by MRI joint space narrowing (Watson 1996; Watson 1996). Joint space narrowing is typical of mid-late stage OA, but there is evidence that bone changes can occur before any such irreversible cartilage changes. Quasnichka et al investigated OA in DH guinea pigs and noted that an increased bone density in the subchondral and epiphyseal regions occurred concomitantly with the first signs of cartilage pathology at 24 weeks. The irreversible cartilage damage such as fibrillation occurred much later at 40 weeks (irreversible cartilage damage is a pathognomonic sign of OA whereas reversible cartilage damage is not). In the DH strain it has been shown that MMP-2 and collagenase levels are elevated in the bone even earlier (at 16 and 20 weeks), compared to the control strain (Anderson-MacKenzie 2005). This suggests that elevated bone turnover actually occurs four to eight weeks before any histological cartilage changes; this

biochemical change may drive the bone morphology changes. There are further studies in which bone changes have been observed before cartilage changes (Carlson 1996; Newberry 1997; Saied 1997). Other studies argue that cartilage degradation precedes bone change (Brandt 1991; Dedrick 1993; Yamada 2002). Bone changes occurring before cartilage does not necessarily implicate bone as an initiator of OA, but it does suggest the possibility. Botter et al. (Botter 2009) investigated subchondral bone changes in ADAMTS-5 knockout mice with DMM surgery. The knockout mice exhibited significantly less bone remodelling compared to wild type mice, suggesting a link between bone and cartilage damage and subchondral bone changes. There are a number of proposed mechanisms by which bone may initiate cartilage damage. These include: 1) biochemical cross-talk between the bone and cartilage, 2) advancement of calcified cartilage and tidemark and 3) changing of the mechanical properties of bone, which alters stresses in the cartilage.

Biochemical Signals between Bone and Cartilage

Bone and cartilage have been described as a functional unit in OA, capable of 'cross-talk' by permitting the perfusion of biochemical signals between the two tissues (Lajeunesse 2003). It is likely that the relationship between bone and cartilage is disrupted by an imbalance in the tissues, preventing normal maintenance (Goldring 2010). Biological agents such as cytokines and growth factors produced in the subchondral bone can pass through the calcified cartilage and induce a negative response in the chondrocytes. Work by Mori et al. and Sokoloff et al. (Sokoloff 1993; Mori 1993a) identified channels and cracks in the bone and calcified cartilage; vascular channels extending in the calcified cartilage have also been identified (Clark 1990). Hepatocyte growth factor (HGF) is a possible agent, found in the deep layers of OA cartilage, but only produced by osteoblasts. Osteoblasts from osteoarthritic bone have been shown to exhibit higher than normal HGF production (Lajeunesse 2003). HGF causes the production of collagenase-3 in chondrocytes which are involved in cartilage degradation. Osteoblasts also produce osteoblast stimulating factor I,

derived from vitamin A which stimulates cartilage degradation (Kubo 2002). IGFs are important growth factors for regulating bone metabolism (Hock 1988): IGF-1 inhibits bone MMPs, increased IGF-1 levels found in OA subchondral bone may increase bone remodelling. TGF-β1 production is increased in osteoblasts from OA tissue. TGF-β is involved in matrix turn over; it stimulates the synthesis of bone matrix and increases collagenase activity (Palcy 1999), both TGF-β and IGF-1 have a catabolic effect on the chondrocyte. Prostaglandin E_2 (Masuko-Hongo 2004), IL-6 (Sanchez 2008), and oncostatin M (Sanchez 2004) have also been suggested as possible molecules involved in cross talk between the tissues.

Recent studies have demonstrated that the regulation of bone and cartilage formation by the Wnt pathway may be an important factor contributing to the pathogenesis of OA, as increased signalling through the Wnt pathway has been implicated in increased cartilage damage and increased bone density (Lories 2007). In particular there is evidence to suggest that WNT signalling may be responsible for regulating the interactions that occur between the cartilage and bone in the development of OA (Lories 2007).

The Wnt signalling proteins constitute a large family of signalling proteins that bind to cell surface receptor proteins of the Frizzled family (Fzd). Four downstream cascades have been identified to be activated by binding of Wnt, these pathways have been shown to regulate osteogenesis through various mechanisms; although the Wnt/β-catenin pathway is of particular importance to osteoarthritis (Hoang 1996). A number of antagonists to the Wnt/β-catenin pathway have been identified, one such molecule is FRZB, which competitively binds to the cell surface receptor protein Frizzled in place of Wnt. One study investigating the effect of FRZB knockdown in a murine OA model observed increased cartilage damage compared to wild type mice (Lories 2007). The increase in cartilage damage observed was associated with an increase in Wnt signalling via the Wnt/β-catenin pathway, due to loss of the inhibitory antagonistic FRZB signal. An increase was also observed in the expression of the tissue destructive enzyme, matrix metalloproteinase 3 (MMP3), as FRZB directly

inhibits MMP3 expression. Alongside the changes observed in the cartilage of FRZB knockout mice, alterations were also observed to take place in the structure of the bone including an increase in the cortical thickness, bone density and mineral content, and greater periosteal bone formation following mechanical stimulation. These alterations in the biomechanical properties of bones resulted in stiffer long bones, and had further influence the cartilage-bone biomechanical unit by altering the load in cartilage, further contributing to the progression of OA (Lories 2007).

Alongside the morphological changes observed in the FRZB knockdown mice, additional studies investigating voluntary running wheel exercise performance confirmed the findings that FRZB contributed to OA development, as wild type mice showed greater exercise performance in comparison to FRZB knockout mice (Lories 2009).

The findings from this FRZB knockout murine study are supported by genetic association studies which have identified the presence of polymorphisms in the FRZB gene that are associated with the development of OA (Enomoto-Iwamoto 2002).

Dickkopf-1 (DKK-1) is another antagonist of Wnt signalling, which binds to LPR5/6 receptor (of the Wnt signal complex) and its co-receptor Kremen-1/2 inducing receptor internalisation and preventing activation of the Wnt pathway. One recent study performed which demonstrates the key role of Wnt signalling in the progression of OA investigated the capacity of an anti-DKK antibody to stimulate the development of OA in a transgenic mouse model of rheumatoid arthritis. Depletion of DKK resulted in stimulation of Wnt signalling, which reversed bone resorptive nature in rheumatoid arthritis and instead created a pattern of bone formation that resembled osteoarthritis, preventing resorption and inducing osteophyte formation (Diarra 2007).

Thickening of Calcified Cartilage

Another hypothesis regarding the involvement of bone in OA is that thickening of the calcified cartilage and advancement of the tidemark are features of OA (Lane 1980; Bullough 2004), which contributes to the thinning of articular cartilage and increases the stress in the deep zones of cartilage by increasing the stiffness gradient(Burr 2004). Advancement of the tidemark is possibly caused by release of angiogenic factors by hypertrophic chondrocytes (Walsh 2007) or by focal remodelling of micro cracks in subchondral bone (Goldring 2009). Damage to subchondral bone incurred from high impact injuries may initiate OA even without cartilage damage (Vellet 1991). Micro cracks in subchondral bone can stimulate focal remodelling (Trueta 1963). Their repair involves mineral resorption, vascular in-growth and bone deposition in the resorption space (Mori 1993b). In calcified cartilage the same process occurs but requires vascular invasion from the subchondral bone. This suggests a relationship between calcified cartilage and micro damage, in which remodelling of calcified cartilage micro damage may play a role in initiation or progression of OA (Burr 1997; Burr 2004; Burr 2004).

Change of Mechanical Environment by Subchondral Bone

The most frequently proposed method of bone involvement in OA is that of altered mechanics. Radin et al (Radin 1986) proposed that hardening or sclerosis of the subchondral bone increased the stresses on cartilage during loading by creating non-uniform regions of subchondral bone stiffness, with subchondral bone peripheral to the habitually loaded areas less stiff than loaded areas. In these regions a stiffness gradient will exist, which increases shear stresses in the cartilage (Brown 1984) and causes fibrillation (Radin 1986). More recent research has found that, despite an increase of bone volume in OA, the stiffness of subchondral bone tissue actually decreases (Li 1997a; Li 1997b; Day 2001; Ding 2003). However, despite a decrease of stiffness in osteoarthritic subchondral bone a stiffness gradient may still be present, where there will be an increase in shear stresses in the

cartilage. Furthermore, weakening of the bone will reduce cartilage support and increase deformation when loaded. The decrease of OA bone mechanical properties has been attributed to an increase in bone turnover (Seibel 1989; Sowers 1991; Li 1999; Pacicca 2003), a decrease of mineralisation (Bailey 2004), and an increase in osteoid (Grynpas 1991; Zysset 1994; Mansell 1998).

2.5 Summary and Hypothesis

There is evidence for the involvement of subchondral bone in the progression or initiation of OA, various theories exist as to how the subchondral bone is involved, but none are as yet accepted as being definitive. Both the timing and nature of subchondral bone changes in relation to cartilage damage is also unclear, with different bone changes having been reported in different models. OA is a chronic disease in which different tissues exhibit different characteristics between early and late stages; hence, there is a necessity to fully understand tissue changes in OA models. Surgical instability models are frequently used in OA research, in general there is a lack of longitudinal investigations focussing on bone changes, and limited characterisation of laxity in many of these models.

The DMM model is widely used in the investigation of OA. The work in this thesis hypothesises that meniscal destabilisation will result in a change of joint laxity, and this change in laxity will correspond to tissue changes in both bone and cartilage. These tissue changes may vary between different mouse strains and across different stages of OA. The purpose of the work in this thesis is to understand the morphology changes that take place in both the bone and cartilage, and investigate these changes in relation to any measured change of joint instability. This work will also allow for the enhancement and development of various imaging methods used to investigate these changes.

3. Investigation of OA in C57Bl/6 DMM model of OA

3.1 Introduction

In mice, a widely used and well validated instability model involves destabilisation of the medial meniscus (DMM), by surgically transecting the medial menisco-tibial ligament (Glasson 2007).

The DMM model has been used most notably for investigating biochemical and genetic factors in OA (Imhof 1999; Glasson 2004; Glasson 2005; Ma 2007; Shi-Lu 2009). In these studies, histological coronal sections were semi-quantitatively graded from 0 - 6, depending on the degree of cartilage degeneration (Glasson 2004; Glasson 2005; Glasson 2007; Ma 2007; Ma 2007; Botter 2009; Glasson 2010) and indicated mild to moderate OA at four weeks and moderate OA at eight weeks, with lesions focused on the 'central weight-bearing region' (Glasson 2007).

It is well known that joint laxity can lead to OA in animal models and humans (Pritzker 1994; van Osch 1995; Bendele 2001; Ameye 2006). The meniscus is important in dissipating transmitted load from the femoral condyles and also has a role in stabilising the joint (McDermott 2006). Experiments in human and dog cadaveric legs suggest meniscectomy introduces rotational and tensile laxity (Wang 1974; Oretorp 1978). However, other studies suggest meniscal tears and other damage that compromises the meniscus' ability to withstand hoop stresses results in an increase in contact area and therefore, increased peak local contact stress (Baratz 1986). A change in joint mechanics undoubtedly occurs after DMM surgery which causes secondary OA. It is uncertain whether this is because meniscal destabilisation introduces laxity into the joint altering the alignment of the articular surfaces, or because the meniscus loses its ability to support hoop stresses thereby increasing articular contact stresses. Though the DMM model is described as "destabilised", the changes in joint mechanics after DMM surgery have not been previously investigated. Clinically, measures of knee joint stability are often used after suspected injury to cruciate ligaments (anterior-drawer or Lachman test) or collateral ligaments (varus-valgus rotation assessment). In humans it has

been demonstrated that reduced anterior-posterior and varus-valgus knee stability is a risk factor for OA (van der Esch 2008).

Blankevoort and van Osch et al (van Osch 1995; Blankevoort 1996) developed two rigs for the in-vitro testing of murine knee joint laxity. The laxity rigs measure the laxity in anterior-posterior (AP) translation and varus-valgus (VV) rotation. These devices were used to investigate the effect of a collagenase injection on the laxity of murine knee joints, and they found that collagenase produced an increase in laxity (van Osch 1995; Blankevoort 1996). Further investigation found that freezing had no effect on laxity (van Osch 1995).

Previous studies with the DMM model have used histological techniques on the cartilage to describe tissue and cellular changes with limited quantitative analysis. Histological sections provide high resolution images for tissue characterisation and are currently the gold standard for assessing cartilage and bone degeneration. Histological thin sections are taken in one plane at a regular spacing across the sample, this provides two dimensional sampling of the joint. Recent work has demonstrated the utility of multimodal imaging for concomitant analysis of cartilage and bone using confocal scanning laser microscopy (CSLM) and x-ray micro-computed tomography (micro-CT), respectively. This method has recently been proven successful in quantifying and visualizing both cartilage and bone changes in three dimensions in the STR/ort spontaneous OA mouse model and provides a 3D representation of morphology changes in the joint (Stok 2009c). There have been no three dimensional quantifications of cartilage loss in the DMM model.

In OA, bone changes occur concomitant with cartilage degradation (Radin 1986; Burr 1998; Imhof 1999; Bailey 2001). Subchondral bone can become sclerotic and the underlying epiphyseal trabecular bone may undergo trabecular resorption (Blumenkrantz 2004; Botter 2008). Only a few studies have examined bone changes in the DMM model (Kamekura 2005; Kadri 2008; Botter 2009), and none in relation to altered mechanics of the joint.

This study will investigate the effect of DMM surgery on the laxity of the murine knee. 3D multi-modal imaging methods will be developed. These methods will be used to quantify and visualise changes in cartilage volume, cartilage topology and subchondral bone as OA progresses from four to eight weeks. It is hypothesised that the changes in joint laxity will correspond with patterns of tissue degradation of the bone and cartilage observed with multi-modal imaging.

3.2 Methods

3.2.1 Surgical Induction of OA

All procedures were performed with institutional ethical approval. Thirty-eight male mice (C57Bl6, Harlan, UK) aged twelve weeks underwent DMM surgery of the right limb, the left limb was unoperated. Surgery was performed by an experienced technician (Kennedy Institute of Rheumatology, Imperial College, London, UK). Mice were anaesthetised with an intra peritoneal injection of a 1:1 mixture of a 1:1 dilution of Hypnorm® (0.315 mg/ml fentanyl citrate and 10 mg/ml fluanisone; VetaPharma Ltd., Leeds, UK) and a 1:1 dilution of Hypnovel® (1 mg/ml midazolam; Roche Products Ltd., UK), at a dose of 5-10 ml/ mg body weight. The right knee was shaved and prepared with 70% alcohol solution. With the aid of a dissecting microscope the joint capsule was entered medially to the patella, and the cranial horn of the medial meniscus was transected from the tibia by cutting with an ophthalmic scalpel. To reduce the likelihood of damaging the ACL, the meniscus was first hooked with a bent needle and displaced away from the joint. After transection the capsule and skin were sutured. A complete description of the DMM procedure is in Appendix B. The mice were sacrificed in three groups: (1) at the time of surgery (0-week DMM, n = 15), (2) Four weeks after surgery (4 week DMM, n = 11) and (3) Eight weeks after surgery (8 week DMM, n = 12).

C57Bl/6 mice are known to develop spontaneous OA (Stanescu 1993). Therefore control C57Bl/6 mice with no DMM surgery were examined for occurrence of spontaneous OA at the same time

points (4 week control, n = 8; 8 week control, n = 8). These mice underwent confocal microscopy and micro-CT and did not undergo laxity testing.

3.2.2 Joint Laxity Testing

Mice in the zero week group were culled then received DMM surgery. The contralateral (left) and DMM operated (right) hind limbs were subject to the laxity testing protocol described by Blankevoort *et al.* (van Osch 1995; Blankevoort 1996).

The proximal femur and distal tibia were dissected from the overlying soft tissues. Tissue around the capsule was left intact to prevent specimen dehydration, all other tissue was stripped from the femur and tibia. During preparation the sample was wrapped with PBS soaked gauze to prevent dehydration.

Potting rig

The Potting device (Figure 3-1) used vernier adjustment of fine clamps that matched the landmarks of the femur and tibia. Laxity testing of the knee joint, varus-valgus rotation in particular, is highly sensitive to axial alignment. The vernier adjustment allowed positioning of a slit to hold the third trochanter, a cup to hold the femoral head and two opposing grooves to clamp the femur. This setup allowed reproducible positioning of the femur. Two additional clamps then positioned the tibia. The femur and tibia were embedded using pMMA (Simplex®), within the pMMA two steel rods were embedded to provide a mechanical connection to the testing rigs. The pMMA was applied by syringe injection into the potting rig. The samples were tested on two separate rigs. To prevent damage during handling a protective steel bridge was incorporated into the potting rig, which was removed with the potted sample attached.

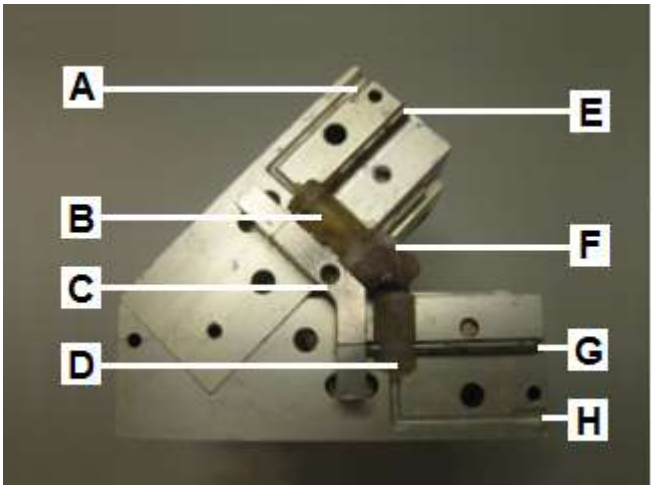

Figure 3-1. Photograph of half of the embedding rig, with a mouse leg embedded. A. pMMA injection point for tibia. B. Potted tibia. C. Protective bridge (removable). D. Potted femur. E. Steel pin to connect tibia to the rigs. F. Specimen. G. Steel pin to connect femur to the rigs. H. pMMA injection point for femur.

AP Drawer Test

The AP rig (Figure 3-2) used a linear variable differential transformer (LVDT) and a load cell, to measure tibial displacement and applied force. The load cell had a working range of ± 1 N and the LVDT had a range of 2.54 mm. Loads were applied through a spindle, which was mechanically connected to the LVDT and load cell with a spring. The spring smoothed the application of force and reduced any torsional forces on the load cell or bearings. Tibia motion was controlled in the anterior-posterior direction. The femur was free to translate parallel to the tibial axial direction, to minimise any contact restraint caused by contacting articular surfaces. Once embedded, the samples were clamped in testing rigs and preconditioned with five full cycles of load then tested with three full cycles of load. Force was controlled in the AP direction from 0 to ± 1 N. The knees were tested at an angle of 60° flexion, in this position there was minimal restraint from the capsule. Appendix C contains a detailed protocol for AP laxity testing.

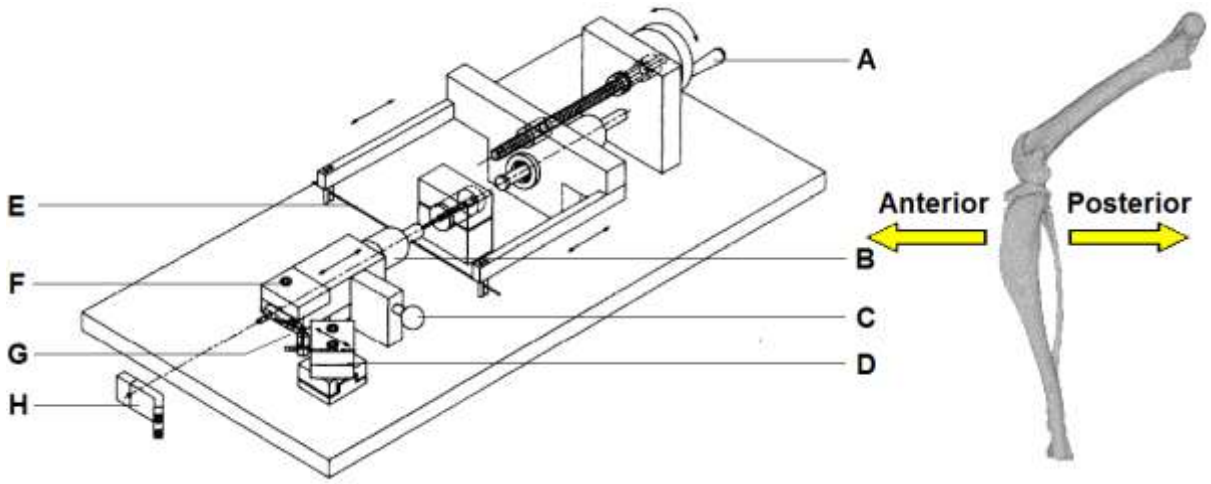

Figure 3-2. Schematic diagram of the AP rig (Blankevoort 1996) and illustration of anterior and posterior directions. A. Handle to apply load. B. Load cell. C. Locking pin. D. Femur clamp on linear bearings. E. Spring for smooth application of force. F. Tibia Clamp. G. Specimen. H. Protective bridge for specimen.

VV Rotation Test

The VV rig (Figure 3-3) used a rotation encoder to record angular position accurate to 1/3°, and a load cell connected to a 22 mm moment arm. The load cell moment arm used a working range of ± 5 Nmm. The VV rig used the same specimen configuration as the AP rig, only the tibia was free to rotate in the VV direction about the knee joint, instead of the AP direction. As with the AP rig, a load was applied via a handle, the applied force was smoothed with a spring. Torque was controlled in the VV direction from 0 to ± 5 Nm. The knees were tested at an angle of 60° flexion in the knee. Appendix C contains a detailed protocol for VV laxity testing.

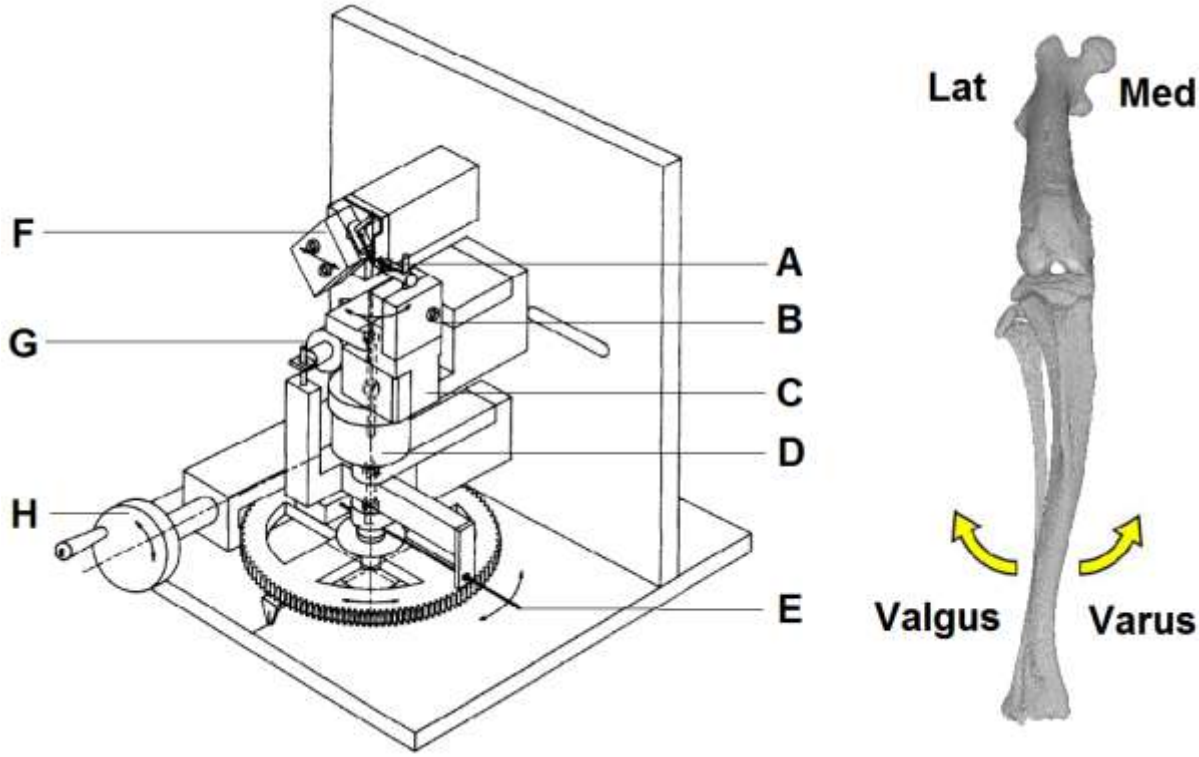

Figure 3-3. Schematic diagram of the VV rig (Blankevoort 1996) and illustration of Varus and Valgus rotation. A. Specimen. B. Tibia clamp. C. Moment arm. D. Rotation encoder. E. Spring to smooth load application. F. Femur clamp mounted on linear bearings. G. Load cell. H. Handle to apply load.

Data Acquisition

Signals from the load cells, rotation encoder and LVDT were acquired by a data acquisition (DAQ) unit (Flyde FE-MM-8 with a combined Flyde FE-USB-356-USB digital interface, Flyde Electronics Laboratory, Preston, UK). The DAQ unit provided an excitation circuit for the instrumentation. The load cells were connected to the DAQ with full bridge configuration. Amplification was configured to give maximum resolution. The DAQ unit is capable of sampling between 1 to 50 KHz. The rotation encoder produced two signals that featured voltage spikes every 1/3° of rotation. To ensure that no spikes were omitted from sampling, a test signal was created with a displacement of 45° applied in ten seconds, to represent a high loading rate. The signal had a maximum frequency of 13.5 Hz, Nyquist theorem states that the minimum sampling rate should be twice the frequency of the signal. The signal was originally sampled at a rate of 1000 Hz, it was then decimated by a factor of ten to

have an effective sample rate of 100 Hz. This was analysed using the automated code, no omission of spikes occurred when compared to a manual count and to the original undecimated signal. As a result of this a sample rate of 100 Hz with ×10 decimation being used for the rotation encoder in subsequent experiments. As only absolute values are required in the LVDT and load cell signals, aliasing would not occur, therefore, a sampling of 1 Hz was used.

Data Processing and Analysis

Data processing was performed using two Matlab programs. The programs averaged each of the three loading cycles and plotted load against displacement. Appendix D contains annotated code for the programs.

Graphs of load versus displacement were obtained from the data consistent with Blankevoort et al. (Blankevoort 1996). Plotting load on the x axis and displacement on the y axis means compliance is represented by the gradient of the curve (compliance is the inverse of stiffness). The laxity curves are closed graphs with four parts representing elements of the loading cycle (Figure 3-4). A and C represent loading in the anterior and posterior direction: B and D represent the unloading. The differences between unloading and loading curves are due to hysteresis, i.e. the energy dissipated within the joint during the loading cycle. At the zero point, compliance is high, as load increases compliance decreases nonlinearly until a linear region is reached. As with previous laxity testing work (Edixhoven 1987) the joint was characterised by determining the total displacement between loading limits, in both directions, and compliance in the linear region of loading (defined as 80% of maximum load). Other studies have used compliance at the zero point. However it was felt that this was too unreliable because at low loads the laxity curves were heavily influenced by bearing friction and articular contact, especially in the varus-valgus test. Matlab software was used to produce the curves and to analyse the laxity curves.

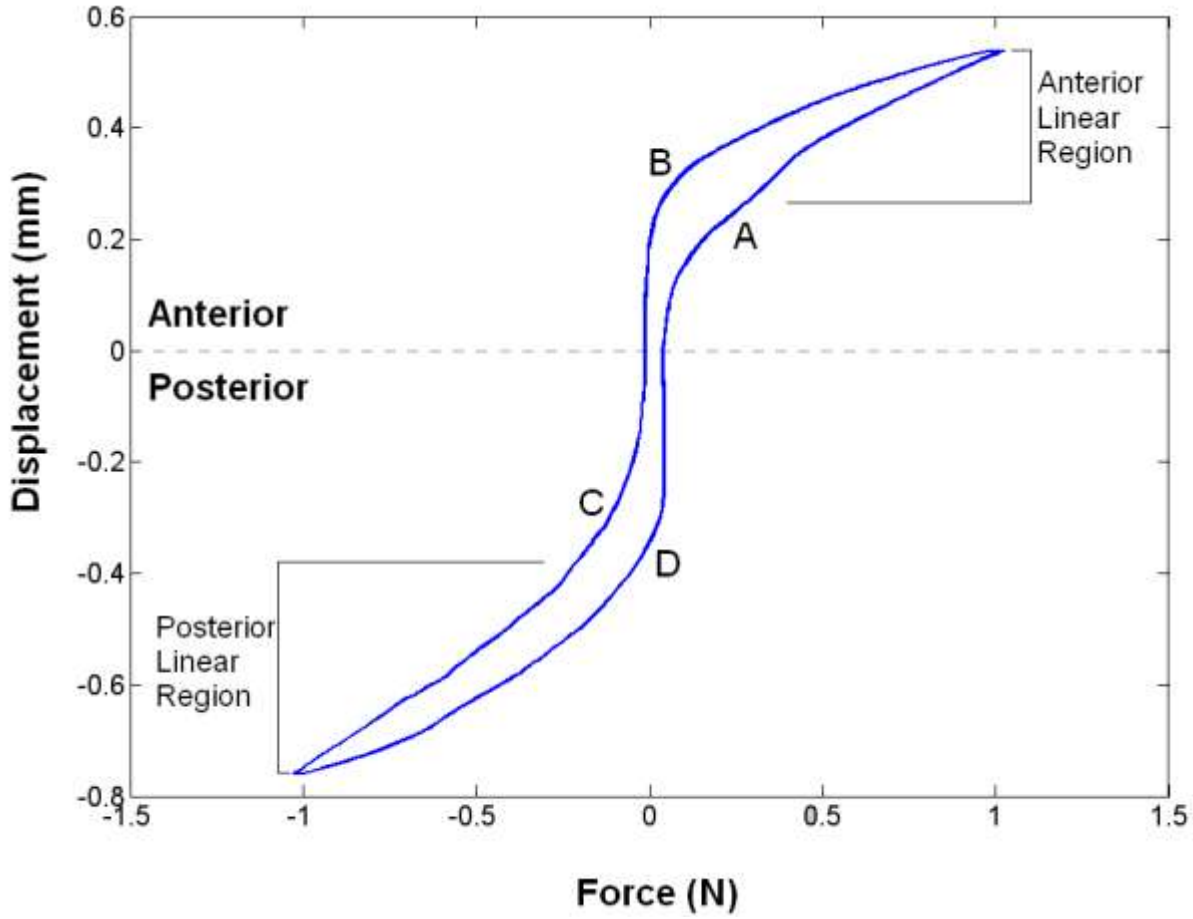

Figure 3-4. An example of a compliance curve. Portions of the curve labelled A and C represent loading in the anterior and posterior directions respectively, B and D represent the unloading curves from anterior and posterior positions.

Large forces can be required to remove sample from the potting rig which place the samples at risk of damage, as a precaution eight samples were discarded after the embedding process, thus reducing the group sizes (n = 10 DMM limb, n = 12 contra lateral limb) and prohibiting the use of a paired test. A Student's t-test was used to compare the means (significance measured as $p < 0.05$).

3.2.3 Bone Analysis

DMM (right) and contralateral (left) hind limbs were dissected from mice in the four and eight week groups. The limbs were manipulated into 0° flexion and imaged using micro-CT, set at 50 kVp and 160 µA (µCT40, Scanco Medical AG, Brüttisellen, Switzerland). The limbs were scanned from the

mid-femoral diaphysis to the mid-tibial diaphysis with an isotropic voxel size of 12 µm, resulting in a stack of 630 dicom axial slices.

The stacks were individually aligned to a constant orientation. Regions of interest (ROI) were identified on the lateral and medial tibial plateaus by defining two volumes bounded by consistent fractions of the breadth and width of the tibial plateau, omitting any artificial increase in width and breadth due to osteophytes (Figure 3-5). Typically in animal instability models the most significant bone changes occur under regions of cartilage damage (Muraoka 2007; Botter 2009). Previous studies on the DMM model suggest cartilage legions on the central part of the medial plateau (Glasson 1997). The ROI was centred in the tibial plateaus.

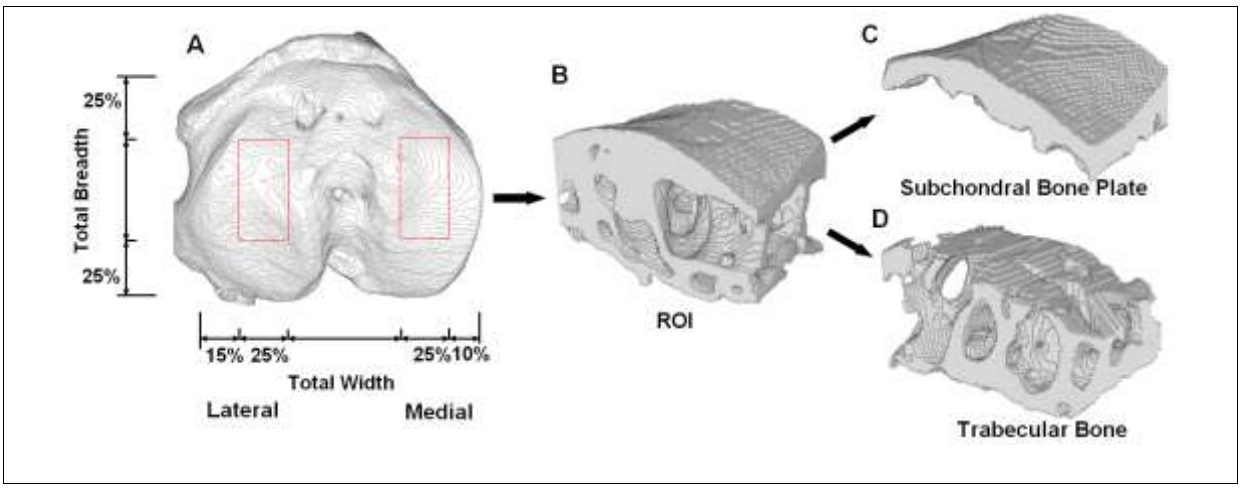

Figure 3-5. A 3D micro-CT reconstruction of a proximal tibia illustrating the selection of regions of interest (red boxes on lateral and medial plateaus are the ROIs). Fractions of the total width and total breadth define the position and size of both regions of interest. B is a 3D reconstruction of a medial region of interest. C and D are 3D reconstructions of subchondral bone and trabecular bone separated from B.

Bone distal to the growth plate was removed from the scans, the remaining volume was manually segmented into epiphyseal trabecular and subchondral bone plate using ImageJ3dViewer (Schmid 2007). The remaining bone was thresholded with the Otsu thresholding method (Otsu 1975). A number of investigations used automated methods to segment subchondral bone from epiphyseal bone (Botter 2009; Stok 2009c). As bone changes were variable amongst animals, automated

methods were unreliable. Consequently a manual method for segmentation was necessary. Problems with automated ROI selection are compounded in the mouse as the subchondral plate is of a comparable thickness to the epiphyseal trabecular bone. It is challenging for an automated algorithm to detect differences between the two. Some published studies separate the subchondral cortical bone from subchondral bone plate by observing a difference in pixel intensity (Kohler 2005; Stok 2009b). Density differences were not visible in the scans used in this study.

Average subchondral plate thickness was measured using BoneJ, an ImageJ plug-in which utilises a greatest sphere fitting algorithm (Dougherty 2007; Doube M 2010). In the epiphyseal trabecular bone, trabecular thickness (Tb.Th), spacing (Tb.Sp) and bone volume per total volume (BV/TV) were calculated using MicroView (GE Healthcare). MicroView and BoneJ use the same method for calculating thickness. The shortest distance from a bone voxel to a non-bone voxel is calculated. The largest sphere that fits within the bone structure is then determined for each bone voxel. Tb.Th is the mean value applied to all bone voxels. Tb.Sp uses the same method but only applied to bone marrow voxel (Hildebrand 1997; GE 2005).

The DMM limb was compared to the contralateral limb using a two way ANOVA with a Bonferroni post hoc test. All data conformed to a Gaussian distribution as assessed by Levene's test.

3.2.4 Cartilage Analysis

The tibiae from the four and eight week groups were carefully disarticulated from the femurs. All soft tissue including the menisci and capsule were removed. The tibiae were cut at the mid-length and glued onto a custom holder (Figure 3-6). Samples were left at room temperature for one hour. The holder was placed into a tissue culture well filled with phosphate buffered saline with the proximal end of the tibiae orientated toward the bottom of the tissue culture well. The well was placed on an inverted confocal laser microscope (Leica SP5) stage and scanned with a 10× dry

objective and a 466 nm laser. The laser was powered for a minimum of 30 minutes before scanning, to ensure a steady state temperature was reached as fluorescence varies with temperature (Pawley 2006). The photo multiplier was set to collect for all available wavelengths above 488 nm, with a gain of 625 V and an offset of -2%, 512 × 512 images were made with a laser speed of 400 Hz. To ensure reproducibility all parameters were maintained throughout all scans. Images were obtained at 5.80 µm intervals in the Z-direction throughout the thickness of the cartilage, with a resolution of 3.03 µm in the XY plane. During post-processing the XY images were downsampled to 5.80 µm to form isotropic voxels. The protocol was modified from Stok et al (Stok 2009b; Stok 2009c). Four to six stacks of images in the axial plane were made for each tibia and stitched together to encompass a whole tibial plateau. Stitching was performed automatically by Leica software. The full protocol is contained in Appendix E.

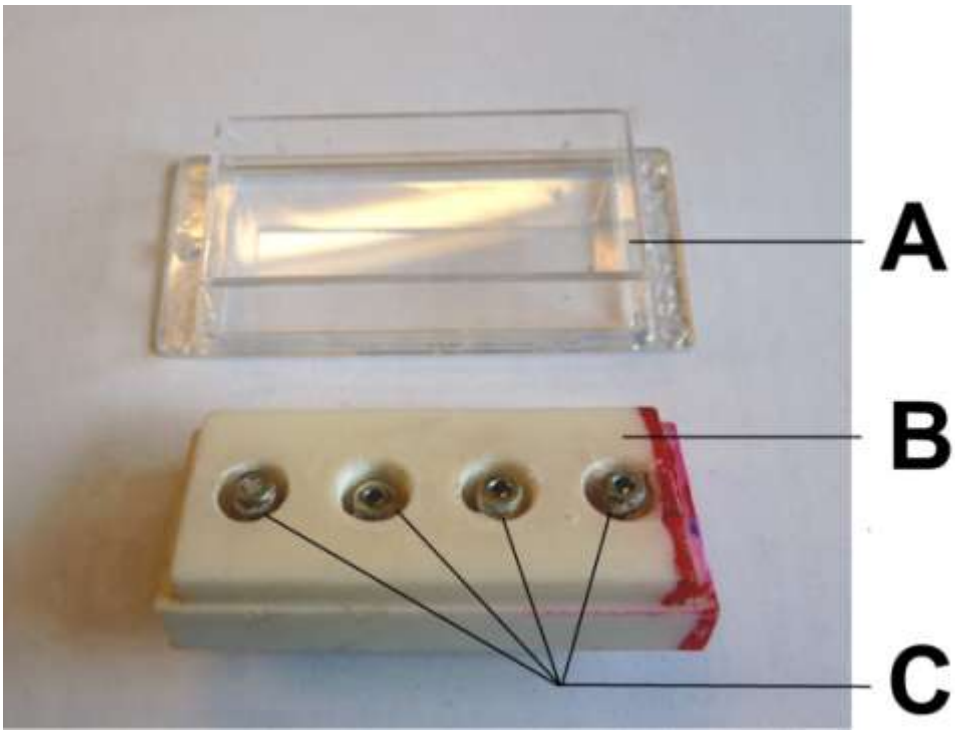

Figure 3-6. Tibia holder. A. Cell culture well. B. Polymer tibia holder. C. Screws, tibia are glued into the screw caps and height adjusted. Once the tibiae are glued into place, the culture well is filled with phosphate buffered saline (PBS) and the tibia holder is turned upside down and pressed into the culture well.

The CSLM image stacks were converted into 3D images (ImageJ3D viewer). Cartilage was manually segmented by identifying and removing all surplus soft tissue (i.e. ligaments and meniscus fragments) from the 3D scans. The remaining cartilage was segmented using the IsoData method (Ridler 1978) (Figure 3-7). Volume was analysed by summing the thresholded voxels and multiplying by voxel volume. Local thickness was calculated from the reconstructions. A measure of average cartilage thickness was not included because DMM limbs exhibited full thickness cartilage loss on the posterior plateau. Therefore, any average thickness calculations would omit these regions of loss and return an artificially large value from the remaining cartilage. Cartilage volume was analysed using a two way ANOVA with a Bonferroni post hoc test. All data conformed to a Gaussian distribution as assessed by Levene's test.

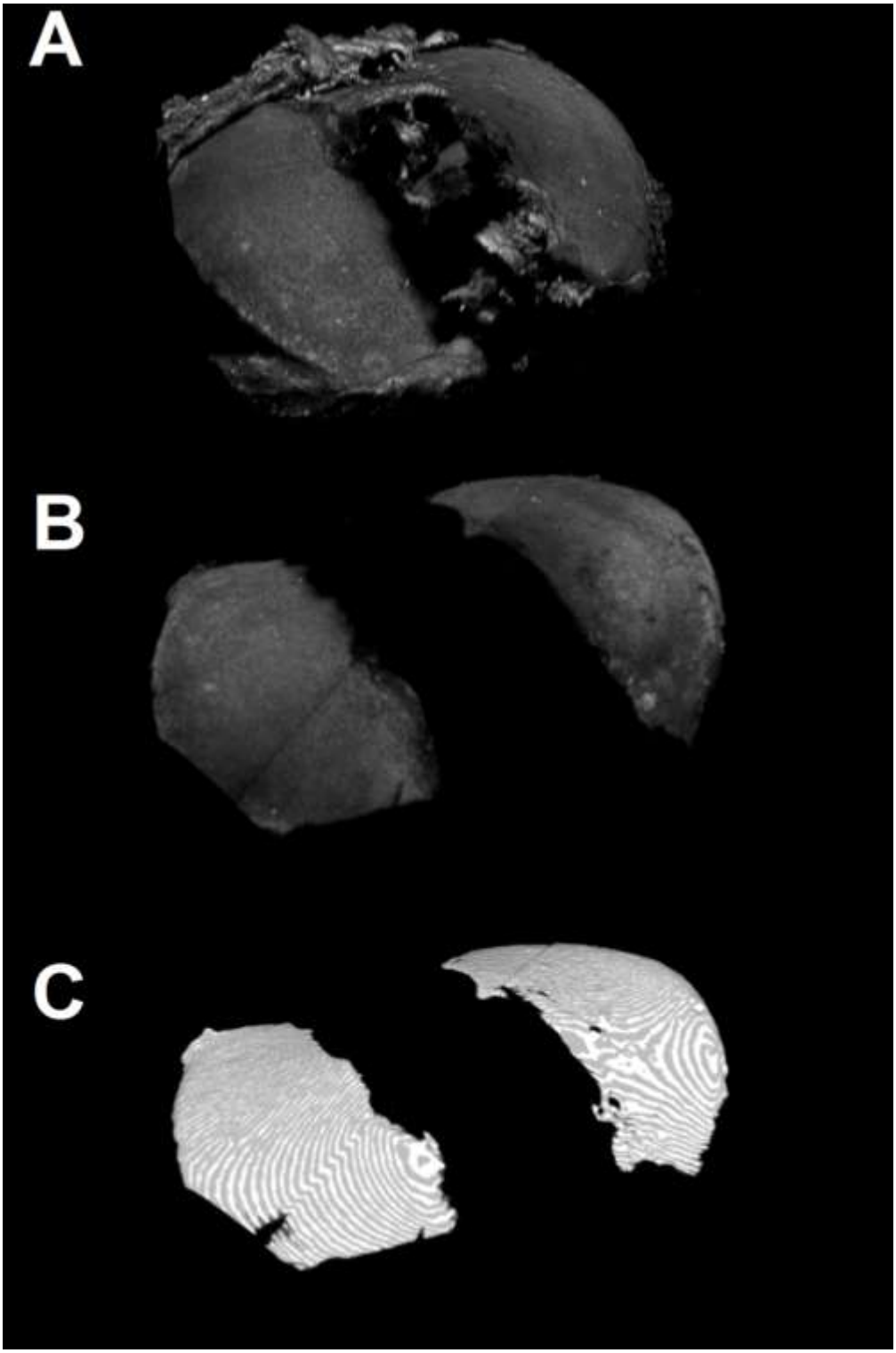

Figure 3-7. Post processing of cartilage stacks. A. Unprocessed reconstruction of CSLM stack of lateral and medial tibial plateau. B. Reconstruction of stack after soft tissue has been removed. C. Reconstruction of a thresholded stack.

3.3 Results

3.3.1 Laxity changes

The anterior-posterior compliance curve (displacement vs. load for a loading and unloading cycle) demonstrated characteristic hysteresis in the joints (Figure 3-8). A significant increase of anterior-posterior range of motion with DMM surgery was observed with an increase particularly in the anterior direction. The mean displacement in the posterior direction increased with a similar magnitude, but this increase was not statistically significant (Table 3-1). Total range of anterior-posterior motion increased with DMM surgery by 49%. There was no significant increase of displacement in the varus and valgus directions and total range of motion with DMM surgery.

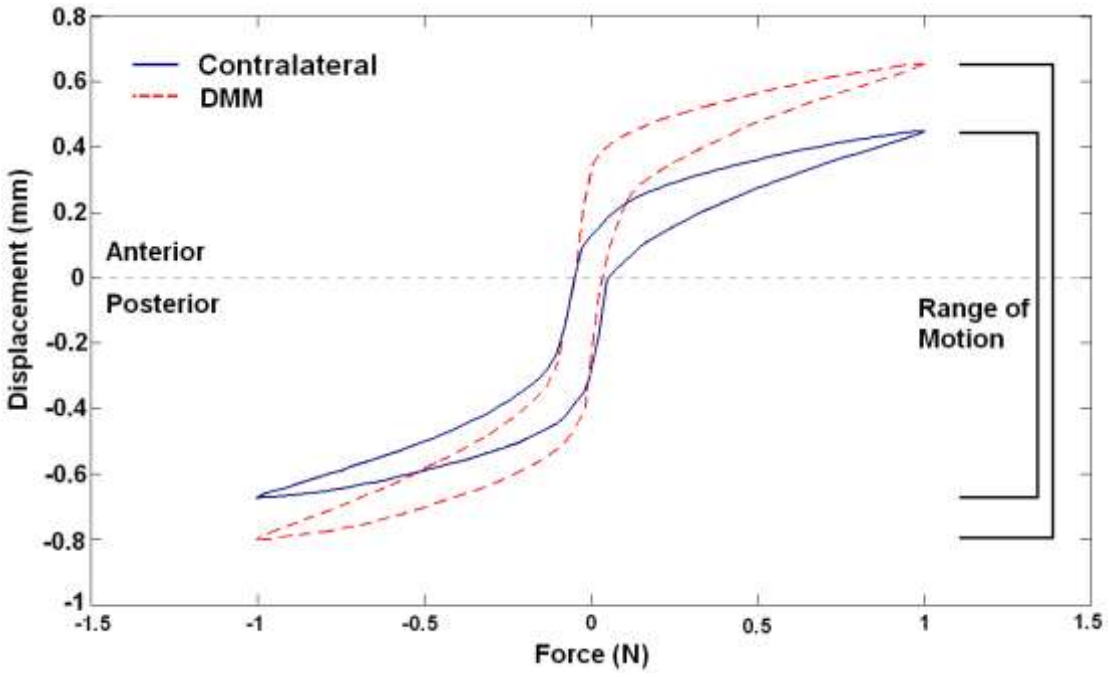

Figure 3-8. Mean anterior-posterior compliance curve for all contralateral (left) and DMM (right) legs.

	Contralateral (left)	DMM (right)	
	n = 12	n = 10	P
Anterior displacement at 0.8 N (mm)	0.45 ± 0.10	0.66 ± 0.36	< 0.05
Posterior displacement at 0.8 N (mm)	-0.58 ± 0.34	-0.83 ± 0.44	ns
Anterior-Posterior Range (mm)	1.04 ± 0.374	1.55 ± 0.54	< 0.05
Varus displacement at 4 Nm (°)	10.33 ± 4.37	11.91 ± 5.77	ns
Valgus displacement at 4 Nm (°)	-10.47 ± 4.39	-11.44 ± 3.63	ns
Varus Valgus Range (°)	20.80 ± 5.33	23.35 ± 5.17	ns

Table 3-1. Table of laxity testing tibia displacements, mean ± SEM, p < 0.05.

3.3.2 Bone Analysis

Four weeks after DMM surgery, the medial epiphysis of the DMM leg had lower bone volume fraction (BV/TV) than the contralateral medial epiphysis (Table 3-2). There was no significant difference for all other parameters. After eight weeks in the DMM group, there was a further decrease in BV/TV and trabecular thickness decreased suggesting a loss of trabecular bone. Subchondral plate thickness increased significantly on the DMM leg compared to the contralateral leg at eight weeks. There were no significant changes in the lateral ROI between DMM and contralateral legs except for a decrease in BV/TV at eight weeks. The control groups showed no significant change in any parameter from week four to week eight (Table 3-3).

	Contralateral (left) **4 weeks**	DMM (right) **4 weeks**		Contralateral (left) **8 weeks**	DMM (right) **8 weeks**	
Medial	n = 11	n = 11	p	n = 12	n = 12	p
Sb.Pl.Th / (mm)	0.243±0.029	0.259±0.078	ns	0.236±0.040	0.292±0.126	<0.01
Tb.Th / (mm)	0.070±0.009	0.063±0.011	ns	0.074±0.012	0.060±0.001	<0.01
Tb.Sp / (mm)	0.104±0.015	0.110±0.022	ns	0.109±0.016	0.131±0.002	ns
BV/TV	0.503±0.050	0.409±0.088	<0.01	0.511±0.053	0.356±0.085	<0.001
Lateral						
Sb.Pl.Th / (mm)	0.172±0.012	0.205±0.060	ns	0.166±0.008	0.181±0.046	ns
Tb.Th / (mm)	0.047±0.004	0.053±0.007	ns	0.048±0.003	0.048±0.009	ns
Tb.Sp / (mm)	0.126±0.018	0.127±0.018	ns	0.134±0.018	0.139±0.014	ns
BV/TV	0.376±0.049	0.336±0.059	ns	0.374±0.028	0.281±0.059	<0.001

Table 3-2. Bone parameter means ± SEM. Significance (p) compares contralateral to DMM leg, $p < 0.05$ is considered significant. Sb.Pl.Th is subchondral bone plate thickness, Tb.Th is trabecular thickness, Tb.Sp is trabecular spacing, BV/TV is bone volume / total volume, n = 11 at 4 weeks, n = 12 at 8 weeks.

	Control left **4 weeks**	Control right **4 weeks**		Control left **8 weeks**	Control right **8 weeks**	
Medial	n = 8	n = 8	p	n = 8	n = 8	p
Sb.Pl.Th / (mm)	0.177 ± 0.024	0.203 ± 0.037	ns	0.166 ± 0.011	0.182 ± 0.020	ns
Tb.Th / (mm)	0.050 ± 0.007	0.050 ± 0.007	ns	0.060 ± 0.005	0.060 ± 0.007	ns
Tb.Sp / (mm)	0.095 ± 0.020	0.091 ± 0.014	ns	0.121 ± 0.022	0.105 ± 0.021	ns
BV/TV	0.336 ± 0.045	0.360 ± 0.056	ns	0.334 ± 0.055	0.326 ± 0.050	ns
Lateral						
Sb.Pl.Th / (mm)	0.147 ± 0.009	0.165 ± 0.020	ns	0.130 ± 0.010	0.135 ± 0.005	ns
Tb.Th / (mm)	0.044 ± 0.005	0.043 ± 0.004	ns	0.051 ± 0.007	0.050 ± .004	ns
Tb.Sp / (mm)	0.118 ± 0.014	0.124 ± 0.015	ns	0.122 ± 0.029	0.120 ± 0.013	ns
BV/TV	0.333 ± 0.036	0.315 ± 0.028	ns	0.357 ± 0.046	0.375 ± 0.023	ns

Table 3-3. Control bone results, means ± SEM. Significance (p) compares contralateral to DMM leg. Sb.Pl.Th is subchondral bone plate thickness, Tb.Th is trabecular thickness, Tb.Sp is trabecular spacing, and BV/TV is bone volume / total volume.

Three dimensional reconstructions of the tibiae were created from the micro-CT data (MIMICS, Leuven, Belgium). At both four and eight weeks on the DMM affected limbs, extensive changes of morphology of the posterior tibial head were observed in 13 out of 23 specimens (4 weeks: 6 out of 11, 8 weeks: 8 out of 12) (Figure 3-9). Bone loss occurred on the posterior portion of the medial plateau, and on more severe examples, bone loss appeared to extend through the epiphyseal bone, with damage to the tibia extending distally beyond the growth plate. The bone loss was typically accompanied by periosteal bone growth occurring around the growth plate on the posterior aspect, distal to the site of bone loss. In bones with no posterior growth, large changes were seen anteriorly (Figure 3-10). In all DMM tibias at both time points, there was extensive bone remodelling observed on the micro-CT reconstructions at the joint periphery that was not included in the ROI and therefore not captured in the quantitative micro-CT analysis. Various bone changes were seen in DMM affected femurs, these changes were not investigated or quantified.

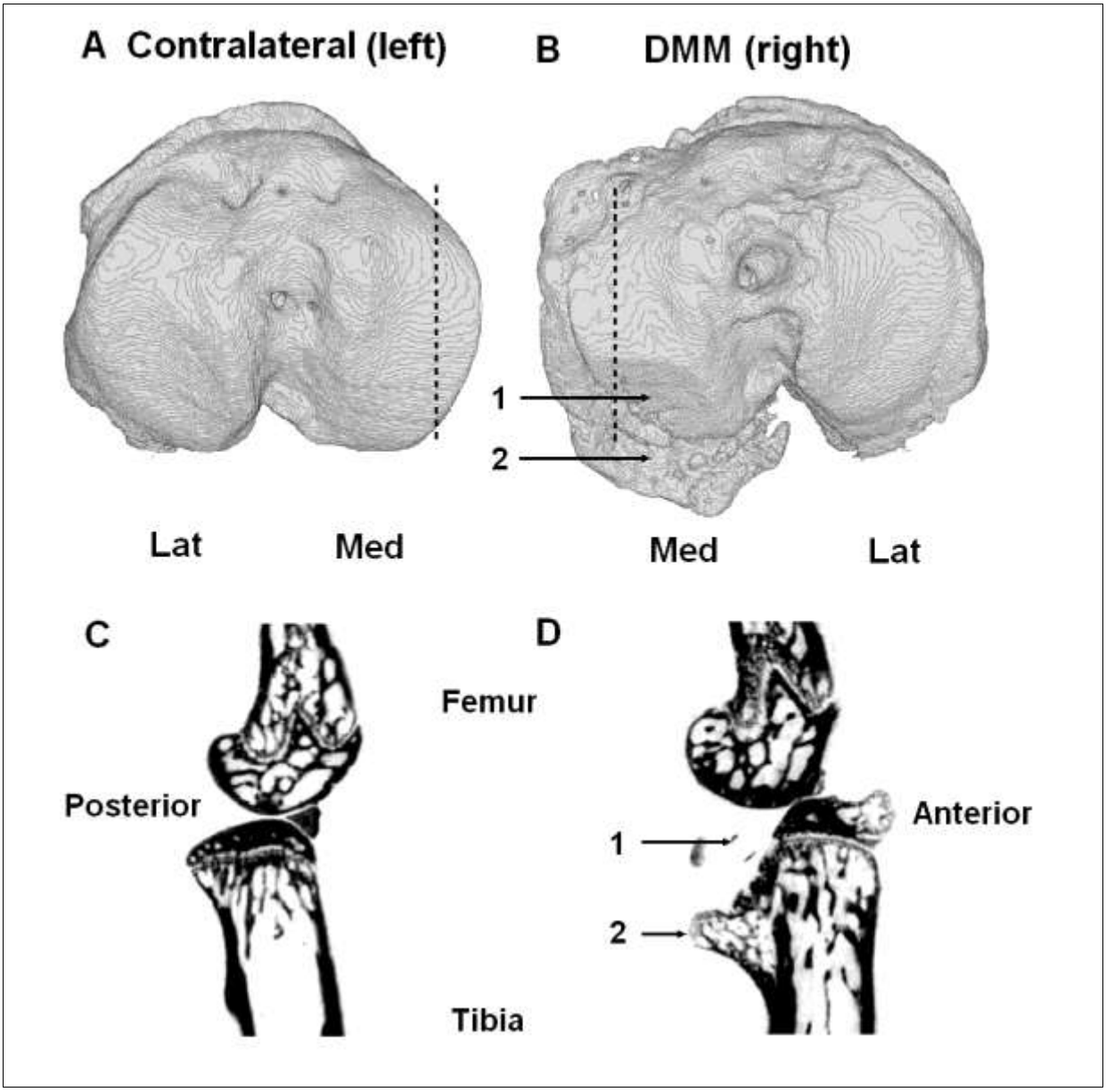

Figure 3-9. 3D bone reconstructions and corresponding sagittal tomograms of tibial heads from a mouse 8 weeks after DMM surgery. A: Contralateral (left) tibia. B: DMM (right) tibia. 1. Indicates region of bone loss, 2. Indicates bone growth. C and D: micro-CT sagittal tomograms from A and B respectively, approximate location indicated by dashed line. Posterior subchondral bone loss is evident and damage to the tibia extends beyond the growth plate, distal to the region of bone loss, bone remodelling is evident.

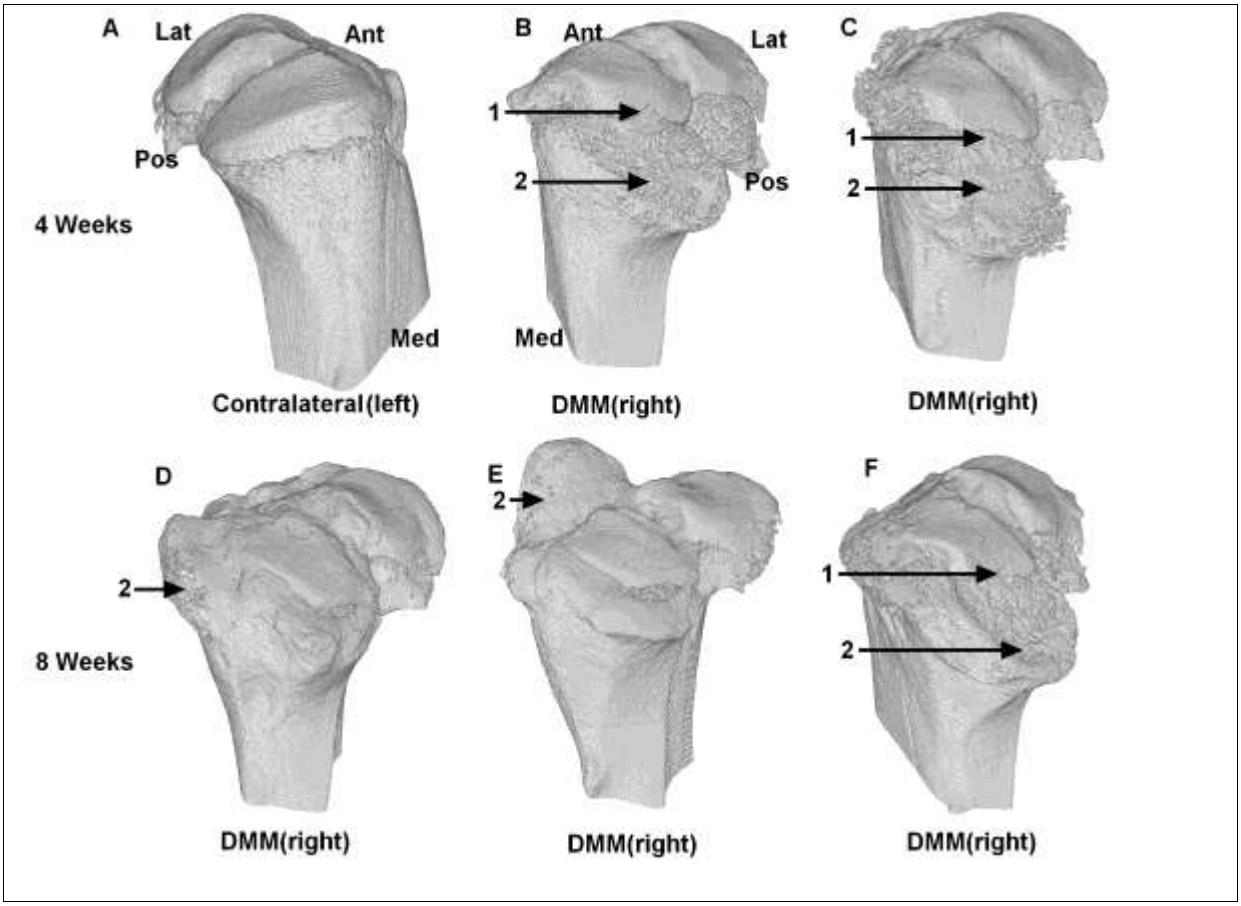

Figure 3-10. Micro-CT reconstructions of proximal tibiae, the medial plateau is in the foreground. A: Contralateral (left) leg 4 weeks after surgery. B: DMM (right) leg 4 weeks after surgery, significant bone growth can be seen on the posterior of the tibial head. C: DMM (right) leg 4 weeks after surgery, extensive bone loss on the medial posterior plateau. D: DMM (right) leg 8 weeks after surgery, minimal posterior bone loss but growth on anterior and medial aspect. E: DMM (right) leg 8 weeks after surgery, extensive anterior bone formation. F: DMM (right) leg 8 weeks after surgery, characteristic posterior bone loss and bone growth on posterior medial plateau. 1. Indicates region of bone loss, 2. Indicates bone growth.

3.3.3 Cartilage analysis

Quantitative analysis of cartilage volume indicated a significant decrease of cartilage volume on the medial plateau of the DMM leg compared to the contralateral leg at four and eight weeks. There were no significant changes on the lateral plateau (Table 3-4). Three dimensional reconstructions of the CSLM data indicated loss of cartilage on the DMM leg was consistent on the posterior region of the medial plateau (Figure 3-11). The region of loss corresponded with the same regions of bone loss

observed by micro-CT. The occurrence of this characteristic loss was 6 mice from 11 at four weeks and 9 mice from 12 at eight weeks.

Volume ($\times 10^{-3}$ mm^3)	Contralateral (left) **4 weeks** n = 11	DMM (right) **4 weeks** n = 11	P	Contralateral (left) **8 weeks** n = 12	DMM (right) **8 weeks** n = 12	p
Medial	1.276± 0.151	1.022 ± 0.243	< 0.05	1.238± 0.231	0.948 ± 0.210	<0.01
Lateral	1.454 ± 0.230	1.429 ± 0.398	ns	1.620± 0.157	1.623 ± 0.225	ns

Table 3-4. Table of cartilage volumes for lateral and medial tibial plateau of DMM and contralateral legs. Volume change compares contralateral to DMM legs, p < 0.05 is considered significant, n = 11 at 4 weeks, n = 12 at 8 weeks.

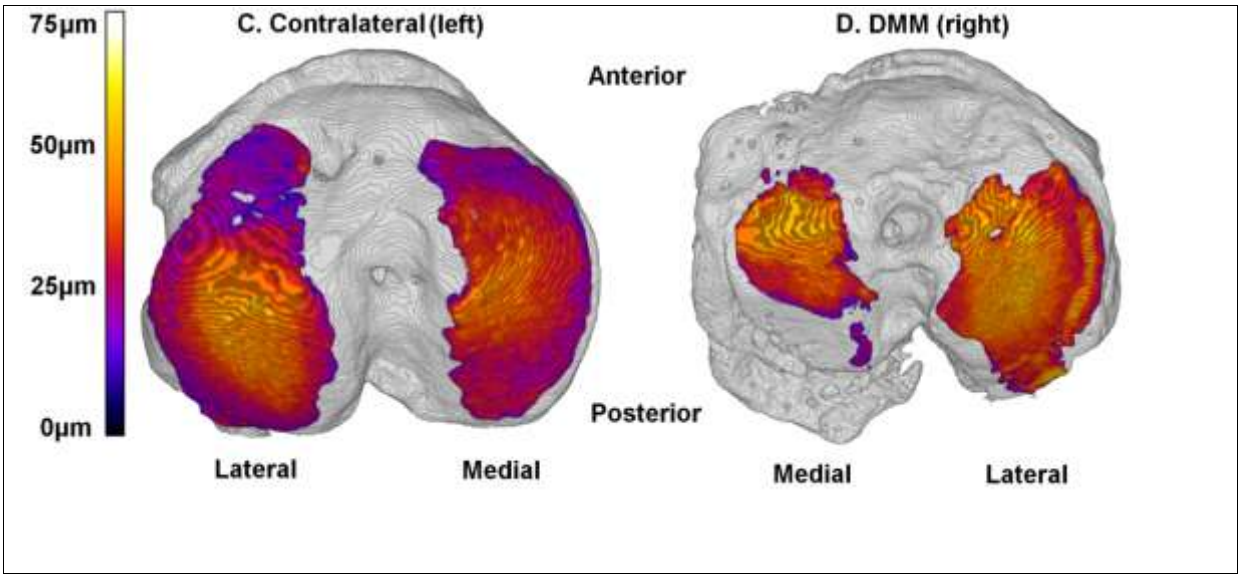

Figure 3-11. CSLM 3D cartilage thickness reconstructions from a mouse 8 weeks after DMM surgery superimposed on micro-CT reconstruction of bone. A: Tibial cartilage from contralateral (left) leg. B: Tibial cartilage from DMM (right) leg. Characteristic region of cartilage loss is visible on the posterior aspect of the medial plateau and corresponds with regions of bone loss.

3.4 Discussion

3.4.1 Laxity in the DMM model

DMM surgery caused a significant increase of tibial AP range of motion, particularly with the tibia moving in the anterior direction with respect to the femur. This change in joint dynamics repositioned the point of contact between the femur and the tibia posteriorly. The severity of bone and cartilage damage was surprising given previous reports of moderate damage in the mid-plateau region (Glasson 2007). The medial menisco-tibial ligament is located close to the tibial insertion of the ACL. Therefore, it is conceivable that during medial menisco-tibial transection the ACL was damaged. The medial menisco-tibial incision in DMM surgery is parallel to the ACL fibre orientation so any accidental damage would, however, be limited. Knees were examined in vivo and after sacrifice for ligament damage, but none was apparent. The CLSM protocol required disarticulation of the joint, which prohibited detailed histological analysis of the ACL. A complete transection of the ACL results in an obvious increase in joint laxity and would have been discarded prior to investigation. Partial ACL damage could, however, explain the increase in AP range of motion and posterior tissue damage as well as the large variance. The damage patterns observed in the four and eight week mice are similar to described changes in a murine ACL transection model (Glasson 2007). However, it is possible the increase in laxity could be caused by surgical entry into the capsule or accidental damage to the medial collateral ligament, as no sham controls were performed it is impossible to rule this out. A study in which a capsular incision was performed on rabbits reported the development of OA symptoms, this however, was most likely a result of increased bleeding and inflammation (Fahlgren 2006).

There was a varying range of bone morphology outcomes for DMM affected limbs. For example (Figure 3-10) (B), (C) and (F) exhibit different extents of posterior tibial bone remodelling, in half the mice (52%), extensive bone loss occurred in the posterior subchondral plate region. Those that lacked posterior damage frequently exhibited marked anterior bone remodelling, (Figure 3-10) (D)

and (E) exhibit two entirely different remodelled bone structures on the anterior tibia. This variation may be as a result of surgery affecting the ACL to different extents across a group. Normal control mice showed no significant bone changes, therefore, the changes in the DMM legs cannot be attributed to spontaneous OA.

Laxity testing of the 0 week group was performed immediately after DMM surgery to determine how release of the medial meniscus altered joint mechanics. This group was not analysed with micro-CT or CSLM. DMM surgery was performed immediately after culling; therefore no changes in bone or cartilage were expected. DMM surgery significantly increased anterior motion and tended to increase VV laxity. A post-hoc analysis of statistical power for VV laxity suggested that a sample size of 23 would be required to produce a statistically significant difference. Therefore it is possible that DMM surgery also increased VV laxity, but because of large variance it was not measurable in this study. Internal-external rotation is also relevant for assessing the integrity of the menisci and will be addressed in Chapter 5. The variance for the laxity testing was unexpectedly high when compared to previous work using the laxity rigs (van Osch 1995). This may be as a result of varying degrees of ACL surgical damage across each experimental group of mice.

Sham surgery controls were not used as previous studies have shown no statistically significant difference of histological OA scores up to twelve weeks after surgery between the sham and contralateral legs (Chia 2007; Glasson 2007; Inglis 2008). As mentioned above, this is a severe limitation of the study. The control group (no surgery) was used to demonstrate that OA does not spontaneously develop at this age in this strain of mouse.

3.4.2 Changes in Bone

The regions of interest in the micro-CT quantitative analysis were focused on the regions beneath the lateral and medial tibial plateaus. It is evident that remodelling had taken place within these regions by eight weeks however, more substantial changes occurred around the perimeter of the

epiphyseal cortex which was not included in the ROI. Quantitative analysis of bone in the periphery and standardising a ROI to capture meaningful quantitative data from the periphery remains a challenge.

It is well known that bone changes occur concomitantly with cartilage loss (Bailey 1997; Burr 1998; Bailey 2001; Brandt 2006). In the DMM model using a different strain (129/SvEv), Botter et al. found that subchondral bone plate thickness increased on the medial plateau with no significant change in trabecular parameters eight weeks after surgery, but published tomograms showed a clear increase of epiphyseal bone (Botter 2009). In the C57Bl/6 mice there was a similar increase of subchondral bone plate thickness and an additional loss of trabecular bone at eight weeks. There were also extensive bone changes at the joint periphery which were not reported in the 129/SvEv mouse. Differences between the two studies may be a consequence of using different strains, as the C57Bl/6 strain has lower bone mineral density and a thinner subchondral bone plate compared to the 129/SvEv strain (Beamer 1996; Botter 2008; Jackson-Laboratory 2009). Furthermore, the mice used had an unusually high activity and required separation due to fighting, this may have encouraged OA progression. These however, are unlikely to account for such extreme differences of bone damage. It must be noted that a study using an ACLT mouse model described similar bone changes to those seen in this study (Glasson 2007).

In a study using the DMM model in C57Bl/6 mice a decrease of BV/TV, Tb.Th and an increase of Tb.Sp was reported. Histological thin sections were used to look at bone changes six weeks after surgery instead of micro-CT. They reported trabecular bone changes similar to the changes in this study, suggesting the possibility that ACL damage is not uncommon with the DMM model (Kadri 2008).

3.4.3 Changes in the Cartilage

Using 129/SvEv mice with DMM model, Glasson et al. found mild to moderate OA at four weeks and moderate OA at eight weeks from histological coronal sections from the central part of the plateau (Glasson 2007). Cartilage loss from the posterior region did not occur. CSLM images in this study indicated that full thickness loss of cartilage was occurring on approximately 70% of the DMM affected limbs in the posterior region but did not identify changes in the central plateau. The disparity may arise for a number of different reasons: possible damage to the ACL, mouse strain (as discussed above) and differences in assessment technique. Coronal histological section in mid-plateau may overlook the loss occurring in the posterior region. CSLM, on the other hand, may lack the resolution to detect fibrillation and lesions that were observed on histological sections from early degeneration of osteoarthritic cartilage. Hence the use of CSLM in this study has been limited to volume measurements and visualisation of gross morphology. With this limitation it is conceivable that lesions and fibrillation previously described in the centre of the DMM medial plateau were present, but their effect on cartilage thickness was not extensive enough to be detected by CSLM.

Quantitative measurements of cartilage from CSLM images must be validated using histology. Cartilage thickness was calculated from confocal reconstructions of non-DMM legs using the local thickness plug-in of BoneJ (Doube M 2010), which utilises a sphere fitting algorithm (Dougherty 2007). The average cartilage thickness calculated from confocal reconstructions was approximately 0.035 mm on both plateaus, which is in the range of previously reported values from histological sections (0.03 -0.083 mm) (William 1970; Stockwell 1971; Cao 2006) and CSLM (Stok 2009a). Previous work compared histological sections with CSLM measurements and demonstrated that with the application of a correction factor, CSLM thickness measurements can match histological thickness measurements from thin sections (Stok 2009a).

The DMM model produced significant bone remodelling and cartilage loss only four weeks after surgery compared to the contralateral leg. Using CSLM and micro-CT it was possible to quantify the

changes in the region of the tibial plateaus and visualise the changes peripherally. Though remodelling changes were variable within a group, 3D multimodal imaging techniques were able to capture differences which may not be observed on standard histological sections. Micro-CT and CSLM are non-destructive and can be used to complement histological thin sections, indicating particular sites of interest for further histological analysis.

The locations of regions of cartilage and bone remodelling detected by CSLM and micro-CT were consistent with the measured changes of laxity in the mouse knee after surgery. It is likely that laxity of the tibia allowed the femur to contact more posteriorly (tibia moves anteriorly) and may have contributed to the degradation of bone and cartilage, however, this cannot be verified without histological evaluation.

4. Early Stage Osteoarthritis in the DMM Model

4.1 Early Stage OA

Osteoarthritis is a degenerative disease and is rarely reversible. Late stage treatments are focussed on pain management and maintaining joint function; they are unable to restore lost cartilage. Hence, early detection of OA is important for developing treatments. The involvement of bone in early stage OA and the timing of onset of bone changes in relation to cartilage changes is currently disputed (Felson 2004a).

Early bone changes in human OA

In the clinic, cartilage is assessed directly using MRI or indirectly by examining joint space narrowing using radiography. Both techniques lack the sensitivity to detect early stage structural changes, such as proteoglycan loss, fibrillation, and osteoid formation. Analysis of early stage OA bone from human cadavers suggest the subchondral plate and epiphyseal bone increase in volume (Grynpas 1991; Ding 2003) with an accompanying decrease of bone tissue stiffness (Li 1997a; Li 1997b; Ding 2003). A mathematical model of early stage bone estimated that the bone tissue elastic modulus decreased by 60% percent, this caused the bone to respond by increasing volume to restore stiffness (Day 2001). In early stage OA the subchondral bone plate and trabecular bone also decrease in matrix density (Li 1997a; Li 1997b; Yamada 2002). The reduction of density and elastic modulus in bone are attributed to an increase of turnover, causing increased osteoid content and hypomineralisation in the bone (Bailey 2004). There have however, been a few studies that challenge the conception that human OA increases bone volume by suggesting early stage resorption does occur in human OA. A reduction of radiographic bone mineral density (BMD) in mild idiopathic OA has been reported (Karvonen 1998), as has a decrease of BMD in patients with complete ACL rupture (Leppala 1999), and number of MRI studies have observed the formation of lesions in epiphyseal bone, which predict regions of cartilage loss (Felson 2003; Hunter 2006; Roemer 2009). Additionally, an increase

of bone resorption markers have been observed in the urine of patients with progressive OA (Bettica 2002).

These abnormal changes in bone metabolism and structure seen in OA have led to the pursuit of therapeutic agents to target abnormal bone metabolism. One such strategy involves the use of a class of drugs called bisphosphonates. Bisphosphonates have a chemical structure similar to that of pyrophosphate (PP_i) and are able to inhibit osteoclast resorption. Studies using various surgical animal models have suggested that bisphosphonates have a chondroprotective effect, as well as suppressing subchondral bone resorption and osteophytosis (Hayami 2004; Moreau 2011). The success seen in animal trials has not been replicated in clinical trials, for example a bisphosphonate called risedronate did not have disease modifying effects in a phase III clinical trial (Bingham 2006). One frequently proposed reason for this difference of outcome is that for the bisphosphonates to be effective they may have to be applied in the early stages of the disease to reduce any bone resorption (Martel-Pelletier 2011). In surgical animal models the bisphosphonates are typically applied after induction, whereas in human trials the timings of treatment in relation to the stage of disease are more variable.

Early bone changes in animal OA

Depending on the animal, the method of OA induction, the time point examined, and the method of assessment, animal models of OA exhibit bone resorption or formation in the early or late stages of OA (Figure 4-1 for summary). A number of surgical models show bone resorption (or decreased formation) takes place in the early stages. Early stage bone resorption is seen in the subchondral plate and epiphyseal bone in rat and dog ACL transaction models and guinea pig meniscectomy models (Dedrick 1993; Pastoureau 1999; Pelletier 2004; Hayami 2006; McErlain 2008). Early stage subchondral plate bone loss is also seen in cartilage trauma models, in the ovine fetlock and canine stifle joint (Intema 2008; Mastbergen 2008; Intema 2010). In some models (canine groove, canine

ACLT, and collagenase murine models) bone resorption is also seen in later stage OA, coinciding with moderate and severe cartilage damage (Botter 2006; Botter 2008; Intema 2010). This early stage resorption is potentially analogous to the formation of bone marrow lesions in trabecular bone of human OA.

A number of researchers attribute trabecular resorption in OA to disuse osteopenia (Botter 2008; Intema 2010). For example dogs reduced peak forces in ACLT legs by 60% (O'Connor 1989) and both epiphyseal and metaphyseal trabecular bone loss occurred in ACLT legs (Intema 2010). Weight bearing, however, was not affected in a canine trauma model and trabecular bone loss did not occur. Both canine ACLT and trauma models exhibited progressive cartilage degeneration and subchondral plate thinning (Intema 2010). This highlights the difference between bone changes in the subchondral plate and trabecular bone. Changes in weight bearing seem to affect the trabecular bone more than the subchondral plate. However, because subchondral plate thinning is seen even when weight-bearing is unaffected, such as in the canine groove and trauma models (Mastbergen 2008; Intema 2010), factors other than mechanical load must contribute to bone resorption. Thinning of the subchondral bone may contribute to cartilage degeneration by decreasing mechanical support for the cartilage (Dedrick 1993; Behets 2004) or increasing perfusion of biochemical factors from the bone to the cartilage (Intema 2010).

Not all surgical animal models of OA demonstrate bone resorption. For example, DMM in the mouse, guinea pig meniscectomy (subchondral plate only) and guinea pig gluteal myectomy all demonstrate increased bone formation with progression or onset of OA (Layton 1988; Pastoureau 2003; McErlain 2008; Botter 2009). Spontaneous OA models, such as the DH guinea pig and STR/oRT mouse also exhibit increased bone formation with no evidence of resorption (Anderson-MacKenzie 2005; Tomoya 2007; Stok 2009c). It is possible that resorption occurs in spontaneous models but is difficult to observe because of variable timing of OA onset. A more likely explanation is that spontaneous models do not result in limb unweighting to the extent of surgical models.

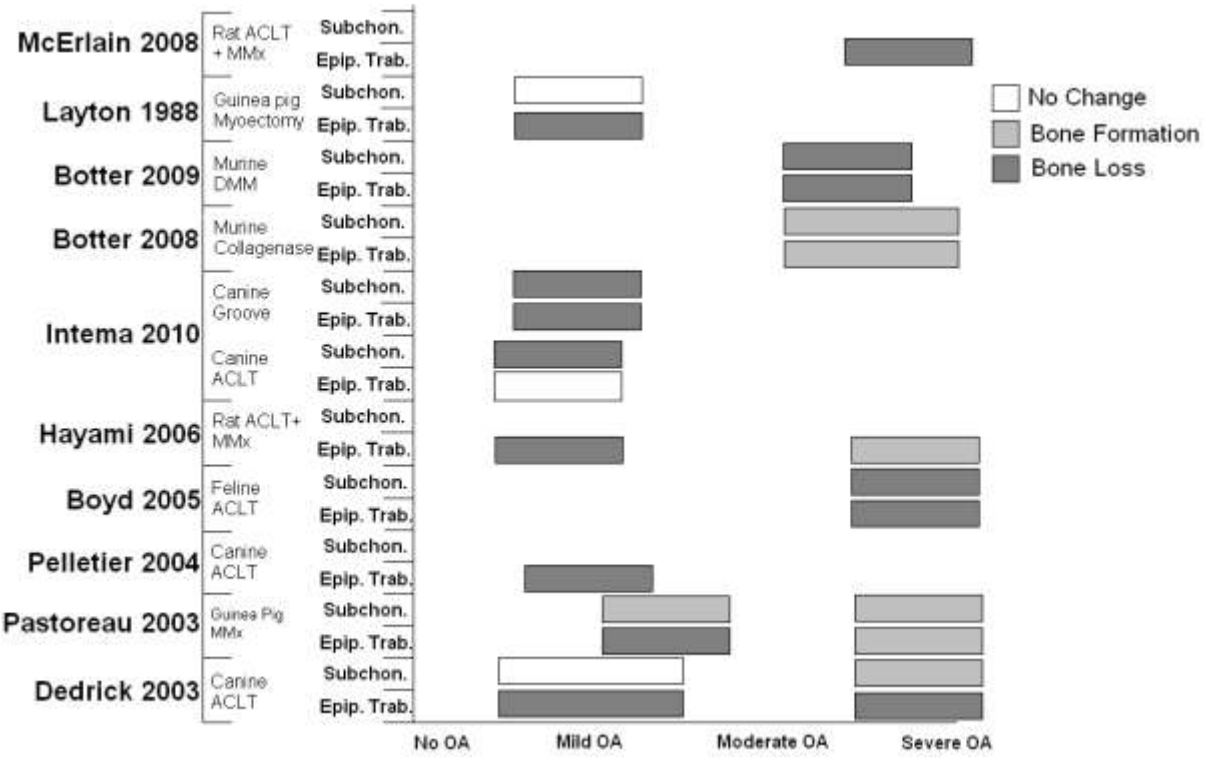

Figure 4-1. Chart of bone responses in OA models.

Despite a large number of OA investigations using murine models for OA research, there are few studies that examine bone changes in murine OA (Kamekura 2005; Botter 2006; Botter 2008; Kadri 2008; Botter 2009; Stok 2009c), and only two investigating bone changes in the DMM model (Kadri 2008; Botter et al. 2009). In one of these studies, histological methods were used to measure bone changes six weeks postoperatively, finding a reduction of epiphyseal bone and thinning of the subchondral plate (Kadri 2008). Another study using micro-CT, and different time points found no significant changes of trabecular parameters in the epiphyseal bone (Botter 2009). No studies have examined the early stage bone changes in the DMM model.

I hypothesise that bone changes occur early in the DMM model and before structural changes can be measured, an increase in bone cell activity will be evident. Micro-CT, CSLM and histological thin sections are used to detect structural and histological changes. CSLM and micro-CT operate at the micro scale and only image one phase within the tissue (collagen matrix in cartilage and mineral

phase in bone, respectively). These techniques provide only morphological information. An increase of osteoid, for example, which indicates increased turnover, would be neglected by micro-CT. Histological techniques allow the measurement of pre-structural changes, such as the ratio of osteoid to mineralised bone. Herein all three techniques were combined to provide a thorough analysis of early bone changes in the murine tibia two weeks after DMM surgery.

4.2 Methods

4.2.1 Surgical Induction of OA

All procedures were performed with institutional ethical approval. Ten male mice (C57Bl6, Harlan, UK) aged twelve weeks, underwent DMM surgery of the right limb, and five mice underwent a sham surgery on the right leg. Surgery was performed by an experienced technician (Kennedy Institute of Rheumatology, Imperial College, London, UK). The technician was different to the one used in Chapter 3. For this study the surgical procedure was consistent with the DMM model (Glasson 2007).

4.2.2 Calcein Labelling

Calcein was dissolved into a saline solution with sodium bicarbonate on a magnetic stirrer until completely dissolved. The calcein saline solution was filter sterilised prior to use. Mice received a dose of 30 mg/kg via intra peritoneal injection. Mice were injected three and six days before culling. The mice were sacrificed two weeks after surgery.

4.2.3 Micro-CT Analysis

All mice tibiae underwent micro-CT bone analysis. The tibiae were imaged using micro-CT, set at 135 kVp and 160 µA (XT H 225, X-Tek, Hertfordshire, UK). The tibiae were scanned with an isotropic voxel

size of 9 µm. A region of interest (ROI) was identified on the medial tibial plateau only. The lateral plateau was not examined because the previous study found no changes on the lateral tibia at later time points, and other studies suggest that significant changes occur in the medial plateau (Botter 2009). The ROI was defined using the same method as described in section 3.3.3. Consistent fractions of the breadth and width of the tibial plateau were found, omitting any artificial increase in breadth and width due to osteophytes. Epiphyseal trabecular bone and subchondral bone were identified within the ROIs, using ImageJ3dViewer (Schmid 2007). A threshold was applied using the Otsu method (Otsu 1975). Average subchondral plate thickness was measured using BoneJ (Doube M 2010). In the epiphyseal trabecular bone, trabecular thickness (Tb.Th), spacing (Tb.Sp) and bone volume/total volume (BV/TV) were calculated using BoneJ. The DMM limb was compared to the contralateral limb using a Student's t-test. All data conformed to a Gaussian distribution assessed by Levene's test.

4.2.4 Confocal Microscopy

All mice tibiae underwent CSLM. Confocal microscopy was performed consistent with the method used in section 3.2.4. However the Z-stack spacing was decreased from 5.8 µm to 3.03 µm. The previous study used isotropic voxels of 5.8 µm to ensure scans were comparable with other published work (Stok 2009a). In this study the Z-stack spacing was reduced to 3.03 µm to improve image quality and reduce post processing.

4.2.5 Histological Techniques

After micro-CT and confocal scanning, soft tissue was removed from all samples and fixed overnight in formalin. Samples were dehydrated in graded ethanols and embedded in pMMA (Appendix F). Micro-CT data and visual inspection of five tibiae from a previous study revealed that the angle between the sagittal plane and a plane formed from the tibial cranial crest, the lateral tubercle

(Gerdy's tubercle in humans) and the distal tibia was 32°. Embedded samples were placed on a diamond saw (Buehler IsoMet low speed saw, Illinois, USA) and a 32° section cut away from the previously described plane, to produce a flat face parallel with the sagittal plane, this ensured future microtome cuts were parallel with the sagittal plane. Samples were ground and polished (Beuhler Alpha twin wheel grinder-polisher). Using a microtome (tungsten-carbide knife, Leica, Germany), sections of 4 µm thickness were cut in the sagittal plane (SP2265 Leica, Germany). Three sections were taken at six locations across the tibial plateau (Figure 4-2). Sections were mounted on microscope slides and stained with either toluidine blue, safranin O or left unstained for observance of calcein labels. A protective cover slip was placed over all sections and adhered with DePex solution.

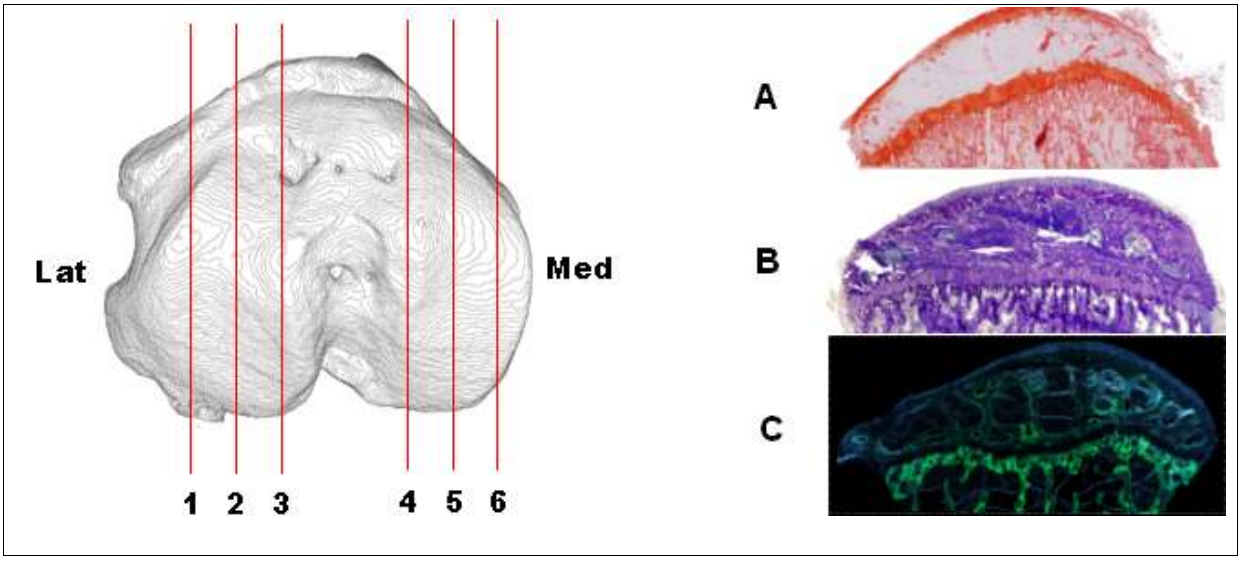

Figure 4-2. Locations of histological sections. At each location, three sections were obtained and stained for Safranin O (A), Toluidine Blue (B) and unstained for fluorescent imaging of calcein (C).

Sections were viewed using an Olympus BX 51m Microscope (Olympus, Japan) an X-Cite 120Q fluorescent lamp (Lumen Dynamics Group, Canada), DP-BSW Controller software (Olympus, Japan) and a 20x objective. Sections stained with safranin O and toluidine blue were viewed in light field mode, unstained sections were viewed using the fluorescent lamp. Multiple high resolution images

across each section were made (with approx 25% overlap), and stitched with Adobe Photoshop CS5, to form one high resolution image for each section.

Unstained fluorescent images were converted into HSL (Hue, Saturation and Luminance) colour space using ImageJ. This enabled a colour threshold to be applied to the frequency associated with fluorescent calcein labels. With the chosen microscope filter, calcein fluoresced green (approx 530 nm, whereas bone auto-fluoresced blue (approx 430 nm), HSL colour space places blue and green further apart in the colour domain than with other colour spaces, allowing the two colours to be easily separated for thresholding (Figure 4-3). Calcein labelled bone bordering a marrow space was defined as a mineralising surface. A ratio of mineralising surface against total bone surface was calculated (MS/BS). Osteoid was identified on toluidine blue stained slides and normalised against bone surface (OS/BS). Both measures were performed in ImageJ software and where possible conformed to the standards defined by Parfitt (Parfitt 1988).

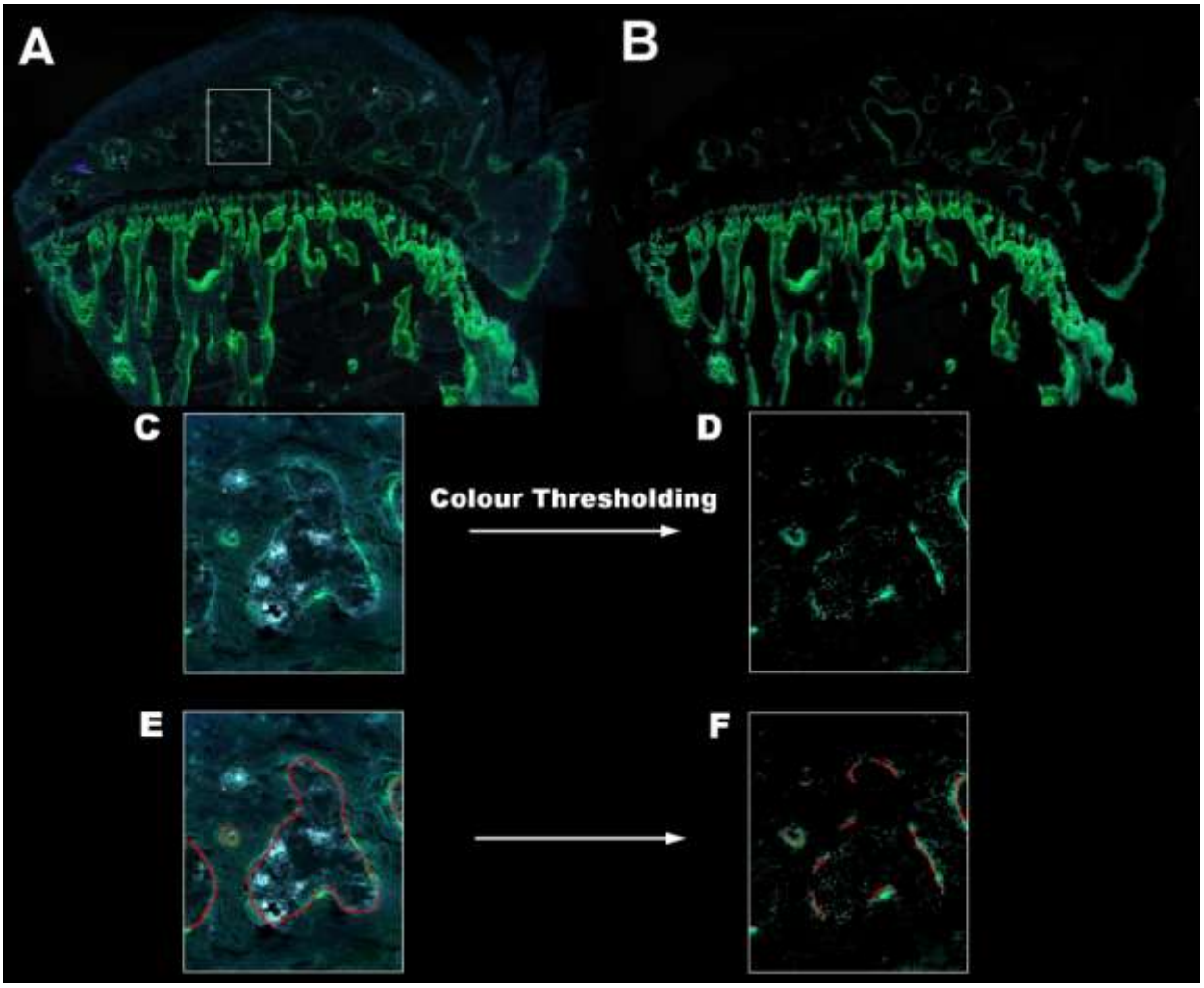

Figure 4-3. A) Example of calcein labelled section. B) Colour thresholded calcein labelled section. C) Enlarged section of epiphyseal bone. D) Colour Threshold applied. E) Red denotes bone surface. F) Red denotes mineralised surface.

Safranin O stained sections were scored by an independent assessor. The severity of joint damage was assessed using a simple scoring system based on the system first described by Chambers et al. and later modified by Glasson et al. (Chambers 1997; Glasson 2005). The cartilage damage was graded using a validated 6-point scoring system (Figure 4-4):

0. Healthy cartilage.
1. Superficial fibrillations only.
2. Minor fibrillations with delamination of superficial layer but no ulceration.
3. Ulceration of superficial, non-calcified cartilage only, less than 20% overall cartilage loss.

4. Major fibrillations down to calcified cartilage and/or bone.
5. Major ulceration involving calcified cartilage layer, <80% overall cartilage loss.
6. Major ulceration with >80% cartilage loss.

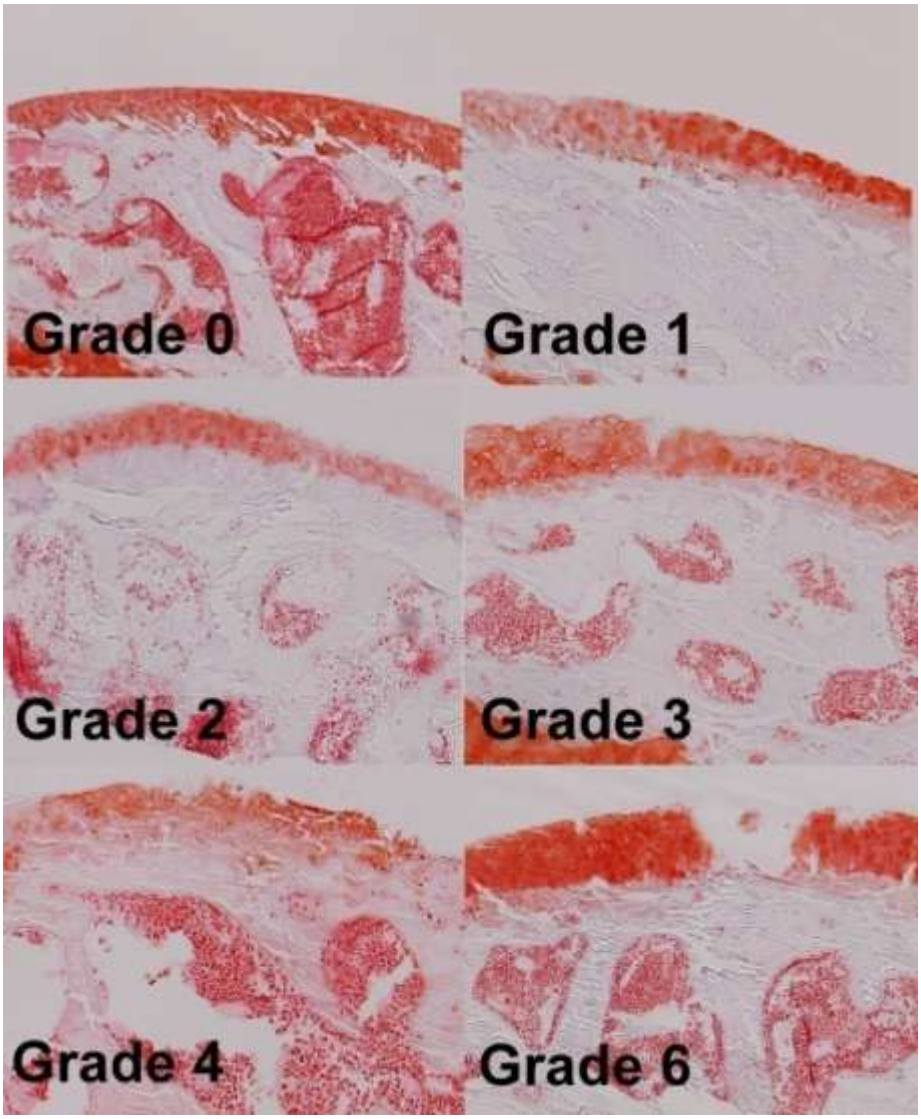

Figure 4-4. Examples of cartilage scoring grades. Images are taken from non-decalcified sagittal sections of the medial compartment of the hind knee, stained with Safranin O. sections were produced as part of this thesis (Original magnification 200x).

4.3 Results

4.2.1 Micro-CT and CSLM Results

On inspection of bone reconstructions, there were no extreme bone changes resembling those seen in Chapter 3. There was no sign of bone loss or formation on the posterior plateau. Small osteophytes were present on the periphery of the medial plateau (Figure 4-5), and were more of an extension of the plateau than nodules found in human OA.

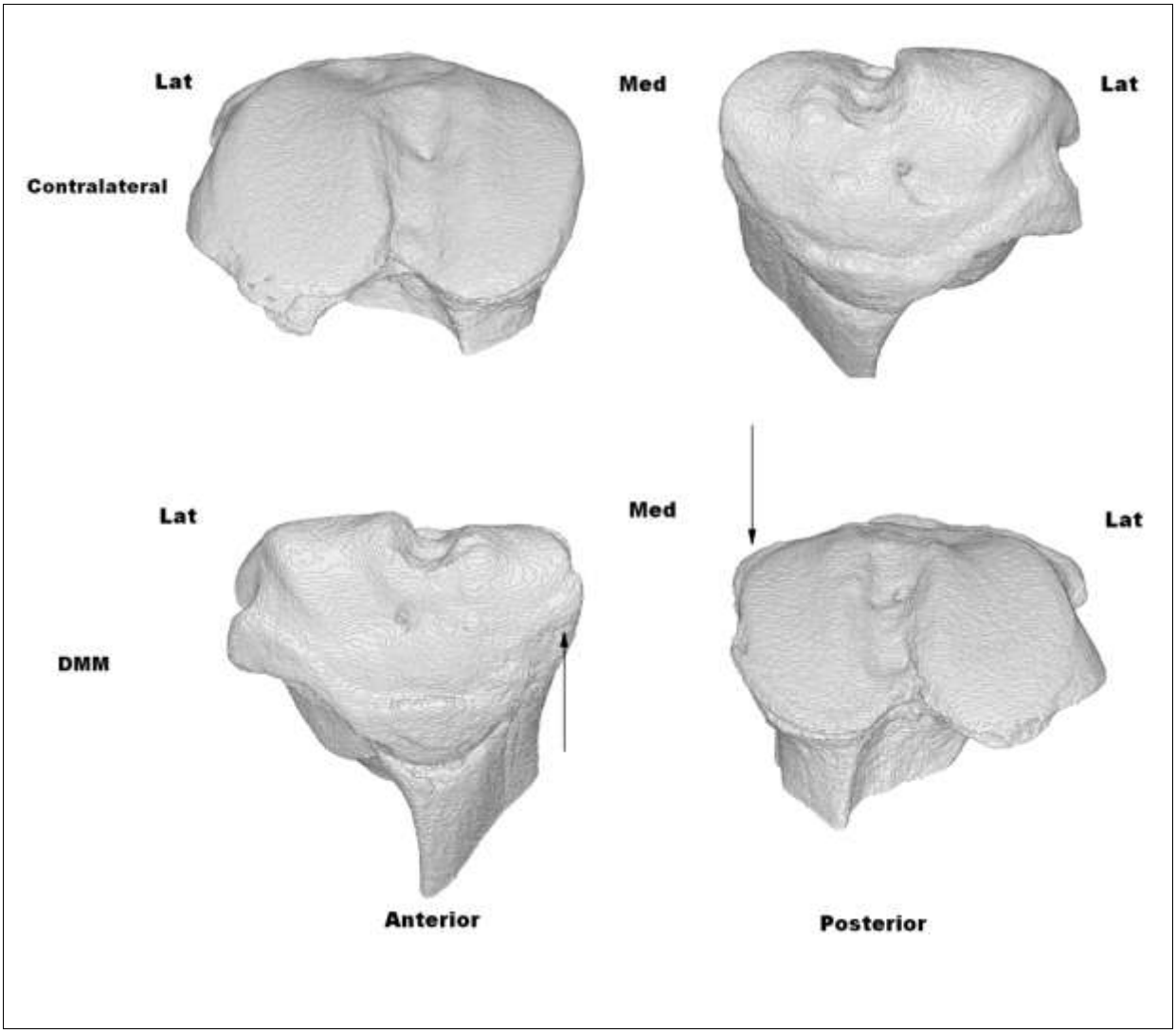

Figure 4-5. 3D reconstruction of tibia from the contralateral (left) leg and DMM (right) leg of C57Bl/6 mice at 2 weeks post operatively. Osteophyte labelled with arrows.

Tomograms from the central tibia suggest the volume of trabecular bone is increasing in the medial epiphyseal compartment on DMM affected legs (Figure 4-6A). Tomograms also display structure of osteophyte on medial plateau (Figure 4-6B).

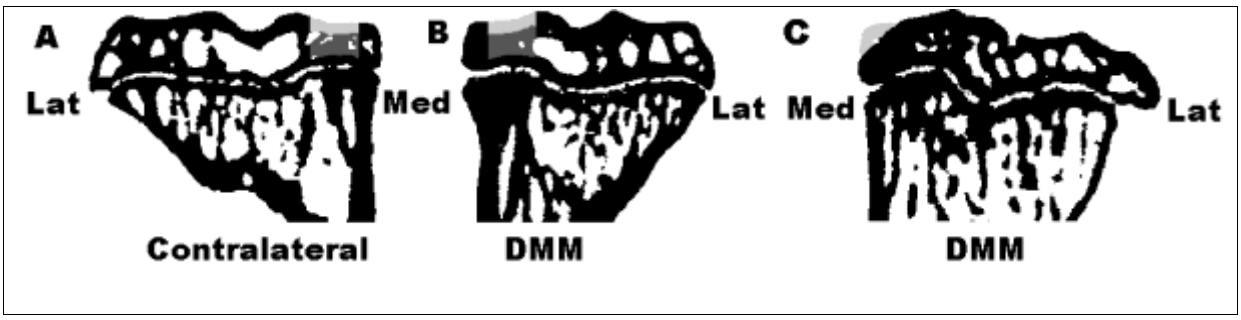

Figure 4-6. Coronal tomogram of tibia from: A contralateral (left) and B DMM (right) legs. Light grey represents subchondral bone ROI and dark grey represents epiphyseal ROI. Tomograms approximately through the tibia centre. C) Coronal tomogram displaying osteophyte structure on medial plateau of DMM leg. Osteophyte is coloured grey.

Two weeks after DMM surgery, there was a no significant difference of subchondral bone plate thickness or bone volume fraction (BV/TV). There was, however, a significant decrease in trabecular spacing in the DMM limb (Table 4-1).

	Left (contralateral) leg n = 10	Right (DMM) leg n = 10	Percent Change	p
BV mm^3	0.041 ±0 .033	0.031 ± 0.010	-23.5	ns
TV mm^3	0.199 ± 0.044	0.134 ± 0.030	-32.5	ns
BV/TV	0.203 ± 0.068	0.229 ± 0.065	12.8	ns
Tb.Th mm	0.069 ± 0.017	0.059 ± 0.015	-13.9	ns
Tb.Sp mm	0.417 ± 0.107	0.319 ± 0.105	-23.5	0.036
Sb.Pl.Th mm	0.144 ± 0.028	0.125 ± 0.011	-13.5	ns
Cartilage Volume mm^3	0.009 ± 0.002	0.008 ± 0.002	-2.1	ns

Table 4-1. Cartilage and micro-CT results, parameter means ± SEM. Significance (p) compares contralateral to DMM leg, $p \leq 0.05$ is considered significant. Sb.Pl.Th is subchondral bone plate thickness, Tb.Th is trabecular thickness, Tb.Sp is trabecular spacing, BV/TV is bone volume / total volume. n = 10.

CSLM quantification of cartilage volume produced no significant difference between DMM and contralateral legs. The 3D cartilage reconstructions revealed no full thickness defects (Figure 4-7). The thickness of reconstructed cartilage appeared approximately uniform across each plateau.

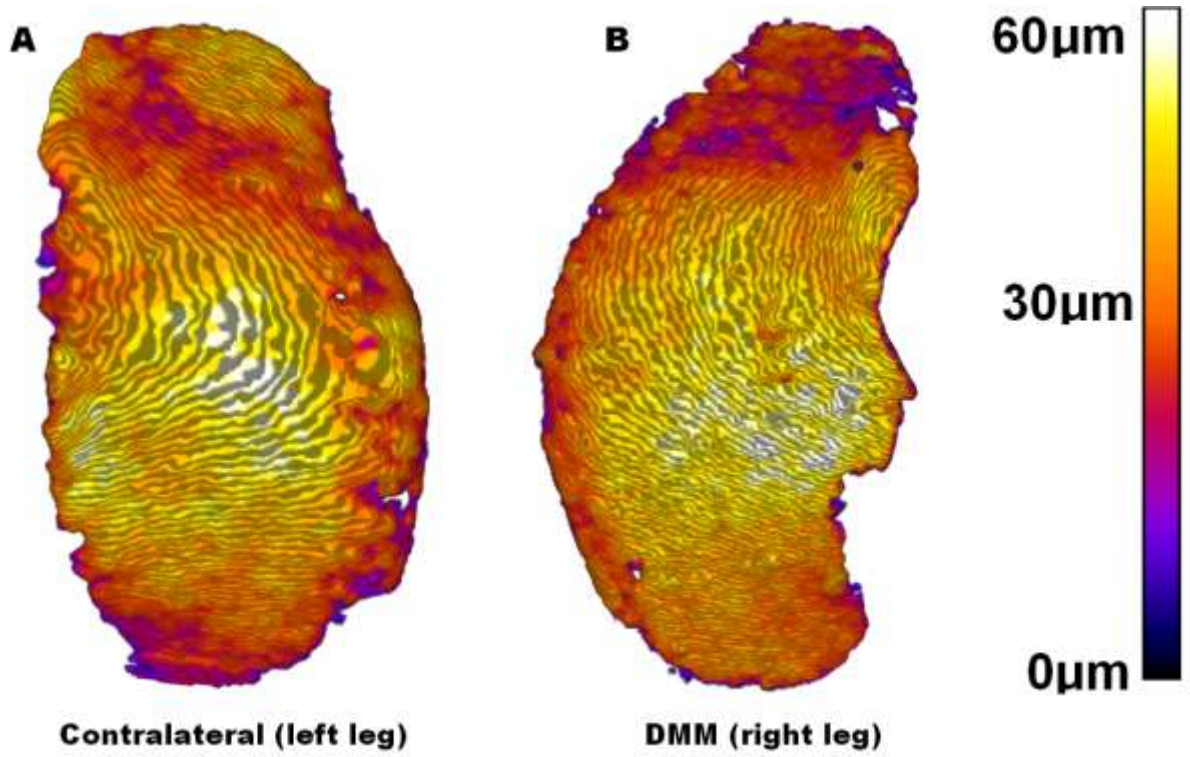

Figure 4-7. Example 3D CSLM reconstructions of cartilage from the medial tibial plateaus from: A Contralateral (left) leg, B DMM (right) leg.

4.2.2 Histology Results

Calcein fluorescence on epiphyseal bone was less intense and less extensive than in the metaphysis. In the epiphysis, calcein was exclusively deposited on bone surfaces adjacent to epiphyseal spaces. There was no calcein labelling in the subchondral plate or in the calcified cartilage. The ratio of mineralised surface to bone surface was greater in the DMM affected leg compared to the contralateral leg (Figure 4-8, Table 4-2). Note MS/BS failed Levene's equal variances, analysed by t-test equal variances not assumed.

Toluidine blue stained sections indicated little difference between DMM and contralateral legs on visual inspection, and no major morphological bone changes similar to those seen in Chapter 3. The DMM leg had a weakly significant increase of osteoid to bone surface ratio.

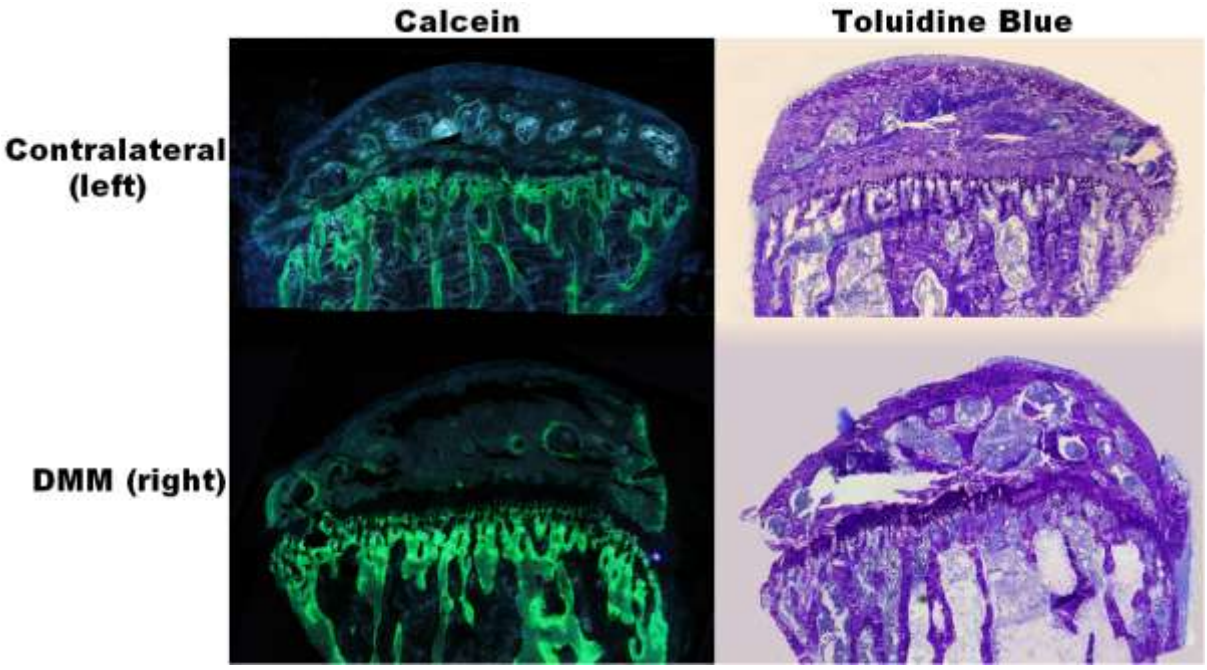

Figure 4-8. Example calcein and toluidine blue staining of the proximal tibia, sectioned in the sagittal plane. Tibia width is approx 2.5mm. Composite images are formed from multiple images made with × 20 magnifications.

	Left (contralateral) leg n = 5	Right (DMM) leg n = 5	Percent Change	p
MS/BS	0.226 ± 0.090	0.349 ± 0.121	+54.4	0.045
OS/BS	0.083 ± 0.032	0.132 ± 0.044	+59.0	0.050

Table 4-2. Histology results. Significance (p) compares contralateral to DMM leg, $p \leq 0.05$ is considered significant. MS/BS is Mineralised Surface/Bone Surface.

Scoring of safranin O stained cartilage produced an average score of 1 in the contralateral leg (n = 3), and 2.6 for the DMM leg (n = 7) indicating mild OA. The cutting of pMMA embedded tibia frequently damaged the cartilage, due to a difference of stiffness between the two substances. Only 25% of the total numbers of sections made were acceptable for scoring. However, the process of scoring did

allow identification of clefts, fibrillation and proteoglycan loss that were attributed to pathological changes rather than cutting artefact (Figure 4-9).

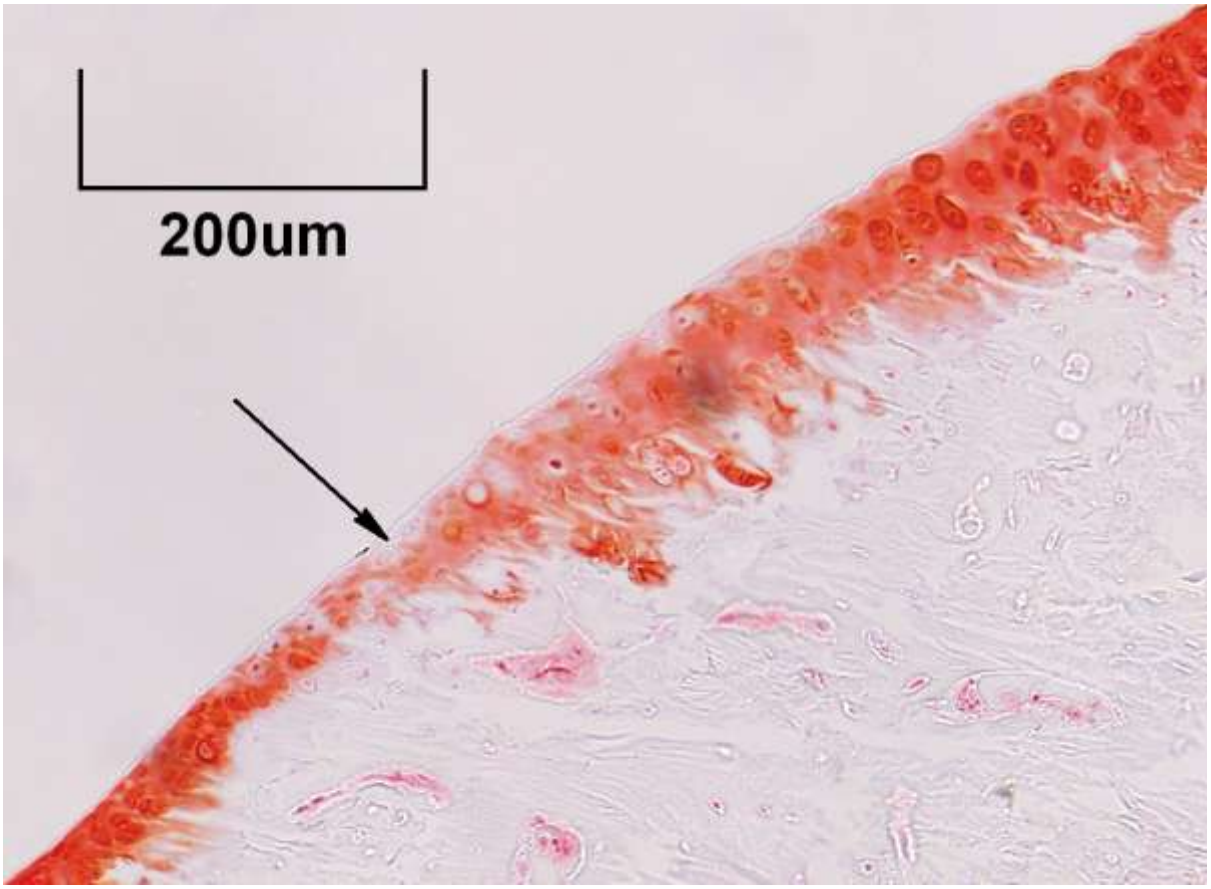

Figure 4-9. Example of thin section of cartilage, stained with safranin O from the medial plateau of a DMM (right) leg. Cartilage on the medial plateau of DMM legs exhibit regions of degeneration associated with OA, in this example the arrow denotes proteoglycan loss.

4.3 Discussion

4.3.1 Changes in Bone

Two weeks after DMM surgery a significant decrease of trabecular bone spacing had occurred in the tibial medial plateau and small osteophyte growth was visible (but unquantified) on 3D micro-CT reconstructions, there was no significant change in any other bone parameter. This suggests that as early as two weeks postoperatively the DMM mouse may be exhibiting some mild trabecular

resorption. However, significant increases of osteoid surface and mineralising surface indicated that at the cellular level, new bone was being formed.

Neither histology nor micro-CT indicated that early stage bone loss occurred in the DMM model two weeks post operatively. In a larger species (ACLT rat model), early stage resorption was present at the same time point (two weeks after surgery) (Hayami 2006). Early stage bone resorption in the DMM model cannot be ruled out as bone turnover is rapid in the C57Bl/6 mouse. It is possible that if early stage bone resorption had occurred, it could have occurred prior to the two week time point. Previous studies using the DMM model have found a reduction of weight bearing occurs 0-1 days after surgery, and restores to 77% of normal loading three days after surgery (Chia 2007). If unweighting is the cause of trabecular resorption, then resorption might occur in this brief period. Osteoclast activity was not assessed as TRAP staining was not used, therefore, the presence of resorption was not properly assessed in this study.

Botter et al. (Botter 2009) investigated bone changes in the DMM model eight weeks post operatively in C57Bl/6 mice. They found an increase of subchondral bone plate thickness, representing subchondral sclerosis. Coronal tomograms of the DMM and control tibia are reproduced in Figure 4-10, similarities between these and the tomograms in Figure 4-6 are immediately apparent, despite Botter et al. culling a further four weeks after DMM surgery.

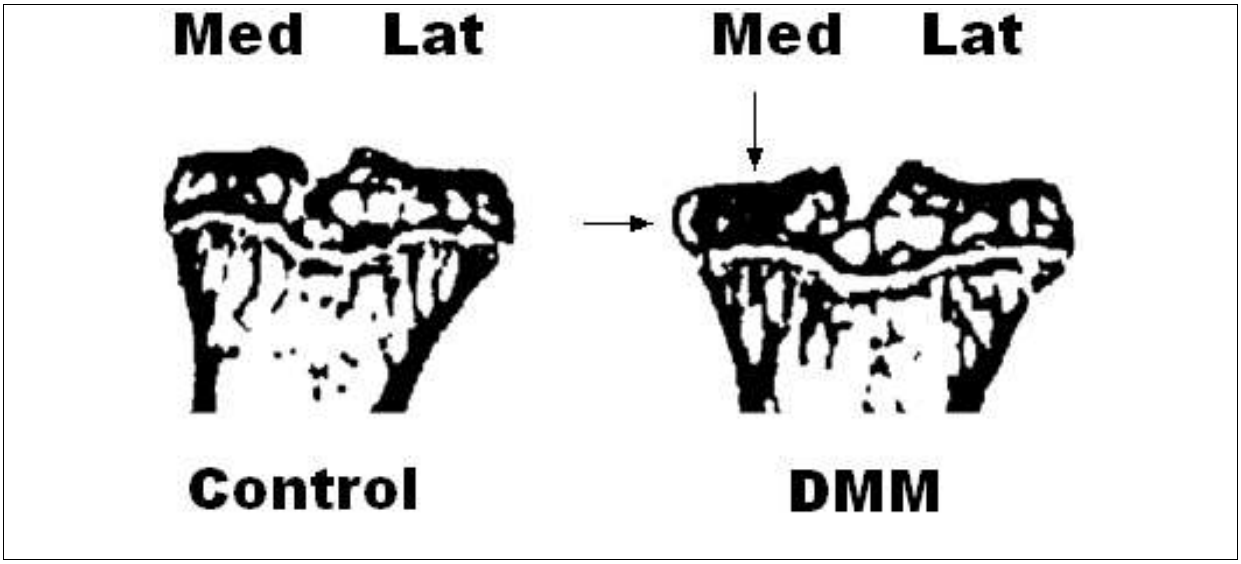

Figure 4-10. Representative tomogram from wild type C57Bl/6 tibia 8 weeks after surgery, from Botter et al (Botter 2009). Arrows label subchondral sclerosis and osteophyte formation.

Botter et al. did not report a significant increase of BV/TV in the medial epiphysis, despite an apparent increase as shown in Figure 4-10. This may result from a failure of the methodology to distinguish accurately between bone of the epiphysis and subchondral plate. As bone volume in the epiphysis increases it becomes difficult to distinguish between trabeculae and cortical bone, leading to errors in ROI selection. Bias will always be given when selecting one bone region from the other; in the case of Botter et al, this may have been in favour of the subchondral plate (at the expense of epiphyseal BV/TV). The method used in this study was performed manually, using predefined selection criteria based on morphology; this has the potential to be equally biased when selecting regions. The tibiae were investigated two weeks post operatively, producing less extensive bone changes, consequently distinguishing between subchondral plate and epiphyseal bone was less problematic. Kadri et al. (Kadri 2008) found bone changes that were contradictory to both Botter et al. and those found in this study. They used the same model and mouse strain but sacrificed six weeks time post operatively, using histological thin sections to examine bone morphology. Kadri et al. found a decrease of epiphyseal BV/TV, suggesting trabecular resorption had occurred. The number of thin sections and ROI used for analysis were not described: it is possible the tibia were

under sampled. The erroneous DMM surgery used in Chapter 3 produced a significant decrease of BV/TV similar to Kadri et al. it is plausible that unwanted ACL damage in the DMM model may have effected Kadri's results, as ligament integrity was not assessed in their study.

4.2.1 Changes in cartilage

There were no significant changes in cartilage thickness when measured by CSLM, however, histological sections indicated regions of cartilage damage. The early stages of cartilage degeneration involve the loss of proteoglycan from the cartilage matrix. CSLM detects auto fluorescence from collagen fibres in cartilage matrix. The early loss of proteoglycan may have no effect on the collagen fibres, and therefore the fluorescence may be unchanged in early stage OA. As OA progresses, fibrillation (followed by lesions) of the cartilage surface occurs, these features are of the order of approximately 2 - 20 μm wide. The image resolution for confocal microscopy in this application is 3.03 μm making the resolution too low to detect small fibrillations. In the previous study CSLM microscopy was effective in mapping full thickness cartilage loss. This study indicated that the resolution of CSLM limits the utility in detecting early damage.

CSLM was unable to detect early stage cartilage changes and traditional histological scoring was limited due to the difficulty in maintaining cartilage in mineralised histology. No reliable cartilage analysis was available to identify the stage of degeneration in the DMM tibia. It is known that at two weeks after DMM surgery, C57Bl/6 had mild OA as assessed by histological scoring (Chia 2007). Evidence of cartilage damage on my histological sections indicates that degeneration has begun at two weeks. It can therefore be assumed that the cartilage damage seen resembles mild OA at this time point. However, the lack of accurate cartilage scoring prevents us from defining precisely the state of cartilage degeneration, making it difficult to compare with bone changes.

Cartilage and bone in osteoarthritic joints experience increasing levels of degeneration from early to late stage of the disease (Buckwalter 1995; Hayami 2006). These time dependent tissue changes

present opportunities and also problems for therapeutic interventions. Different treatments will have different efficacies when applied at different stages of degeneration. For example, alendronate (a bisphosphonate that inhibits bone resorption) had a chondroprotective effect when administered to ACLT rats after surgery (Hayami 2004). The nature of early stage bone resorption in OA may have a significant effect on therapies that target bone changes, and could partially explain the varied outcomes seen with such treatments. In order to effectively investigate therapeutic effects in animal models it is important to have prior knowledge of the sequence and timing of tissue changes in that model. This study helps to provide this by establishing that two weeks after DMM surgery there was an observable increase of epiphyseal bone.

5. Mouse Strain Differences and its effect on the DMM model

5.1 Effects of Subchondral Bone Structure on OA

Patients with OA have higher BMD at sites remote from the effected joint (e.g. in the vertebrae with hip OA) (Dieppe 1993; Dequeker 1995; Nevitt 1995; Dequeker 1997; Goker 2000; Bruyere 2003). This introduces the possibility that those with naturally higher BMD are at greater risk of OA. It is likely that those with increased BMD have higher subchondral stiffness prior to pathology (Ferretti 1996; Boivin 2000; Ong 2000; Follet 2004). Epidemiological studies found an increase of OA in African Americans compared to Caucasians (Nelson 2010, Braga 2009), African Americans typically have a higher BMD (Henry 2000; Finkelstein 2002) providing further evidence for a link between subchondral stiffness and OA. Aside from epidemiological studies there is limited direct evidence between the two. Studies have injected pMMA into the epiphysis to increase subchondral stiffness, which typically resulted in OA (Lu 2010). There is however, some doubt over these results because a calcium phosphate substitute for pMMA, which has a similar modulus but is histologically superior to pMMA, does not induce degeneration. This suggests that the pMMA induced-degeneration arose from histological factors (possibly thermal necrosis) rather than mechanical factors (Hisatome 2002).

Twenty years ago it was proposed that changes in the subchondral bone initiated cartilage damage. The hypothesis was that non-uniform changes in subchondral bone architecture create regions of differing stiffness with habitually loaded area of subchondral bone stiffer than peripheral bone. The stiffness gradient at these regions results in increased shear stress in the cartilage, causing cartilage fibrillation (Radin 1986). Finite element analysis suggested increased bone stiffness does increase shear stress in the cartilage (Brown 1984).

Instability models alter the force distribution across an articular surface. The subchondral bone protects cartilage by deforming to attenuate loads to a greater extent than the overlying cartilage (Radin 1970; Burr 2004). An articular joint with a thinner subchondral plate or lower BMD will experience larger subchondral strains induced by the new loading pattern. Bone mechanoadaptation

is strain driven (Duncan 1995), so joints with lower BMD would produce a greater or more rapid response in bone, or respond at a lower load threshold. Joint surfaces in non-pathologic bones respond to gradually increased exercise by increasing the thickness of the cartilage, calcified cartilage and subchondral bone plate (Oettmeier 1992). However, this process does not occur when loading changes in instability induced OA; instead a pathologic bone response occurs. A possible early stage bone resorption takes place in the trabecular and subchondral plate (Dedrick 1993; Wohl 2001; Behets 2004). Then towards the later stages of OA the subchondral plate and trabeculae increase in volume, prior to cartilage loss (Carlson 1996; Buckland Wright 2000; Buckland Wright 2004). At this point there is an increase of bone turnover (Seibel 1989; Sowers 1991; Mansell 1998; Li 1999; Pacicca 2003), and rapid bone changes occur, producing hypomineralised woven bone (Grynpas 1991; Zysset 1994; Mansell 1998; Bailey 2004). This causes the bone tissue to become less stiff, with increased porosity, reduced matrix density and reduced stiffness (Grynpas 1991; Li 1997a; Li 1997b). These changes in bone quality may cause the increase of bone volume (subchondral sclerosis) as a failed attempt to restore stiffness (Burr 2004). It is hypothesised that this reduced stiffness results in increased deformation of the subchondral bone plate, which increases shear stresses in the cartilage, contributing to its degeneration (Manicourt 2005).

Presumably, for the reasons mentioned previously, a joint with low BMD would be less stiff and more susceptible to mechanical driving factors associated with instability induced OA. This is at odds with the hypothesis proposed by Radin in 1986 (Radin 1986) and evidence derived from epidemiological studies, namely, high BMD as a risk factor for OA. One experimental study supports this idea, in which guinea pigs with a thinner subchondral bone plate actually had a higher incidence of OA than those with a thicker subchondral bone plate (Tomoya 2007). The role of subchondral stiffness in OA is unclear. It seems increased BMD predisposes to OA, yet in early stage OA there are bone changes that reduce bone volume (and therefore stiffness) and late stage material changes that reduce subchondral stiffness. There is no direct evidence that links the thickness or stiffness of subchondral bone to OA.

In the following study bone changes of similarly sized mouse strains with different BMD and subchondral thickness prior to pathology are compared, to determine how initial structure affects subchondral bone response to OA.

Different mice strains have different skeletal bone mineral densities. The C57Bl/6 is amongst the lowest; C3H/HeJ is usually reported as having the highest; and the BALB/c is closer to the C3H/HeJ (Beamer 1996). Ignoring the effects of bone morphology, the BALB/c mouse has a higher degree of mineralisation than the C57Bl/6. Externally the C56Bl/6 and the BALB/c femur length and femur volume are closely matched between the strains (Beamer 1996). Internally the BALB/c has 20% higher BMD than the C57Bl/6. The BALB/c also has greater average trabeculae thickness and double the number of trabeculae in the femur (Judex 2002). In the epiphysis of the distal femur the BALB/c has a BV/TV of 28.4 % whereas the C57Bl/6 is 20.1 % (Judex 2004). Note that these analyses have been confined to the femur; reconstructions of C57Bl/6 and BALB/c tibia are included in Figure 5-1.

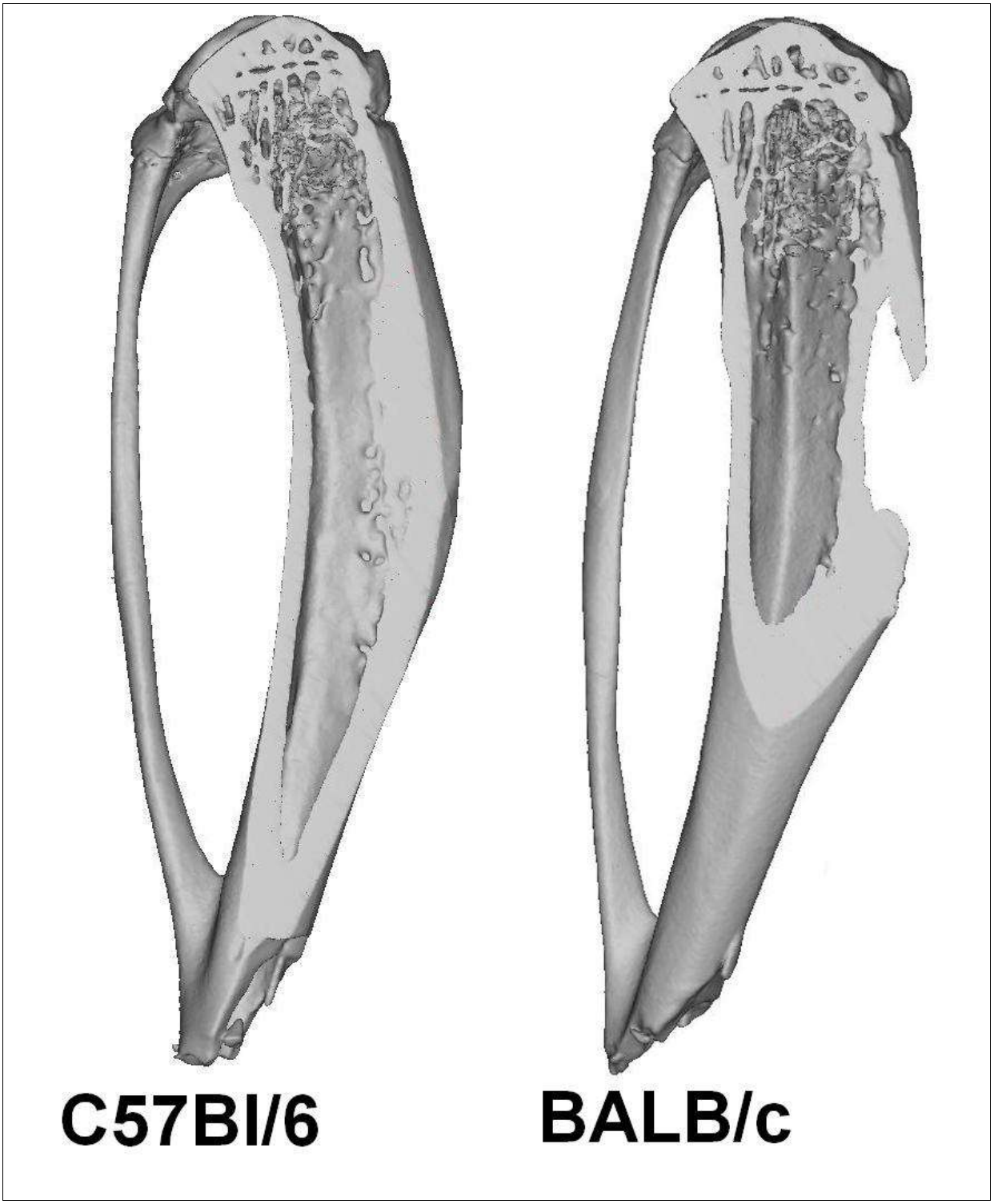

Figure 5-1. Reconstructed micro-CT images of the left tibia from a C57Bl/6 and a BALB/c mouse. Tibia are cut through the medial plateau in the sagittal plane.

Different strains also respond to mechanostimulation differently. For example C57Bl/6 responds to a vibrating plate by increasing bone formation whereas BALB/c mice do not. BALB/c increase bone

resorption rate in the femur during disuse, whereas C57Bl/6 mice do not (Judex 2002). C57Bl/6 mice have been shown to have an increased adaptive remodelling response to changes in mechanical load compared to mouse strains with higher bone mineral density (Akhter 1998; Judex 2002; Webster 2010). A genetic predisposition to low bone mass and a thinner subchondral bone plate paralleled by an enhanced sensitivity to signals anabolic to the skeleton, may contribute to differences of OA progression seen between mice strains.

The BALB/c and C57Bl/6 mice bone response to OA are compared in this study. The DMM surgical instability model used was consistent with Chapter 4 (same surgical technician). Laxity was also investigated to ensure that DMM produced similar joint instability because differences in ligament laxity have been implicated in OA (Anderson-MacKenzie 1999). Laxity was investigated immediately after surgery as well as eight weeks post operatively to investigate if OA bone changes act to stabilise the knee. Results in Chapter 4 indicated that DMM surgery in C57Bl/6 mice produced osteophyte formation at two weeks (note, this was not quantified but observed between DMM and control reconstructions). One hypothesis concerning the formation of osteophytes is that they form as a result of altered loading within the joint (Felson 2005), and that osteophytes may be a repair mechanism to stabilise the joint (Pottenger 1990).

5.2 Methods

5.2.1 Surgical Induction of OA/experimental design

Two experimental groups, comprising of 16 BALB/c and 16 C56Bl/6 mice, received DMM surgery in the right hind leg at twelve weeks of age. DMM surgery was performed by the same technician and method as in section 4.2.1 (different from Chapter 3). The mice received calcein intra peritoneally, three and six days before sacrifice by the same method outlined in section 4.2.2. Both groups of mice were sacrificed at eight weeks after surgery (twenty weeks of age). An additional group of ten BALB/c mice were culled at twelve weeks of age, and received DMM surgery in the right hind leg.

The purpose of this group was to compare initial joint laxity with the C57Bl/6 laxity group used in Chapter 3. This group did not receive calcein injections. The surgery was performed prior to establishing that the C57Bl/6 group used in Chapter 3 had probably received erroneous DMM and ACLT surgery.

5.2.2 Laxity

The same laxity testing protocol as described in 3.3.3 was used for AP and VV testing. Laxity testing was performed on ten mice from each of the three groups. In addition to anterior-posterior drawer and varus-valgus rotation tests, the VV rig was adapted to perform internal-external rotation laxity tests (Figure 5-2). A modified mounting system allowed the sample to be mounted with the long axis of the tibia concentric with the centre of rotation of the VV rig instrumented moment arm. As internal-external tests are highly sensitive to position, care was taken to ensure that the rig centre of rotation was aligned with the knee joint; the knee was accurately positioned using callipers from a reference point. The femur was free to move in the tibial axial direction to reduce artefacts from contacting articular surfaces (Figure 5-3). Maximum moments of ± 4 Nmm were slowly applied as described in section 3.2.2. All other operations of the internal-external rig were identical in usage to the VV rig.

Figure 5-2. Illustration of internal and external rotation.

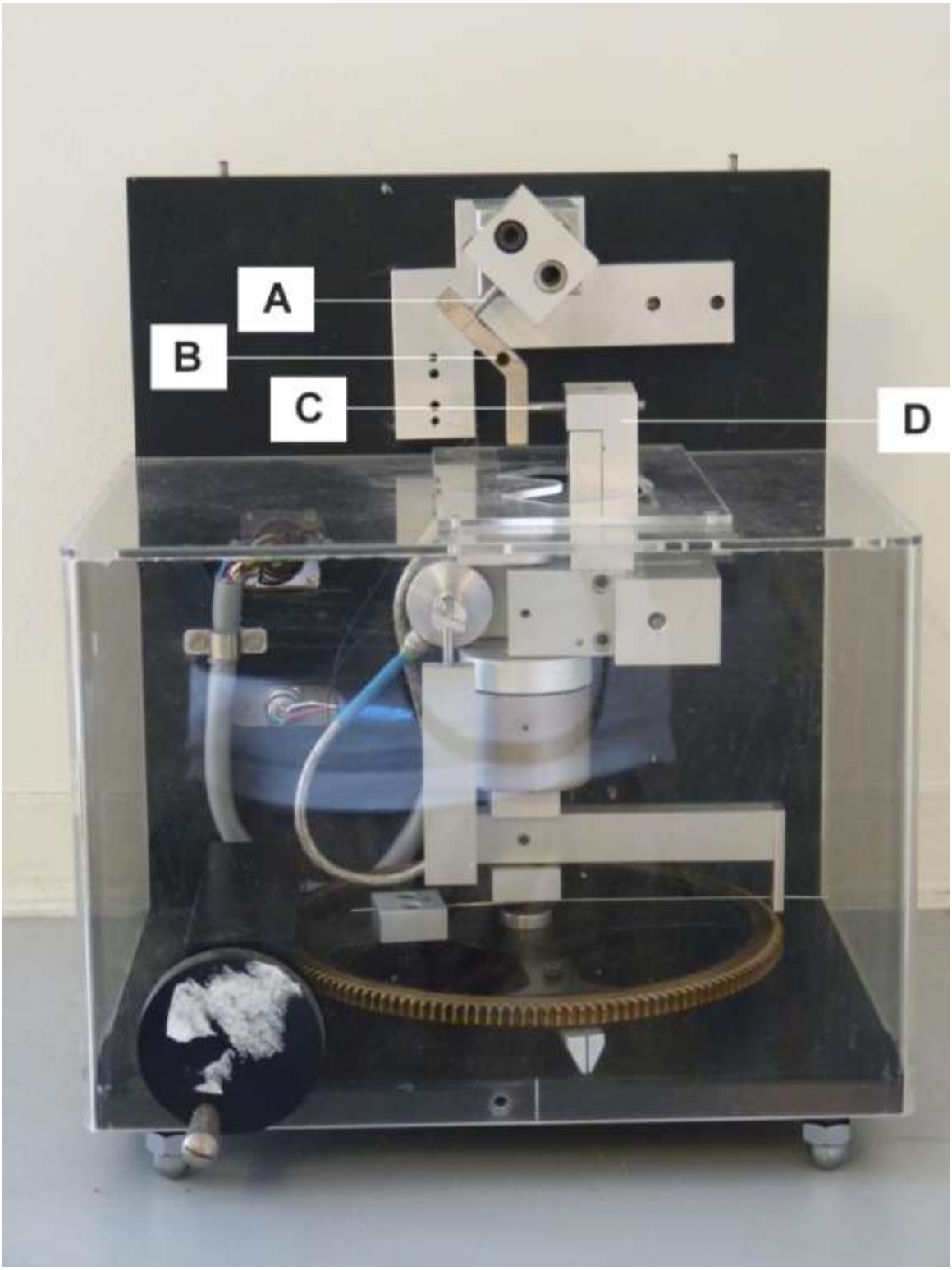

Figure 5-3. Photograph of the internal-external laxity rig. The mouse leg is potted to the steel rods labelled in A and C, with the tibia toward C and the femur toward A. B is the protective bridge that is removed prior to testing. D is the moment arm that rotates about the same axis as the tibia to apply internal and external rotation.

5.2.3 Cartilage Analysis

All tibiae from the eight week post operative groups underwent confocal scanning laser microscopy. The cartilage analysis was identical to the method in section 4.2.4. The DMM limb was compared to the contralateral limb using a two way ANOVA. All data conformed to a Gaussian distribution assessed by Levene's test.

5.2.4 Bone Analysis

All tibiae from the eight week post operative groups underwent micro-CT. The bone analysis was identical to the method outlined in section 4.2.3. Subchondral bone plate thickness (Sb.Pl.Th), trabecular thickness (Tb.Th), trabecular spacing (Tb.Sp) and bone fraction (BV/TV) were calculated. The DMM limb was compared to the contralateral limb using a two way ANOVA. All data conformed to a Gaussian distribution assessed by Levene's test.

5.2.5 Histological Analysis

The same histology method in section 4.3.5 was applied to ten of the tibiae from the eight week post operative C57Bl/6 and BALB/c groups. Osteoid area and mineralised surface were calculated as ratios of bone surface (Os/Bs and Ms/Bs). Cartilage was scored using the same method described in section 4.2.5.

The length of cartilage on safranin O stained histological sections was measured, and used to estimate location on the corresponding CSLM reconstructions from the same leg. The reconstructions were sliced (using ImageJ) to the approximate location of the histological sections. Cartilage thickness measurements were made at anterior, central and posterior locations on

histological sections, and using ImageJ, on CSLM reconstructions. These two sets of measurements were then compared to see if they correlated.

5.3 Results

5.3.1 Laxity Results

Laxity results for BALB/c mice culled prior to surgery are contained in Table 5-1.There was no significant effect of DMM surgery on any laxity parameter for the BALB/c mice culled prior to surgery. Unfortunately this dataset could not be compared to C57Bl6 mice in Chapter 3 as different surgeries were performed.

	BALB/c 0 Weeks		
	Contralateral (left) n = 10	DMM (right) n = 10	P
Anterior (mm)	0.451 ± 0.070	0.462 ±0.091	ns
Posterior (mm)	-0.426 ± 0.091	-0.444 ± 0.087	ns
AP Range (mm)	1.023 ± 0.176	1.024 ± 0.0186	ns
Varus (°)	7.792 ± 2.174	5.741 ± 1.164	ns
Valgus (°)	-7.250 ± 1.943	-9.922 ± 1.859	ns
VV Range(°)	18.000 ± 3.282	18.629 ± 2.795	ns

Table 5-1 Laxity results for BALB/c mice 0 weeks post operatively, values ± SEM.

Laxity results for the C57Bl/6 and BALB/c mice eight weeks after surgery are contained in Table 5-2. The contralateral (left) legs and DMM (right) legs were compared between strains (p value leg, listed in Table 5-2). The effect of DMM surgery on both strains was also compared by comparing values for the left and right legs (p value strain). There was no significant effect of strain for any parameters

suggesting BALB/c and C57Bl/6 share similar laxity characteristics. There was no significant effect produced by DMM surgery, suggesting that the meniscus does not provide restraint in the AP or VV directions in the murine knee.

	BALB/c 8 Weeks		C57Bl/6 8 Weeks		P	
	Contralateral (left) n = 16	DMM (right) n = 16	Contralateral (left) n = 16	DMM (right) n = 16	Leg	Strain
Anterior (mm)	0.331 ± 0.054	0.391 ± 0.110	0.404 ± 0.098	0.402 ± 0.180	ns	ns
Posterior (mm)	-0.324 ± 0.084	-0.343 ± 0.104	-0.336 ± 0.050	-0.378 ± 0.165	ns	ns
AP Range (mm)	0.715 ± 0.058†	0.841 ± 0.202†	0.846 ± 0.157	0.915 ± 0.372	ns	ns
Varus (°)	3.999 ± 0.666†	4.572 ± 2.250†	3.094 ± 1.387	3.417 ± 1.411	ns	ns
Valgus (°)	-4.600 ± 1.278†	-5.381 ± 1.671†	-4.542 ± 2.462	-5.370 ± 1.380	ns	ns
VV Range (°)	10.067 ± 1.921†	11.286 ± 3.171†	10.462 ± 5.941	10.333 ± 2.676	ns	ns

Table 5-2 Laxity result for C56Bl/6 and BALB/c 8 weeks post operatively, values ± SEM. † denotes significance between BALB/c at 0 weeks (Table 5-1) and BALB/c at 8 weeks post operatively (p≤0.005).

Anterior posterior range and all varus valgus laxity parameters exhibited a significant reduction of laxity for BALB/c mice from 0 to eight weeks postoperatively (Table 5-2). This age related reduction of laxity was seen in both the contralateral and DMM legs.

The purpose of internal-external rotation was to investigate the role of the meniscus at restricting rotation; however, it was observed that at 4 Nmm the collateral ligaments were providing the restraint, not the meniscus. Compliance curves for over half of the internal-external rotation tests had artefacts caused by tibio-femoral surface contact or meniscal restraint, which resulted in spikes on the loading curve (Figure 5-4 and Figure 5-5). Interestingly, slipping artefacts occurred in only 7% of the DMM 8 weeks (right) legs, and 77% of the contralateral (left) legs. This implies that internal-external slipping was caused by the meniscus. Therefore, it is possible that at low loads, the meniscus reduces the internal-external laxity. At higher loads, in internal-external rotation, the

collateral ligaments restrain the joint. Though these qualitative differences were evident in the laxity curves, the artefacts caused by slipping prevented any quantification of internal-external laxity.

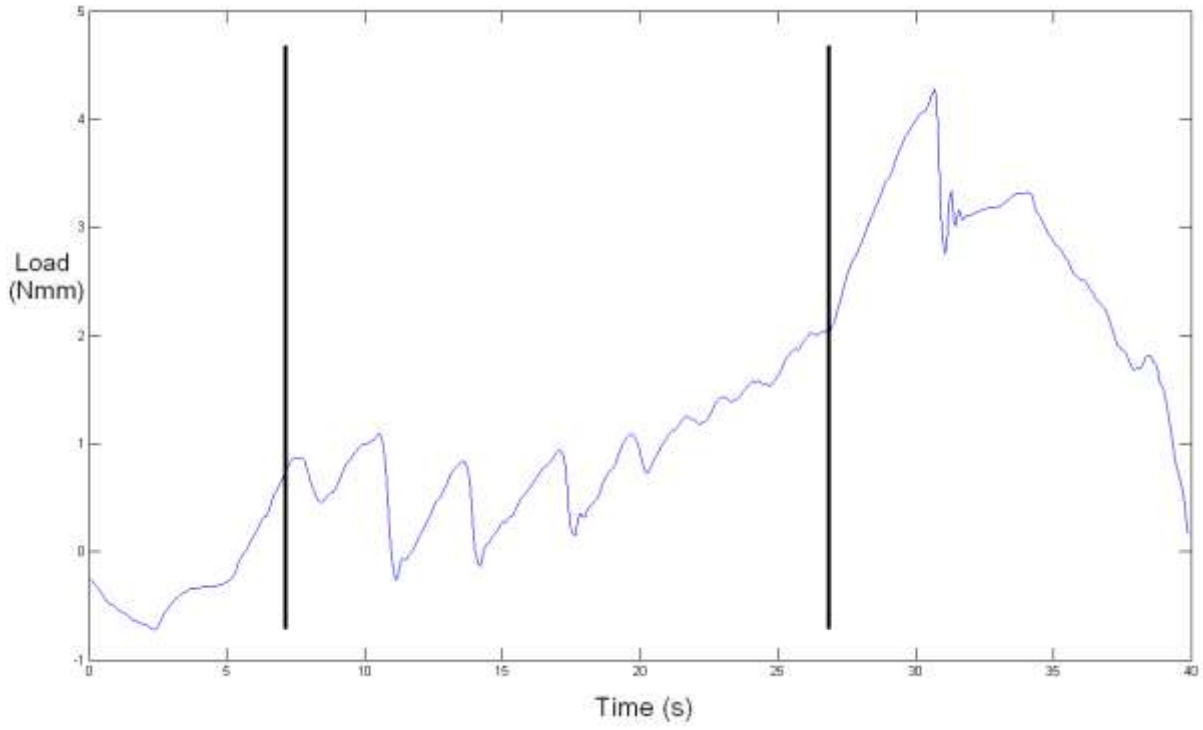

Figure 5-4. Example loading curve loading curve for internal-external rotation from a C57Bl/6 contralateral (left) leg 8 weeks post operatively. One cycle of loading from 0 – 4 – 0 N is applied over 40 seconds. The peaks caused by slipping occur between 5 and 27 seconds, whereas the smooth loading of collateral ligaments occurs between 27 and 31 seconds.

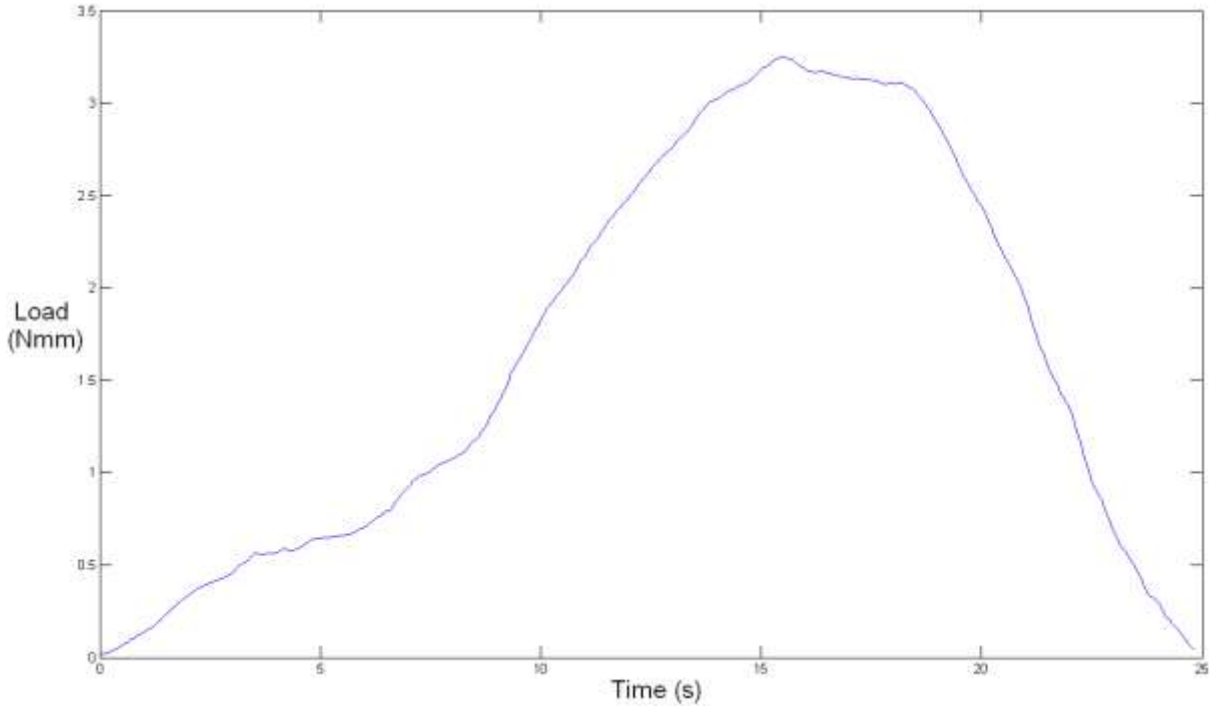

Figure 5-5. Example loading curve Loading curve for internal-external rotation from a C57Bl/6 DMM (right) leg eight weeks post operatively. One cycle of loading from 0 – 3.5 – 0 N is applied over 25 seconds. No slipping occurs.

5.3.2 Bone Analysis

Frontal tomograms suggest C57Bl/6 have a greater volume of epiphyseal trabeculae than BALB/c mice (Figure 5-6). BALB/c had taller epiphyses, producing greater ROI volume, equivalent to an increased total volume (TV) (Table 5-3). Reconstructions of BALB/c and C57Bl/6 contralateral tibiae had no major external structural differences between the strains (Figure 5-7).

As OA progressed in the DMM affected limbs, more trabecular bone formed i.e. the BV/TV increased in both strains. In the C57Bl/6 it almost formed a solid bone unit extending from the subchondral plate to the growth plate (Figure 5-8). Medial osteophytes were visible on reconstructions for DMM affected legs of both strains (Figure 5-9).

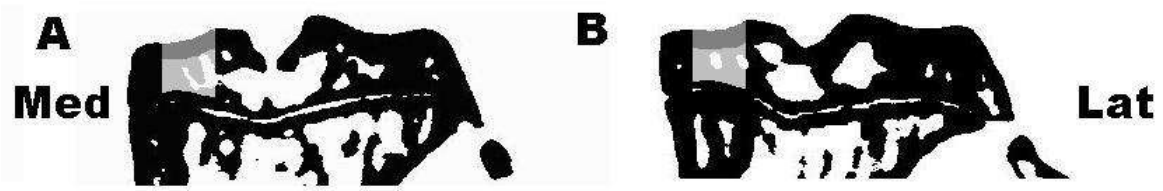

Figure 5-6. Tomograms in the sagittal plane of the proximal tibia from the contralateral (left) legs of: A. BALB/c and B. C57Bl/6 mice. Tomograms are from the approximate centre of the tibia. Grey region indicates medial plateau region of interest analysed for trabecular bone and subchondral plate properties.

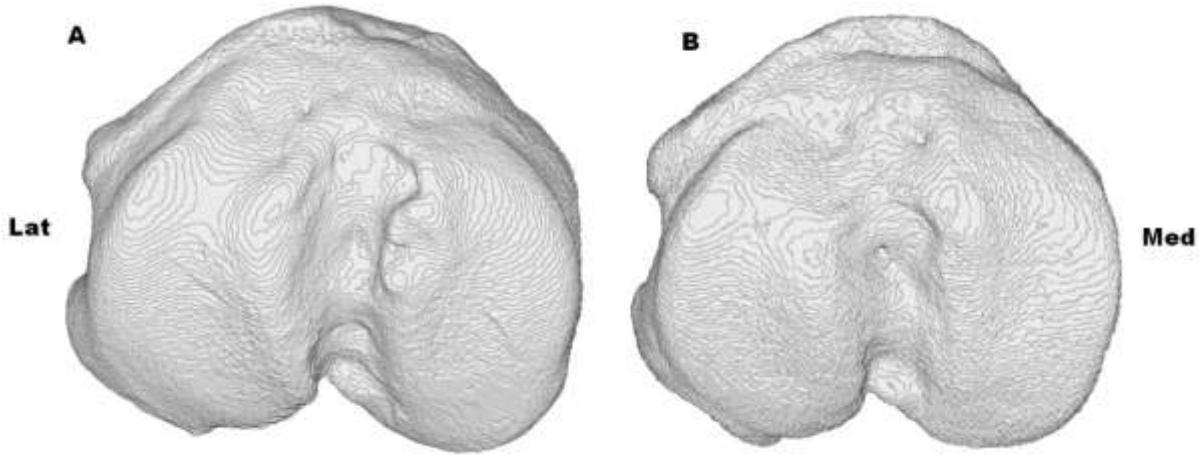

Figure 5-7. 3D micro-CT Reconstructions of the proximal tibia from contralateral (left) legs of A. BALB/c, and B C57Bl/6 mice. The tibias are similar in appearance and lack and osteophytes.

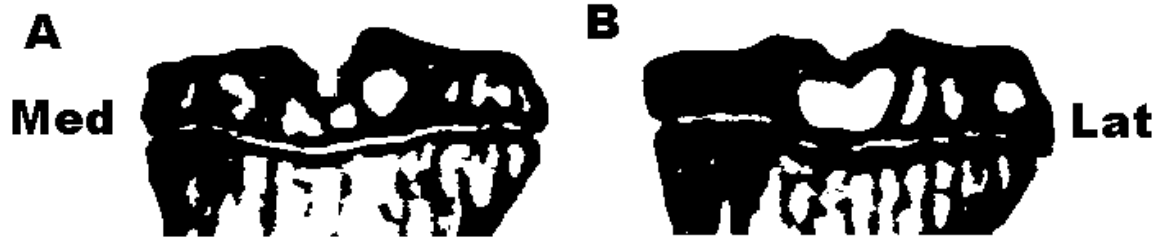

Figure 5-8. Tomograms in the sagittal plane of the proximal tibia from the DMM (right) legs of: A. BALB/c and B. C57Bl/6 mice. Tomograms are from the approximate centre of the tibia. Note the increase of bone on the medial plateaus in both strains, compared to Figure 5-6.

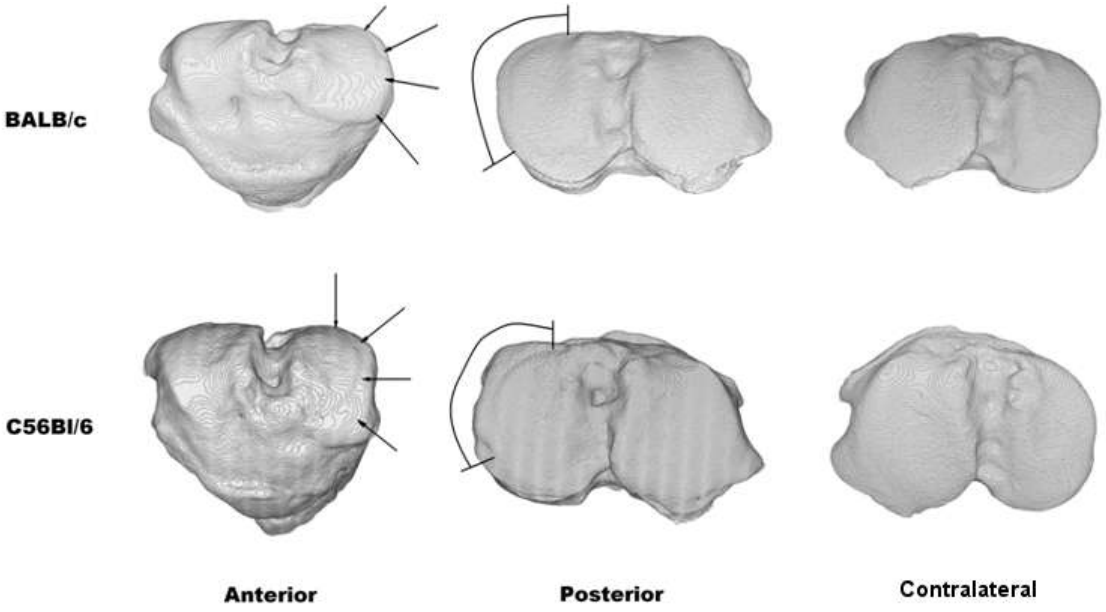

Figure 5-9. 3D reconstructions of a BALB/c and C57Bl/6 for DMM (right) and contralateral (left) tibia, showing anterior and posterior views of the same tibiae. Osteophytes are labelled with arrows in the anterior view, and brackets mark the extent of each osteophyte in the posterior view (tibia in posterior view only).

Table 5-3 contains the bone analysis results. There was a significant difference for all parameters between strains. BALB/c mice exhibited a significantly thicker subchondral bone plate than C57Bl/6 mice. In general the BALB/c had less bone volume per total volume within the epiphysis (primarily due to a greater total epiphyseal volume). The strain difference of bone volume is also reflected in the trabecular parameters.

The bone changes described by the quantitative bone analysis in the DMM leg demonstrated that onset of OA increased the volume of epiphyseal trabecular bone, as reflected by a significant increase of BV/TV and a decrease of Tb.Sp in DMM legs. The subchondral plate thickness also increased in DMM legs in both strains. However, as epiphyseal bone volume increased, distinguishing subchondral plate from trabecular bone became difficult, particularly in the C57Bl/6.

	BALB/c		C57Bl/6		p	
	Contralateral (left) **8 weeks** n = 16	DMM (right) **8 weeks** n = 16	Contralateral (left) **8 weeks** n = 16	DMM (right) **8 weeks** n = 16	Strain	Leg
Sb.Pl.Th (mm)	0.173 ± 0.0059	0.184 ± 0.014	0.149 ± 0.016	0.176 ± 0.019	<0.0001	<0.0001
TV	0.309 ± 0.060	0.304 ± 0.045	0.232 ± 0.040	0.241 ± 0.053	<0.0001	ns
BV/TV	0.222 ± 0.031	0.281 ± 0.053	0.340 ± 0.027	0.394 ± 0.059	<0.0001	<0.0001
Tb.Th (mm)	0.081 ± 0.005	0.088 ± 0.007	0.116 ± 0.022	0.126 ± 0.009	<0.0001	ns
Tb.Sp (mm)	0.449 ± 0.148	0.347±0.0520	0.525 ± 0.131	0.424 ± 0.073	0.001	0.002

Table 5-3. Bone analysis results, parameter means ± SEM. Significance (p) compares contralateral to DMM leg, p ≤ 0.05 is considered significant. Sb.Pl.Th is subchondral bone plate thickness, Tb.Th is trabecular thickness, Tb.Sp is trabecular spacing, BV/TV is bone volume / total volume. n = 16.

There was no significant difference of MS/BS or OS/BS between DMM and contralateral legs (Table 5-4). There was a weakly significant effect from strain, MS/BS and OS/BS were greater in the C57Bl/6 mice; this effect was due primarily to a difference in bone surface, evident in Figure 5-7 and Figure 5-9.

	BALB/c		C57Bl/6		p	
	Contralateral (left) n = 6	DMM (right) n = 5	Contralateral (left) n = 4	DMM (right) n = 4	Strain	Leg
Ms/Bs	0.229 ± 0.063	0.247 ± 0.047	0.412 ± 0.159	0.330 ± 0.099	ns	ns
Os/Bs	0.0625 ± 0.0136	0.0956 ± 0.0294	0.1995 ± 0.0887	0.2061 ± 0.0921	ns	ns

Table 5-4. Histological bone analysis results, parameter means ± SEM. Significance (p) compares contralateral to DMM leg, p ≤ 0.05 is considered significant.

5.3.3 Cartilage Analysis

Table 5-5 contains CSLM analysis of mean plateau cartilage volumes. There was no significant difference for any parameter when comparing strains or DMM (leg). There were no characteristic regions of loss or obvious morphology changes on the 3D reconstructions that were similar to those seen in chapter 3 (Figure 5-10). However, the 3D reconstructions did illustrate that thickness varies across the plateau, which is not reflected by the volume analysis in Table 5-5. The C57Bl/6 reconstructions in Figure 5-10 suggest a difference of thickness between the two plateaus, this difference is most likely attributable to errors in the CSLM method. Errors from soft tissue cover (exemplified in C57Bl/6 DMM reconstructions in Figure 5-10) may act to reduce this difference when measuring the cartilage volume, potentially explaining why the cartilage volume measures exhibited no significant difference.

	BALB/c		C57Bl/6		p	
	Contralateral (left) leg n = 16	DMM (right) Leg n = 16	Contralateral (left) leg n= 16	DMM (right) leg n = 16	Strain	Leg
Cartilage Volume (mm^3)	0.0076 ± 0.0026	0.0071 ± 0.0016	0.0069 ± 0.0005	0.0087 ± 0.0035	ns	ns

Table 5-5. CSLM cartilage analysis results, parameter means ± SEM. Significance (p) compares contralateral to DMM leg, $p \leq 0.05$ is considered significant.

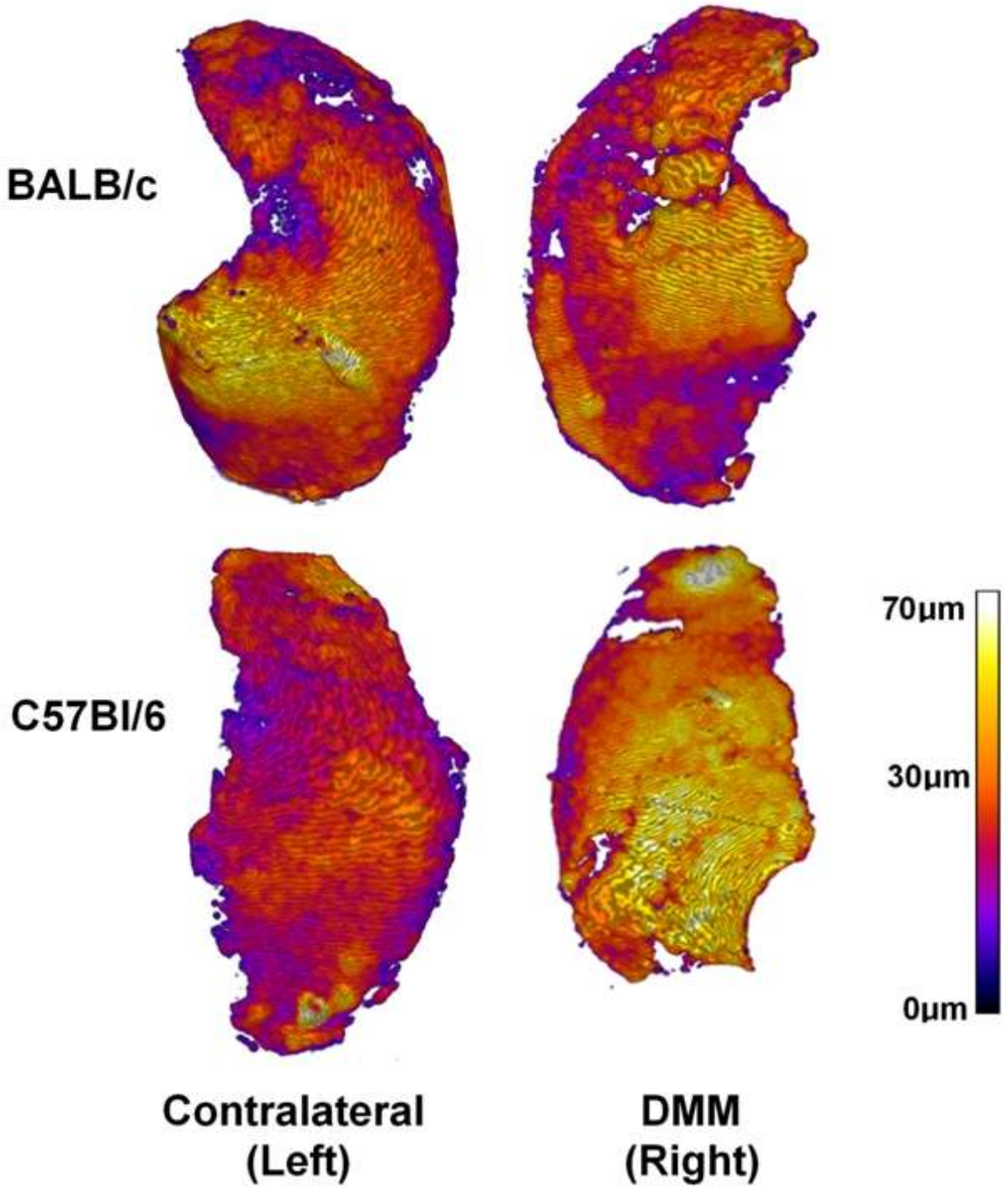

Figure 5-10. CSLM 3D reconstructions of the medial plateau cartilage from DMM and contralateral legs of a BALB/c and a C57Bl/6 mouse. Note, a small region posterior region has been omitted on the reconstruction for the C57Bl/6 DMM, because this region was obscured by soft tissue during scanning.

Fluorescent tissue peripheral to the medial plateau was observed on eight week CSLM images with both strains. This material was removed at the post processing stage and not included as cartilage when calculating cartilage volume. The tissue was located superior and peripheral (medial and anterior) to the articular cartilage (Figure 5-11). Osteophyte formation on micro-CT reconstructions formed a continuous band on the anterio-medial aspect of the medial plateau (Figure 5-9), the same region in which fluorescent tissue appeared peripheral to the cartilage in the CSLM scans (Figure 5-11).

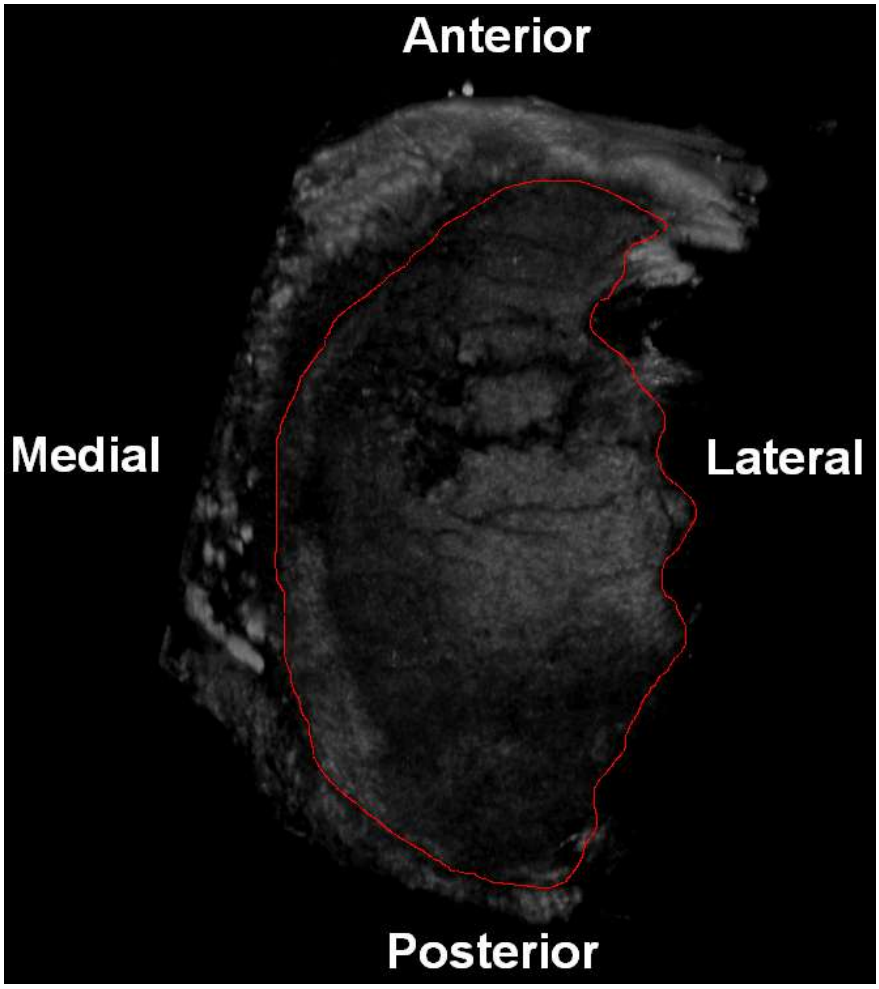

Figure 5-11. CLSM (not thresholded) 3D reconstruction of a medial tibial plateau from a DMM leg (BALB/c 8weeks). Area bordered in red illustrates cartilage plateau. Fluorescent material is evident peripheral to this border on the anterio-medial edge of the cartilage. Note, CSLM field of view limit on the medial aspect.

5.3.4 Cartilage Scoring

Experimental design did not support scoring of cartilage as group sizes were too small, and unexpected damage from sectioning reduced the group size further. Sections were not decalcified and therefore cartilage was prone to damage, making it difficult to distinguish between OA damage and microtome damage. However, clear features of OA such as PG loss, clefts and fibrillation were evident on the sections. CLSM exhibited similar evidence of lesions that occurred on weight bearing regions of the medial plateau in the DMM legs of three C57Bl/6 and five BALB/c mice (Figure 5-12). However, it is difficult to distinguish these features from foreign material or damage caused during disarticulation.

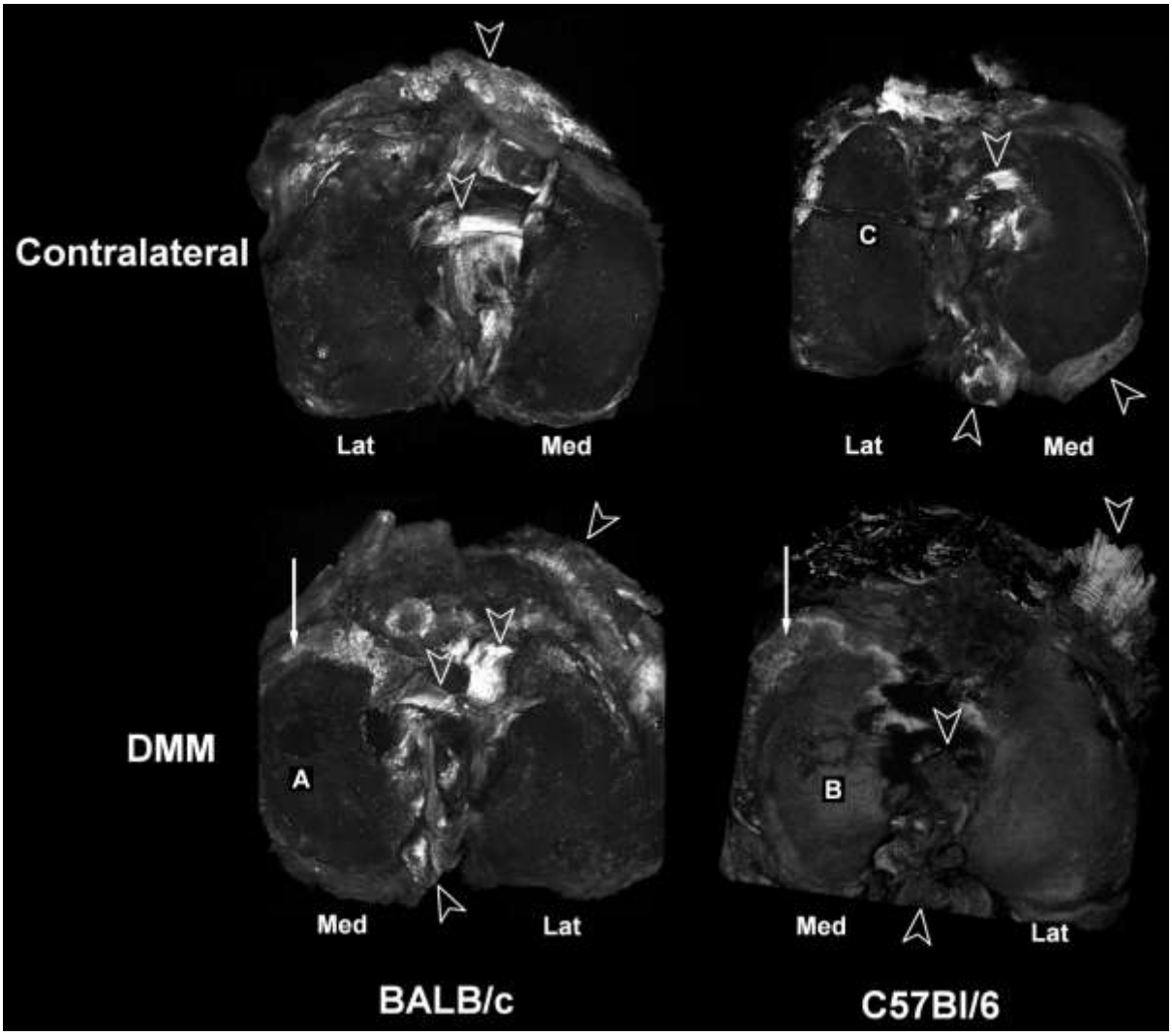

Figure 5-12. Example Z projection images of contralateral and DMM tibial plateaus from BALB/c and C57Bl/6 mice. Z projections are formed from the maximum intensity pixel in each slice of a stack. Arrow heads denote soft tissue from the capsule or ligaments. Solid arrows denote soft tissue formation on the perimeter of OA affected plateaus. A is an example of a possible lesion on a DMM BALB/c medial plateau. B is an example of a possible lesion on a DMM C67Bl/6 medial plateau. C is an example of soft tissue or foreign material obscuring the cartilage of a contralateral C57Bl/6 lateral plateau.

Scoring of safranin O stained cartilage produced an average score of 1.3 (σ = 0.58) (n = 3) in the contralateral leg, and in the 1.6 (σ = 0.58) DMM leg of BALB/c mice (n = 3). In C57Bl/6 mice scoring produced an average score of 1 (σ = 0) (n = 2) for contralateral legs and 1.3 (σ= 0.98) (n = 7) for DMM legs (Figure 5-13).

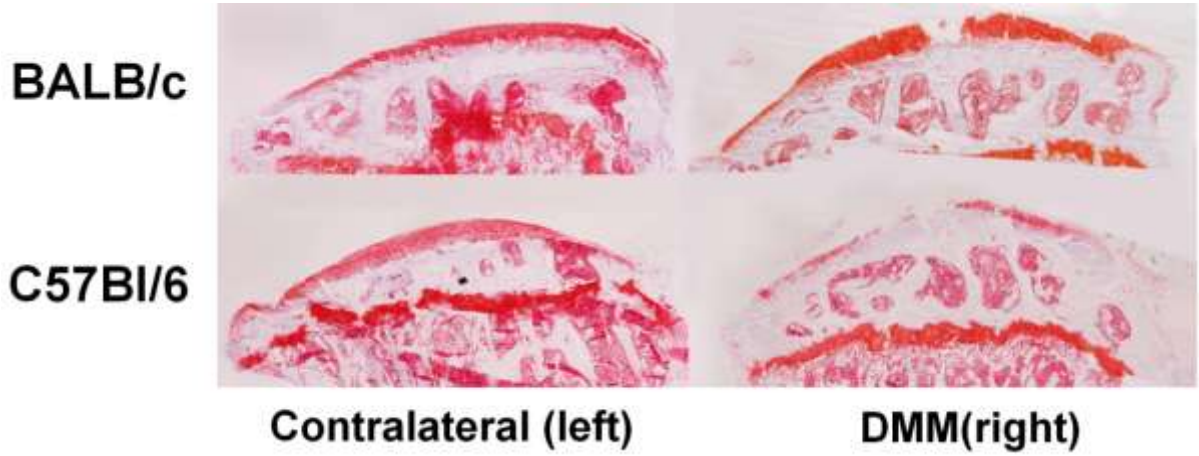

Figure 5-13. Histology images for BALB/c and C57Bl/6 contralateral and DMM tibia. Safranin O stained sections are from the medial plateau in the sagittal plane. The tibiae in the images are approx. 2mm in depth on the sagittal plane. Cartilage loss can be seen in the middle of the plateau on the DMM tibia of both strains. Note, cutting artefacts have deformed the epiphyseal area on the contralateral tibia for both strains.

5.3.5 Comparison of CSLM and histological cartilage thickness measurements

The average thickness measurement determined from Safranin O stained histology and corresponding CSLM images are contained in Table 5-6. There is little variation across the plateau for CSLM, which fails to mirror the natural variance of cartilage thickness across the plateau, as measured by histology. A further example of this is presented in Figure 5-15, which shows a thickness profile for CSLM vs. a histological section. The thickness was measured every 100 µm from posterior to anterior by CSLM and histology (Figure 5-14). There appears to be little correlation between the two measurements. However, the thickness measurements are of the right order of magnitude, unlike previous CSLM studies (Stok 2009a; Stok 2009b; Stok 2009c).

	Anterior n = 16	Central n = 16	Posterior n = 16	Average
CSLM (μm)	27.8 ± 0.109	32.6 ± 0.157	29.2 ± 0.191	29.5 ± 0.152
Histological Section (μm)	45.3 ± 0.301	55.8 ± 0.330	38.0 ± 0.208	46.9 ± 0.280

Table 5-6. Comparison of CSLM and histology cartilage thickness measurements by location on the medial tibial plateau. Mean value ± coefficient of variation.

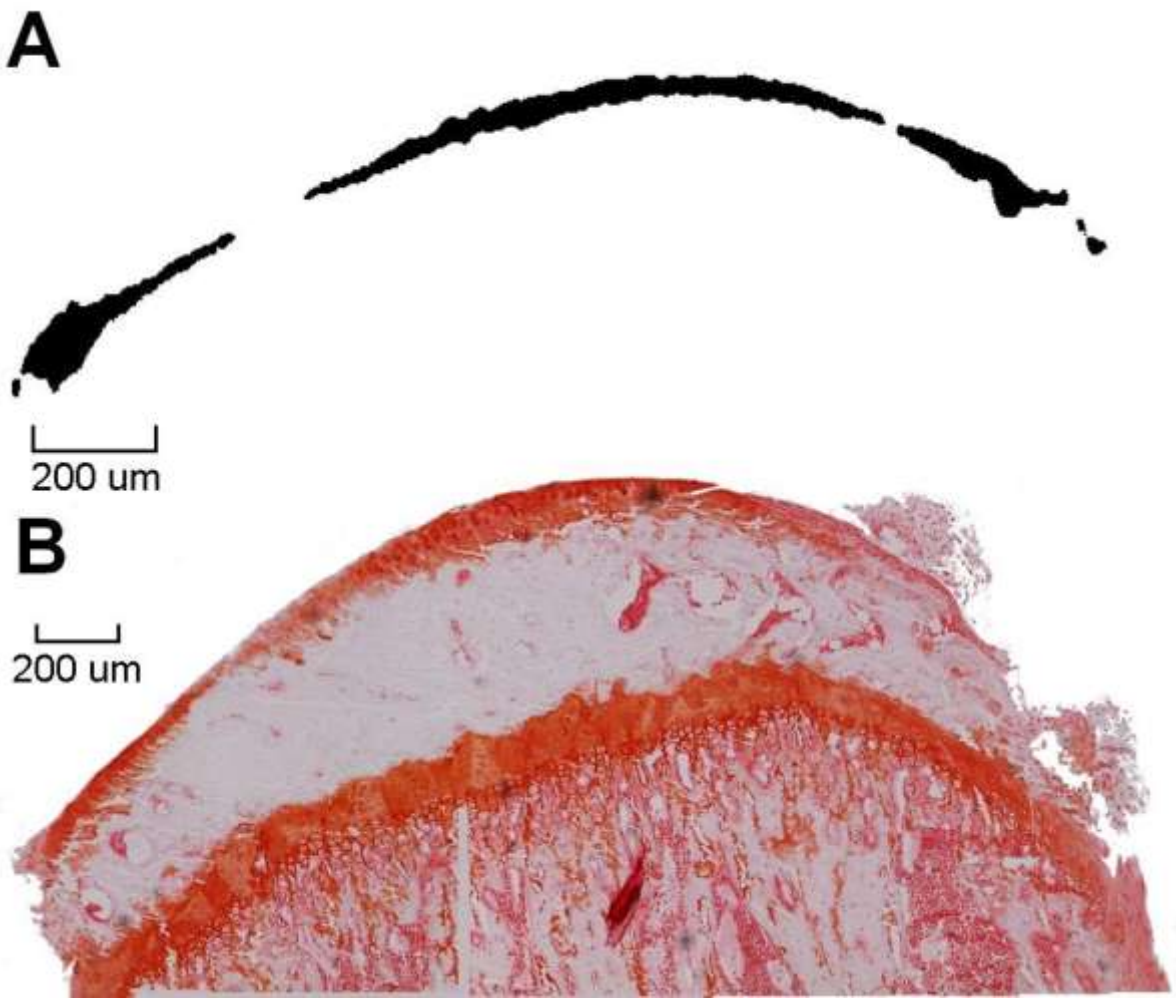

Figure 5-14. A CLSM image and safranin O histological section used to make Figure 5-15. A is a sagittal section of a CSLM reconstructed plateau, black represents thresholded cartilage. B is a sagittal section from the same tibia in the same region as A.

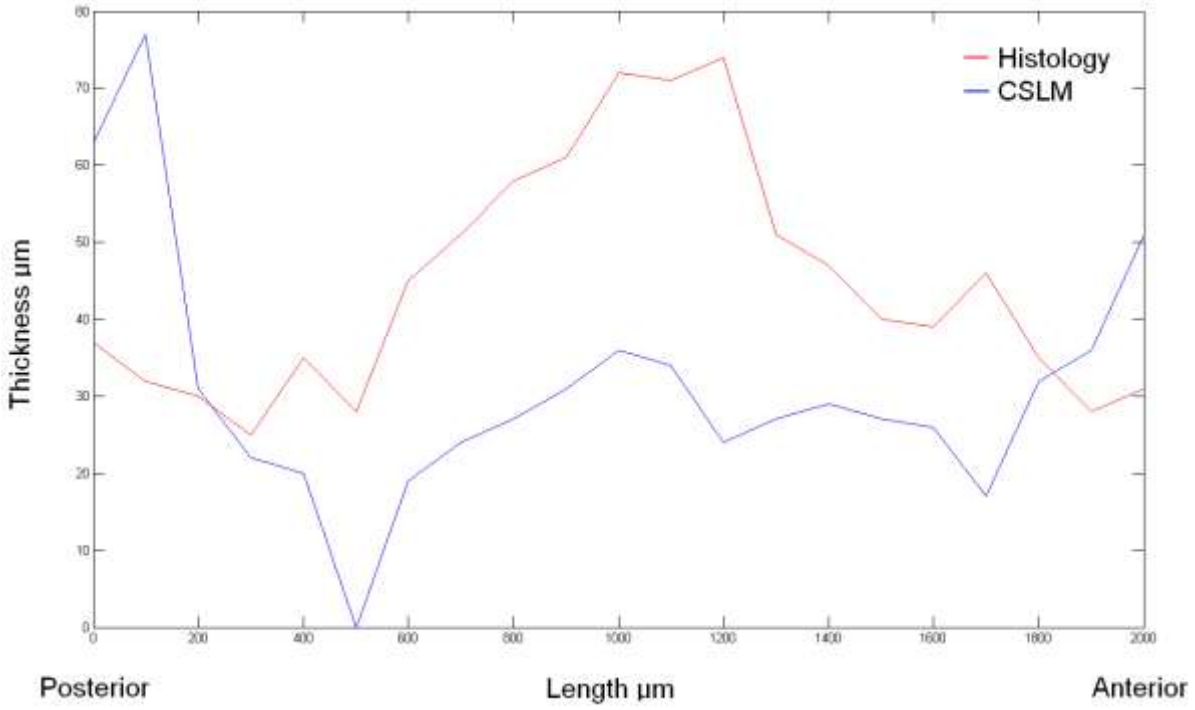

Figure 5-15. Thickness profile of cartilage for one sagittal histological section compared to corresponding CSLM measurements. There is little correlation between the two measurement techniques.

Histology thickness measurements ranged from 18 µm to 126 µm, whereas CSLM ranged from 17 µm to 44 µm. All pairs of thickness values used in Table 5-6 were plotted as a scatter plot in Figure 5-16. The least squares method was used to obtain a best fit line to the scatter plot, the line had a gradient of -0.2, with a Pearson's Correlation coefficient of r = 0.02, suggesting that no correlation occurred between CSLM and histological thickness measurements.

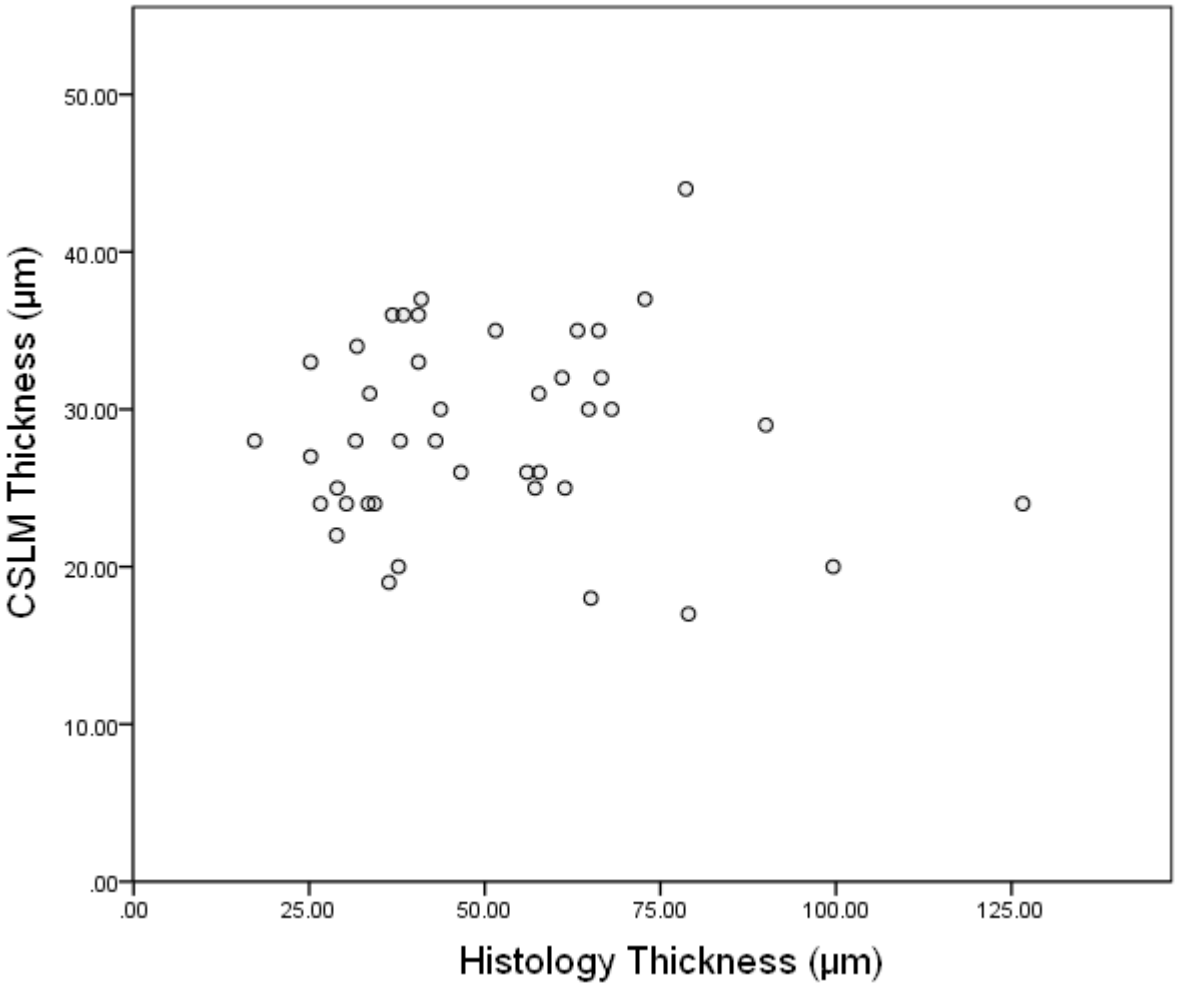

Figure 5-16. Scatter plot for thickness measurement by CSLM Vs. histological sections, demonstrating no correlation between the measurement techniques.

5.3.6 Retrospective Comparisons of C57Bl/6 Two and Eight Weeks after Surgery

Bone and cartilage were compared between C57Bl/6 mice at two weeks after surgery (Chapter 4) and C57Bl/6 mice eight weeks after surgery. There was an age related increase of all bone parameters (except trabecular spacing). Cartilage showed no significant difference between time points, as did MS/BS. OS/BS exhibited a significant age related increase (Table 5-7).

	C57Bl/6				p	
	Contralateral (left) 2 weeks n = 10 (unless stated)	DMM (right) 2 weeks n = 10 (unless stated)	Contralateral (left) 8 weeks n = 16 (unless stated)	DMM (right) 8 weeks n = 16 (unless stated)	Age	leg
Sb.Pl.Th / (mm)	0.144 ± 0.028	0.125 ± 0.011	0.149 ± 0.016	0.176 ± 0.019	<0.0001	ns
Tb.Th / (mm)	0.069 ± 0.017	0.059 ± 0.015	0.116 ± 0.022	0.126 ± 0.009	<0.0001	ns
Tb.Sp / (mm)	0.417 ± 0.107	0.319 ± 0.105	0.525 ± 0.131	0.424 ± 0.073	ns	ns
BV/TV	0.203 ± 0.068	0.229 ± 0.065	0.340 ± 0.027	0.394 ± 0.059	<0.0001	ns
MS/BS	0.226 ± 0.090 (n = 5)	0.349 ± 0.121 (n = 5)	0.412 ± 0.159 (n = 4)	0.330 ± 0.099 (n = 4)	ns	ns
OS/BS	0.083 ± 0.032 (n = 5)	0.132 ± 0.044 (n = 5)	0.1995 ± 0.0887 (n = 4)	0.2061 ± 0.0921 (n = 4)	0.003	Ns
Cartilage Volume (mm^3)	0.0087 ± 0.002	0.0080 ± 0.002	0.0069 ± 0.0005	0.0087 ± 0.0035	ns	ns

Table 5-7. Comparison of C57Bl/6 mice 2 weeks of age (Chapter 4) and C57Bl/6 mice 8 weeks of age, parameter means ± SEM. Significance (p leg) compares contralateral to DMM leg and (p age) compares 2 weeks to 8 weeks, $p \leq 0.05$ is considered significant. Sb.Pl.Th is subchondral bone plate thickness, Tb.Th is trabecular thickness, Tb.Sp is trabecular spacing, BV/TV is bone volume / total volume, MS/BS is mineralising surface / bone surface and OS/BS is osteoid surface / bone surface.

5.4 Discussion

5.4.1 Comparison of Bone changes between strains

Micro-CT quantification of epiphyseal bone demonstrated that the bone response to DMM at the eight week time point was similar between strains. Both mice strains exhibited a significant increase

of epiphyseal bone volume, with an associated decrease of trabecular spacing. C57Bl/6 mice had a significantly higher epiphyseal bone volume in the contralateral leg compared to BALB/c (Table 5-3), which was increased further in the DMM leg. Judex et al (Judex 2002) reported that the epiphysis of the distal femur of C57Bl/6 mice had a lower BV/TV than BALB/c mice. It is possible that this difference occurs because different sites were investigated in the two studies, but it could also be the early signs of spontaneous OA in the tibia of the C57Bl/6. Within the tibial ROI the C57Bl/6 has a greater BV/TV, however, at other skeletal sites the BALB/c has a greater BV/TV. These results support the hypothesis that greater bone volume produces a smaller bone response in OA. The BALB/C had a medial epiphyseal BV/TV that was 34% lower than the C57Bl/6 in the contralateral leg, and epiphyseal BV/TV in the DMM leg increased by 21% in the BALB/c. In the C57Bl/6BV/TV increased by only 13% compared to the contralateral, suggesting the strain with the smallest BV/TV exhibits the greatest increase of bone. A study comparing the response of two mice strains with different BMD (C57Bl/6 and C3H/HeJ with a higher BMD) to a collagenase model of OA, found a similar extent of cartilage degeneration and bone resorption between the C57Bl/6 and the C3H/HeJ strains. The C3H/HeJ strain exhibited trabecular resorption and experienced greater changes on the medial plateau, whereas the C57Bl/6 experience more bone changes and cartilage damage on the lateral plateau, attributed to different tibial alignment (Botter 2008). Both strains exhibited bone resorption with the collagenase model, probably due to inflammation typical with such models causing unweighting and bone resorption.

Botter used a similar micro-CT analysis on DMM 129/SvEv mice eight weeks post operatively. No significant difference was found in bone parameters. However, tomograms suggested that epiphyseal bone volume was increasing. The similarities between tomograms suggest that the DMM surgery was comparable with Botter et al. A comparison with Botter et al. and Kadri et al was made in Chapter 4 (Figure 4-10), and is also applicable in this study. The convention for analysing micro-CT bone scans is to perform a quantitative assessment of trabecular parameters. This study has highlighted some limitations of this when applied to mice. A qualitative assessment of tomograms

from the epiphysis proved more indicative of changes (such as increased epiphyseal bone volume) than the quantitative analysis, whose values only partially reflected the changes (see Figure 5-6, Figure 5-8 and trabecular parameters of Table 5-3). At both two and eight weeks post operatively the volume of epiphyseal bone directly beneath the medial plateau increased in such a manner that separation of the subchondral and trabecular bone was difficult. Due do the small size of the epiphyseal ROI, (2 mm^3 and containing approximately twelve trabeculae) it is prone to error. Furthermore, the epiphyseal architecture of the mouse tibia does not resemble that of other larger mammals. Murine tibial epiphyseal trabeculae are of comparable thickness to the subchondral plate and extend from the growth plate to the subchondral plate in continuous vertical struts with little connectivity. Comparison of their contribution to subchondral support with other mammal forms of bone architecture is therefore difficult. This study questions the utility of quantifying these parameters in the murine epiphysis.

It was observed that osteophytes formed peripheral to the medial plateau on DMM legs of both mice strains, forming in a band or ridge adjacent to the cartilage, starting on the anterior aspect of the medial plateau and extending beyond the medial aspect. The osteophytes were continuous in shape, and they did not form in discrete regions or nodules as with human OA. Osteophyte extent, shape and location were similar between strains. Fluorescent tissue on CSLM images occurred in the same region as the osteophytes (Figure 5-11). Histological sections of this region indicate the presence of cartilage and fibrocartilage on the surface of the osteophytes (Figure 5-17 and Figure 5-18). Osteophytes in toluidine blue stained sections appeared fully mineralised. The histological images, CLSM and micro-CT reconstructions considered together, suggest that in response to the DMM model, osteophyte formation may be acting to increase the surface area of the plateau (in a continuous band on the anterio-medial plateau). DMM has been reported as a model that does not produce osteophytes (Glasson 2007). The osteophyte pictured in Figure 5-17 is located anteriorly, usually histological sections used to analyse DMM joints are taken in the frontal plain and may overlook the anterior region. However, this study also reported osteophytes on the medial aspect on

the plateau, it is highly unlikely medial osteophytes would have been overlooked in other studies had they been present. Therefore, based on their location, it is possible that the osteophytes are a reaction to accidental damage during the resection of the menisco-tibial ligament.

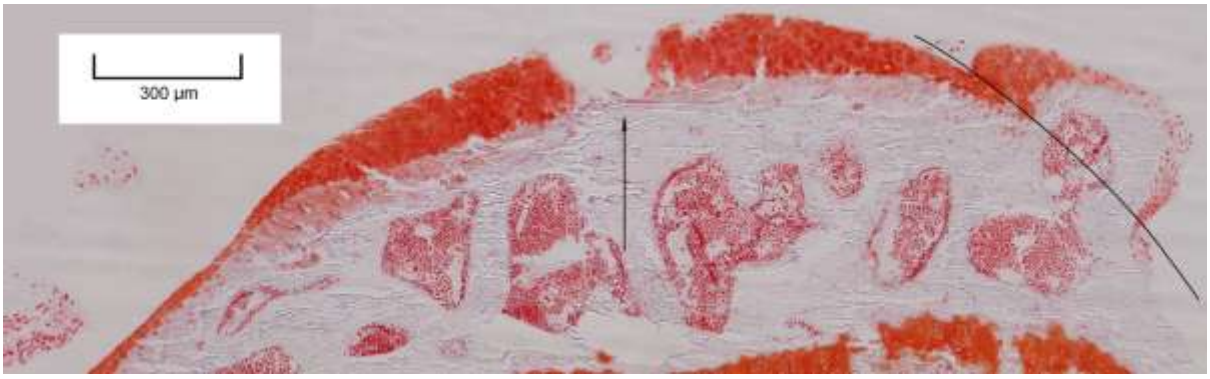

Figure 5-17. Safranin O stained histological section in the sagittal plane from a DMM leg (BALB/c 8weeks). Note anterior osteophyte with cartilage and fibrocartilage on the surface. Osteophyte on the right hand side of image is bisected from the tibia by a black line. Arrow marks region of cartilage loss.

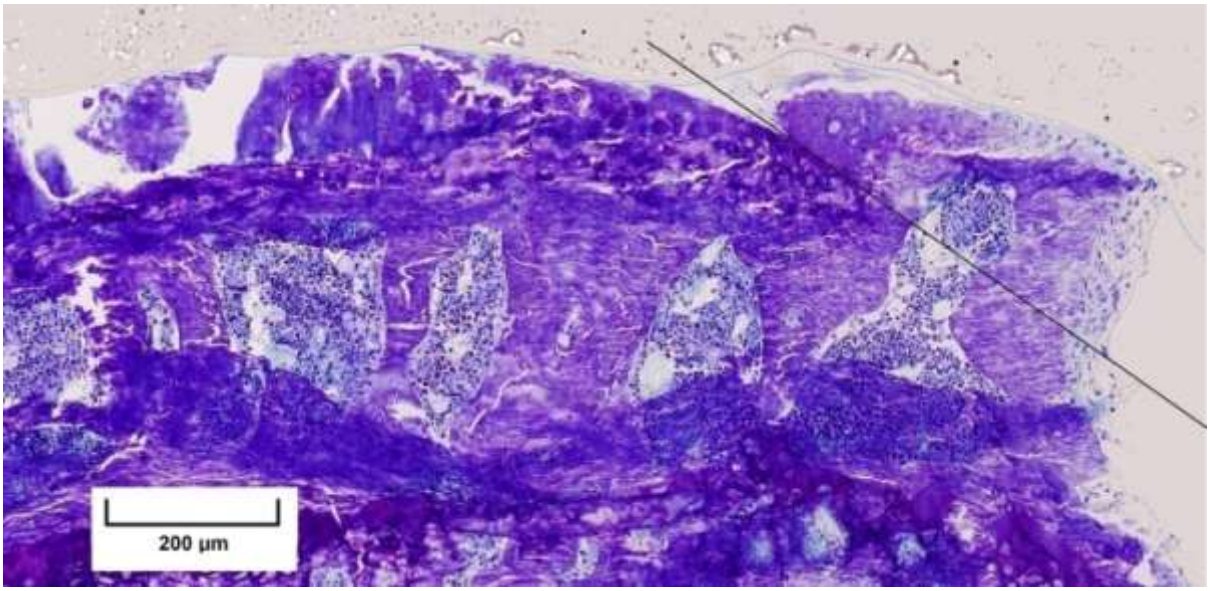

Figure 5-18. Toluidine blue stained histological section in the sagittal plane from a DMM leg (BALB/c 8weeks). Note anterior osteophyte with cartilage and fibrocartilage on the surface. This section is damaged by folding near the growth plate during the sectioning process.

Osteoid surface and mineralised surface exhibited no significant difference due to the effect of DMM surgery (Table 5-4). In the previous study, as described in Chapter 4, these parameters exhibited a

significant increase with DMM surgery two weeks post operatively. The lack of a significant increase eight weeks post operatively suggested that there is no hypomineralisation or increased bone formation taking place at this time point, to assess this properly requires further investigation using dynamic measures and TRAP staining for osteoclasts and osteoblasts. It is possible an increased turnover of bone at two weeks may have been attenuated by the eight week time point, and the result of early mineralisation seen at the two week time point in Chapter 4 is seen in the structural differences in micro-CT measures by eight weeks. However, without direct assessment of bone turnover rate it cannot be verified.

5.4.2 Cartilage Analysis and CSLM

There were no significant differences of cartilage volume between DMM and contralateral legs. CSLM was used in Chapter 3 and a significant difference of cartilage volume was observed. This was because a more extreme model was inadvertently used, which produced full thickness cartilage loss. CSLM was able to reliably detect large regions of full thickness loss, but correct application of the DMM model does not produce full thickness cartilage loss; instead moderate cartilage damage is reported in the DMM model at eight weeks (Glasson 2007). As a result CSLM was unable to measure any significant difference between DMM and contralateral plateaus. Possible lesions were visible on the weight bearing regions on the medial plateaus the five of the DMM BALB/c and three of the C57Bl/6 tibia. Cartilage defects that did not resemble lesions were also visible on the CSLM scans. These were caused by damage during disarticulation and foreign material or soft tissue obscuring the cartilage.

CSLM detects auto fluorescence from collagen (primarily from pyridinoline and pentosidine cross links) but also from substances contained within cells (Uchiyama 1991; Wong 2001). The early stage of OA involves PG loss from the cartilage matrix (Goldring 2000a) followed by an increase of water into the ECM. It is unclear how such changes may affect CSLM thickness measurements. The collagen

in cartilage is degraded and reformed at varying rates throughout the stages of degeneration in OA. It is likely that this imbalance will result in a non-linear change of fluorescent signal as degeneration progresses. This should be validated by studying fluorescence of articular cartilage at varying stages of degeneration. As OA progresses, fibrillation and lesions occur, as mentioned in Chapter 4, but confocal microscopy may not have the resolution to detect fibrillation. However, CSLM does still have a use. In Chapter 3 it was used effectively to demonstrate full thickness cartilage loss on the posterior plateau of a DMM + ACLT model. CSLM use should therefore, be restricted to models in which full thickness loss is expected, whereby it benefits of ease of use and 3D qualitative analysis become apparent. CSLM does have a practical limitation, for a quantitative analysis, its use should always performed in conjunction with histology for validation.

In Table 5-6 the CSLM average thickness measurement was 62 % of the average histology thickness. Whereas Stok et al. found that CSLM thickness measurements were 312 % larger than histology thickness measurements (Stok 2009a). The CSLM technique used in this thesis provided more accurate cartilage thickness measurements than CLSM methods used elsewhere, because a ×10 objective was used instead of a ×5. It is likely a ×5 objective has a Z axis (axis parallel to cartilage thickness) resolution greater than the thickness of murine cartilage. Reconstructions of medial tibial cartilage from the same specimen by the two CSLM methods are provided in Figure 5-19, from which the effect of Z resolution is immediately apparent.

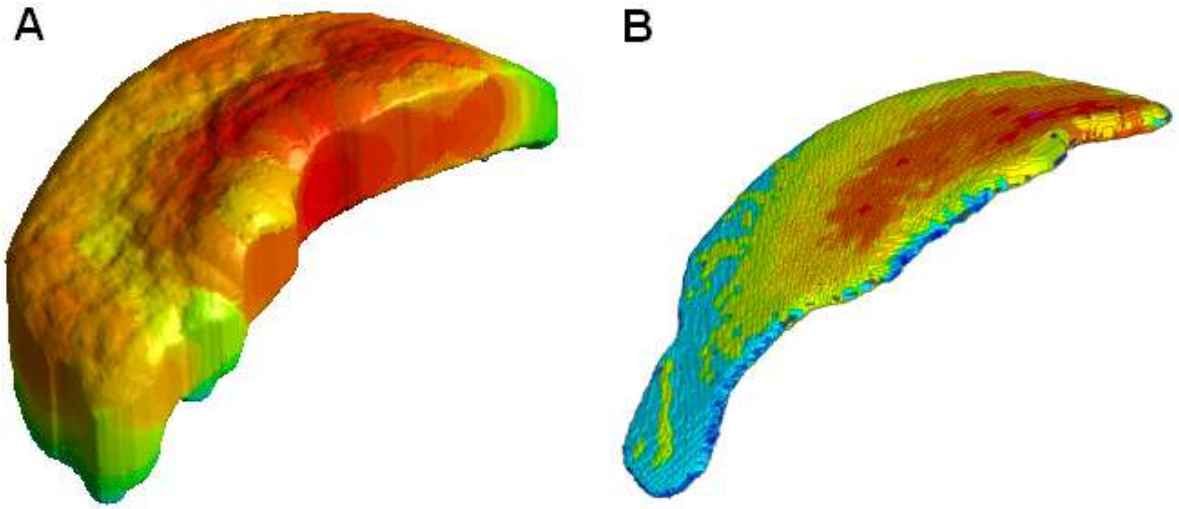

Figure 5-19. Cartilage reconstructions of a medial tibial plateau. A. with protocol defined in Stok et al 2009. B. With protocol defined by (Moodie 2010) used within this thesis. Note colours approximate thickness for each sample independently with red representing thicker cartilage.

CSLM and histological section thickness measurements did not correlate. CSLM produced reconstructions that exhibited less variation than in histological sections, i.e. CSLM reconstructions were more uniform across the plateau. This could be due to surface effects dominating the signal, and therefore neglecting a contribution from deeper lying cartilage. Alternatively, this could be caused by aggressive thresholding in the post processing stage. This effect can be minimised in future studies by increasing the signal intensity in the post processing stage, making it proportional to depth dependent attenuation of the incident beam.

5.4.3 Laxity

There was no significant difference of laxity between strains at eight weeks, therefore it can be assumed that DMM surgery affects the mechanics and loading pattern of both joints to a similar extent.

There were no observable laxity differences between the operated and non operated legs in either strain at eight weeks. This suggests that as in the humans, the meniscus provides no measurable

restraint in either AP drawer or VV rotation when the cruciate and collateral ligaments are intact. The laxity testing lacked any sham surgery controls, therefore, the effect of arthrotomy on laxity, or a physiological reaction to arthrotomy cannot distinguished from the effect of DMM surgery alone.

The effect of meniscal destabilisation on internal and external rotation could not be quantified, but evidence suggests that the meniscus may play a role in providing some restraint. Unlike humans the articulating surfaces of the murine femur and tibia are highly convex, and the meniscus forms a comparatively more substantial structure, which would be expected to play a more significant role in joint stability. The meniscus appears to contribute to stability at low loads only, with greater loads attenuated by the collateral ligaments. Therefore, investigation of the meniscal contribution to joint stability in mice will remain challenging, because laxity testing on the scale of a mouse means that changes of laxity at low loads are often concealed by friction effects. It was for this reason that no analysis of the zero point was conducted at any stage of laxity testing described in this chapter and Chapter 3.

It could be argued that the lack of significant results suggests that the apparatus lacked the sensitivity to work on the scale of mice limbs. However, previous studies using the same apparatus, suggesting that limited sensitivity was not an issue (van Osch 1995; Blankevoort 1996). Additionally significant differences were observed in Chapter 3 with a hypothesized transaction of the ACL. The sensitivity of the apparatus was not directly investigated, but could be investigated by transecting various structures of the knee, such as the cruciate ligaments, and assessing the magnitude of any resulting change of laxity.

Laxity reduced with age in the BALB/c mice in both the contralateral and DMM leg. A similar age related reduction of laxity is seen in humans (Beighton 1973; Cheng 1991; Jansson 2004). Both the DMM and contralateral legs were affected to a similar extent, therefore there was no pathologic effect on the cruciate and collateral ligaments as OA progressed. This suggests that these structures are not affected by turn over as OA progresses, nor does osteophyte formation act to reduce motion

in the AP and VV directions. Pottenger et al. removed osteophytes from human cadaveric knees and found an increase of varus-valgus motion, suggesting osteophyte growth acted to reduce instability (Pottenger 1990). This was not the case in the BALB/c mice, however, DMM surgery did not produce an increase of varus-valgus laxity, so it is unlikely that osteophyte formation would have cause to reduce laxity in this direction. Furthermore, osteophytes form in discrete nodules in human OA, in the DMM model they form in a continuous periarticular band and so may not affect laxity in the same manner.

The zero week post operative BALB/c group could not be compared with the corresponding C57Bl/6 group as described in Chapter 3, because different technicians operated on the different groups. For the same reason, C57Bl/6 mice at zero and eight weeks could not be compared.

5.4.4 Summary

BALB/c and C57Bl/6 mice produced a similar pattern of bone response to DMM. The two strains increased bone volume by different amounts, reflecting strain differences of BV/TV. The strain with the lowest BV/TV produced the largest increase of bone. This difference may affect the rate of progression of OA.

BALB/c and C57Bl/6 strains responded to DMM surgery by forming a continuous osteophyte with a cartilage and fibrocartilage surface, which resembled new joint surface. This could have important implications for understanding the role of osteophyte formation. Furthermore, this observation may have been overlooked if histology alone was used to examine the tibiae. Instead micro-CT and CSLM were able to provide valuable 3D reconstructions of both the soft and mineralised tissues.

The CSLM was substantially more accurate using the methods described in this study than those used elsewhere, and this methodology is recommended for future use. Concerns remain over the ability of CSLM to detect fibrillation and receive signals from deeper layers cartilage. However

peripheral soft tissue growth and lesions on the weight bearing region of the plateau were visualised, thus demonstrating its utility. Possible lesions were visualised, with further investigation this may provide the ability to map lesions across the whole plateau. This may provide opportunities to investigate damage patterns in murine OA models. CSLM remains a useful technique with potential but still requires more thorough investigation.

Meniscectomy had no observable effect on anterior-posterior or varus-valgus laxity (and a possible stabilising effect in internal-external rotation). This implies that in the DMM model cartilage degradation may be induced by increasing articular contact pressure resulting from the meniscus being unable to support hoop stresses, rather than the redistribution of loading caused by increased laxity. This could provide a link between loading and cartilage degeneration.

6. Conclusions

This thesis contains important contributions to the understanding of biomechanics and tissue changes in the DMM model. It also includes the development of novel techniques for investigating tissue changes.

DMM contributions:

1. Improperly conducted DMM surgery can include accidental ACLT damage. The DMM model and DMM + ACLT model produce two distinct bone formation patterns. DMM surgery produces mild bone changes on the proximal tibia. A small profile, but continuous osteophyte forms peripheral to the cartilage, around the anterio-medial aspect. Bone formation occurs within the medial epiphyseal compartment. When the ACL is damaged or transected (Moodie 2010) excessive bone loss occurs on the posterior plateau with an associated rapid bone formation that occurs both distal and posterior to this. Due to the severe morphological changes occurring elsewhere on the tibia, epiphyseal bone volume decreases. These bone changes are extreme and DMM with ACLT damage does not represent human OA, because damage extends through the growth plate. Other research groups have reported epiphyseal bone loss when examining bone changes (Kadri 2008), therefore, it is conceivable that ACL damage may been inadvertently used in other studies. Care should be taken to ensure surgical accuracy when using the DMM model. Assessment of ACL integrity should be incorporated into studies, either by anterior-posterior laxity testing or histological thin sections.

2. Micro-CT suggested that osteophyte formation occurs in a band peripheral to the cartilage on the medial plateau. CSLM displayed auto fluorescent soft tissue across the surface of the osteophyte. Histological sections and CSLM suggest that osteophytes have cartilage or

fibrocartilage on the surface. Osteophyte formation resembles an attempt to increase joint surface in the DMM model.

3. The BALB/c mice had less bone in the medial ROI compared to the C57Bl/6 and had a greater increase of bone in response to OA. This might not be representative of bone structure throughout the skeleton, but care should be taken when identifying mice as high/low bone mass as the differences may be site specific as demonstrated in this study.

4. Murine medial meniscus does not contribute to primary AP or VV laxity. This is the same as in humans and other mammals. There is evidence, however, that the medial meniscus may contribute to resisting internal/external rotation at low loads.

Methodological contributions:

1. Confocal microscopy can be used for 3D qualification of joint morphology. It may have an additional use for 3D quantification of full thickness lesions, but would require histological validation. CSLM is of limited use for quantifying more subtle cartilage changes.

2. Lesions can be seen on confocal images, but confocal microscopy is relatively insensitive to small cartilage thickness variations. As a result confocal microscopy could be used to identify regions of interest to refine histological analysis.

3. CSLM produces images that are representative of cartilage thickness when a 10× objective is used instead of a 5×. With a 5× objective the Z-resolution is less than the thickness of the cartilage, further use of CSLM for cartilage analysis should use a 10× objective.

4. Qualitative observations of tomograms were used in addition to the micro-CT quantitative analysis. In the tomograms an increase of bone volume was evident, whereas this was only partially reflected in the quantitative analysis, because bone in the medial epiphyseal compartment increased in volume to make separation of the trabecular bone and subchondral plate difficult. Increased resolution may allow the two bone types to be distinguished by differences of density.

7. Further Work

This thesis has highlighted several key areas of research that will require further investigation. These are split, between furthering the knowledge of OA in the DMM model and the enhancement of current investigative techniques.

Further investigations into the DMM model:

1. Validation of the DMM model

Sham surgery was not performed in any of the studies; as a result they should be repeated with a sham control. This is applicable not just for the bone and cartilage changes, but also for the laxity analysis. The pathological changes reported in this thesis could be the result of inflammation or capsular entry and not just DMM surgery.

The samples should be validated with histology to ensure that a correct DMM procedure had been performed. In Chapter 3, the anomalous tissue changes and laxity results were attributed to a hypothesised erroneous ACLT. In Chapter 5 changes such as osteophyte formation were present which were not reported in existing literature, therefore, the samples themselves should have been assessed for ligament integrity.

2. Validation of methodologies

The magnitude of laxity changes that can be measured using the laxity apparatus is unclear. This requires further investigation with the use of positive controls, whereby a ligament is transacted and the corresponding change in laxity is quantified. The accuracy of the apparatus itself was not tested; the laxity testing of a linearly elastic material of known stiffness should also be performed over the entire displacement range. Micro-CT analysis needs to be performed at a resolution superior to the size of the structure under investigation, further investigation is required to confirm if the resolution used in this thesis was sufficient. Further investigation of the CSLM method is also required, (discussed in the next section).

The CSLM and micro-CT methodologies require significant user specific image analysis, therefore, an analysis of inter user variability needs to be performed for both methods. Intra user variability was not investigated for any methodology in this thesis, this should also be performed on all of the measures.

3. Looking for evidence of bone resorption.

Two weeks after surgery, bone volume had increased in the DMM model and there was evidence of cartilage degeneration. A similar procedure should be repeated one week after surgery, but with additional decalcified histology to score cartilage degeneration in place of CSLM. This may indicate if cartilage changes are evident. Non-decalcified histology should be combined with TRAP (tartrate-resistant acid phosphatase) staining for the identification of osteoclasts and ALP (alkaline phosphatase) staining for osteoblasts, this will yield more accurate information on the nature of early stage bone changes (i.e. early stage bone resorption or deposition). Dynamic measures should also be included which would have required more appropriate use of calcein labels.

4. Bone stiffness in the DMM model

The change of BV/TV in DMM induced OA was extensive in the medial epiphysis. Future work should consider mechanical testing to determine subchondral plate stiffness (and material modulus). It would be most useful to observe how plate stiffness changes with such massive bone formation. A study should be performed to determine how subchondral plate stiffness varies with OA progression. This would be valuable as both the material properties and the bone volume change with OA progression.

5. Osteophyte formation of new joint surface.

Tissue changes in the DMM model suggested that osteophyte formation may be the formation of new joint surface. Osteophytes were present at two weeks, and by eight weeks the osteophyte spans a 90° arc around the medial plateau. There has been much speculation regarding the role of

osteophytes in OA (Pottenger 1990; Neuman 2003; Felson 2005; Felson 2005). Studies carried out as part of this thesis suggest that osteophyte formation is forming new bone surfaces. This hypothesis should be investigated further, with a bone and cartilage analysis focused on the joint periphery

Further development of imaging methods:

1. Further investigation of the CSLM technique.

CSLM may not be able to detect some OA induced cartilage changes. Larger lesions and full thickness loss can be detected, but PG loss, fibrillation, and collagen fibre damage all affect the cartilage matrix, and the effect of these changes on cartilage auto-fluorescence has not been investigated. These early stage cartilage changes could potentially be detected by confocal microscopy. For example fibrillation produces an irregular surface to the cartilage, which will reduce the ratio of reflected light by increasing beam scattering. Pyridinoline and pentosidine cross links are a major cartilage fluorophore, and a marker for degradation in OA (Robins 1986; Uchiyama 1991; Senolt 2005). Further investigation of confocal microscopy should focus specifically on the loss of cross links and possibly link intensity of cartilage auto fluorescence to cartilage degradation.

There are a number of unknowns that need to be resolved in CSLM. It has been assumed that the laser penetrates the full depth of cartilage with only minimal attenuation. However, CSLM thickness measurements were consistently less than those measured by histology. This suggests that auto fluorescence in deeper cartilage layers was not contributing to the recorded signal. Otherwise, if the deep layers were auto fluorescing, it would be expected that the CSLM at a very minimum would equal the thickness of cartilage. There is however, the possibility that the application of a high threshold during post processing of the CSLM scans reduces the thickness. If lack of penetration into cartilage is a limitation, then the alignment of the tibial plateau will also be a limitation. Different tibial alignments will affect the distance an incident beam travels through the cartilage, and therefore, affect beam attenuation. CSLM can be used to provide a qualitative overview of cartilage

changes across the whole plateau. This may be useful for tracking the spatial distribution of focal lesions. However, for a quantitative analysis, CSLM would require a validation with histology, meaning the technique has little added value over histology itself, other than to provide an overview of gross morphology changes.

2. Synchrotron CT for porosity measurements

Theories on the involvement of subchondral bone in OA progression and initiation are not limited to a mechanical role. One theory is that subchondral bone is not an impermeable barrier between the epiphysis and the cartilage (Sokoloff 1993; Lajeunesse 2003; Goldring 2010), as it permits the movement of those biochemical agents responsible for degeneration. If this is the case then the porosity of subchondral bone is an important factor in osteoarthritic bone structure. The micro-CT equipment used in this thesis did not facilitate the measurement of porosity. By switching to high resolution synchrotron CT, the extent of pores and channels in osteoarthritic subchondral bone could be detected. Alternatively the permeability could be measured directly by measuring perfusion in sclerotic and normal subchondral bone, by removing the tibial head at the growth plate and driving fluid through the subchondral plate. Developing early marker of OA and understanding the tissue changes that occur will help in developing new diagnostics and therapies for treating OA.

8. Bibliography

Aagaard, H. and R. Verdonk (1999). "Function of the normal meniscus and consequences of meniscal resection." Scandinavian Journal of Medicine & Science in Sports **9**(3): 134-140.

Abu, E. O. (1997). "The expression of thyroid hormone receptors in human bone." Bone **21**(2): 137.

Aigner, T., U. Dietz, H. Stoss and K. von der Mark (1995). "Differential expression of collagen types I, II, III, and X in human osteophytes." Lab Invest **73**(2): 236-43.

Akhter, M. P., D. M. Cullen, E. A. Pedersen, D. B. Kimmel and R. R. Recker (1998). "Bone response to in vivo mechanical loading in two breeds of mice." Calcified Tissue International **63**(5): 442.

Alaaeddine, N. (2001). "Production of the chemokine RANTES by articular chondrocytes and role in cartilage degradation." Arthritis & Rheumatism **44**(7): 1633.

Aldegheri, R., G. Trivella and M. Saleh (1994). "Articulated distraction of the hip. Conservative surgery for arthritis in young patients." Clinical orthopaedics and related research(301): 94.

Altman, R., E. Asch, D. Bloch, G. Bole, D. Borenstein, K. Brandt, et al. (1986). "Development of criteria for the classification and reporting of osteoarthritis. Classification of osteoarthritis of the knee. Diagnostic and Therapeutic Criteria Committee of the American Rheumatism Association." Arthritis Rheum **29**(8): 1039-49.

Ameye, L. G. (2006). "Animal models of osteoarthritis: lessons learned while seeking the'Holy Grail'." Current opinion in rheumatology **18**(5): 537.

Amin, A. R. (1995). "The expression and regulation of nitric oxide synthase in human osteoarthritis-affected chondrocytes: evidence for up-regulated neuronal nitric oxide synthase." The Journal of experimental medicine **182**(6): 2097.

Amin, A. R. (1997). "Superinduction of cyclooxygenase-2 activity in human osteoarthritis-affected cartilage. Influence of nitric oxide." J Clin Invest **99**(6): 1231.

Anderson-MacKenzie, J. M. (2005). "Fundamental subchondral bone changes in spontaneous knee osteoarthritis." The international journal of biochemistry **37**(1): 224.

Anderson-MacKenzie, J. M., M. E. Billingham and A. J. Bailey (1999). "Collagen remodeling in the anterior cruciate ligament associated with developing spontaneous murine osteoarthritis." Biochem Biophys Res Commun **258**(3): 763-7.

Aspden, R. M. and D. W. L. Hukins (1981). "Collagen Organization in Articular Cartilage, Determined by X-Ray Diffraction, and its Relationship to Tissue Function." Proceedings of the Royal Society of London. Series B. Biological Sciences **212**(1188): 299-304.

Ayral, X. (2005). "Synovitis: a potential predictive factor of structural progression of medial tibiofemoral knee osteoarthritis-results of a 1 year longitudinal arthroscopic study in 422 patients." Osteoarthritis and Cartilage **13**(5): 361.

Bab, I. (2007). Micro-Tomographic Atlas of the Mouse Skeleton, Springer Science + Business Media LLC.

Bae, D. K., K. H. Yoon and S. J. Song (2006). "Cartilage Healing After Microfracture in Osteoarthritic Knees." Arthroscopy: The Journal of Arthroscopic & Related Surgery **22**(4): 367-374.

Bailey, A. J. (2004). "Biochemical and mechanical properties of subchondral bone in osteoarthritis." Biorheology **41**(3): 349.

Bailey, A. J., C. Buckland-Wright and D. Metz (2001). "The role of bone in osteoarthritis." Age and Ageing **30**(5): 374.

Bailey, A. J. and J. P. Mansell (1997). "Do subchondral bone changes exacerbate or precede articular cartilage destruction in osteoarthritis of the elderly?" Gerontology **43**(5): 296-304.

Baratz, M. E., F. H. Fu and R. Mengato (1986). "Meniscal tears: The effect of meniscectomy and of repair on intraarticular contact areas and stress in the human knee: A preliminary report." Am J Sports Med **14**(4): 270-275.

Beamer, W. G., L. R. Donahue, C. J. Rosen and D. J. Baylink (1996). "Genetic variability in adult bone density among inbred strains of mice." Bone **18**(5): 397.

Behets, C. (2004). "Effects of calcitonin on subchondral trabecular bone changes and on osteoarthritic cartilage lesions after acute anterior cruciate ligament deficiency." Journal of Bone and Mineral Research **19**(11): 1821.

Beighton, P. H. (1973). "Articular mobility in an African population." Annals of the Rheumatic Diseases **32**(5): 413.

Bendele, A. M. (2001). "Animal models of osteoarthritis." Journal of musculoskeletal & neuronal interactions **1**(14): 363.

Benderdour, M. (2002). "Interleukin 17 (IL-17) induces collagenase-3 production in human osteoarthritic chondrocytes via AP-1 dependent activation: differential activation of AP-1 members by IL-17 and IL-1beta." Journal of rheumatology **29**(6): 1262.

Bettica, P., G. Cline, D. J. Hart, J. Meyer and T. D. Spector (2002). "Evidence for increased bone resorption in patients with progressive knee osteoarthritis: Longitudinal results from the Chingford study." Arthritis & Rheumatism **46**(12): 3178-3184.

Beuf, O., S. Ghosh, D. C. Newitt, T. M. Link, L. Steinbach, M. Ries, et al. (2002). "Magnetic resonance imaging of normal and osteoarthritic trabecular bone structure in the human knee." Arthritis & Rheumatism **46**(2): 385-393.

Biewener, A. A., N. L. Fazzalari, D. D. Konieczynski and R. V. Baudinette (1996). "Adaptive changes in trabecular architecture in relation to functional strain patterns and disuse." Bone **19**(1): 1-8.

Bilezikian, J. P. (2008). Principles of bone biology.

Billinghurst, R. C. (1997). "Enhanced cleavage of type II collagen by collagenases in osteoarthritic articular cartilage." The Journal of clinical investigation **99**(7): 1534.

Bingham, C. O., 3rd, J. C. Buckland-Wright, P. Garnero, S. B. Cohen, M. Dougados, S. Adami, et al. (2006). "Risedronate decreases biochemical markers of cartilage degradation but does not decrease symptoms or slow radiographic progression in patients with medial compartment osteoarthritis of the knee: results of the two-year multinational knee osteoarthritis structural arthritis study." Arthritis Rheum **54**(11): 3494-507.

Blankevoort, L., G. J. van Osch, B. Janssen and E. E. Hekman (1996). "In vitro laxity-testers for knee joints of mice." Journal of Biomechanics **29**(6): 799.

Blom, A. B., P. L. van Lent, A. E. Holthuysen, P. M. van der Kraan, J. Roth, N. van Rooijen, et al. (2004). "Synovial lining macrophages mediate osteophyte formation during experimental osteoarthritis." Osteoarthritis Cartilage **12**(8): 627-35.

Blumenkrantz, G., C. T. Lindsey, T. C. Dunn, H. Jin, M. D. Ries, T. M. Link, et al. (2004). "A pilot, two-year longitudinal study of the interrelationship between trabecular bone and articular cartilage in the osteoarthritic knee." Osteoarthritis and Cartilage **12**(12): 997.

Bobinac, D., J. Spanjol, S. Zoricic and I. Maric (2003). "Changes in articular cartilage and subchondral bone histomorphometry in osteoarthritic knee joints in humans." Bone **32**(3): 284-90.

Boivin, G. Y. (2000). "Alendronate increases bone strength by increasing the mean degree of mineralization of bone tissue in osteoporotic women." Bone **27**(5): 687.

Botter, S. M., S. S. Glasson, B. Hopkins, S. Clockaerts, H. Weinans, J. P. T. M. van Leeuwen, et al. (2009). "ADAMTS5-/- mice have less subchondral bone changes after induction of osteoarthritis through surgical instability: implications for a link between cartilage and subchondral bone changes." Osteoarthritis and Cartilage **17**(5): 636-645.

Botter, S. M., G. J. V. M. van Osch, J. H. Waarsing, J. S. Day, J. A. N. Verhaar, H. A. P. Pols, et al. (2006). "Quantification of subchondral bone changes in a murine osteoarthritis model using micro-CT." Biorheology **43**(3-4): 379.

Botter, S. M., G. J. V. M. van Osch, J. H. Waarsing, J. C. van der Linden, J. A. N. Verhaar, H. A. P. Pols, et al. (2008). "Cartilage damage pattern in relation to subchondral plate thickness in a collagenase-induced model of osteoarthritis." Osteoarthritis and Cartilage **16**(4): 506.

Brandt, K. D. (1991). "Osteoarthritic changes in canine articular cartilage, subchondral bone, and synovium fiftyâ□□four months after transection of the anterior cruciate ligament." Arthritis & rheumatism **34**(12): 1560.

Brandt, K. D. (1991). "Osteoarthritic changes in canine articular cartilage: subchondral bone, and synovium fifty-four months after transection of the anterior crucitate ligament." Arthritis and rheumatism **34**(12): 1560.

Brandt, K. D., E. L. Radin, P. A. Dieppe and L. van de Putte (2006). "Yet more evidence that osteoarthritis is not a cartilage disease." Annals of the rheumatic diseases **65**(10): 1261.

Bronner, F., M. C. Farach-Carson and J. E. Rubin (2005). Bone Resorption, Springer-Verlag London Ltd.

Brown, T. D., R. C. Johnston, C. L. Saltzman, J. L. Marsh and J. A. Buckwalter (2006). "Posttraumatic Osteoarthritis: A First Estimate of Incidence, Prevalence, and Burden of Disease." Journal of orthopaedic trauma **20**(10): 739-44.

Brown, T. D., E. L. Radin, R. B. Martin and D. B. Burr (1984). "Finite element studies of some juxtarticular stress changes due to localized subchondral stiffening." Journal of Biomechanics **17**(1): 11-21, 23-24.

Brujan, E. (2011). Cavitation in Non-Newtonian Fluids.

Bruyere, O. (2003). "Subchondral tibial bone mineral density predicts future joint space narrowing at the medial femoro-tibial compartment in patients with knee osteoarthritis." Bone **32**(5): 541.

Buckland Wright, C. (2004). "Subchondral bone changes in hand and knee osteoarthritis detected by radiography." Osteoarthritis and cartilage **12**: 10.

Buckland Wright, J. C. (2000). "Early radiographic features in patients with anterior cruciate ligament rupture." Annals of the Rheumatic Diseases **59**(8): 641.

Buckwalter, J. A. (1994). "Operative treatment of osteoarthrosis. Current practice and future development." Journal of bone and joint surgery **76**(9): 1405.

Buckwalter, J. A. (1996). "Aging, Sports, and Osteoarthritis." Sports medicine and arthroscopy review **4**(3): 276.

Buckwalter, J. A. and H. J. Mankin (1997). "Instructional Course Lectures, The American Academy of Orthopaedic Surgeons - Articular Cartilage. Part II: Degeneration and Osteoarthrosis, Repair, Regeneration, and Transplantation." J Bone Joint Surg Am **79**(4): 612-32.

Buckwalter, J. A. and J. Martin (1995). "Degenerative joint disease." Clin Symp **47**(2): 1-32.

Bullough, P. G. (2004). "The role of joint architecture in the etiology of arthritis1." Osteoarthritis and cartilage **12**: 2.

Burr, D. (2004). "The importance of subchondral bone in the progression of osteoarthritis." Journal of rheumatology. Supplement **70**: 77-80.

Burr, D. B. (1997). "The involvement of subchondral mineralized tissues in osteoarthrosis: quantitative microscopic evidence." Microscopy research and technique **37**(4): 343.

Burr, D. B. (1998). "The importance of subchondral bone in osteoarthrosis." Current opinion in rheumatology **10**(3): 256-62.

Burr, D. B. (2004). "Anatomy and physiology of the mineralized tissues: role in the pathogenesis of osteoarthrosis." Osteoarthritis and Cartilage **12**: 20.

Cao, L., I. Youn, F. Guilak and L. A. Setton (2006). "Compressive Properties of Mouse Articular Cartilage Determined in a Novel Micro-Indentation Test Method and Biphasic Finite Element Model." Journal of Biomechanical Engineering **128**(5): 766-771.

Carlson, C. S. (1996). "Osteoarthritis in cynomolgus macaques III: effects of age, gender, and subchondral bone thickness on the severity of disease." Journal of bone and mineral research **11**(9): 1209.

Carter, D. R. (1988). "The role of mechanical loading histories in the development of diarthrodial joints." Journal of Orthopaedic Research **6**(6): 804.

Chadjichristos, C. (2003). "Sp1 and Sp3 transcription factors mediate interleukin-1β down-regulation of human type II collagen gene expression in articular chondrocytes." Journal of Biological Chemistry **278**(41): 39762.

Chambers, M. G., M. T. Bayliss and R. M. Mason (1997). "Chondrocyte cytokine and growth factor expression in murine osteoarthritis." Osteoarthritis Cartilage **5**(5): 301-8.

Chappard, C. (2006). "Subchondral bone micro-architectural alterations in osteoarthritis: a synchrotron micro-computed tomography study." Osteoarthritis and Cartilage **14**(3): 215.

Chen, Q. (1995). "Progression and recapitulation of the chondrocyte differentiation program: cartilage matrix protein is a marker for cartilage maturation." Developmental Biology **172**(1): 293.

Cheng, J. C. Y. (1991). "Joint laxity in children." Journal of pediatric orthopedics **11**(6): 752.

Chenu, C., A. Valentin-Opran, P. Chavassieux, S. Saez, P. J. Meunier and P. D. Delmas (1990). "Insulin like growth factor I hormonal regulation by growth hormone and by 1,25(OH)2D3 and activity on human osteoblast-like cells in short-term cultures." Bone **11**(2): 81-86.

Chia, S., J. J. Inglis, D. Essex, D. Preston, R. Williams, J. Saklatvala, et al. (2007). 53rd Annual Meeting of the Orthopaedic Research Society. 53rd Annual Meeting of the Orthopaedic Research Society, San Diego, ORS.

Clark, J. M. (1990). "The structure of vascular channels in the subchondral plate." Journal of anatomy **171**: 105.

Clements, K. M., J. S. Price, M. G. Chambers, D. M. Visco, A. R. Poole and R. M. Mason (2003). "Gene deletion of either interleukin-1β, interleukin-1β–converting enzyme, inducible nitric oxide synthase, or stromelysin 1 accelerates the development of knee osteoarthritis in mice after surgical transection of the medial collateral ligament and partial medial meniscectomy." Arthritis & Rheumatism **48**(12): 3452-3463.

Colombo, C., M. Butler, E. O'Byrne, L. Hickman, D. Swartzendruber, M. Selwyn, et al. (1983). "A new model of osteoarthritis in rabbits. I. Development of knee joint pathology following lateral meniscectomy and section of the fibular collateral and sesamoid ligaments." Arthritis Rheum **26**(7): 875-86.

Cserjesi, P., D. Brown, K. L. Ligon, G. E. Lyons, N. G. Copeland, D. J. Gilbert, et al. (1995). "Scleraxis: a basic helix-loop-helix protein that prefigures skeletal formation during mouse embryogenesis." Development **121**(4): 1099-1110.

Davies, J. (1989). "The osteoclast functional antigen, implicated in the regulation of bone resorption, is biochemically related to the vitronectin receptor." The Journal of cell biology **109**(4): 1817.

Day, J. S., M. Ding, J. C. van der Linden, I. Hvid, D. R. Sumner and H. Weinans (2001). "A decreased subchondral trabecular bone tissue elastic modulus is associated with pre-arthritic cartilage damage." Journal of Orthopaedic Research **19**(5): 914-918.

de Hooge, A. S. K., F. A. J. van de Loo, M. B. Bennink, O. J. Arntz, P. de Hooge and W. B. van den Berg (2005). "Male IL-6 gene knock out mice developed more advanced osteoarthritis upon aging." Osteoarthritis and Cartilage **13**(1): 66-73.

Dedrick, D. K. (1993). "A longitudinal study of subchondral plate and trabecular bone in cruciate-deficient dogs with osteoarthritis followed up for 54 months." Arthritis & Rheumatism **36**(10): 1460.

Deie, M. (2007). "A New Articulated Distraction Arthroplasty Device for Treatment of the Osteoarthritic Knee Joint: A Preliminary Report." Arthroscopy **23**(8): 833.

Dekel, S. and S. L. Weissman (1978). "Joint changes after overuse and peak overloading of rabbit knees in vivo." Acta Orthop Scand **49**(6): 519-28.

Dequeker, J. (1997). "Bone density and local growth factors in generalized osteoarthritis." Microscopy research and technique **37**(4): 358.

Dequeker, J., L. Mokassa and J. Aerssens (1995). "Bone density and osteoarthritis." Journal of rheumatology. Supplement **43**: 98-100.

Diarra, D., M. Stolina, K. Polzer, J. Zwerina, M. S. Ominsky, D. Dwyer, et al. (2007). "Dickkopf-1 is a master regulator of joint remodeling." Nat Med **13**(2): 156-163.

Dieppe, P. (1993). "Prediction of the progression of joint space narrowing in osteoarthritis of the knee by bone scintigraphy." Quality & Safety in Health Care **52**(8): 557.

Ding, M. (2003). "Changes in the three-dimensional microstructure of human tibial cancellous bone in early osteoarthritis." Journal of bone and joint surgery **85**(6): 906.

Doube M, K. M., Arganda-Carreras I, Cordelires F, Dougherty RP, and S. B. Jackson J, Hutchinson JR, Shefelbine SJ. (2010). "Extensible Bone Image Analysis in ImageJ. ." Bone (In press), from http://www.bonej.org.

Dougados, M., A. Gueguen, M. Nguyen, A. Thiesce, V. Listrat, L. Jacob, et al. (1992). "Longitudinal radiologic evaluation of osteoarthritis of the knee." J Rheumatol **19**(3): 378-84.

Dougherty, R. (2007). "Computing local thickness of 3D structures with ImageJ." Microscopy and Microanalysis **13**(S02E): 1678.

Ducy, P., R. Zhang, V. r. Geoffroy, A. L. Ridall and G. r. Karsenty (1997). "Osf2/Cbfa1: A Transcriptional Activator of Osteoblast Differentiation." Cell **89**(5): 747-754.

Dumond, H. (2003). "Evidence for a key role of leptin in osteoarthritis." Arthritis & Rheumatism **48**(11): 3118.

Duncan, R. L. (1995). "Mechanotransduction and the functional response of bone to mechanical strain." Calcified tissue international **57**(5): 344.

Eckstein, F. (2005). "In vivo cartilage deformation after different types of activity and its dependence on physical training status." Annals of the Rheumatic Diseases **64**(2): 291.

Edixhoven, P. (1987). "Accuracy and reproducibility of instrumented knee-drawer tests." Journal of Orthopaedic Research **5**(3): 378.

Ehrlich, M. G., H. J. Mankin, H. Jones, A. Grossman, C. Crispen and D. Ancona (1975). "Biochemical confirmation of an experimental osteoarthritis model." Journal of Bone and Joint Surgery; American volume **57**(3): 392-396.

Enomoto-Iwamoto, M., J. Kitagaki, E. Koyama, Y. Tamamura, C. Wu, N. Kanatani, et al. (2002). "The Wnt Antagonist Frzb-1 Regulates Chondrocyte Maturation and Long Bone Development during Limb Skeletogenesis." Developmental Biology **251**(1): 142-156.

Fahlgren, A., S. Chubinskaya, K. Messner and P. Aspenberg (2006). "A capsular incision leads to a fast osteoarthritic response, but also elevated levels of activated osteogenic protein-1 in rabbit knee joint cartilage." Scandinavian Journal of Medicine & Science in Sports **16**(6): 456-462.

Felson, D. T. (2004a). "Osteoarthritis: is it a disease of cartilage or of bone?" Arthritis & rheumatism **50**(2): 341.

Felson, D. T. (2004b). "Risk factors for osteoarthritis: understanding joint vulnerability." Clinical orthopaedics and related research(427 Suppl): S16-21.

Felson, D. T. (2005). "Osteophytes and progression of knee osteoarthritis." Rheumatology **44**(1): 100.

Felson, D. T., D. R. Gale, M. Elon Gale, J. Niu, D. J. Hunter, J. Goggins, et al. (2005). "Osteophytes and progression of knee osteoarthritis." Rheumatology **44**(1): 100-104.

Felson, D. T., S. McLaughlin, J. Goggins, M. P. LaValley, M. E. Gale, S. Totterman, et al. (2003). "Bone Marrow Edema and Its Relation to Progression of Knee Osteoarthritis." Annals of Internal Medicine **139**(1): 330-336.

Felson, D. T. and M. C. Nevitt (1998b). "The effects of estrogen on osteoarthritis." Current Opinion in Rheumatology **10**(3): 269-272.

Felson, D. T. and Y. Zhang (1998a). "An update on the epidemiology of knee and hip osteoarthritis with a view to prevention." Arthritis & Rheumatism **41**(8): 1343-1355.

Ferretti, J. L. (1996). "Mechanical validation of a tomographic (pQCT) index for noninvasive estimation of rat femur bending strength." Bone **18**(2): 97.

Finkelstein, J. S. (2002). "Ethnic variation in bone density in premenopausal and early perimenopausal women: effects of anthropometric and lifestyle factors." The Journal of clinical endocrinology and metabolism **87**(7): 3057.

Follet, H. (2004). "The degree of mineralization is a determinant of bone strength: a study on human calcanei." Bone **34**(5): 783.

Frisbie, D. D., G. W. Trotter, B. E. Powers, W. G. Rodkey, J. R. Steadman, R. D. Howard, et al. (1999). "Arthroscopic Subchondral Bone Plate Microfracture Technique Augments Healing of Large Chondral Defects in the Radial Carpal Bone and Medial Femoral Condyle of Horses." Veterinary Surgery **28**(4): 242-255.

Furman, W. (1976). "The anterior cruciate ligament. A functional analysis based on postmortem studies." Journal of Bone and Joint Surgery; American volume **58**(2): 179.

Ganey, T. M., J. A. Ogden, N. Abou-Madi, B. Colville, J. M. Zdyziarski and J. H. Olsen (1994). "Meniscal ossification. II. The normal pattern in the tiger knee." Skeletal Radiol **23**(3): 173-9.

GE, H. (2005) GE Healthcare, eXplore MicroView v. 2.0 Software Guide. **Volume**, DOI:

Ge, Z., Y. Hu, B. C. Heng, Z. Yang, H. Ouyang, E. H. Lee, et al. (2006). "Osteoarthritis and therapy." Arthritis and rheumatism **55**(3): 493-500.

Gilbert, S. F. (2000). Developmental Biology 6th edition. Sunderland (MA), Sinauer Associates.

Gill, T. J., L. E. DeFrate, C. Wang, C. T. Carey, S. Zayontz, B. Zarins, et al. (2003). "The Biomechanical Effect of Posterior Cruciate Ligament Reconstruction on Knee Joint Function." The American Journal of Sports Medicine **31**(4): 530-536.

Glasson, S. S. (2004). "Characterization of and osteoarthritis susceptibility in ADAMTS-4-knockout mice." Arthritis and rheumatism **50**(8): 2547.

Glasson, S. S. (2010). "The OARSI histopathology initiative-recommendations for histological assessments of osteoarthritis in the mouse." Osteoarthritis and cartilage **18**: S17.

Glasson, S. S., R. Askew, B. Sheppard, B. Carito, T. Blanchet, H. L. Ma, et al. (2005). "Deletion of active ADAMTS5 prevents cartilage degradation in a murine model of osteoarthritis." Nature **434**(7033): 644-8.

Glasson, S. S., R. Askew, B. Sheppard, B. Carito, T. Blanchet, H. L. Ma, et al. (2005). "Deletion of active ADAMTS5 prevents cartilage degradation in a murine model of osteoarthritis." Nature **434**: 644-648.

Glasson, S. S., R. Askew, B. Sheppard, B. A. Carito, T. Blanchet, H.-L. Ma, et al. (2004). "Characterization of and osteoarthritis susceptibility in ADAMTS-4–knockout mice." Arthritis & Rheumatism **50**(8): 2547-2558.

Glasson, S. S., T. J. Blanchet and E. A. Morris (2007). "The surgical destabilization of the medial meniscus (DMM) model of osteoarthritis in the 129/SvEv mouse." Osteoarthritis and Cartilage **15**(9): 1061-9.

Goker, B. (2000). "Bone mineral density varies as a function of the rate of joint space narrowing in the hip." Journal of rheumatology **27**(3): 735.

Goldring, M. B. (2000a). "The role of the chondrocyte in osteoarthritis." Arthritis Rheum **43**(9): 1916-26.

Goldring, S. R. (2009). "Role of bone in osteoarthritis pathogenesis." Med Clin North Am **93**(1): 25-35, xv.

Goldring, S. R. (2010). "Bone and cartilage in osteoarthritis: is what's best for one good or bad for the other?" Arthritis Research & Therapy **12**(5): 143.

Gomoll, A., G. Filardo, L. de Girolamo, J. Esprequeira-Mendes, M. Marcacci, W. Rodkey, et al. (2011). "Surgical treatment for early osteoarthritis. Part I: cartilage repair procedures." Knee Surgery, Sports Traumatology, Arthroscopy: 1-17.

Gray, H. (2008). Gray's Anatomy: The Anatomical Basis of Clinical Practice.

Grynpas, M. D. (1991). "Subchondral bone in osteoarthritis." Calcified Tissue International **49**(1): 20.

Hadjidakis, D. J. (2006). "Bone remodeling." Annals of the New York Academy of Sciences **1092**(1): 385.

Hannan, M. T. (1990). "Estrogen use and radiographic osteoarthritis of the knee in women." Arthritis & rheumatism **33**(4): 525.

Harris, W. H. (1986). "Etiology of osteoarthritis of the hip." Clinical orthopaedics and related research **213**: 20.

Harwin, S. F. (1999). "Arthroscopic Debridement for Osteoarthritis of the Knee: Predictors of Patient Satisfaction." Arthroscopy: The Journal of Arthroscopic & Related Surgery **15**(2): 142-146.

Hatori, M., K. J. Klatte, C. C. Teixeira and I. M. Shapiro (1995). "End labeling studies of fragmented DNA in the Avian growth plate: Evidence of apoptosis in terminally differentiated chondrocytes." Journal of Bone and Mineral Research **10**(12): 1960-1968.

Havdrup, T. (1976). "The subchondral bone in osteoarthritis and rheumatoid arthritis of the knee: a histological and microradiographical study." Acta orthopaedica Scandinavica **47**(3): 345.

Havdrup, T. (1977). "Papain-induced changes in the knee joints of adult rabbits." Acta orthopaedica Scandinavica **48**(2): 143.

Hayami, T. (2004). "The role of subchondral bone remodeling in osteoarthritis: reduction of cartilage degeneration and prevention of osteophyte formation by alendronate in the rat anterior cruciate ligament transection model." Arthritis & rheumatism **50**(4): 1193.

Hayami, T. (2006). "Characterization of articular cartilage and subchondral bone changes in the rat anterior cruciate ligament transection and meniscectomized models of osteoarthritis." Bone **38**(2): 234.

Henderson, B. (1989). "Arthritogenic actions of recombinant IL-1 and tumour necrosis factor alpha in the rabbit: evidence for synergistic interactions between cytokines in vivo." Clinical and experimental immunology **75**(2): 306.

Henry, Y. M. (2000). "Ethnic and gender differences in bone mineral density and bone turnover in young adults: effect of bone size." Osteoporosis international **11**(6): 512.

Hildebrand, T. (1997). "A new method for the independent assessment of thickness in three-dimensional images." Journal of microscopy **185**(1): 67.

Hill, P. A. (1998). "Bone remodelling." Journal of orthodontics **25**(2): 101.

Hisatome, T. (2002). "Effects on articular cartilage of subchondral replacement with polymethylmethacrylate and calcium phosphate cement." Journal of biomedical materials research. Part B, Applied biomaterials **59**(3): 490.

Hoang, B. (1996). "Primary structure and tissue distribution of FRZB, a novel protein related to Drosophila frizzled, suggest a role in skeletal morphogenesis." Journal of Biological Chemistry **271**(42): 26131.

Hock, J. M. (1988). "Insulin-like growth factor I has independent effects on bone matrix formation and cell replication." Endocrinology **122**(1): 254.

Hofbauer, L. C. (2000). "The roles of osteoprotegerin and osteoprotegerin ligand in the paracrine regulation of bone resorption." Journal of Bone and Mineral Research **15**(1): 2.

Hofbauer, L. C. (2004). "Clinical implications of the osteoprotegerin/RANKL/RANK system for bone and vascular diseases." JAMA (Chicago, Ill.) **292**(4): 490.

Hou, P. (1997). "Identification and Characterization of the Insulin-like Growth Factor I Receptor in Mature Rabbit Osteoclasts." Journal of Bone and Mineral Research **12**(4): 534.

Hsieh, H. H. and P. S. Walker (1976). "Stabilizing mechanisms of the loaded and unloaded knee joint." J Bone Joint Surg Am **58**(1): 87-93.

Hsu, H. (1999). "Tumor necrosis factor receptor family member RANK mediates osteoclast differentiation and activation induced by osteoprotegerin ligand." Proceedings of the National Academy of Sciences of the United States of America **96**(7): 3540.

Hughes, L. C. (2005). "The ultrastructure of mouse articular cartilage: collagen orientation and implications for tissue functionality. A polarised light and scanning electron microscope study and review." European cells & materials **9**: 68.

Hung, S. C. (1997). "Effects of Continuous Distraction on Cartilage in a Moving Joint: An Investigation on Adult Rabbits." Journal of Orthopaedic Research **15**: 381.

Hunt, S., L. Jazrawi and O. Sherman (2002). "Arthroscopic management of osteoarthritis of the knee." Journal of the American Academy of Orthopaedic Surgeons **10**(5): 356-363.

Hunter, D. J. (2006). "Osteoarthritis." BMJ **332**(7542): 639.

Hunter, D. J., Y. Zhang, J. Niu, J. Goggins, S. Amin, M. P. LaValley, et al. (2006). "Increase in bone marrow lesions associated with cartilage loss: A longitudinal magnetic resonance imaging study of knee osteoarthritis." Arthritis & Rheumatism **54**(5): 1529-1535.

Hunziker, E. B. (2002). "Articular cartilage repair: basic science and clinical progress. A review of the current status and prospects." Osteoarthritis and Cartilage **10**(6): 432.

Ilic, M. Z. (2007). "Distinguishing aggrecan loss from aggrecan proteolysis in ADAMTS-4 and ADAMTS-5 single and double deficient mice." Journal of Biological Chemistry **282**(52): 37420.

Imai, K. (1997). "Expression of membrane-type 1 matrix metalloproteinase and activation of progelatinase A in human osteoarthritic cartilage." The American journal of pathology **151**(1): 245.

Imhof, H., M. Breitenseher, F. Kainberger, T. Rand and S. Trattnig (1999). "Importance of subchondral bone to articular cartilage in health and disease." Topics in magnetic resonance imaging **10**(3): 180-92.

Inglis, J. J., K. E. McNamee, S. L. Chia, D. Essex, M. Feldmann, R. O. Williams, et al. (2008). "Regulation of pain sensitivity in experimental osteoarthritis by the endogenous peripheral opioid system." Arthritis and rheumatism **58**(10): 3110.

Intema, F. (2010). "Similarities and discrepancies in subchondral bone structure in two differently induced canine models of osteoarthritis." Journal of Bone and Mineral Research **25**(7): 1650.

Intema, F., J. DeGroot, B. Elshof, M. E. Vianen, S. Yocum, A. Zuurmond, et al. (2008). "The canine bilateral groove model of osteoarthritis." Journal of Orthopaedic Research **26**(11): 1471-7.

Jackson-Laboratory. (2009). "JAX® Mice Database." from http://jaxmice.jax.org/query/f?p=205:1:3633989967120115798.

Jansson, A. (2004). "General joint laxity in 1845 Swedish school children of different ages: ages and genders□specific distributions." Acta paediatrica **93**(9): 1202.

Jefferson, R. J. (1990). "The role of the quadriceps in controlling impulsive forces around heel strike." Proceedings of the Institution of Mechanical Engineers; Part H; Journal of Engineering in Medicine **204**(18): 21.

Joosten, L. A. B. (1997). "Role of interleukin-4 and interleukin-10 in murine collagense induced arthritis. Protective effect of interleukin-4 and interleukin-10 treatment on cartilage destruction." Arthritis & rheumatism **40**(2): 249.

Judex, S. (2004). "Genetically Based Influences on the Site-Specific Regulation of Trabecular and Cortical Bone Morphology." Journal of bone and mineral research **19**(4): 600.

Judex, S., L. R. Donahue and C. Rubin (2002). "Genetic predisposition to low bone mass is paralleled by an enhanced sensitivity to signals anabolic to the skeleton." FASEB J.: 01-0913fje.

Junqueira, L. C. (2005). Basic histology.

Jurvelin, J., I. Kiviranta, M. Tammi and J. H. Helminen (1986). "Softening of canine articular cartilage after immobilization of the knee joint." Clinical orthopaedics and related research(207): 246-52.

Kadri, A. (2008). "Osteoprotegerin inhibits cartilage degradation through an effect on trabecular bone in murine experimental osteoarthritis." Arthritis and rheumatism **58**(8): 2379.

Kajiwara, R., O. Ishida, K. Kawasaki, N. Adachi, Y. Yasunaga and M. Ochi (2005). "Effective repair of a fresh osteochondral defect in the rabbit knee joint by articulated joint distraction following subchondral drilling." Journal of Orthopaedic Research **23**(4): 909-15.

Kamekura, S., K. Hoshi, T. Shimoaka, U. Chung, H. Chikuda, T. Yamada, et al. (2005). "Osteoarthritis development in novel experimental mouse models induced by knee joint instability." Osteoarthritis and Cartilage **13**(7): 632-641.

Kapoor, M. (2011). "Role of proinflammatory cytokines in the pathophysiology of osteoarthritis." Nature Reviews Rheumatology **7**(1): 33.

Karadam, B. (2005). "No beneficial effects of joint distraction on early microscopical changes in osteoarthrotic knees." Acta orthopaedica **76**(1): 95.

Karvonen, R. L. (1998). "Periarticular osteoporosis in osteoarthritis of the knee." Journal of rheumatology **25**(11): 2187.

Kellgren, J. H., J. S. Lawrence and F. Bier (1963). Genetic Factors in Generalized Osteo-Arthrosis.

Ker, R. F. (2002). "The implications of the adaptable fatigue quality of tendons for their construction, repair and function." Comparative Biochemistry and Physiology - Part A: Molecular & Integrative Physiology **133**(4): 987-1000.

Kerkhof, H. J. M. (2010). "A genome wide association study identifies an osteoarthritis susceptibility locus on chromosome 7q22." Arthritis & Rheumatism **62**(2): 499.

Kilts, T., L. Ameye, F. Syed-Picard, M. Ono, A. D. Berendsen, A. Oldberg, et al. (2009). "Potential roles for the small leucine-rich proteoglycans biglycan and fibromodulin in ectopic ossification of tendon induced by exercise and in modulating rotarod performance." Scandinavian Journal of Medicine & Science in Sports **19**(4): 536-546.

KIR (2007). MMD Excerpt.

Kirkley, A. (2008). "A randomized trial of arthroscopic surgery for osteoarthritis of the knee." The New England journal of medicine **359**(11): 1097.

Knäuper, V. (1996). "Biochemical characterization of human collagenase-3." Journal of Biological Chemistry **271**(3): 1544.

Kohler, T. (2005). "Compartmental bone morphometry in the mouse femur: Reproducibility and resolution dependence of microtomographic measurements." Calcified Tissue International **77**(5): 281.

Kreuz, P. C., M. R. Steinwachs, C. Erggelet, S. J. Krause, G. Konrad, M. Uhl, et al. (2006). "Results after microfracture of full-thickness chondral defects in different compartments in the knee." Osteoarthritis and Cartilage **14**(11): 1119-1125.

Kubo, M. (2002). "Articular cartilage degradation and de-differentiation of chondrocytes by the systemic administration of retinyl acetate-ectopic production of osteoblast stimulating factor-1 by chondrocytes in mice." Osteoarthritis and cartilage **10**(12): 968.

Lafeber, F. (1992). "Intermittent hydrostatic compressive force stimulates exclusively the proteoglycan synthesis of osteoarthritic human cartilage." Rheumatology **31**(7): 437.

Lafeber, F. (2006). "Unloading joints to treat osteoarthritis, including joint distraction." Current opinion in rheumatology **18**(5): 519.

Lajeunesse, D. (2003). "Subchondral bone in osteoarthritis: a biologic link with articular cartilage leading to abnormal remodeling." Current Opinion in Rheumatology **15**(5): 628.

Lane, L. B. (1980). "Age-related changes in the thickness of the calcified zone and the number of tidemarks in adult human articular cartilage." Journal of bone and joint surgery. British volume **62**(3): 372.

Lapvetelainen, T., T. Nevalainen, J. J. Parkkinen, J. Arokoski, K. Kiraly, M. Hyttinen, et al. (1995). "Lifelong moderate running training increases the incidence and severity of osteoarthritis in the knee joint of C57BL mice." Anat Rec **242**(2): 159-65.

Laupattarakasem, W., M. Laopaiboon, P. Laupattarakasem and C. Sumananont (2008). "Arthroscopic debridement for knee osteoarthritis." Cochrane database of systematic reviews(1): CD005118-CD005118.

Layton, M. W. (1988). "Examination of subchondral bone architecture in experimental osteoarthritis by microscopic computed axial tomography." Arthritis & Rheumatism **31**(11): 1400.

Lee, M. S. (2002). "Effects of shear stress on nitric oxide and matrix protein gene expression in human osteoarthritic chondrocytes in vitro." Journal of Orthopaedic Research **20**(3): 556.

Lee, M. S. (2003a). "Intermittent hydrostatic pressure inhibits shear stress-induced nitric oxide release in human osteoarthritic chondrocytes in vitro." Journal of rheumatology **30**(2): 326.

Lee, M. S. (2003b). "Protective effects of intermittent hydrostatic pressure on osteoarthritic chondrocytes activated by bacterial endotoxin in vitro." Journal of Orthopaedic Research **21**(1): 117.

Leppala, J. (1999). "Effect of anterior cruciate ligament injury of the knee on bone mineral density of the spine and affected lower extremity: a prospective one-year follow-up study." Calcified tissue international **64**(4): 357.

Leroux, M. A., H. S. Cheung, J. L. Bau, J. Y. Wang, D. S. Howell and L. A. Setton (2001). "Altered mechanics and histomorphometry of canine tibial cartilage following joint immobilization." Osteoarthritis Cartilage **9**(7): 633-40.

Levy, I. M., P. A. Torzilli and R. F. Warren (1982). "The effect of medial meniscectomy on anterior-posterior motion of the knee." J Bone Joint Surg Am **64**(6): 883-888.

Li, B. (1997b). "Mechanical and material properties of the subchondral bone plate from the femoral head of patients with osteoarthritis or osteoporosis." Quality & Safety in Health Care **56**(4): 247.

Li, B. and R. M. Aspden (1997a). "Composition and Mechanical Properties of Cancellous Bone from the Femoral Head of Patients with Osteoporosis or Osteoarthritis." Journal of Bone and Mineral Research **12**(4): 641-651.

Li, B., D. Marshall, M. Roe and R. M. Aspden (1999). "The electron microscope appearance of the subchondral bone plate in the human femoral head in osteoarthritis and osteoporosis." Journal of Anatomy **195**(1): 101-110.

Lindsey, C. T. (2004). "Magnetic resonance evaluation of the interrelationship between articular cartilage and trabecular bone of the osteoarthritic knee." Osteoarthritis and Cartilage **12**(2): 86.

Little, C. (2008). "Animal Models of Osteoarthritis." Current Rheumatology Reviews **4**: 175-182.

Little, C. B., C. T. Meeker, S. B. Golub, K. E. Lawlor, P. J. Farmer, S. M. Smith, et al. (2007). "Blocking aggrecanase cleavage in the aggrecan interglobular domain abrogates cartilage erosion and promotes cartilage repair." J Clin Invest **117**(6): 1627-1636.

Lories, R. J. U. (2007). "Articular cartilage and biomechanical properties of the long bones in Frzb-knockout mice." Arthritis & Rheumatism **56**(12): 4095.

Lories, R. J. U. (2009). "Deletion of frizzled-related protein reduces voluntary running exercise performance in mice." Osteoarthritis and Cartilage **17**(3): 390.

Lotz, M., R. Terkeltaub and P. M. Villiger (1992). "Cartilage and joint inflammation. Regulation of IL-8 expression by human articular chondrocytes." The journal of immunology **148**(2): 466-473.

Loughlin, J. (2006). "The CALM1core promoter polymorphism is not associated with hip osteoarthritis in a United Kingdom Caucasian population." Osteoarthritis and Cartilage **14**(3): 295.

Loughlin, J. (2010). "Osteoarthritis year 2010 in review: genetics." Osteoarthritis and Cartilage **19**(4): 342-345.

Lu, J.-P. (2010). "An experimental Osteoarthritis Induced by Implanting Composite Material into Subchondral Bone of Rabbit Knee." Orthopedic Journal of China **18**(3): 250-254.

Ma, H. L. (2007). "Osteoarthritis severity is sex dependent in a surgical mouse model." Osteoarthritis and Cartilage **15**(6): 695.

Ma, H. L., T. J. Blanchet, D. Peluso, B. Hopkins, E. A. Morris and S. S. Glasson (2007). "Osteoarthritis severity is sex dependent in a surgical mouse model." Osteoarthritis and Cartilage **15**(6): 695-700.

MacGregor, A. J. (2000). "The genetic contribution to radiographic hip osteoarthritis in women." Arthritis & Rheumatism **43**(11): 2410.

Maffulli, N. (2005). Tendon Injuries.

Mahmoodian, R., J. Leasure, P. Philip, N. Pleshko, F. Capaldi and S. Siegler (2011). "Changes in mechanics and composition of human talar cartilage anlagen during fetal development." Osteoarthritis and Cartilage **19**(10): 1199-1209.

Majumdar, M. K. (2007). "Double-knockout of ADAMTS-4 and ADAMTS-5 in mice results in physiologically normal animals and prevents the progression of osteoarthritis." Arthritis & Rheumatism **56**(11): 3670.

Manicourt, D. (2005). "Rationale for the potential use of calcitonin in osteoarthritis." Journal of musculoskeletal & neuronal interactions **5**(3): 285.

Manninen, P., H. Riihimaki, M. Heliovaara and P. Makela (1996). "Overweight, gender and knee osteoarthritis." Int J Obes Relat Metab Disord **20**(6): 595-7.

Mansell, J. P. and A. J. Bailey (1998). "Abnormal cancellous bone collagen metabolism in osteoarthritis." J Clin Invest **101**(8): 1596-603.

Marguerite, R. (2008). "Rheological investigation on hyaluronan-fibrinogen interaction." International Journal of Biological Macromolecules **43**(5): 444-450.

Marijnissen, A. (2002b). "Clinical benefit of joint distraction in the treatment of severe osteoarthritis of the ankle." Arthritis and rheumatism **46**: 2893.

Marijnissen, A. C., P. M. van Roermund, N. Verzijl, J. M. Tekoppele, J. W. Bijlsma and F. P. Lafeber (2002a). "Steady progression of osteoarthritic features in the canine groove model." Osteoarthritis Cartilage **10**(4): 282-9.

Martel-Pelletier, J., L. M. Wildi and J.-P. Pelletier (2011). "Future therapeutics for osteoarthritis." Bone(0).

Martin, J. A. (2002). "Aging, articular cartilage chondrocyte senescence and osteoarthritis." Biogerontology **3**(5): 257.

Mason, R. M., M. G. Chambers, J. Flannelly, J. D. Gaffen, J. Dudhia and M. T. Bayliss (2001). "The STR/ort mouse and its use as a model of osteoarthritis." Osteoarthritis and cartilage **9**(2): 85-91.

Mastbergen, S. C. (2008). "The groove model of osteoarthritis applied to the ovine fetlock joint." Osteoarthritis and Cartilage **16**(8): 919.

Masuko-Hongo, K. (2004). "Up-regulation of microsomal prostaglandin E synthase 1 in osteoarthritic human cartilage: Critical roles of the ERK-1/2 and p38 signaling pathways." Arthritis & Rheumatism **50**(9): 2829.

Masuya, H., K. Nishida, T. Furuichi, H. Toki, G. Nishimura, H. Kawabata, et al. (2007). "A novel dominant-negative mutation in Gdf5 generated by ENU mutagenesis impairs joint formation and causes osteoarthritis in mice." Human Molecular Genetics **16**(19): 2366-2375.

Mathieu, M. D. P., M. D. T. Conrozier, M. D. E. Vignon, M. D. Y. Rozand and D. M. R. Ph (2009). "Rheologic Behavior of Osteoarthritic Synovial Fluid after Addition of Hyaluronic Acid: A Pilot Study." Clinical Orthopaedics and Related Research® **467**(11): 3002-3009.

McDermott, I. D. and A. A. Amis (2006). "The consequences of meniscectomy." J Bone Joint Surg Br **88-B**(12): 1549-1556.

McErlain, D. D. (2008). "Study of subchondral bone adaptations in a rodent surgical model of OA using in vivo micro-computed tomography." Osteoarthritis and Cartilage **16**(4): 458.

Media, N. M. (1999-2011). Ligaments of the Knee. Atlanta US.

Messner, K. and J. Gao (1998). "The menisci of the knee joint. Anatomical and functional characteristics, and a rationale for clinical treatment." Journal of Anatomy **193**(2): 161-178.

Mizuno, Y. (1994). "Immunocytochemical identification of androgen receptor in mouse osteoclast-like multinucleated cells." Calcified Tissue International **54**(4): 325.

Mohtai, M. (1996). "Expression of interleukin-6 in osteoarthritic chondrocytes and effects of fluid-induced shear on this expression in normal human chondrocytes in vitro." Journal of Orthopaedic Research **14**(1): 67.

Moodie, J. P., K. S. Stok, R. Müller, T. L. Vincent and S. J. Shefelbine (2010). "Multimodal imaging demonstrates concomitant changes in bone and cartilage after destabilisation of the medial meniscus and increased joint laxity." Osteoarthritis and Cartilage **19**(2): 163-170.

Moreau, M. (2011). "Tiludronate treatment improves structural changes and symptoms of osteoarthritis in the canine anterior cruciate ligament model." Arthritis research & therapy **13**(3): R98.

Mori, S. and D. B. Burr (1993b). "Increased intracortical remodeling following fatigue damage." Bone **14**(2): 103-109.

Mori, S., R. Harruff and D. B. Burr (1993a). "Microcracks in articular calcified cartilage of human femoral heads." Arch Pathol Lab Med **117**(2): 196-8.

Moseley, J. B., K. O'Malley, N. J. Petersen, T. J. Menke, B. A. Brody, D. H. Kuykendall, et al. (2002). "A Controlled Trial of Arthroscopic Surgery for Osteoarthritis of the Knee." New England Journal of Medicine **347**(2): 81-88.

Moskowitz, R. W. (1999). "Bone remodeling in osteoarthritis: subchondral and osteophytic responses." Osteoarthritis and Cartilage **7**(3): 323.

Moskowitz, R. W., W. Davis, J. Sammarco, M. Martens, J. Baker, M. Mayor, et al. (1973). "Experimentally induced degenerative joint lesions following partial meniscectomy in the rabbit." Arthritis Rheum **16**(3): 397-405.

Mototani, H., A. Mabuchi, S. Saito, M. Fujioka, A. Iida, Y. Takatori, et al. (2005). "A functional single nucleotide polymorphism in the core promoter region of CALM1 is associated with hip osteoarthritis in Japanese." Human Molecular Genetics **14**(8): 1009-1017.

Muraoka, T. (2007). "Role of subchondral bone in osteoarthritis development: a comparative study of two strains of guinea pigs with and without spontaneously occurring osteoarthritis." Arthritis & Rheumatism **56**(10): 3366.

Murshed, M., D. Harmey, J. L. MillÃ¡n, M. D. McKee and G. Karsenty (2005). "Unique coexpression in osteoblasts of broadly expressed genes accounts for the spatial restriction of ECM mineralization to bone." Genes & Development **19**(9): 1093-1104.

Nadkar, M. Y., R. S. Samant, S. S. Vaidya and N. E. Borges (1999). "Relationship between osteoarthritis of knee and menopause." The Journal of the Association of Physicians of India **47**(12): 1161-1163.

Naruse, K. (2009). "Osteoarthritic changes of the patellofemoral joint in STR/OrtCrlj mice are the earliest detectable changes and may be caused by internal tibial torsion." Connective tissue research **50**(4): 243.

Naski, M. C. and D. M. Ornitz (1998). "FGF signaling in skeletal development." Front Biosci **3**: d781-94.

Neuman, P., A. Hulth, B. Lindén, O. Johnell and L. Dahlberg (2003). "The role of osteophytic growth in hip osteoarthritis." International Orthopaedics **27**(5): 262-266.

Nevitt, M. C. (1995). "Radiographic osteoarthritis of the hip and bone mineral density." Arthritis & Rheumatism **38**(7): 907.

Newberry, W. N., D. K. Zukosky and R. C. Haut (1997). "Subfracture insult to a knee joint causes alterations in the bone and in the functional stiffness of overlying cartilage." Journal of Orthopaedic Research **15**(3): 450-455.

Nielsen, S. (1984). "Rotatory instability of cadaver knees after transection of collateral ligaments and capsule." Archives of orthopaedic and trauma surgery **103**(3): 165.

Nordin, M. (2012). Basic biomechanics of the musculoskeletal system.

Nuki, G. (1999). "Osteoarthritis: a problem of joint failure." Zeitschrift für Rheumatologie **58**(3): 142.

O'Connor, B. L. (1989). "Gait alterations in dogs after transection of the anterior cruciate ligament." Arthritis & Rheumatism **32**(9): 1142.

O'Connor, K. M. (1997). "Unweighting Accelerates Tidemark Advancement in Articular Cartilage at the Knee Joint of Rats." Journal of Bone and Mineral Research **12**(4): 580-589.

O'Hara, B. P. (1990). "Influence of cyclic loading on the nutrition of articular cartilage." Annals of the Rheumatic Diseases **49**(7): 536.

Oettmeier, R. (1992). "Quantitative study of articular cartilage and subchondral bone remodeling in the knee joint of dogs after strenuous running training." Journal of Bone and Mineral Research **7**(S2): S419.

Ong, F. R. (2000). "Evaluation of bone strength: correlation between measurements of bone mineral density and drilling force." Proceedings of the Institution of Mechanical Engineers. Part B, Journal of engineering manufacture **214**(4): 385.

Oretorp, N. (1978). "Immediate effects of meniscectomy on the knee joint: The effects of tensile load on knee joint ligaments in dogs." Acta orthopaedica Scandinavica **49**(4): 407.

Oretorp, N. (1978). "Immediate Effects of Meniscectomy on the Knee Joint: The Effects of Tensile Load on Knee Joint Ligaments in Dogs." Acta orthopaedica **49**(4): 407.

Ortega, N., D. J. Behonick and Z. Werb (2004). "Matrix remodeling during endochondral ossification." Trends in Cell Biology **14**(2): 86-93.

Otsu, N. (1975). "A threshold selection method from gray-level histograms." Automatica **11**: 285.

Ozawa, H. (2008). "Current concepts of bone biomineralization." Journal of oral biosciences **50**(1): 1.

Pacicca, D. M. (2003). "Expression of angiogenic factors during distraction osteogenesis." Bone **33**(6): 889.

Pacquelet, S. (2002). "Interleukin 17, a nitric oxide-producing cytokine with a peroxynitrite-independent inhibitory effect on proteoglycan synthesis." Journal of rheumatology **29**(12): 2602.

Palcy, S. and D. Goltzman (1999). "Protein kinase signalling pathways involved in the up-regulation of the rat alpha1(I) collagen gene by transforming growth factor beta1 and bone morphogenetic protein 2 in osteoblastic cells." Biochem J **343 Pt 1**: 21-7.

Palmoski, M. J. (1982). "Immobilization of the knee prevents osteoarthritis after anterior cruciate ligament transection." Arthritis and rheumatism **25**: 1201.

Palmoski, M. J., R. A. Colyer and K. D. Brandt (1980). "Joint motion in the absence of normal loading does not maintain normal articular cartilage." Arthritis and rheumatism **23**(3): 325-34.

Panula, H. E., H. J. Helminen and I. Kiviranta (1997). "Slowly Progressive Osteoarthritis After Tibial Valgus Osteotomy in Young Beagle Dogs." Clinical Orthopaedics and Related Research **343**: 192-202.

Parfitt, A. M. (1988). "Bone histomorphometry: Standardization of nomenclature, symbols and units (summary of proposed system)." Bone **9**(1): 67-69.

Pastoureau, P. (2003). "Quantitative assessment of articular cartilage and subchondral bone histology in the meniscectomized guinea pig model of osteoarthritis." Osteoarthritis and Cartilage **11**(6): 412.

Pastoureau, P. C., A. C. Chomel and J. Bonnet (1999). "Evidence of early subchondral bone changes in the meniscectomized guinea pig. A densitometric study using dual-energy X-ray absorptiometry subregional analysis." Osteoarthritis and Cartilage **7**(5): 466-473.

Pawley, J. B. (2006). Handbook of Biological Confocal Microscopy.

Pazzaglia, U., T. Congiu, G. Zarattini, M. Marchese and D. Quacci (2011). "The fibrillar organisation of the osteon and cellular aspects of its development." Anatomical Science International **86**(3): 128-134.

Pearle, A. D. (2005). "Basic Science of Articular Cartilage and Osteoarthritis." Arthroscopy **24**(1): 1.

Pelletier, J. P. (2001). "Osteoarthritis, an inflammatory disease: potential implication for the selection of new therapeutic targets." Arthritis & Rheumatism **44**(6): 1237.

Pelletier, J. P. (2004). "The inhibition of subchondral bone resorption in the early phase of experimental dog osteoarthritis by licofelone is associated with a reduction in the synthesis of MMP-13 and cathepsin K." Bone **34**(3): 527.

Petrtyl, M. (1996). "Spatial organization of the haversian bone in man." Journal of biomechanics **29**(2): 161.

Piecha, D. (2010). "Novel selective MMP-13 inhibitors reduce collagen degradation in bovine articular and human osteoarthritis cartilage explants." Inflammation research **59**(5): 379-389.

Ploegmakers, J. J. W. (2005). "Prolonged clinical benefit from joint distraction in the treatment of ankle osteoarthritis." Osteoarthritis and Cartilage **13**(7): 582.

Pond, M. J. and G. Nuki (1973). "Experimentally-induced osteoarthritis in the dog." Annals of the Rheumatic Diseases **32**(4): 387-388.

Pottenger, L. A., F. M. Phillips and L. F. Draganich (1990). "The effect of marginal osteophytes on reduction of varus-valgus instability in osteoarthritic knees." Arthritis Rheum **33**(6): 853-8.

Poulet, B., R. W. Hamilton, S. Shefelbine and A. A. Pitsillides "Characterizing a novel and adjustable noninvasive murine joint loading model." Arthritis Rheum **63**(1): 137-47.

Pritzker, K. P. (1994). "Animal models for osteoarthritis: processes, problems and prospects." Annals of the rheumatic diseases **53**(6): 406.

Puxkandl, R., I. Zizak, O. Paris, J. Keckes, W. Tesch, S. Bernstorff, et al. (2002). "Viscoelastic properties of collagen: synchrotron radiation investigations and structural model." Philosophical Transactions of the Royal Society of London. Series B: Biological Sciences **357**(1418): 191-197.

Qiu, S., D. S. Rao, S. Palnitkar and A. M. Parfitt (2009). "Dependence of bone yield (volume of bone formed per unit of cement surface area) on resorption cavity size during osteonal remodeling in human rib: implications for osteoblast function and the pathogenesis of age-related bone loss." Journal of Bone and Mineral Research **25**(2): 423-430.

Quasnichka, H. L. (2006). "Subchondral bone and ligament changes precede cartilage degradation in guinea pig osteoarthritis." Biorheology **43**(3): 389.

Quasnichka, H. L., J. M. Anderson-MacKenzie, J. F. Tarlton, T. J. Sims, M. E. Billingham and A. J. Bailey (2005). "Cruciate ligament laxity and femoral intercondylar notch narrowing in early-stage knee osteoarthritis." Arthritis Rheum **52**(10): 3100-9.

Radin, E. L. (1972). "Role of mechanical factors in pathogenesis of primary osteoarthritis." The Lancet **299**(7749): 519.

Radin, E. L., M. G. Ehrlich, R. Chernack, P. Abernethy, I. L. Paul and R. M. Rose (1978). "Effect of Repetitive Impulsive Loading on the Knee Joints of Rabbits." Clinical Orthopaedics and Related Research **131**: 288-293.

Radin, E. L., I. L. Paul and M. Lowy (1970). "A comparison of the dynamic force transmitting properties of subchondral bone and articular cartilage." Journal of Bone and Joint Surgery; American volume **52**(3): 444-456.

Radin, E. L. and R. M. Rose (1986). "Role of subchondral bone in the initiation and progression of cartilage damage." Clinical orthopaedics and related research **213**: 34-40.

Radin, E. L., K. H. Yang, C. Riegger, V. L. Kish and J. J. O'Connor (1991). "Relationship between lower limb dynamics and knee joint pain." Journal of Orthopaedic Research **9**(3): 398-405.

Raggatt, L. J. and N. C. Partridge (2010). "Cellular and Molecular Mechanisms of Bone Remodeling." Journal of Biological Chemistry **285**(33): 25103-25108.

Rauch, F. (2005). "Bone growth in length and width: the Yin and Yang of bone stability." Journal of musculoskeletal & neuronal interactions **5**(3): 194.

Ridler, T. W. (1978). "Picture thresholding using an iterative selection method." IEEE transactions on systems, man and cybernetics. Part B. Cybernetics **8**(8): 630.

Robertson, C. M. (2006). "Characterization of pro-apoptotic and matrix-degradative gene expression following induction of osteoarthritis in mature and aged rabbits." Osteoarthritis and Cartilage **14**(5): 471.

Robins, S. P. (1986). "Measurement of the cross linking compound, pyridinoline, in urine as an index of collagen degradation in joint disease." Annals of the rheumatic diseases **45**(12): 969.

Roemer, F. W., A. Guermazi, M. K. Javaid, JÂ A. Lynch, J. Niu, Y. Zhang, et al. (2009). "Change in MRI-detected subchondral bone marrow lesions is associated with cartilage loss: the MOST Study. A longitudinal multicentre study of knee osteoarthritis." Annals of the Rheumatic Diseases **68**(9): 1461-1465.

Ross, M. (2006). Histology: A Text and Atlas, Lippincott Williams & Wilkins.

Rutsch, F., N. Ruf, S. Vaingankar, M. R. Toliat, A. Suk, W. Hohne, et al. (2003). "Mutations in ENPP1 are associated with 'idiopathic' infantile arterial calcification." Nat Genet **34**(4): 379-381.

Säämänen, A.-M., M. Tammi, J. Jurvelin, I. Kiviranta and H. J. Helminen (1990). "Proteoglycan alterations following immobilization and remobilization in the articular cartilage of young canine knee (stifle) joint." Journal of Orthopaedic Research **8**(6): 863-873.

Saied, A. (1997). "Assessment of articular cartilage and subchondral bone: subtle and progressive changes in experimental osteoarthritis using 50 MHz echography in vitro." Journal of bone and mineral research **12**(9): 1378.

Saklatvala, J. (1986). "Tumour necrosis factor alpha stimulates resorption and inhibits synthesis of proteoglycan in cartilage." Nature **322**(6079): 547-549.

Sanchez, C. (2008). "Phenotypic characterization of osteoblasts from the sclerotic zones of osteoarthritic subchondral bone." Arthritis & Rheumatism **58**(2): 442.

Sanchez, C., M. A. Deberg, S. Burton, P. Devel, J.-Y. L. Reginster and Y. E. Henrotin (2004). "Differential regulation of chondrocyte metabolism by oncostatin M and interleukin-6." Osteoarthritis and Cartilage **12**(10): 801-810.

Saunders, J. B. (1933). "The Knee Joint-Its Functional Anatomy and the Mechanism of Certain Injuries." Cal West Med **39**(2): 83-5.

Schmid, B. (2007). "ImageJ 3D Viewer." from http://132.187.25.13/home/?category=Download&page=Viewer3D.

Schünke, M., E. Schulte, M. Lawrence, U. Schumacher, D. Edward and M. Voll (2006). Thieme Atlas of Anatomy: General Anatomy and Musculoskeletal System, Thieme.

Scott, J. E. (1981). "Proteoglycan-collagen arrangements in developing rat tail tendon. An electron microscopical and biochemical investigation." Biochemical journal **195**(3): 573.

Seer (2001). U.S. National Cancer Institute's Surveillance, Epidemiology and End Results (SEER) Program Introduction to Collaborative Stage, ICD-O-3, National Cancer Institute.

Segal, N. A. (2006). "Other surgical techniques for osteoarthritis." Baillière's best practice & research. Clinical rheumatology **20**(1): 155.

Seibel, M. J. (1989). "Urinary hydroxy-pyridinium crosslinks provide indices of cartilage and bone involvement in arthritic diseases." Journal of rheumatology **16**(7): 964.

Senolt, L., M. Braun, M. Glejarova, A. Forejtova, J. Gatterova and K. Pavelka (2005). "Increased pentosidine, an advanced glycation end product, in serum and synovial fluid from patients with knee osteoarthritis and its relation with cartilage oligomeric matrix protein." Annals of the Rheumatic Diseases **64**(6): 886-890.

Sharma, L. (1997). "Is knee joint proprioception worse in the arthritic knee versus the unaffected knee in unilateral knee osteoarthritis?" Arthritis & rheumatism **40**(8): 1518.

Sharma, L. (2000). "The mechanism of the effect of obesity in knee osteoarthritis: the mediating role of malalignment." Arthritis & rheumatism **43**(3): 568.

Sharma, L. (2001). "The role of knee alignment in disease progression and functional decline in knee osteoarthritis." JAMA (Chicago, Ill.) **286**(2): 188.

Sharma, L. (2004). "The role of proprioceptive deficits, ligamentous laxity, and malalignment in development and progression of knee osteoarthritis." J Rheumatol Suppl **70**: 87-92.

Sharma, L. and Y.-C. Pai (1997). "Impaired proprioception and osteoarthritis." Current Opinion in Rheumatology **9**(3): 253-258.

Shi-Lu, C., S. Yasunobu, B. Annika, M. Celia, I. Julia, S. Jeremy, et al. (2009). "Fibroblast growth factor 2 is an intrinsic chondroprotective agent that suppresses ADAMTS-5 and delays cartilage degradation in murine osteoarthritis." Arthritis & Rheumatism **60**(7): 2019-2027.

Shimizu, S. (2007). "Prevention of cartilage destruction with intraarticular osteoclastogenesis inhibitory factor/osteoprotegerin in a murine model of osteoarthritis." Arthritis & rheumatism **56**(10): 3358.

Shoemaker, S. C. (1986). "The role of the meniscus in the anterior-posterior stability of the loaded anterior cruciate-deficient knee. Effects of partial versus total excision." Journal of Bone and Joint Surgery; British volume **68**(1): 71.

Silberberg, R. and M. Silberberg (1964). "Pathogenesis of Osteoarthrosis." Pathol Microbiol (Basel) **27**: 447-57.

Silbermann, M. (1977). "Age-related changes in the cellular population of the growth plate of normal mouse." Cells tissues organs **97**(4): 459.

Silver, F. H., J. W. Freeman and G. P. Seehra (2003). "Collagen self-assembly and the development of tendon mechanical properties." Journal of biomechanics **36**(10): 1529-1553.

SkeleTech (2001). Bone Histology Presentation. Bothell, WA 98021.

Slemenda, C., K. D. Brandt, D. K. Heilman, S. Mazzuca, E. M. Braunstein, B. P. Katz, et al. (1997). "Quadriceps Weakness and Osteoarthritis of the Knee." Annals of Internal Medicine **127**(2): 97-104.

Smith, R. L. (1996). "In vitro stimulation of articular chondrocyte mRNA and extracellular matrix synthesis by hydrostatic pressure." Journal of Orthopaedic Research **14**(1): 53.

Smith, R. L. (2000). "Time-dependent effects of intermittent hydrostatic pressure on articular chondrocyte type II collagen and aggrecan mRNA expression." Journal of rehabilitation research and development **37**(2): 153.

Sokoloff, L. (1993). "Microcracks in the calcified layer of articular cartilage." Arch Pathol Lab Med **117**(2): 191-5.

Somerville, J. M. (2004). "Growth of C57Bl/6 Mice and the Material and Mechanical Properties of Cortical Bone from the Tibia." Calcified tissue international **74**(5): 469-475.

Sosic, D., B. Brand-Saberi, C. Schmidt, B. Christ and E. N. Olson (1997). "Regulation of Paraxis Expression and Somite Formation by Ectoderm and Neural Tube Derived Signals." Developmental Biology **185**(2): 229-243.

Sowers, M., D. Zobel, L. Weissfeld, V. M. Hawthorne and W. Carman (1991). "Progression of osteoarthritis of the hand and metacarpal bone loss. A twenty-year followup of incident cases." Arthritis Rheum **34**(1): 36-42.

Srivastava, S., G. Toraldo, M. N. Weitzmann, S. Cenci, F. P. Ross and R. Pacifici (2001). "Estrogen Decreases Osteoclast Formation by Down-regulating Receptor Activator of NF-1B Ligand (RANKL)-induced JNK Activation." Journal of Biological Chemistry **276**(12): 8836-8840.

Stanescu, R., A. Knyszynski, M. P. Muriel and V. Stanescu (1993). "Early lesions of the articular surface in a strain of mice with very high incidence of spontaneous osteoarthritic-like lesions." J Rheumatol **20**(1): 102-10.

Steadman, J. R. (2003). "Outcomes of microfracture for traumatic chondral defects of the knee: average 11-year follow-up." Arthroscopy **19**(5): 477.

Stockwell, R. A. (1971). "The interrelationship of cell density and cartilage thickness in mammalian articular cartilage." Journal of anatomy **109**(Pt 3): 411.

Stok, K. and R. Müller (2009a). "Morphometric characterization of murine articular cartilage - Novel application of confocal laser scanning microscopy." Microscopy Research and Technique **72**(9): 650-658.

Stok, K. S., G. Pelled, Y. Zilberman, I. Kallai, D. Gazit and R. Mueller (2009b). "Whole joint imaging allows quantification of bone and cartilage degeneration in a murine model of osteoarthritis." Bone **44**(Supplement 1): S156-S157.

Stok, K. S., G. Pelled, Y. Zilberman, I. Kallai, J. Goldhahn, D. Gazit, et al. (2009c). "Revealing the interplay of bone and cartilage in osteoarthritis through multimodal imaging of murine joints." Bone **45**(3): 414-422.

Stoop, R. (1999). "Denaturation of type II collagen in articular cartilage in experimental murine arthritis. Evidence for collagen degradation in both reversible and irreversible cartilage damage." The Journal of pathology **188**(3): 329.

Tetlow, L. C., D. J. Adlam and D. E. Woolley (2001). "Matrix metalloproteinase and proinflammatory cytokine production by chondrocytes of human osteoarthritic cartilage: Associations with degenerative changes." Arthritis & Rheumatism **44**(3): 585-594.

Tomoya, M., H. Hiroshi, O. Toru, E. Makoto and T. Ryota (2007). "Role of subchondral bone in osteoarthritis development: A comparative study of two strains of guinea pigs with and without spontaneously occurring osteoarthritis." Arthritis & Rheumatism **56**(10): 3366-3374.

Tortora J R, G. S. R. (2002). Principles of Anatomy and Physiology, Wiley.

Towheed, T. E. (2006). "Pennsaid therapy for osteoarthritis of the knee: a systematic review and metaanalysis of randomized controlled trials." J Rheumatol **33**(3): 567-573.

Treuting, P. M. (2011). Comparative Anatomy and Histology : A Mouse and Human Atlas.

Trindade, M. C. D. (2004). "Intermittent hydrostatic pressure inhibits matrix metalloproteinase and pro-inflammatory mediator release from human osteoarthritic chondrocytes in vitro* 1." Osteoarthritis and Cartilage **12**(9): 729.

Trueta, J. (1963). "Studies on the etiopathology of osteoarthritis of the hip." Clinical orthopaedics and related research **31**: 7.

Uchiyama, A., T. Ohishi, M. Takahashi, K. Kushida, T. Inoue, M. Fujie, et al. (1991). "Fluorophores from Aging Human Articular Cartilage." Journal of Biochemistry **110**(5): 714-718.

Valdes, A. M. (2008a). "Genome-wide association scan identifies a prostaglandin-endoperoxide synthase 2 variant involved in risk of knee osteoarthritis." American journal of human genetics **82**(6): 1231.

Valdes, A. M. (2009). "The Contribution of Genes to Osteoarthritis." Arthroscopy **93**(1): 45.

Valdes, A. M., M. Doherty and T. D. Spector (2008b). "The additive effect of individual genes in predicting risk of knee osteoarthritis." Annals of the Rheumatic Diseases **67**(1): 124-127.

van Beuningen, H. M., H. L. Glansbeek, P. M. van der Kraan and W. B. van den Berg (1998). "Differential effects of local application of BMP-2 or TGF-Î²1 on both articular cartilage composition and osteophyte formation." Osteoarthritis and Cartilage **6**(5): 306-317.

van Beuningen, H. M., H. L. Glansbeek, P. M. van der Kraan and W. B. van den Berg (2000). "Osteoarthritis-like changes in the murine knee joint resulting from intra-articular transforming growth factor-[beta] injections." Osteoarthritis and Cartilage **8**(1): 25-33.

van Beuningen, H. M., P. M. van der Kraan, O. J. Arntz and W. B. van den Berg (1994). "Transforming growth factor-beta 1 stimulates articular chondrocyte proteoglycan synthesis and induces osteophyte formation in the murine knee joint." Lab Invest **71**(2): 279-90.

Van de Loo, F. A. (1997). "Interleukin-6 reduces cartilage destruction during experimental arthritis. A study in interleukin-6-deficient mice." The American journal of pathology **151**(1): 177.

van den Berg, W. B. (1999). "The role of cytokines and growth factors in cartilage destruction in osteoarthritis and rheumatoid arthritis." Zeitschrift fur Rheumatologie **58**(3): 136.

van der Esch, M., M. Steultjens, J. Harlaar, N. Wolterbeek, D. L. Knol and J. Dekker (2008). "Knee varus-valgus motion during gait - a measure of joint stability in patients with osteoarthritis?" Osteoarthritis and Cartilage **16**(4): 522-525.

van der Kraan, P. M., E. L. Vitters, H. M. van Beuningen, L. B. van de Putte and W. B. van den Berg (1990). "Degenerative knee joint lesions in mice after a single intra-articular collagenase injection. A new model of osteoarthritis." Journal of experimental pathology **71**(1): 19-31.

van Osch, G. J., L. Blankevoort, P. M. van der Kraan, B. Janssen, E. Hekman, R. Huiskes, et al. (1995). "Laxity characteristics of normal and pathological murine knee joints in vitro." Journal of Orthopaedic Research **13**(5): 783.

van Roermund, P. M., A. C. A. Marijnissen and F. P. J. G. Lafeber (2002). "Joint distraction as an alternative for the treatment of osteoarthritis." Foot and Ankle Clinics of North America **7**(3): 515-527.

van Valburg, A. A. (2000). "Joint distraction in treatment of osteoarthritis (II): effects on cartilage in a canine model." Osteoarthritis and Cartilage **8**(1): 1.

van Valburg, A. A., P. M. van Roermund, J. Lammens, J. van Melkebeek, A. J. Verbout, E. P. Lafeber, et al. (1995). "Can Ilizarov joint distraction delay the need for an arthrodesis of the ankle? A preliminary report." J Bone Joint Surg Br **77-B**(5): 720-725.

Vellet, A. D. (1991). "Occult posttraumatic osteochondral lesions of the knee: prevalence, classification, and short-term sequelae evaluated with MR imaging." Radiology **178**(1): 271.

Venn, M. (1977). "Chemical composition and swelling of normal and osteoarthrotic femoral head cartilage. I. Chemical composition." Annals of the Rheumatic Diseases **36**(2): 121.

Videman, T. (1982). "Experimental osteoarthritis in the rabbit: comparison of different periods of repeated immobilization." Acta Orthop Scand **53**(3): 339-47.

Walsh, D. A., C. S. Bonnet, E. L. Turner, D. Wilson, M. Situ and D. F. McWilliams (2007). "Angiogenesis in the synovium and at the osteochondral junction in osteoarthritis." Osteoarthritis Cartilage **15**(7): 743-51.

Walton, M. (1977). "Studies of degenerative joint disease in the mouse knee joint; scanning electron microscopy." J Pathol **123**(4): 211-7.

Wang, C.-J. and P. S. Walker (1974). "Rotatory Laxity of the Human Knee Joint." J Bone Joint Surg Am **56**(1): 161-170.

Wang, J. (2004). "Evidence supporting dual, IGF-I-independent and IGF-I-dependent, roles for GH in promoting longitudinal bone growth." Journal of Endocrinology **180**(2): 247.

Warshawsky, H. (1980). "Direct in vivo demonstration by radioautography of specific binding sites for calcitonin in skeletal and renal tissues of the rat." The Journal of cell biology **85**(3): 682.

Watson, M., S. T. Brookes, A. Faulkner and J. Kirwan (2006). "Non-aspirin, non-steroidal anti-inflammatory drugs for treating osteoarthritis of the knee." Cochrane Database Syst Rev(1): CD000142.

Watson, P. J. (1996). "Degenerative joint disease in the guinea pig. Use of magnetic resonance imaging to monitor progression of bone pathology." Arthritis & rheumatism **39**(8): 1327.

Watson, P. J., T. A. Carpenter, L. D. Hall and J. A. Tyler (1996). "Cartilage swelling and loss in a spontaneous model of osteoarthritis visualized by magnetic resonance imaging." Osteoarthritis and Cartilage **4**(3): 197-207.

Webster, D., E. Wasserman, M. Ehrbar, F. Weber, I. Bab and R. Müller (2010). "Mechanical loading of mouse caudal vertebrae increases trabecular and cortical bone mass-dependence on dose and genotype." Biomechanics and Modeling in Mechanobiology.

Wedge, J. H. (1991). "Minor anatomic abnormalities of the hip joint persisting from childhood and their possible relationship to idiopathic osteoarthrosis." Clinical orthopaedics and related research **264**: 122.

Weiner, S., W. Traub and H. D. Wagner (1999). "Lamellar Bone: Structure-Function Relations." Journal of Structural Biology **126**(3): 241-255.

Weinstein, R. S. (1998). "Inhibition of osteoblastogenesis and promotion of apoptosis of osteoblasts and osteocytes by glucocorticoids. Potential mechanisms of their deleterious effects on bone." J Clin Invest **102**(2): 274.

William, H. S. (1970). "Scale effects in animal joints. I. articular cartilage thickness and compressive stress." Arthritis & Rheumatism **13**(3): 244-255.

Wohl, G. R., R. C. Shymkiw, J. R. Matyas, R. Kloiber and R. F. Zernicke (2001). "Periarticular cancellous bone changes following anterior cruciate ligament injury." Journal of Applied Physiology **91**(1): 336-342.

Wong, B. J. F. (2001). "Two-photon excitation laser scanning microscopy of human, porcine, and rabbit nasal septal cartilage." Tissue engineering **7**(5): 599.

Wong, M. (1996). "Zone-specific cell biosynthetic activity in mature bovine articular cartilage: A new method using confocal microscopic stereology and quantitative autoradiography." Journal of Orthopaedic Research **14**(3): 424.

Xu, L. X. (1996). "Osteoclasts in normal and adjuvant arthritis bone tissues express the mRNA for both type I and II interleukin-1 receptors." Laboratory Investigation **75**(5): 677.

Yamada, K. (2002). "Subchondral bone of the human knee joint in aging and osteoarthritis." Osteoarthritis and Cartilage **10**(5): 360-369.

Zhai, G. (2007). "Genetic influence on the progression of radiographic knee osteoarthritis: a longitudinal twin study1." Osteoarthritis and Cartilage **15**(2): 222.

Zysset, P. K., M. Sonny and W. C. Hayes (1994). "Morphology-mechanical property relations in trabecular bone of the osteoarthritic proximal tibia." J Arthroplasty **9**(2): 203-16.

APPENDIX A - Joint Distraction

A-1 Joint Distraction

Joint distraction is a technique for treating osteoarthritis (OA) by unloading the articular surfaces. This is achieved by applying an articulated external fixation across a joint. Joint distraction aims to increase joint space width whilst maintaining weight bearing (van Roermund 2002; Segal 2006). The mechanism by which distraction repairs cartilage damage is unclear. However, it has been theorised that a decrease in mechanical loading reduces damage to the articular surface (Lafeber 2006). Obesity, physically demanding occupations and sports all increase the risk of developing OA by increasing the loading on a joint (Buckwalter 1996; Felson 2004b). Additionally joint injury can lead to permanent instability and therefore increased contact stresses on the articular surfaces (Buckwalter 1996; Brown 2006). The rationale for joint distraction is that unloading may prevent or reduce any further progression (van Roermund 2002; Lafeber 2006). Osteotomy and muscle release work with this principle. A decrease in loading allows chondrocytes to initiate repair and encourages osteopenia of sclerotic subchondral bone (Segal 2006).

Removal of joint loading has been shown to induce cartilage degeneration (Jurvelin 1986), and joint motion alone is not sufficient to prevent degeneration (Palmoski 1980). Joint distraction reduces cartilage loading but does not induce cartilage degeneration because it maintains mechanostimulation from intermittent pressure fluctuations generated during loading, even if there is no cartilage-cartilage contact. Intermittent hydrostatic fluid pressure without mechanical stress has been shown to enhance the proteoglycan synthesis rate for OA cartilage in-vitro (Lafeber 1992). Fluid motion may prevent apoptosis of the chondrocyte and increase nourishment of the cartilage. Intra-articular fluid pressure was measured during joint distraction in one study on human ankles and was found to vary throughout loading cycles by 3.0 ± 0.5 kPa to 10.3 ± 0.6 kPa, which is comparable to a normal physiological pressure range(van Valburg 1995).

Joint distraction produces a reduction in sclerosis of the subchondral bone. By analysing the density of subchondral bone in radiographs, Marijnissen et al found an average decrease in subchondral bone density of 10% one year following distraction surgery for patients with severe ankle OA (Marijnissen 2002b). Reducing subchondral thickening may reduce pain symptoms but also accommodate cartilage repair. Reducing the density of subchondral bone will reduce its stiffness and therefore it will absorb more stress during loading, reducing the loading experienced by cartilage (Moskowitz 1999). However, it is also a possibility that cartilage repair protects the subchondral bone leading to a decrease in density. In addition the external framework may reduce joint instability which is a cause of secondary OA.

A-1.1 Clinical Trials

Aldegheri et al. used articulated hip distraction to treat 80 patients with a variety of hip diseases such as OA, osteonecrosis and chondrolysis (Aldegheri 1994). Patients had an age range of 9-69 years. A monolateral axial fixator was used to increase the joint space width by 5 mm, flexion and extension were permitted by the external framework. The treatment lasted from six to ten weeks. Patients were assessed by radiographic studies, clinical examination and questionnaire. Good results were found in patients under 45 in 42 out of 59 in that group. The results were poor for those over 45 or those with inflammatory arthroplasty. There were three criteria that were classed as a good result; a return to normal activities with no pain or mild pain after prolonged exercise, a range of motion with 90^{o} flexion 20^{o} in adduction, abduction and internal and external rotation or independent ambulation for 30 minutes. The authors concluded that joint distraction of the hip is a minimally invasive method of improving OA symptoms and delaying the need for hip arthroplasty.

Van Valburg et al. treated post-traumatic OA of the ankle using joint distraction on eleven patients all considered for arthrodesis. Distraction was maintained for 12-22 weeks. Pain decreased in all patients, six of the patients had increased range of motion, and three out of those six patients had

an increase in joint space width; two of which the joint space continued to increase with time. They also concluded that joint distraction shows promise as a treatment for delaying the need for arthrodesis (van Valburg 1995). A two year follow up was then conducted on 17 patients with severe OA. Distraction with full weight bearing was applied to each patient for three months; clinical examination was performed before, and after surgery and annually. 75% of the patients showed an increase in mobility, which continued to improve to the two year follow up. In four out of 17 patients there was no clinical improvement, and in all the patients there was no average change in joint space width.

Marjinissen et al. performed a randomised trial for joint distraction, out of a group of 57 all of whom had severe ankle OA and were considered for arthrodesis (Marijnissen 2002b). Distraction was applied for three months. One year after surgery average scores for pain decreased 38%, function increased 69% and clinical condition increased 120%. Improvement continued with time, with a statistically significant improvement at three years compared to one year after surgery. In a separate trial to compare distraction to debridement, involving seventeen patients, nine of the seventeen underwent joint distraction and the remaining eight received debridement. Debridement produced less significant changes compared to distraction at one year. These results were then incorporated into a prolonged study in which 73% of patients received clinical benefit from joint distraction of severe ankle OA which was maintained for at least seven years (Ploegmakers 2005).

Deie et al. investigated articulated distraction for the treatment of OA in the knee joint. Distraction was applied to the knees of six patients between 45 and 58 years old for a period ranging from seven to thirteen weeks with a follow up period of one to three and a half years. The joint distraction was combined with a bone-marrow stimulating method, by drilling or micro fracturing the arthritic lesions with a sharpened K-wire. They reported that all cases showed a significant improvement in joint space width, range of motion and clinical assessment of OA (Deie 2007).

The current OA treatments have limited success or require extensive surgery; there is a need for a minimally invasive procedure to reliably treat or at least slow the progression of OA. Further work is required to understand the mechanism of action and the most suitable way of employing distraction.

A-1.2 Animal Trials

Hung et al applied joint distraction to adult rabbits to study the effect of non-weight bearing on articular cartilage (Hung 1997). Joint distraction was not used as a treatment but as a method of simulating non weight bearing without immobilising the joint. Histological evaluation was used to compare distracted joints with the contralateral joints. Cartilage thickness was the same in the distracted and non distracted groups. At three and six weeks the chondrocytes increased in volume in the superficial and intermediate zones. At nine weeks in the superficial zone cell volume and matrix volume per cell decreased and numerical cell density increased. The study concluded that continuous distraction produced morphological chondrocyte changes which resulted in cartilage degeneration.

Kajiwara et al used the same apparatus as Hung but applied an osteochondral defect on the medial femoral condyles of the rabbits. The contralateral knee was used as a control with an osteochondral defect drilled but no fixator applied. Histology was used to assess the morphology of the cartilage (Kajiwara 2005). At four weeks the control group had an enlarged defect whereas the distracted group had partially repaired tissue. At eight weeks osteophyte formation and defect increase occurred in the control group, whereas in the distraction group there was little osteophyte formation and four out of six defects had almost repaired. The remaining two had partial repair tissue in the defect.

Van Valburg et al induced osteoarthritis in 13 canines using an anterior cruciate ligament transection model (van Valburg 2000). During joint distraction intermittent fluid pressure and mechanical

separation of articulating surfaces were measured. Nine weeks after distraction the joints were analysed. After joint distraction proteoglycan metabolism had returned to a level comparable with the control joints. Cartilage degeneration and proteoglycan content had not improved.

Karadam et al performed joint distraction on rabbit joints in which osteoarthritis had been induced 6 weeks prior with a papain injection (Karadam 2005). The rabbits were divided into groups receiving either articulated distraction, non-articulated distraction, non distracted application of fixation and a control of papain induced OA only. Culled after six weeks, non-articulated distraction produced significantly worse results than the other three groups in which there was no significant difference.

To the author's knowledge there is no murine model of joint distraction. A murine model has the advantage that transgenic animals can be used, biochemical and cellular assays are more readily available and time and cost of experiment are reduced. A murine model of distraction would provide an effective platform for investigating the mechanism of repair in joint distraction.

Matthew Gardiner of the Kennedy Institute of Rheumatology (KIR) developed an external fixator for murine joint distraction; which was applied first to healthy mice. The next step was to apply distraction to mice which had OA due to medial meniscal destabilisation. The trials at the KIR never progressed beyond healthy mice. Mechanical failings of the external fixator caused rotation of the femur rather than distraction. Histological results reported extensive inflammation and damage to the articular cartilage. Following this result the project ended.

A-2 Objectives

The overall aim of this work was to develop a murine model of joint distraction. In order to achieve this aim the following objectives needed be met:

- Develop methods to quantify bone and cartilage changes using micro-CT and confocal laser scanning microscopy.

- Determine laxity in DMM knees and laxity in knees with an external fixator applied.
- Develop an external fixator for applying distraction to murine knee joints.
- Characterise the effect of an external fixator on the biomechanics of a murine knee joint.
- Use the external fixator in a pilot study and subsequently, a full trial.

The DMM model was to be investigated using confocal microscopy and micro-CT. This would provide a method necessary to study changes within murine cartilage and bone in a live trial. The effects on laxity of DMM surgery and application of an external fixator would be investigated with AP drawer and VV rotation tests. Finally an external fixator will be developed and fully characterised, prior to a live trial. Characterisation will determine how the distractor will affect the mechanics of the knee, if the results of characterisation were suitable a pilot trial would commence.

A-3 Design Requirements and Considerations

The minimum criterion for the external fixator as dictated by ethical review was that the external fixator must weight under 1g, and create no obstruction to the flank of the mouse so as to cause harm when walking.

The external fixator must be capable of producing distraction, this must be demonstrated prior to use in a live trial. To apply the external fixator the surgical procedure must be appropriate for an anaesthetised mouse and the fixator must be stable when the mouse is mobile. The external fixator must allow some flexion and extension of the knee, it must also separate the articulating surfaces; the extent of these must be quantified and reviewed prior to live use.

A-4 Original External Fixator

An external fixator for joint distraction of a murine knee was developed by Matthew Gardiner (Kennedy Institute of Rheumatology). The external fixator used two 27g needles through the femoral metaphysis attached to a nylon bar. This bar was fixed to a brass hinge which allowed knee articulation. The hinge was connected to a nylon bolt which controlled the distraction. The bolt inserted into a tibial ring which used two 27g needles drilled into the tibia, arranged in an 'x' shape to provide stability (Figure A-1)

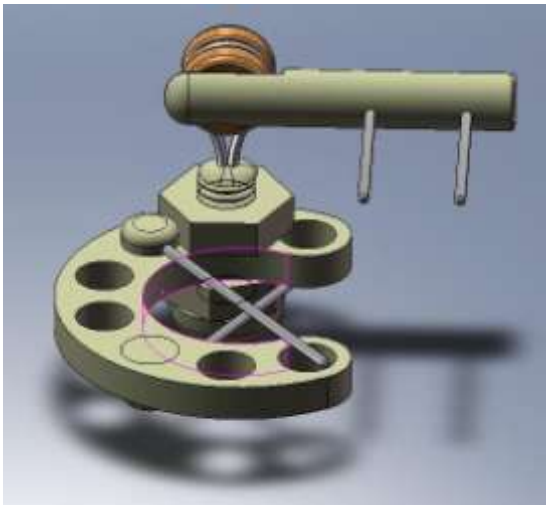

Figure A-1. Murine external fixator

Figure A-2. External fixator on cadaveric mouse

External fixators were placed in three cadaveric mice (Figure A-2) and then scanned using micro CT with 0.5 mm distraction. Reconstructions showed that the external fixator was distracting the lateral condyle but compressing the medial condyle against the tibia. There was also some rotation of the femur about its long axis, rather than straight distraction (Figure A-3). This was because the femoral pins were deflecting due to their monolateral support. The 27g needles have an outer diameter of 0.78mm: in a monolateral configuration 27g needles are unable to support the required loads. A brass nut formed the hinge, this was secured in place with a wire loop; the loop also reduced the overall stiffness of the external fixator. The loop was inserted into a nylon bolt which allowed

additional rotation. For distraction to be successful the stiffness needed to be improved and the rotation of the femur limited.

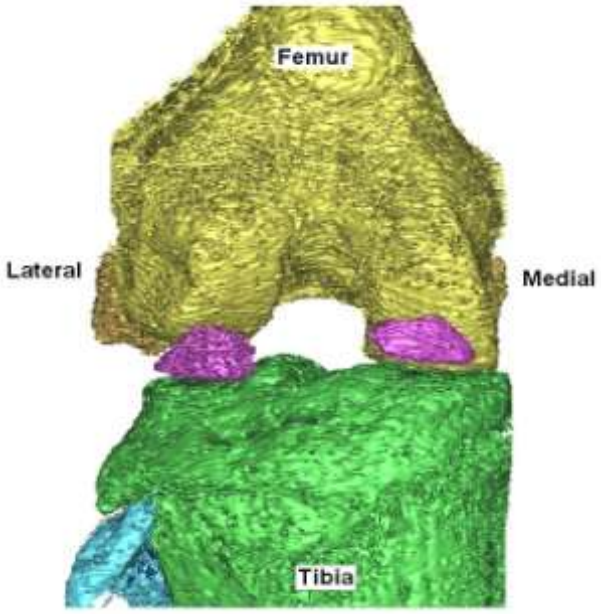

Figure A-3. Frontal view of a 3D reconstruction of distracted right leg. A raised lateral condyle and compression of the medial condyle against the tibia is visible. Note poor quality is due artefacts from metallic components of external fixator.

A-5 Redesigned External Fixator

A new external fixator was designed (Figure A-4). The needle stiffness could not be increased as 27g was the largest hypodermic needle that could be drilled into the femur without fracturing it. Instead the pins in the new external fixator were bilaterally supported to prevent bending. However, the mouse has soft tissue from the medial side of the upper leg to the flank; this limits the options for medial support of the pins. The only accessible part of the femur on the medial side is the around the distal end of the femur. Instead of two pins in the femoral metaphysis, one pin was placed through the femoral condyles approximately along the axis that marks the centre of rotation between the femur and tibia. This was inserted at either end into holes on a partial ring and allowed

to rotate, therefore allowing the leg to articulate. This design discards the large hinge which was permitting femoral axial rotation. Additionally, the nylon bolt was replaced with a stainless steel bolt for increased stiffness. Steel nuts would have increased the weight of the device past the 1g target weight, instead the tibial ring thickness was increased and its outer diameter reduced, and the steel bolt inserted into a threaded hole in the tibial ring. The tibial ring was made out of ployetheretherketone (PEEK) instead of nylon. PEEK is considerably stiffer than Nylon and nylon is unable to hold shallow threads. PEEK on stainless steel has a very low coefficient of friction allowing the pins to rotate freely. The redesigned prototype weighed 0.89g, lighter than the original, and was more robust. However, one centrally placed bolt gives little control over the distraction. A two pin version was also created so that each bolt could control the distraction and to some extent, rotation of the femur (Figure A-5). This device weighs 1.01g and is more difficult to use. Should the one pin version produce unsuitable distraction then the two pin version can be used instead.

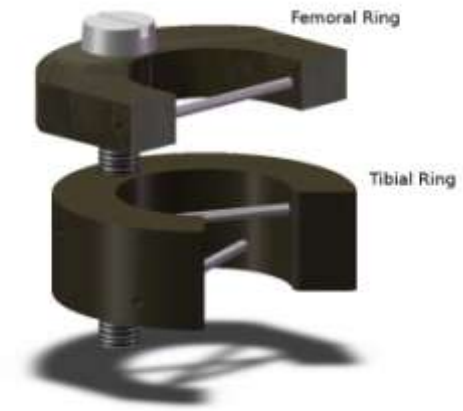

Figure A-4. Drawing of redesigned fixator.

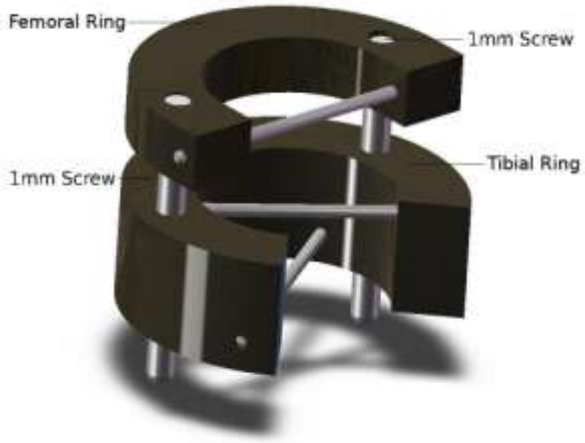

Figure A-5. Drawing of 2-pin redesigned fixator.

Proposed Surgical Procedure

A surgical protocol was trialled in cadaveric mice (Figure A-6). The protocol consisted of:

- Intra-peritoneal injection, shaving of the leg followed by creation of aseptic field (A).

- Incision created proximally and laterally to the patella, extending to the mid length of the femur. Using blunt dissection through the intramuscular septum separate tissues to expose the femur (B).

- Use the third trochanter and the exposed femur to place the drill guide and PEEK femoral ring. Drill a 27g needle through the hole on the femoral ring and drill through the femur to the opposing hole on the femoral ring. Cut crimp and fold the needle to hold in place (C).

- Suture incision (D).

- Apply the steel bolt, nut and tibial ring to the femoral ring (E).

- Placement of the tibial ring over the tibia. Using the holes in the femoral ring as guides drill two 27g needle into the tibia and super glue in place (F).

- Check the positioning of the external fixator, and the range of motion of the leg (G).

- Treatment mouse with analgesics. Allow recovery in a warm environment (H).

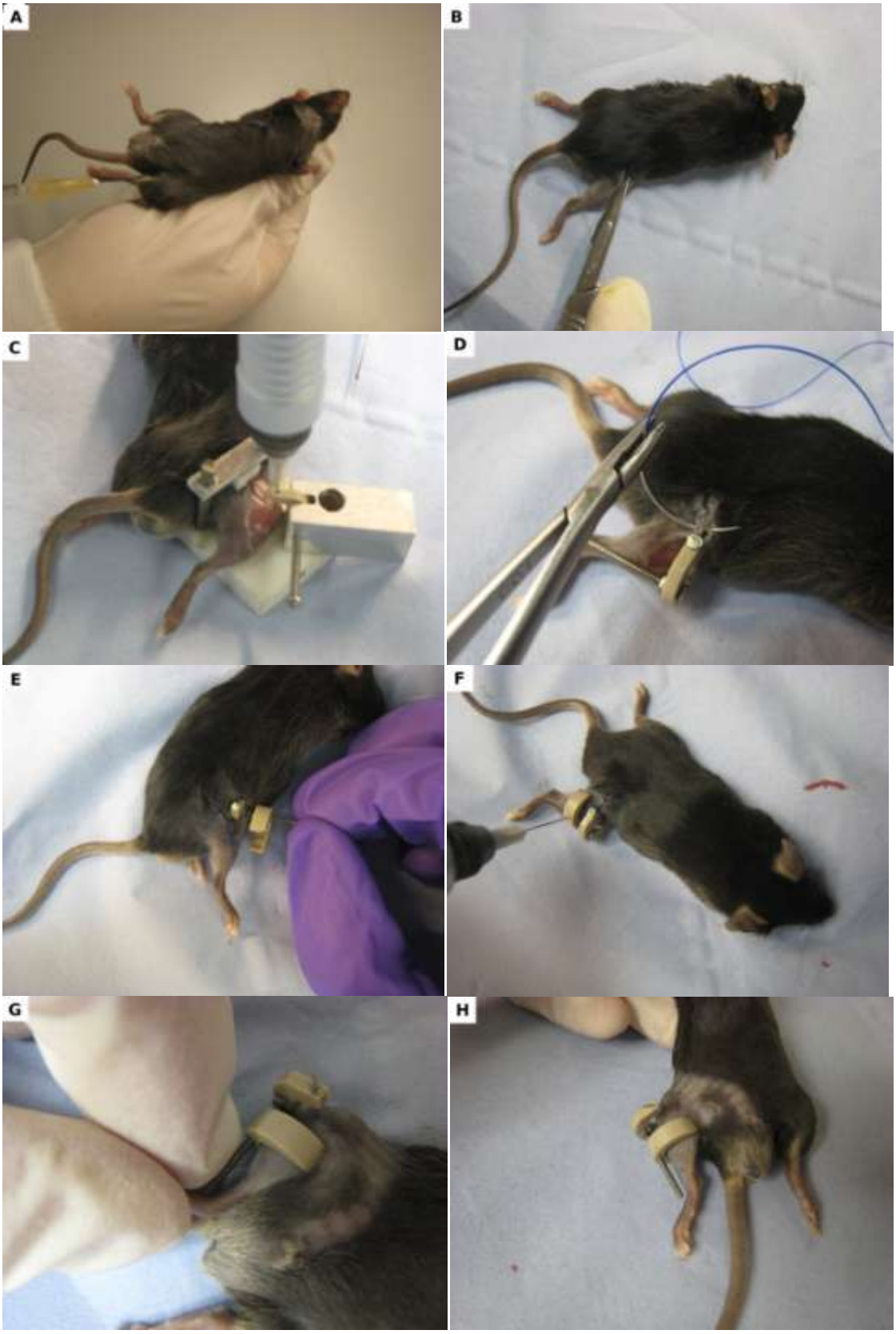

Figure A-6. Photographic series for surgical procedure.

A-6 Characterisation of External Fixator

A-6.1 Characterisation of Distraction

The one pin external fixator was applied to three cadaveric specimens, which were then scanned with a micro CT scanner undistracted. A 1 mm of distraction was then applied and the specimens rescanned. Due to the high volume of steel in the scanner, large artefacts hindered segmentation of the bone. As an interim solution, 3D reconstructions of the metal work were produced. The distracted reconstructions were registered against the undistracted reconstructions. From this, bolt height (applied distraction) and femoral pin height (approximation of actual distraction) were calculated (Figure A-7).The bolt moved 1 mm with four turns, this was equivalent to 1 mm; 1 mm of bolt displacement created approximately 0.5 mm of distraction of the femoral pin. The scans should be reanalysed to asses bone position, because the reconstruction of metal work does not completely describe bone position. The bones need to be segmented to investigate if 0.5 mm distraction is mid-way between the lateral and medial tibial plateaus and their opposing femoral condyles, and to see if any axial rotation of the femur occurs. To achieve this, the metal can be segmented and removed from the scans, then Hounsfield units reapplied to the remaining scans to increase contrast between bone and artefacts. Failing this, a more time consuming method of manually selecting the bone can be employed.

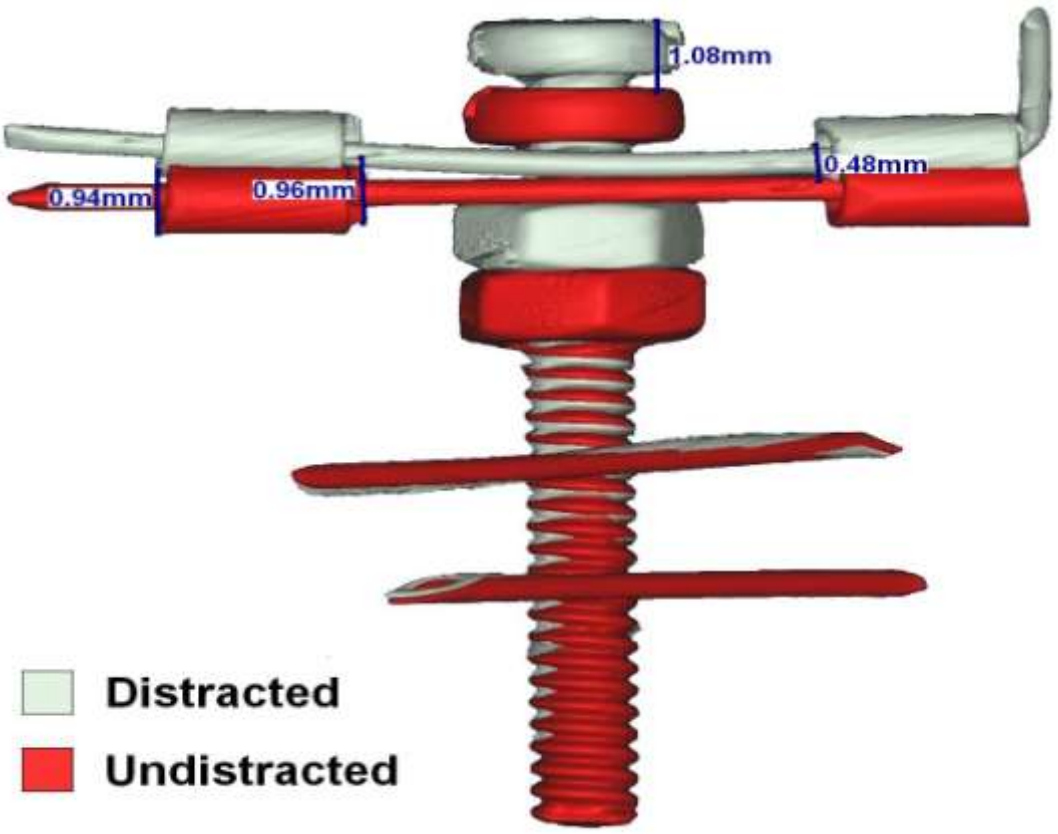

Figure A-7. 3D Reconstructions of distracted framework

A-6.2 Proposed Characterisation of Flexion and Extension

Application of an external fixator will reduce joint motion in flexion and extension; this will affect motion and weight bearing of the limb and therefore must be quantified. A materials testing machine can apply tension to the patello-femoral tendon: it is possible to pull on the patello-femoral tendon using forceps, the other end of the forceps will be attached to the load cell of the materials testing machine. With the femur rigidly fixed the materials testing rig can measure force required to extend the tibia through a specific angle. Flexion angle will be observed using a fixed marker, the load is recorded when the tibia reaches the marker. The force required to extend the tibia of legs with an external fixator is then compared to healthy legs.

A-6.3 Proposed Characterisation of Laxity and Instability

It is assumed that the DMM model introduces instability into the murine joint; if this is the case then it is quite plausible that the application of an external fixator reduces instability. Conversely it may be that the external fixator introduces malalignment or instability by some other unforeseen means. An external fixator should be applied to cadaveric specimens and subjected to the laxity testing protocol described in Chapters 3 and 5.

A-6.4 Proposed Characterisation of Weight Bearing

The effect of weight bearing on the distracted joint must be assed to see if distraction will be maintained during joint use, or if any fluctuations in separation of articular surfaces occur then they must be quantified. A cadaveric leg with an external fixator fitted should be rigidly mounted by the femur, and the tibia subject to compressive forces via a materials testing machine to record displacement.

A-7 Experimental Outline

A pilot trial was to be performed on approximately four mice with healthy cartilage using the original monolateral fixator. The sample size was to be kept small for ethical reasons and restrictions from the animal house veterinary surgeons. This pilot trial should be repeated using the redesigned bilateral fixators. The effect of the external fixator on weight bearing should be assessed using a Linton incapacitance tester. This apparatus uses two balances to calculate a weight a mouse puts through its hind legs when reared up. It should be used to assess the effect of the external fixator on the weight bearing of mice. The activity of mice should also be measured using the Laboras Automated Activity Monitor (Metris, Holland). The Laboras system measures the amount of time a mouse spends active or inactive. Following the pilot trial the animals should to be culled and the cartilage analysed using confocal microscopy or histology. If cartilage significantly worsens then the external fixator will require redeveloping. If no severe degradation occurs then the external fixator is

ready to be applied to animals with the DMM model compared to a sham surgery group in a full trial. The sample size of the full trial would be determined using the results of the pilot trial

A-8 Conclusion

The subchondral and cartilage changes in the DMM model were investigated, using confocal scanning laser microscopy and micro-CT. This has provided useful techniques which will be used for analysing the results of joint distraction on mice. Additionally, this has provided data on bone and cartilage changes for the DMM model, against which the effects of joint distraction could be compared.

The effect of DMM surgery on joint laxity had been investigated. The effect of the external fixator on joint laxity has not yet been investigated. It is a necessary step in the process of characterising the mechanics of the external fixator, prior to live trials.

An external fixator for murine joint distraction was developed. A process for mechanical characterisation was also been defined. Once the external fixator had been characterised and if considered suitable it would be applied to live animals in a pilot trial. The results of the pilot trial would determine if the distractor should be used will be employed in a full trial on mice the OA induced by DMM surgery.

APPENDIX B – Destabilisation on the Medial Meniscus

The mouse is anaesthetised using an intra-peritoneal injection of a 1:1 mixture of a 1:1 dilution of Hypnorm® (0.315 mg/ml fentanyl citrate and 10 mg/ml fluanisone; VetaPharma Ltd., Leeds, UK) and a 1:1 dilution of Hypnovel® (1 mg/ml midazolam; Roche Products Ltd., UK), at a dose of 5-10 ml/ mg body weight. The ventral portion of the knee is shaved, and the surgical field prepared with 70% alcohol solution.

With the aid of a dissecting microscope a midline incision is made over the ventral aspect of the knee with a no. 15 scalpel. The capsule is entered on the medial compartment medial to the patella, damage to the medial collateral ligament quadriceps should be avoided. Sufficient exposure can normally be obtained by creating a small window in the thinned retinacular-capsular tissues medial to the patella. The anterior medial meniscal horn is transacted using a 3 mm ophthalmic scalpel close to where it joins with the tibial plateau. Special care is taken not to injure the anterior cruciate ligament and the cartilage surfaces. Mobility of the medial meniscus is assured with jeweller's forceps, it should be possible to displace the anterior third of the meniscus freely from between the medial femoral condyle and tibial plateau (Figures B-1 and B-2).

Sterile 0.9% saline solution is used to irrigate the joint, and the para-patellar window closed with a fine absorbable suture (6/0 Vicryl®, Ethicon, USA) and the skin is then sutured (5/0 Ethilon®, Ethicon, USA) sutures.

The mice are placed in an incubator at 30°C and monitored until awake. Once recovered the mice, are returned to their original cages. The mice are typically fully mobile eight hours after DMM surgery. There is minimal post operative pain associated with DMM surgery, often analgesics are not required (KIR 2007).

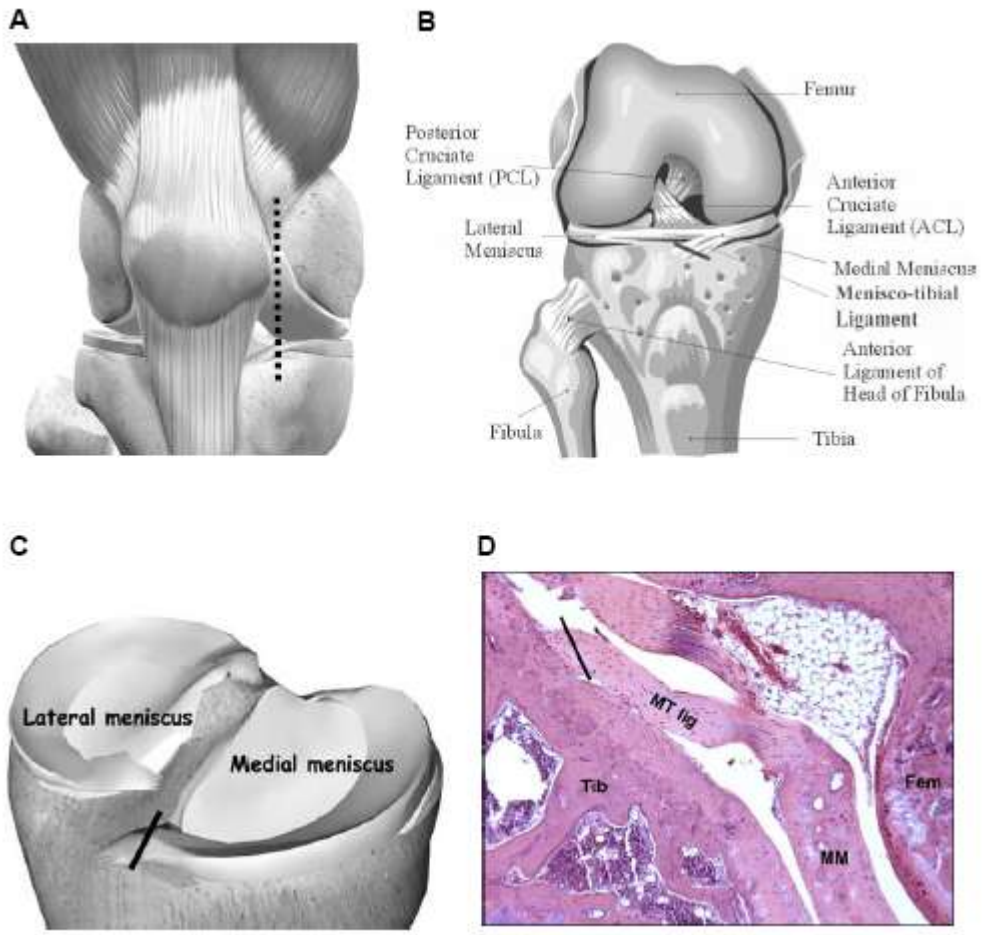

Figure B-1. (A) Diagram of ventral aspect of knee joint. Dotted line marks out the medial para-patellar approach to the knee joint (KIR 2007). (B) Detail of intra-articular structures. The solid line marks out where the medial menisco-tibial ligament is transected (KIR 2007). (C) Plan view of tibial plateau showing position of both menisci. Solid line marks out where the attachment of the anterior horn of the medial meniscus to the tibial plateau is cut during the procedure (KIR 2007). (D) Haemotoxylin & eosin-stained coronal section through the mouse knee. Solid line again marks out where the medial menisco-tibial ligament (MT) is released from the tibial plateau (Tib), hence freeing the anterior portion of the medial meniscus (MM) (KIR, 2007). (Fem—medial femoral condyle) (Original magnification 100x)

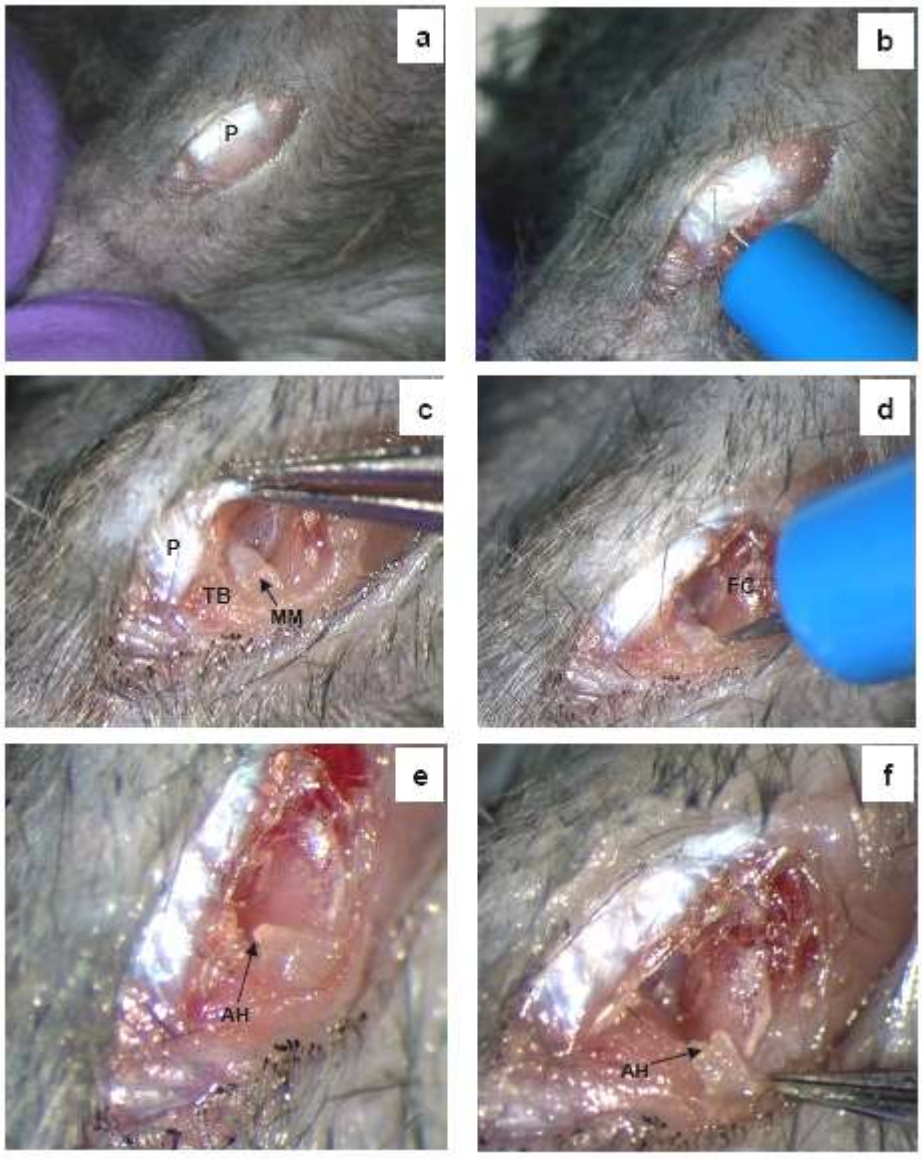

Figure B-2 Pictorial description of MMD technique. (a) Midline ventral skin incision revealing patella (P). (b) Joint is entered via a small medial para-patellar window, without cutting the quadriceps and unduly displacing the patella. The medial collateral ligaments are undisturbed. (c) The anterior rim of the medial tibial plateau (TB) and the medial meniscus (MM) are exposed. (d, e) The menisco-tibial ligament is cut and the anterior horn (AH) of the meniscus is freed. FC—medial femoral condyle. (f) Displacement and mobility of the meniscus is checked—the anterior medial meniscus should be able to move freely out from between the femoral condyle and tibial plateau.

APPENDIX C - Laxity Protocol

Sample Preparation:-

1. Dissect leg from hip, remove foot and strip tissue, retaining skin and musculature from to the mid length of femur to the mid length of the tibia. Clean thoroughly the exposed distal tibia and proximal femur.
2. Prepare potting rig by adding protective bridge and grease all surfaces that contact pMMA. Place specimen in potting rig and close.
3. Use vernier adjustment first to cup femoral head, then to secure third trochanter. Tighten remaining vernier dials until leg is correctly aligned. Tighten all four rig bolts; prior loosening of all vernier dials by half of a turn prevents specimen breakage.
4. In a fume hood mix MMA with catalyst and syringe into both compartments of the potting rig, waiting 5 minutes between injecting pMMA between compartments, prevents pMMA from draining.
5. Cover with gauze and allow polymerisation to complete, approximately 45 minutes. Remove all bolts and open rig in fume hood. Unscrew vernier dials and carefully remove sample.

Anterior Posterior Rig Protocol:-

6. Restore AP rig to neutral position. Remove AP rig locking bolt and zero LVDT and load cell. Reconnect locking bolt.
7. Connect sample to AP rig. Carefully remove protective bridge and locking bolt.
8. Adjust AP position until load displays zero then auto zero LVDT.
9. Apply 5 full cycles of loading to precondition, to ± 1 N.
10. Record LVDT and load cell output for 3 full cycles of load.
11. Return AP locking and reapply protective bridge to sample.
12. Remove specimen from AP rig ready for use in VV rig.

Varus Valgus Rig Protocol:-

13. Unlock moment arm on the VV rig.
14. Rotate moment arm so that both rotation encoder outputs are outputting lowest possible voltage.
15. Zero both rotation encoder and load cell outputs.
16. Connect specimen to the VV rig
17. Adjust moment arm position until load cell displays zero.
18. Auto zero load cell and rotation encoder.
19. Apply 5 full cycles of loading to precondition, to ± 5 Nmm.
20. Record rotation encoder and load cell output for 3 full cycles of load.
21. Return VV lock and reapply protective bridge to sample.
22. Remove specimen from VV rig.

Internal External Rig Protocol:-

As for 13-22 but with external back plate adaptor applied to the VV rig, using callipers to ensure knee is a constant 26 mm from edge of moment arm.

APPENDIX D - Laxity Matlab Programs

D-1 Rotencoder

The following is a program converts the dual sinusoidal signals from the retention encoder and converts to a matrix containing the time points and cumulative position of the rotation encoder, along with corresponding moment values. Rotencoder is based on a signal thresholding method. Rotencoder is intended for use with data recorded with a Fylde amplifier.

```
%Rotencoder is designed to work with data from MADAQ with I1 in channel 5
%and I2 in channel 7 and force (moment)on CH1.
%Once data is imported there will be a time signature on the first column
%right click on file in workspace and click import data...
%Formatting by deleting redundant columns
%data(:,9)=[]; %only necessary if all 8 amplifier channels were used
data(:,7)=[];
data(:,5)=[];
data(:,4)=[];
data(:,2)=[];

g=size(data);
for x=1:g(1,2)
A(:,x)=decimate(data(:,x),12);  %decimates by 2
end
%g=size(A);
%for x=1:g(1,2)
%B(:,x)=decimate(A(:,x),3);  %decimates by 3
%end
data=A;
clear A;

span=3;
window= ones(span,1)/span;
data(:,2)=convn(data(:,2),window,'same');
data(:,2)=convn(data(:,2),window,'same');
span=3;
data(:,3)=convn(data(:,3),window,'same');
data(:,3)=convn(data(:,3),window,'same');
data(:,4)=convn(data(:,4),window,'same');
data(:,4)=convn(data(:,4),window,'same');%Smoothes I1 and I2



%Input is now an array called data, with 4 columns: time, force,I1,I2
%Output is P with columns: , deg change, cumulative change,time, force.
% Z is: I2, I1 spike location, and resultant degree change
%grad and grad2 are measures of gradient on the I1 and I2 curves
grad=0;
grad2=0;
```

```
Z=zeros(1,3);                %Z Contains location of I2 spikes
W=zeros(1,1);                %W Contains location of I1 spikes
Y=zeros(1,1);                %Y Contains Degree changes
Q=zeros(1,1);                %Q Is an array of all the Spike locations on I1
that may correspond to an I2 spike
f=0;                         %f is a count for indexing spikes in Z and W,
used in a for loop
g=size(data);
for x=1:(g(1,1)-2)
      grad=data(x+1,3)- data(x,3);  %takes gradient at a point on I1
      grad2=data(x+2,3)- data(x+1,3);   %takes gradient at next point  I1
      if grad2 <grad && grad>0 && grad2<=0 && data(x,3)>0.05;  %if a
maximum then location is stored in W
         f=f+1;
         W(f,1)=x+1;
      end
end
f=0;
for x=1:(g(1,1)-2)
      grad=data(x+1,4)- data(x,4); %takes gradient at a point on I2
      grad2=data(x+2,4)- data(x+1,4);
      if grad2 <grad && grad>0 && grad2<0 && data(x,4)>0.1; %if a maximum
then location is returned to Z
         f=f+1;
         Z(f,1)=x+1;
      elseif grad2 <grad && grad>0 && grad2==0 && data(x,4)>0.1; %if a
plateau then start and end is located and put in a and b
          f=f+1;
          a=x+1;
          Z(f,3)=a;
      elseif grad2 <grad && grad==0 && grad2<0 && data(x,4)>0.1;
          b=x+1;
          Z(f,1)=b;
      end
end
g=size(Z);
for f=1:g(1,1)
    if Z(f,3)~=0;
        Z(f,1)=round((Z(f,3)+Z(f,1))/2); % averages a and b and returns
location of centre of plateau
    end
end
Z(:,3)=[]; % removes 'a' values from Z
x=1;
h=size(W);                                          %
lower=0;                                            %
upper=Z(2,1);                                       %
    for x=1:(h(1,1)-1)                              %
        if W(x,1)> lower && W(x,1)< upper           %
           Q= [Q W(x,1)];                           %
        end                                         %
    end                                             %This bit is because
    R=Q-Z(f,1);                                     %i am not very good at
```

```
    R=abs(R);                                   %programming so i have to
    [C,I]=min(R);                               %analyse f=1 seperately to
avoid 0 values
    Z(1,2)=(Q(1,I));

for f=2:(g(1,1)-1)
    lower=Z(f-1,1);         %takes a spike on I2 and searches all I1 spikes
that occur between the previous and next I2 spike
    upper=Z(f+1,1);
    for x=1:(h(1,1)-1)
        if W(x,1)> lower && W(x,1)< upper
           Q= [Q W(x,1)];
        end
    end
    R=Q-Z(f,1);
    R=abs(R);               %Finds the spike closest to the selected I2
value
    [C,I]=min(R);
    Z(f,2)=(Q(1,I));
end                         %By this point we should have I2 in Z(:,1) and
I1 in Z(:,2)
f=1;
for f=1:g(1,1)
    if Z(f,1)<=Z(f,2)       %Compare I2 to I1
       Y(f,1)=-1/3;
    else
       Y(f,1)=1/3;          %Y contains the direction of angle change
    end
end



N=data(Z(:,1),1);           %N is an array containing the time at which the
zero line crossings occur
M=data(Z(:,1),2);           %M is an array containing the force at which
the zero line crossings occur
L=cumsum(Y(:,1));           %L is the angle
P= [L N M Y];
Z= [P Z];%Output
'   angle     time      force    deg change'
clear  grad grad2 a b Y W Q R C I g h lower upper f x L M N  span window;


% plot(P(:,2),P(:,1))
plot(P(:,3),P(:,1))
```

D-2 RotencoderGrad

RotencoderGrad is an alternative program to Rotencoder. It returns the same information as Rotencoder only it operates using a combined threshold gradient detection algorithm.

```
%Rotencoder is designed to work with data from MADAQ with I1 in channel 5
%and I2 in channel 7 and force (moment)on CH1.
%Once data is imported there will be a time signature on the first column
%right click on file in workspace and click import data...
%Formatting by deleting redundant columns
%data(:,9)=[]; %only necessary if all 8 amplifier channels were used
data(:,7)=[];
data(:,5)=[];
data(:,4)=[];
data(:,2)=[];

g=size(data);
for x=1:g(1,2)
A(:,x)=decimate(data(:,x),2);  %decimates by 12
end
g=size(A);
for x=1:g(1,2)
B(:,x)=decimate(A(:,x),3);  %decimates by 12
end
data=A;
clear A;

span=3;
window= ones(span,1)/span;
data(:,2)=convn(data(:,2),window,'same');
data(:,2)=convn(data(:,2),window,'same');
span=3;
data(:,3)=convn(data(:,3),window,'same');
data(:,3)=convn(data(:,3),window,'same');
data(:,4)=convn(data(:,4),window,'same');
data(:,4)=convn(data(:,4),window,'same');%Smoothes I1 and I2
```

```
%Input is now an array called data, with 4 columns: time, force,I1,I2
%Output is P with columns: , deg change, cumulative change,time, force.
% Z is: I2, I1 spike location, and resultant degree change
%grad and grad2 are measures of gradient on the I1 and I2 curves
grad=0;
grad2=0;
Z=zeros(1,3);               %Z Contains location of I2 spikes
W=zeros(1,1);               %W Contains location of I1 spikes
Y=zeros(1,1);               %Y Contains Degree changes
Q=zeros(1,1);               %Q Is an array of all the Spike locations on I1
that may correspond to an I2 spike
f=0;                        %f is a count for indexing spikes in Z and W,
used in a for loop
g=size(data);
for x=1:(g(1,1)-2)
      grad=data(x+1,3)- data(x,3);  %takes gradient at a point on I1
```

```
      grad2=data(x+2,3)- data(x+1,3);   %takes gradient at next point  I1
      if grad2 <grad && grad>0 && grad2<=0 && data(x,3)>0.05;  %if a
maximum then location is stored in W
         f=f+1;
         W(f,1)=x+1;
      end
end
f=0;
for x=1:(g(1,1)-2)
      grad=data(x+1,4)- data(x,4); %takes gradient at a point on I2
      grad2=data(x+2,4)- data(x+1,4);
      if grad2 <grad && grad>0 && grad2<0 && data(x,4)>0.1; %if a maximum
then location is returned to Z
         f=f+1;
         Z(f,1)=x+1;
      elseif grad2 <grad && grad>0 && grad2==0 && data(x,4)>0.1; %if a
plateau then start and end is located and put in a and b
          f=f+1;
          a=x+1;
          Z(f,3)=a;
      elseif grad2 <grad && grad==0 && grad2<0 && data(x,4)>0.1;
          b=x+1;
          Z(f,1)=b;
      end
end
g=size(Z);
for f=1:g(1,1)
    if Z(f,3)~=0;
        Z(f,1)=round((Z(f,3)+Z(f,1))/2); % averages a and b and returns
location of centre of plateau
    end
end
Z(:,3)=[]; % removes 'a' values from Z
x=1;
h=size(W);                                          %
lower=0;                                            %
upper=Z(2,1);                                       %
    for x=1:(h(1,1)-1)                              %
        if W(x,1)> lower && W(x,1)< upper           %
           Q= [Q W(x,1)];                           %
        end                                         %
    end                                             %This bit is because
    R=Q-Z(f,1);                                     %i am not very good at
    R=abs(R);                                       %programming so i have to
    [C,I]=min(R);                                   %analyse f=1 seperately to
avoid 0 values
    Z(1,2)=(Q(1,I));

for f=2:(g(1,1)-1)
    lower=Z(f-1,1);         %takes a spike on I2 and searches all I1 spikes
that occur between the previous and next I2 spike
    upper=Z(f+1,1);
    for x=1:(h(1,1)-1)
        if W(x,1)> lower && W(x,1)< upper
           Q= [Q W(x,1)];
        end
    end
    R=Q-Z(f,1);
    R=abs(R);               %Finds the spike closest to the selected I2
value
    [C,I]=min(R);
```

```
    Z(f,2)=(Q(1,I));
end                         %By this point we should have I2 in Z(:,1) and
I1 in Z(:,2)
f=1;
for f=1:g(1,1)
    if Z(f,1)<=Z(f,2)       %Compare I2 to I1
       Y(f,1)=-1/3;
    else
       Y(f,1)=1/3;          %Y contains the direction of angle change
    end
end



N=data(Z(:,1),1);           %N is an array containing the time at which the
zero line crossings occur
M=data(Z(:,1),2);           %M is an array containing the force at which
the zero line crossings occur
L=cumsum(Y(:,1));           %L is the angle
P= [L N M Y];
Z= [P Z];%Output
'   angle     time      force    deg change'
clear  grad grad2 a b Y W Q R C I g h lower upper f x L M N  span window;


% plot(P(:,2),P(:,1))
plot(P(:,3),P(:,1))
```

D-3 AP Interval

AP interval returns a matrix of AP position and load. Rotencoder is intended for use with data recorded with a Fylde amplifier.

```
data(:,3)=[];
span=5;
window= ones(span,1)/span;
data(:,2)=convn(data(:,2),window,'same');
data(:,2)=convn(data(:,2),window,'same');
span=5;
data(:,3)=convn(data(:,3),window,'same');
data(:,3)=convn(data(:,3),window,'same');
%r=10;%Decimation factor
%AA=data(:,1);
%AB=data(:,2);
%AC=data(:,3);
%AA=decimate(AA,r);
%AB=decimate(AB,r);
%AC=decimate(AC,r);
%f=size(AA);
%data2=zeros(f,3);
%data2(:,1)=AA;
%data2(:,2)=AB;
```

```
%data2(:,3)=AC;
%clear AA AB AC;

%data=data2;
%clear data2;


U1=zeros(1,4);    %Unloading matrix,
U2=zeros(1,4);    %Unloading matrix, posterior
L1=zeros(1,4);    %Loading matrix
L2=zeros(1,4);    %Loading matrix, posteror
x=1;   %global unit count
y=1;   %Value detection count for unloading
z=1;    %Value detection count for loading
n=1;   %Multiplier count
g=size(data);
c=21;   %interval for gradient measure set at 100 if file is approx 3000,
or 15 if file is approx 500

x=1;
n=1;
for x=1:(g(1,1)-1)

    a=data(x,2);
    b=data((x+1),2);
         if  a<=n*0.025 && b>n*0.025  %in anterior region
             if data(x-c,2)<data(x+c,2) %Gradient is positive
                 L1(z,1)= a;      %Put data in a matrix for loading
                 L1(z,2)= data(x,3);
                 L1(z,3)= x;
                 L1(z,4)= n*0.025;
                 z=z+1;
                 if n==40
                    n=0;
                 else n=n+1;
                 end
             end
         end

end

x=1;
n=1;
z=1;
for x=1:(g(1,1)-1)

    a=data(x,2);
    b=data((x+1),2);
        if a>=-(n*0.025) && b<-(n*0.025 ) %In posterior region
                if data(x-c,2)>data(x+c,2)    %Gradient is negative
                L2(z,1)= a;
                L2(z,2)= data(x,3);
```

```
                L2(z,3)= x;
                L2(z,4)= -n*0.025;%Put data in a matrix for loading
                z=z+1;
                    if n==40
                    n=0;
                    else n=n+1;
                    end
                end
        end

end
x=1;
n=40;
for x=1:(g(1,1)-1)

    a=data(x,2);
    b=data((x+1),2);
         if  a>=n*0.025 && b<n*0.025  %in anterior region
             if data(x-c,2)>data(x+c,2) %Gradient is negative
                 U1(y,1)= a;      %Put data in a matrix for unloading
                 U1(y,2)= data(x,3);
                 U1(y,3)= x;
                 U1(y,4)= n*0.025;
                 y=y+1;
                 if n==0
                    n=40;
                 else n=n-1;
                 end
             end
         end

end

x=1;
n=40;
y=1;
for x=1:(g(1,1)-1)

    a=data(x,2);
    b=data((x+1),2);
        if a<=-(n*0.025) && b>-(n*0.025 ) %In posterior region
                if data(x-c,2)<data(x+c,2)    %Gradient is positive
                U2(y,1)= a;
                U2(y,2)= data(x,3);
                U2(y,3)= x;%Put data in a matrix for unloading
                U2(y,4)= -n*0.025;
                y=y+1;
                    if n==2
                    n=40;
                    else n=n-1;
                    end
                end
```

```
        end

end
```

D-4 U Average

Rotencoder and APinterval return matrices which contain three cycles of loading and unloading. U average averages each of the cycles into one and returns a laxity curve.

```
Average=zeros(1,4);
g=size(U1);
m=1;
U1avg=zeros(1,4);
Z=zeros(1,4);
j=1;
u1=sortrows(U1,4);
for n=0:0.025:1
    for x=1:(g(1,1)-1)
        if U1(x,4) ==n
            Z(m,1)= U1(x,1);
            Z(m,2)= U1(x,2);
            Z(m,3)= U1(x,3);
            Z(m,4)= U1(x,4);
            m=m+1;
        end
        if x==(g(1,1)-1)
            f=size(Z);
        U1avg(j,1)= (sum (Z(:,1)))/(f(1,1));
        U1avg(j,2)= (sum (Z(:,2)))/(f(1,1));
        U1avg(j,3)= (sum (Z(:,3)))/(f(1,1));
        U1avg(j,4)= (sum (Z(:,4)))/(f(1,1));
        Z=zeros(1,4);
        m=1;
        j=j+1;
        end
    end
end
clear g m Z j;

g=size(U2);
m=1;
U2avg=zeros(1,4);
Z=zeros(1,4);
j=1;
for n=0:0.025:1
    for x=1:(g(1,1)-1)
        if U2(x,4) ==-n
            Z(m,1)= U2(x,1);
            Z(m,2)= U2(x,2);
            Z(m,3)= U2(x,3);
            Z(m,4)= U2(x,4);
            m=m+1;
```

```
        end
        if x==(g(1,1)-1)
            f=size(Z);
        U2avg(j,1)= (sum (Z(:,1)))/(f(1,1));
        U2avg(j,2)= (sum (Z(:,2)))/(f(1,1));
        U2avg(j,3)= (sum (Z(:,3)))/(f(1,1));
        U2avg(j,4)= (sum (Z(:,4)))/(f(1,1));
       Z=zeros(1,4);
        m=1;
        j=j+1;
       end
    end
end


clear g m Z j;
g=size(L1);
m=1;
L1avg=zeros(1,4);
Z=zeros(1,4);
j=1;
for n=0:0.025:1
    for x=1:(g(1,1)-1)
        if L1(x,4) ==n
            Z(m,1)= L1(x,1);
            Z(m,2)= L1(x,2);
            Z(m,3)= L1(x,3);
            Z(m,4)= L1(x,4);
            m=m+1;
        end
        if x==(g(1,1)-1)
            f=size(Z);
        L1avg(j,1)= (sum (Z(:,1)))/(f(1,1));
        L1avg(j,2)= (sum (Z(:,2)))/(f(1,1));
        L1avg(j,3)= (sum (Z(:,3)))/(f(1,1));
        L1avg(j,4)= (sum (Z(:,4)))/(f(1,1));
        Z=zeros(1,4);
        m=1;
        j=j+1;
        end
    end
end
clear g m Z j;

g=size(L2);
m=1;
L2avg=zeros(1,4);
Z=zeros(1,4);
j=1;
for n=0:0.025:1
    for x=1:(g(1,1)-1)
        if L2(x,4) ==-n
            Z(m,1)= L2(x,1);
```

```
            Z(m,2)= L2(x,2);
            Z(m,3)= L2(x,3);
            Z(m,4)= L2(x,4);
            m=m+1;
        end
        if x==(g(1,1)-1)
            f=size(Z);
        L2avg(j,1)= (sum (Z(:,1)))/(f(1,1));
        L2avg(j,2)= (sum (Z(:,2)))/(f(1,1));
        L2avg(j,3)= (sum (Z(:,3)))/(f(1,1));
        L2avg(j,4)= (sum (Z(:,4)))/(f(1,1));
        Z=zeros(1,4);
        m=1;
        j=j+1;
        end
    end
end
U1avg=sortrows(U1avg,-4);
U2avg=sortrows(U2avg,4);
Average = [L1avg;U1avg;L2avg;U2avg];
    plot (Average(:,1),Average(:,2))
```

APPENDIX E – Confocal Scanning Electron Microscopy Protocol

Sample Preparation:-

1. Prepare specimen by removing leg at the pelvis and stripping all musculature.
2. Disarticulate leg at the knee by transecting collateral and cruciate ligaments with no. 12 scalpel, taking care not to damage the articular cartilage.
3. With fine tweezers and scissors remove and surrounding soft tissue, in particular the synovium, meniscus and remnants of cruciate ligaments.
4. Cut tibia with rongeurs at the midlength.
5. Using superglue affix to tibia holder.
6. Place PBS soaked gauze on tibial plateau to prevent dehydration, whilst adhesive hardens.
7. Fill cell culture well with PBS. Ensure all tibia plateaus are clean. Place tibia holder upside down inside Nunc Lab-tek® cell culture well (Sigma Z734535).
8. If necessary allow tibia and PBS to come to room temperature.

CSLM Scanning Protocol (Leica SP5):-

9. Set the 466 nm laser to 30% power and allow 30 minutes to reach steady state temperature.
10. Configure the microscope to allow full range in the z-direction.
11. Set the following parameters:
    a. Gain of 625 V.
    b. Offset of -2 %
    c. Photomultiplier to collect above 480 nm.
    d. An additional photomultiplier can be set to collect reflection at 466 nm (signal not used in analysis). This allows identification of unwanted material obscuring cartilage.
    e. Image size of 512 × 512 and a laser speed of 400 Hz.
12. Using the fluorescent lamp locate the proximal and distal most regions and set to scan every 3.03 μm.
13. Locate anterior, posterior, lateral and medial edges of the plateau, and set these as the boundaries for a tile scan.
14. Scan, and repeat for all tibia in the holder.

Post-processing and Analysis

15. Import scans into ImageJ. Remove reflection signal if second photomultiplier tube was used.
16. Apply a Gaussian filter with radius of 2.
17. Crop to desired plateau.
18. Remove unwanted soft tissue in ImageJ3DViewer.
19. Apply threshold.
20. Analyse using BoneJ, for thickness and volume.
21. Thickness maps can be produced using BoneJ, and viewed in ImageJ3DViewer.

APPENDIX F – Non Decalcified Histology Protocol

From Nikki Horwood at the Kennedy Institute of Rheumatology, London, UK:

Safety precautions
All work is to be carried out in a fume hood unless otherwise stated. Appropriate protective equipment including gloves, lab coat and safety glasses must be worn at all times. Many of the chemical used in this process are organic and may carry health risks especially if you are pregnant. Consult the MSDS for further information on each chemical.

Preparing and Sectioning Bones in Plastic

Reagents required:

Methylmethacrylate	Sigma M55909
Dibutylphthalate	Sigma D2270
Benzoyl peroxide	Sigma 517909
Anhydrous calcium chloride	Sigma C1016
Sodium hydroxide	
Acetone	
Ethanol	
Formaldehyde	

Equipment required:
Glass separating funnel
Glass funnel
Glass scintillation vials Sigma V8255-500EA
Glass topped stirrer
Whatman filter paper circles
Retort stand
37°C dry incubator
Buehler twin beta grinder (sandpaper: fine is 320 Grit/P400 and the course is Grit P60)
Autocut microtome

A. Preparation of destabilised methylmethacrylate (dMMA)

1. Make up 1lt of 0.5% sodium hydroxide (NaOH) in dH_2O
2. Add 500ml of MMA to the separating funnel with 300ml of NaOH
3. Cap tightly and shake vigorously for more than 20 seconds
4. Place on the retort stand and allow it to settle
5. Drain off NaOH (it's heavier so will go to the bottom) into a beaker and discard
6. Repeat steps 3-5 twice using all the NaOH
7. Repeats steps 3-5 three times using dH_2O instead of NaOH

8. Place ~100ml beaker full of anhydrous calcium chloride ($CaCl_2$) into a folded filter paper in the large glass funnel on the retort stand. Place a clean 500ml glass bottle under it and slowly filter the washed MMA through $CaCl_2$ to remove all traces of water
9. Add a small amount of $CaCl_2$ to the bottle of dMMA to absorb excess water, store at 4°C

B. Dehydration and infiltration of samples

1. Cull mice and remove rear legs from the hip joint and carefully strip of skin and muscle
2. Place in 4% formaldehyde in PBS overnight (or longer if required) at 4oC
3. Wash in PBS for 10 minutes
4. Put bones in 70% ethanol
5. Bone can be visualised using the faxitron if available to determine bone lengths and widths using ImageJ software
6. Trim bones to remove any remaining muscle and separate the tibia from the femur by cutting through the knee joint, place into individual glass scintillation vials and dehydrate at 4°C for at least 1 hour in;
    70% acetone
    90% acetone
    100% acetone
    100% acetone (fresh), in all but the last step the acetone is reused.
7. Infiltrate for at least 3 nights in infiltrate mix;
    90% dMMA
    10% dibutylphthalate (DBP)
    0.05% benzoyl peroxide (BPO)
8. Whilst the bones are infiltrating, make sure there are enough bases for embedding the bones. Bases are made using spare infiltrate that is made into embedding solution by adding 5% BPO, stirring and filtering through $CaCl_2$. A plastic transpipette full (~2-3 mls) is placed in a used MMA vial and left to set at 37°C overnight or longer.

C. Embedding samples (day 4 or later)

1. After the bones have infiltrated, make up embedding solution;
    total volume = 5ml x number of samples + 10%
        85% dMMA
        15% DBP
        4% BPO
(* dMMA and DBP can be made up in 100ml lots and stored at 4°C)
2. Cover with parafilm and place on a stirrer until the BPO is dissolved
3. Using a funnel and filter paper, filter through $CaCl_2$ into a clean dry glass beaker
4. Put ~5ml (2 transpipettes) of embedding solution on top of enough bases for the samples to be embedded. Any spare embedding solution is used to make bases for later use.
5. Once the base has softened, remove the bones from the infiltrate and place into the embedding vial with the 'sharks fin' (for tibiae) orientated towards the bottom of the vial. Press the bones in firmly but carefully and close the lid tightly. Tip spare infiltrate back into a bottle and store at 4°C for future use.

6. Put vials in a plastic box, fill with water making sure the vials do not float and place at 37°C overnight or longer.

D. Top layer on samples as a holding base (day 5 or later)

1. Once the sample is encased with plastic, use spare infiltrate to make a holding base
   total volume = 7.5ml x number of samples + 10%
   Add 5% BPO, cover with parafilm and stir until dissolved
   Filter through $CaCl_2$
2. Put 7.5ml of this solution into each vial. Use any spare to make bases for later use
3. Put vials at 37°C (no need for a water bath) for 1-2 nights.

E. Removing embedded bones from the vials (day 6 or later)

Make sure that you are wearing safety goggles and thick rubber gloves

1. When the holding base is solid (check with forceps), put the vials at -20°C for a minimum of 1 hour
2. Take samples out (up to 6 at a time), individually remove the lid and label, place the vial in a thick zip lock bag and hit with a hammer to shatter the glass. Remove the sample from the bag, brush off any remaining glass inside the bag and replace the label.
3. Using a hacksaw and vice clamped to the bench, cut off excess plastic from the top of the sample (this was originally the base of the vial)

F. Grinding samples for sectioning

Make sure that you are wearing safety goggles, thick rubber gloves and facemask

1. Remove the label and grind flat on the coarse paper until the bone is showing, angle to reveal the entire tibial face
2. Once the tibial face is showing, grind the sides so that minimal plastic is on the flat face at either side of the tibia. Grind the top and bottom of the sample so that it can be inserted into the sample holder on the microtome and finally grind the bottom and top edges into a teardrop shape. Replace the label.

G. Plastic sectioning

1. Remove label, place the sample in the sample holder, secure tightly and angle to ensure that the sections are cut evenly
2. Wet the sample with 40% ethanol and then cut 5μm sections
3. Place the section on the slide (2/slide) and put one drop only of 95% ethanol on the section and flatten onto the slide using a combination of tweezers and a fine paint brush
4. Cover the slide with a plastic square (made from empty tip bags baked at 37°C and cut appropriately) followed by a spare glass slide over the top and clamp with a bulldog clip
5. Bake overnight at 37°C

Slide preparation and staining of plastic sections

Reagents required:

Chromium potassium sulphate	Sigma 243361
Gelatin	Sigma 48723
DePex mounting medium	VWR 361254D
2-Ethoxyethyl acetate (cellosolve)	Sigma 00820
Toluidine Blue	Sigma 89640
Fast green	VWR 1.04022.0025
Safranin O	VWR 1.15948.0025
Disodium phosphate	Sigma S7907
Citric acid	
Butanol	
Toluene	
Ethanol	

Equipment required:

Slides, ground edge, frosted end	VWR 631-1553
Coverslips 22x50mm	VWR 631-0137
Glass staining dishes and jars	
Osteomeasure software and microscope	

A. Fol's coating of slides

1. Dissolve 6g of gelatine in 288ml of dH_2O at 60°C
2. Make up 4g of chromium potassium sulphate in 20ml dH_2O at room temperature
3. Allow the gelatine to cool and add 120ml 95% ethanol followed by the dissolved chromium potassium sulphate
4. Rack slides to be coated in a slide holder and dip for 60 seconds per rack
5. Dry overnight but leave for 2 nights if placing them in boxes for use to avoid slides sticking together

B. General Staining Protocol

1. Select the best sections with no visible folds or cracks
2. Deplasticise in cellosolve for 2 x 25 mins
3. Rehydrate in graded ethanols for a minimum of 3 minutes each;
    - 100% ethanol
    - 100% ethanol
    - 80% ethanol
    - 60% ethanol
    - tap water
4. Stain with appropriate stain (see section C)

5. Blot slides on both sides on filter paper
6. Pass the slides through;
    butanol 1 (store at 37°C)
    butanol 2 (store at 37°C)
    50:50 toluene:butanol
    toluene 1
    toluene 2
7. Coverslip with DePex

C. Stains

* To be used at step 4 of the general staining protocol

Toluidine Blue – for general bone and cell architecture

1. Prepare toluidine blue buffer and stain;

Buffer - 1.58g citric acid, 0.75g disodium phosphate, dH_2O to 1 ltr, pH 3.7 at RT

Stain - 2g toluidine blue O in 100ml of buffer, pH 3.7 at RT

2. Place slide in toluidine blue stain for 5 mins
3. Rinse x2 in toluidine blue buffer

Safranin O– for cartilage detection

1. Prepare the stains
    Safranin O - 0.1% safranin O in dH_2O
    Acetic acid - 1% acetic acid in dH_2O
2. Safranin O stain for 3 min, dip in acetic acid wash
3. Check for the balance of orange and green, can restain and wash as required